



National Library
of Canada

Acquisitions and
Bibliographic Services Branch

395 Wellington Street
Ottawa, Ontario
K1A 0N4

Bibliothèque nationale
du Canada

Direction des acquisitions et
des services bibliographiques

395, rue Wellington
Ottawa (Ontario)
K1A 0N4

Your file - Votre référence

Our file - Notre référence

NOTICE

The quality of this microform is heavily dependent upon the quality of the original thesis submitted for microfilming. Every effort has been made to ensure the highest quality of reproduction possible.

If pages are missing, contact the university which granted the degree.

Some pages may have indistinct print especially if the original pages were typed with a poor typewriter ribbon or if the university sent us an inferior photocopy.

Reproduction in full or in part of this microform is governed by the Canadian Copyright Act, R.S.C. 1970, c. C-30, and subsequent amendments.

AVIS

La qualité de cette microforme dépend grandement de la qualité de la thèse soumise au microfilmage. Nous avons tout fait pour assurer une qualité supérieure de reproduction.

S'il manque des pages, veuillez communiquer avec l'université qui a conféré le grade.

La qualité d'impression de certaines pages peut laisser à désirer, surtout si les pages originales ont été dactylographiées à l'aide d'un ruban usé ou si l'université nous a fait parvenir une photocopie de qualité inférieure.

La reproduction, même partielle, de cette microforme est soumise à la Loi canadienne sur le droit d'auteur, SRC 1970, c. C-30, et ses amendements subséquents.

Canada

UNIVERSITY OF ALBERTA

A Numerical Model for Outbursts in Coal Mines

by

Xiaoqin Chen



A THESIS
SUBMITTED TO THE FACULTY OF GRADUATE STUDIES AND RESEARCH
IN PARTIAL FULFILLMENT OF THE REQUIREMENTS FOR THE DEGREE OF

Doctor of Philosophy

IN

Mining Engineering

Department of Mining, Metallurgical and Petroleum Engineering

Edmonton, Alberta

Fall 1994



National Library
of Canada

Acquisitions and
Bibliographic Services Branch

395 Wellington Street
Ottawa, Ontario
K1A 0N4

Bibliothèque nationale
du Canada

Direction des acquisitions et
des services bibliographiques

395, rue Wellington
Ottawa (Ontario)
K1A 0N4

Author's reference

Notre référence

The author has granted an irrevocable non-exclusive licence allowing the National Library of Canada to reproduce, loan, distribute or sell copies of his/her thesis by any means and in any form or format, making this thesis available to interested persons.

L'auteur a accordé une licence irrévocable et non exclusive permettant à la Bibliothèque nationale du Canada de reproduire, prêter, distribuer ou vendre des copies de sa thèse de quelque manière et sous quelque forme que ce soit pour mettre des exemplaires de cette thèse à la disposition des personnes intéressées.

The author retains ownership of the copyright in his/her thesis. Neither the thesis nor substantial extracts from it may be printed or otherwise reproduced without his/her permission.

L'auteur conserve la propriété du droit d'auteur qui protège sa thèse. Ni la thèse ni des extraits substantiels de celle-ci ne doivent être imprimés ou autrement reproduits sans son autorisation.

ISBN 0-315-95162-1

Canada

UNIVERSITY OF ALBERTA

RELEASE FORM

NAME OF AUTHOR: Xiaoqin Chen

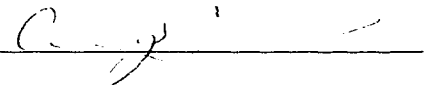
TITLE OF THESIS: A Numerical Model for Outbursts in Coal Mines

DEGREE FOR WHICH THESIS WAS SUBMITTED: Doctor of Philosophy

YEAR THIS DEGREE GRANTED: 1994

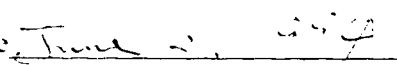
Permission is hereby granted to the UNIVERSITY OF ALBERTA LIBRARY to reproduce single copies of this thesis and to lend or sell such copies for private, scholarly or scientific research purposes only.

The author reserves all other publication right and other rights with the copyright in the thesis, and except as hereinbefore provided neither the thesis nor any substantial portion thereof may be printed or otherwise reproduced in any material form without the author's written permission.

(SIGNED) 

PERMANENT ADDRESS:

c/o Department of Mining, Metallurgical and
Petroleum Engineering
University of Alberta
Edmonton, Alberta
Canada T6G 2G6

Date 

© 1994 Xiaoqin Chen
All rights reserved

子曰：學而不思則罔，
思而不學則殆。

論語 · 為政第二

*The Master said, 'He who learns but does not think,
is lost.'*

*He who thinks but does not learn,
is in great danger.*

Confucian Analects • Book II "The Practice of Government" • 14

Translated by, Arthur Waley (1938)

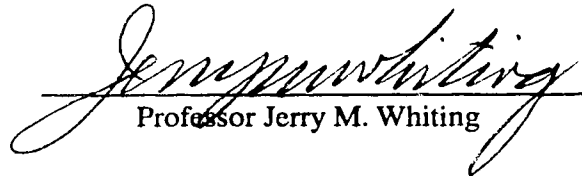
UNIVERSITY OF ALBERTA

FACULTY OF GRADUATE STUDIES AND RESEARCH


The undersigned certify that they have read, and recommend to the Faculty of Graduate Studies and Research, for acceptance, a thesis entitled:

A Numerical Model for Outbursts in Coal Mines

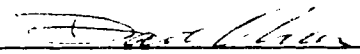
by Xiaoqin Chen in partial fulfilment of the requirements for the degree of Doctor of Philosophy in Mining Engineering




Professor Jerry M. Whiting



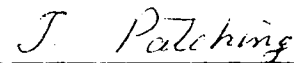
Professor Ken A. Barron



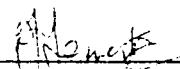
Associate Professor David Chan



Professor D. Scott



Professor Emeritus of Mineral Engineering
Thomas H. Patching



Dr. David Forrester

Date May 17, 1994

Dedication

To my wife and daughter
for their continued encouragement and inspiration
especially for understanding at difficult times

and to my parents
for their persistent supports in my life and studies
and inspiring me to endeavor for the best

ABSTRACT

Outbursts are one of the most serious problems facing underground coal mining operations today. Although many studies and investigations have been carried out, outbursts still threaten lives and reduce mine productivity. This problem is still, therefore, the focus of much research activity throughout the world.

Modeling has always been considered as a major tool to investigate the mechanisms that are responsible for outbursts. This study has developed a new model based on the current knowledge of outburst behavior and the development of numerical modeling technology using the computer. The model can quantitatively evaluate the influence of measurable parameters on the initiation, propagation and cessation of an outburst.

Sandstone outbursts which occurred at #26 colliery, Glace Bay, Nova Scotia, Canada, have been examined against the developed model and comparable results have been achieved. The results suggest that the spalling mechanism postulated in the model can offer a viable explanation of the outburst mechanism. By use of this model, parametric studies have been conducted to investigate the factors influencing outbursts under a range of conditions. It was found, from analyzing modeling results, that initiation, cavity development and cessation of the outbursts will be affected by the gas pressure, the sandstone height, the exposed area of the sandstone in the crown of the excavation, and the field stress ratio. The model may also simulate the "choke up" mechanism proposed by Gray when the outbursts take place in the coal seams. This simulation reveals the significant influence of the gas pressure upon the cavity sizes resulting from the outbursts, which is in general agreement with field observations.

Application of the model to longwall conditions has been attempted. This model produced a cone shape cavity as it was reported in literature, and indicated that the span formed by seam roof has an insignificant effect on the outbursts. Finally the model may be applied to the evaluation of the effectiveness of the potential remedial measures.

ACKNOWLEDGEMENTS

I would like to take this opportunity to thank the program supervisor, Dr. Ken Barron, Chairman of the Mining, Metallurgical and Petroleum Engineering Department, University of Alberta, for his supervision, guidance, encouragement and generosity shown throughout the whole program. Dr. Ken Barron keenly supported this work by ensuring funding and many other resources and by making available his time to discuss with me whenever it was required, and his solid and broad knowledge in mining engineering.

Sincere thanks also go to co-supervisor, Dr. David Chan, Associate Professor of Civil Engineering Department, University of Alberta for his supervision, numerous discussions and many valuable suggestions in development of this model. This program would not have been so successful, and fast to complete without his guidance.

I also wish to express my gratitude to my wife, Xiaoqin, and my father and mother for their support and encouragement.

Dr. David Forrester, Director of Coal Research Center of CANMET, Sydney, Nova Scotia has shown his keen interest and great encouragement for the program. His hospitality shown in the short period of my visit was greatly appreciated.

The help of Mr. Doug Booth, whose assistance, especially in the computer technology and facilities, was indispensable for the completeness of the program, is also greatly appreciated.

TABLE OF CONTENTS

Chapter I INTRODUCTION TO THE THESIS	1
Chapter II INTRODUCTION TO OUTBURSTS.....	3
2.1. Classification of Dynamic Phenomena in Mines.....	4
2.1.1. Definition and classification of outbursts	4
2.1.2. Mining induced seismic activities	7
2.1.3. Gas-outburst (Blower)	8
2.2. Historical Review of Outbursts	9
2.2.1. Outbursts in Europe	9
Belgium:	9
Germany:	10
United Kingdom:	11
France:	12
Poland:	12
Hungary:	13
Soviet Union:	13
Bulgaria:.....	14
Czechoslovakia:.....	14
Yugoslavia:	15
2.2.2. Outbursts in Northern America.....	15
Canada:	15
U.S.A.:	15
2.2.3. Outbursts In Asia	16
China:.....	16
Japan:	16
2.2.4. Outbursts in Australia	17
2.3. Hazards Of Outbursts In Mines	17
2.4. Studies and Research on Outbursts.....	18
2.4.1. Understanding of mechanisms.....	18
2.4.2. Prediction of events	19
2.4.3. Prevention and control measures	21
2.5. Scope of the Thesis.....	21

Chapter III CHARACTERISTICS OF OUTBURSTS AND THE THEORIES.....	22
3.1. Factors Affecting Outbursts.....	22
3.1.1. The factors influencing outbursts	22
3.1.2. Stresses	26
3.1.3. Gas pressure.....	28
3.1.4. Mechanical properties.....	29
3.2 Mechanisms and Theories	30
3.2.1. Gas dominant theories	30
3.2.2. Stress dominant theories	31
3.2.3. Gas and stress combination doctrine	32
3.2.4. Geological structure theories	33
3.2.5. Summary.....	33
3.3. Analysis Methods	33
3.3.1. Descriptive and experimental stage	34
3.3.2. Qualitative and quantitative stage.....	34
3.3.3. Numerical computer aided analysis.....	35
 Chapter IV MODELING OF OUTBURSTS	 36
4.1. Purposes of Outburst Modeling.....	36
4.2. Models Proposed in the Literature.....	36
4.2.1. Energy balance models	37
Karagodin's Model (KARAGODIN, 1983):.....	37
Litwinski's Model (LITWINSKI, 1985):	38
4.2.2. Mechanical failure models.....	40
Gray's Model (GRAY, 1980):.....	40
Hiramatsu's Model (HIRAMATSU, 1983):.....	41
Kristianovich's Model (KRISTIANOVICH, 1983):	42
Khoroshun's model (KHOROSHIUN, 1984):	44
Revalor's model (REVALOR, 1985):.....	46
Paterson's model (PATERSON, 1985):.....	48
Golder Associates Model (GOLDER, 1987):.....	49
Barron and Kullman's model (BARRON, 1991):	50
4.3. Discussions	51

Chapter V STATEMENT OF THE PROBLEM	54
5.1 Statement of the Problem.....	54
5.2 Scope of Thesis.....	55
Chapter VI DERIVATION OF THE MODEL	56
6.1 Description of the Outbursts.....	56
6.2 Selection of the Numerical Method:.....	58
6.3 Model Assumptions.....	59
6.4 Mathematical Derivation of the Model.....	61
6.4.1 Generalized formulation of FEM analysis.....	61
6.4.2 Incremental analysis:	69
6.4.3 Finite element method	72
6.4.4 Gas pressure consideration in FEM.....	75
6.4.5 "Excavation" of the material.....	76
6.5 Model Operation.....	79
6.5.1 Model sequence	79
6.5.2 Inputs for the model.....	82
6.5.3 Output from the model.....	82
6.6 Sample Run Of Model.....	84
Chapter VII APPLICATION OF MODEL TO A DEVELOPMENT ENTRY	85
7.1 Introduction to Outbursts in No. 26 Colliery.....	85
7.1.1 Geological features related to outbursts.....	86
7.1.2 Mining operation at No. 26 Colliery.....	87
7.1.3 Geotechnical properties of rocks	88
7.1.4 In situ gas properties	89
7.1.5 In situ field stresses.....	90
7.2 Initial Conditions for the Modeling.....	91
7.3 Verification of the Model against In Situ Observation.....	94
7.4 Parametric Analysis	101
7.4.1 Outburst initiation.....	101
7.4.2 Gas pressure influence on outburst consequences.....	108
7.4.3 Influence of sandstone height	115
7.4.4 Exposure angle and stress ratio influences	119
7.4.5 Influence of stress level	120
7.5 Filled Cavity Modeling.....	121

7.6 Discussion.....	123
7.7 Summary.....	124
Chapter VIII APPLICATION TO LONGWALL FACE	125
8.1 Statement of the Problem.....	125
8.2 Introduction to MCR outbursts.....	126
8.3 Field Data.....	128
8.4 Input Data for Modeling	130
8.5 Results from the Model Application.....	131
8.6 Summary.....	133
Chapter IX CONCLUSIONS.....	135
9.1 Summary.....	135
9.2 Model Advantages.....	136
9.3 Model Limitations	137
Chapter X FUTURE WORK RECOMMENDED.....	138
REFERENCES	139
APPENDICES	147
Appendix A A Revised General Method for Geometrically Altered Structures	147
Appendix B Patch Test.....	150
Appendix C Development of the Outburst Model Finite Element Program FEOMP	165
Appendix D Sample Run of the Model	172
Appendix E Cavity Shape and Size of #36 and #37 Outbursts	191
Appendix F Cavity Shape and Size Resulting from the Empty Cavity Model	200
Appendix G Cavity Shape and Size Obtained from Filled Cavity Model.....	212

LIST OF TABLES

Table 7.1	Rock Strength and Deformation Properties	88
Table 7.2	In Situ Stresses from Overcoring Tests	90
Table 7.3	Elasto-Plastic Properties and Strength Parameters of the Rock	92
Table 7.4	The Initiation Gas Pressure Under Different Conditions.....	100
Table 7.5	Cavity Size Results from the Model Runs.....	105
Table 7.6	Cavity Size Results from the Model Runs.....	105
Table 7.7	Cavity Size Results from the Model Runs.....	105
Table 7.8	Gas Pressure Influence on Cavity Size for Filled Cavity	116
Table 8.1	Severe Outbursts of LW 102	127
Table 8.2	Strength and Stiffness of Rock and Coal for Pocahontas No. 3 Coalbed.....	129
Table 8.3	Strength and Property Parameters of Rock and Coal for Modeling	131
Table 8.4	Model Results for the Cavity Formed for Longwall Face	132
Table B.1	Material Properties Used for Patch Tests.....	151
Table B.2	Closed Form Solution for Nodal Displacements	152
Table B.3	Closed Form Solution for Nodal Displacements	153
Table B.4	Closed Form Solution for Nodal Displacements	153
Table B.5	Closed Form Solution for Nodal Displacements	154
List B.1	Program Output for Constant σ_y	157
List B.2	Program Output for Constant σ_x	159
List B.3	Program Output for Pure Shear.....	161
List B.4	Program Output for Biaxial Loading with Gas Pressure	163
Table D.1	Format and Definition of GENIN.DAT File.....	172
Table D.2	Format and Definition of EPFECIN.DAT File.....	174
List D.1	Sample of GENIN.DAT File	176
List D.2	Sample of EPFECIN.DAT File	177
List D.3	Sample of FEOMPIN.DAT File	177
List D.4	Sample of EPFEOU.DAT File.....	180
List D.5	Sample of FEOMPRT.DAT File	182

LIST OF FIGURES

Figure 2.1	Classification of Dynamic Phenomena	4
Figure 2.2	Sketch of Gas Pressure Distribution around an Open Face.....	6
Figure 4.1	Sketch of Stress State at the Coal Face	43
Figure 4.2	Stresses around a Circular Hole	47
Figure 4.3	Crescent Shape Cavity (after PATERSON).....	49
Figure 4.4	Outburst Cavity Modeled from the Computer.....	51
Figure 6.1	Sketch of a 3-D Domain	62
Figure 6.2	Sketch of a Discretized 3-D Domain.....	63
Figure 6.3	A 2-D Rectangular Element with Postulated Nodal Forces	64
Figure 6.4	Calculation of the Stress Ratio	71
Figure 6.5	Quadrilateral Element (after WILSON)	72
Figure 6.6	Definition and Displacements of the Typical Triangular Element.....	74
Figure 6.7	Sketch of In-situ Empty Cavity Formation.....	76
Figure 6.8	Sketch of In-situ Filled Cavity Formation.....	77
Figure 6.9	Model Flow Chart	80
Figure 6.10	Relationship among the Input Files and the Programs	83
Figure 7.1	Coal Seam Sequence at Sydney Coalfield (after FORGERON)	86
Figure 7.2	Entry Geometry and Geology	92
Figure 7.3	Sketch for θ Definition.....	93
Figure 7.4	In-situ Outburst Cavity, Longitudinal and selected Cross Sections - No. 26 Colliery, Sydney, Nova Scotia.....	95
Figure 7.5	Comparison of In-situ Cavity Area of Cross Section 12 and Model Result.....	96
Figure 7.6	Comparison of In-situ Cavity Area of Cross Section 10 and Model Result.....	97
Figure 7.7	Comparison of In-situ Cavity Area of Cross Section 7 and Model Result.....	98
Figure 7.8	Comparison of Cavity Size from Field and Model Results.....	99
Figure 7.9	Comparison of In-situ and Model Cavity Areas at Different Exposure Angles	100
Figure 7.10	3-D Plot of Initial Gas Pressure vs Sandstone Height and Exposure Angle for Stress Ratio 0.5	104

Figure 7.11 3-D Plot of Initial Gas Pressure vs Sandstone Height and Exposure Angle for Stress Ratio 1.1	104
Figure 7.12 3-D Plot of Initial Gas Pressure vs Sandstone Height and Exposure Angle for Stress Ratio 2.0	104
Figure 7.13 Initiation Gas Pressure vs. Exposure Angle (Stress Ratio =0.5)	105
Figure 7.14 Initiation Gas Pressure vs. Exposure Angle (Stress Ratio =1.1)	105
Figure 7.15 Initiation Gas Pressure vs. Exposure Angle (Stress Ratio =2.0)	106
Figure 7.16 Initiation Gas Pressure vs. Initial Shear Zone Thickness	107
Figure 7.17 Modeling Results for Different Exposure Angle (θ) with the Sandstone Height 15.8 m	112
Figure 7.18 Modeling Results for Different Exposure Angle (θ) with the Sandstone Height 15.8 m	112
Figure 7.19 Modeling Results for Different Exposure Angle (θ) with the Sandstone Height 15.8 m	112
Figure 7.20 Modeling Results for Different Exposure Angle (θ) with the Sandstone Height 3.8 m	113
Figure 7.21 Modeling Results for Different Exposure Angle (θ) with the Sandstone Height 3.8 m	113
Figure 7.22 Modeling Results for Different Exposure Angle (θ) with the Sandstone Height 3.8 m	113
Figure 7.23 Modeling Results for Different Exposure Angle (θ) with the Sandstone Height 2.8 m	114
Figure 7.24 Modeling Results for Different Exposure Angle (θ) with the Sandstone Height 2.8 m	114
Figure 7.25 Modeling Results for Different Exposure Angle (θ) with the Sandstone Height 2.8 m	114
Figure 7.26 Field Stress Level Effects on the Outbursts	120
Figure 7.27 Stabilized Cavity Area vs. Gas Pressure for a Filled Cavity	122
Figure 8.1 Coal Basin Columnar Section, Pitkin County, Colorado, U.S.	126
Figure 8.2 Longwall Mining at Dutch Creek #1 Mine of MCR	128
Figure 8.3 Setting-up for Longwall Modeling	130
Figure 8.4 Crescent Type of Cavity Formed from the Model	132
Figure 8.5 Cavity Area Variation with Gas Pressure for Different Longwall Spans	133
Figure B.1 Patch Test Elements and Grid Set-up Sketch	151
Figure B.2 Elasto-Plastic Stress Displacement Relationship	155

Figure C.1 Overview of FEOMP Program Flow	166
Figure C.2 Flow Chart of Subroutine STRESS	169
Figure D.1 Sample Run after Iteration 4.....	187
Figure D.2 Sample Run after Iteration 8.....	187
Figure D.3 Sample Run after Iteration 9.....	188
Figure D.4 Sample Run after Iteration 11.....	188
Figure D.5 Sample Run after Iteration 14.....	189
Figure D.6 Sample Run after Iteration 15.....	189
Figure D.7 Sampl Run after Iteration 18	190
Figure D.8 Sample Run after Iteration 21.....	190
Figure E.1 Longitudinal Section of Cavity from Outburst #36 and #37.....	192
Figure E.2 Section 1: Intersection with Cross Cut.....	193
Figure E.3 Section 2: 2.4 m from Cross Cut.....	193
Figure E.4 Section 3: 4.0 m from Cross Cut.....	194
Figure E.5 Section 4: 6.1 m from Cross Cut.....	194
Figure E.6 Section 5: 7.9 m from Cross Cut.....	195
Figure E.7 Section 6: 12.2 m from Cross Cut.....	195
Figure E.8 Section 7: 13.4 m from Cross Cut.....	196
Figure E.9 Section 8: 16.2 m from Cross Cut.....	196
Figure E.10 Section 9: 17.7 m from Cross Cut.....	197
Figure E.11 Section 10: 18.3 m from Cross Cut.....	197
Figure E.12 Section 11: 21.0 m from Cross Cut.....	198
Figure E.13 Section 12: 20.3 m from Cross Cut.....	198
Figure E.14 Section 13: 22.6 m from Cross Cut.....	199
Figure E.15 Section 14: 23.8 m from Cross Cut.....	199
Figure F.1 Stabilized Cavity from Empty Model	201
Figure F.2 Stabilized Cavity from Empty Cavity Model.....	202
Figure F.3 Stabilized Cavity from Empty Cavity Model.....	203
Figure F.4 Stabilized Cavity from Empty Cavity Model.....	204
Figure F.5 Stabilized Cavity from Empty Cavity Model.....	205
Figure F.6 Stabilized Cavity from Empty Cavity Model.....	206
Figure F.7 Stabilized Cavity from Empty Cavity Model.....	207
Figure F.8 Stabilized Cavity from Empty Cavity Model.....	208
Figure F.9 Stabilized Cavity from Empty Cavity Model.....	209
Figure F.10 Stabilized Cavity from Empty Cavity Model.....	210
Figure F.11 Stabilized Cavity from Empty Cavity Model.....	211

Figure G.1 Stabilized Cavity from Filled Cavity Model213
Figure G.2 Stabilized Cavity from Filled Cavity Model214
Figure G.3 Stabilized Cavity from Filled Cavity Model215
Figure G.4 Stabilized Cavity from Filled Cavity Model216
Figure G.5 Stabilized Cavity from Filled Cavity Model217
Figure G.6 Stabilized Cavity from Filled Cavity Model218

NOMENCLATURE

A	constant, cavity area
B	constant
[B]	strain-displacement relationship matrix
c	material cohesion
c_{ij}	constitutive matrix coefficient
D	material density
E	average Young's modulus (Young's modulus)
E_0	initial Young's modulus
E_∞	ultimate Young's modulus
f	constant, failure function
F_i	body forces
G	Lamé constant (shear modulus)
h_1, h_2, h_3	constants for plastic constitutive relation.
H	height of the overburden
J_1	first stress invariant
J_2	second stress invariant
k	permeability, constant associated with material properties
k_0	field stress ratio
K	bulk modulus
[K]	stiffness matrix
$\langle L \rangle$	revised unity vector
m, s	Hoek and Brown constants
M	constant
M_1	magnitude of seismicity
N	constant, shape function
p	pore gas pressure
Δp	coal methane desorption rate
P	gas pressure
P_g	initial gas pressure
$\{P_b\}_e$	element nodal force vector associated with body forces
$\{P_{gp}\}_e$	element nodal force vector associated with gas pressure
$\{P_t\}_e$	element nodal force vector associated with traction on boundary surface

$\langle q \rangle$	global nodal displacement vector
$\langle \bar{q} \rangle_e$	displacement vector in an element
$\langle \underline{q} \rangle_e$	element nodal displacement vector
$\{Q\}'_e$	element nodal force vector associated with internal effective stresses
$\{Q\}'$	global nodal force vector associated with internal effective stresses
R_0	maximum reflectance value for all vitrinite
$\{R\}$	global nodal force vector associated with external forces
s_{ij}	deviatoric stress tensor
s_r	stress ratio
s_{ti}	surface associated with boundary traction
s_{u0}	surface associated with prescribed displacements
t	real world time, sandstone height
T_i	boundary traction
u	potential energy of elastic deformation
u_i	displacement tensor
u_{i0}	prescribed boundary displacements
W_f	work done for fracturing rock
α	constant, angle
β_1	material rheological constant
δ	variational, infinitesimal increment
Δ	incremental
Δ_{ij}	Kronecker delta
ϵ_{ij}	strain tensor
ϵ_x	strain in x direction
ϵ_{xy}	shear strain in 2-D condition
ϵ_y	strain in y direction
ϵ_z	strain in z direction
ϕ	internal friction angle, porosity
γ	material weight
γ_{xy}	shear strain in 2-D condition
μ	gas viscosity, Poisson's ratio
ν_0	Poisson's ratio
θ	exposure angle, angle
$\sigma_1, \sigma_2, \sigma_3$	principle stresses
σ_c	material compressive strength

σ_h	horizontal stress (field stress)
σ_{ij}	total stress tensor
σ'_{ij}	effective stress tensor
σ_{max}	maximum tensile strength in solid phase
σ_t	material tensile strength
σ_v	vertical stress (field stress)
σ_x	stress in x direction
σ_y	stress in y direction
σ_z	stress in z direction
τ	relaxation time
τ'_{xy}	effective shear stress in 2-D condition

SUBSCRIPTS

a, b	identifier
b	broken
e	element
f	final
i, j, k	principal direction, counter
i	initial
n	step counter
u	unbroken

SUPERSCRIPTS

T	transposition
-1	inverse
.	incremental quantity

ABBREVIATIONS

BEM	boundary element method
CANMET	Canada Center for Mineral and Energy Technology

CBDC	Cape Breton Development Corporation
DEM	distinct element method
Eq.	equation
FEM	finite element method
FDM	finite difference method
Fig.	figure
HCS	hybrid computational scheme
MCR	Mid-Continent Resources
MRL	Mining Research Laboratory
N.S.W.	New South Wales
2-D	two dimensional
3-D	three dimensional

SYMBOLS

$\langle \dots \rangle$	row vector
$\{ \vdots \}$	column vector
$[\vdots]$	matrix
$[\vdots \vdots \vdots]$	two-dimensional array

Chapter I

INTRODUCTION TO THE THESIS

Outbursts occurring in underground mining have presented a serious safety problem and have hindered mine's production throughout the world. Many investigations and much research has been done in an attempt to prevent outbursts. This thesis sets the goal of studying this problem in depth, and of comprehensively understanding the phenomenon. Based on this understanding, a numerical model is proposed and developed as the primary goal of this study. The developed model has been verified by a case history, and exercises on solving the problem by use of the model are included.

In Chapter 2, an expanded definition for an outburst is made to distinguish this problem from the other problems which also have dynamic characteristics. The outburst occurrences throughout the world are then reviewed briefly. The results of the study and research of the outburst problem by others are discussed, and the scope of this thesis is defined.

To understand the outburst problem, the characteristics of outbursts have been described as thoroughly as possible in Chapter 3. They are mainly extracted from the previous study and research results. The involvement of gas in the outburst phenomenon has essentially complicated the problem, and makes it unique. The factors directly influencing outbursts reflect this unique characteristic, and are discussed fully in the first section of the chapter. Mechanisms and theories to explain the phenomenon proposed in the past are examined in following section. Comments on, and criticisms are made of these theories. Finally, methods used for studying the problem are summarized, and the trend to use computer numerical modeling as a research tool is recognized.

The important models developed in the past are introduced in Chapter 4. A total of ten models are discussed under the two headings of energy balance models and mechanical failure models. The energy balance models maintain that outbursts occur whenever the energy stored in the medium is greater than that required to break it and to transport the broken material. The physical concept of these models seems reasonable, but mathematical formulation presents very challenging problems. No realistic model has been developed from these theories. The mechanical failure models are easier to formulate mathematically. Among these models, some emphasize the influence of the gas pressure, and some favor field stresses as the primary factor, while others include the combined effects of both gas pressure and field stresses. Discussion in this chapter has

pointed out the limitations and drawbacks while introducing these models. Through this discussion, it is obvious that a better and more practical model is still needed to solve the outburst problem in the mining industry.

Chapter 5 defines the modeling objectives and the scope in which the model will be developed. Chapter 6 details the assumptions in the proposed model and the derivation of the mathematical formulations. A generalized formulation of the finite element method is coupled with a spalling process which deals with both the removal of failed elements in tension and the degassing of the elements failed in the shear mode. The tensile failed elements are removed by the general method for a geometrically altered structure. The sheared elements are degassed according to an algorithm given in section 6.4.4. An empty and a filled cavity model are distinguished by different element removal schemes. Section 6.5 describes the logical flow in the model and the program input preparation. An example run for an empty cavity model is included in section 6.6.

After the model is developed in Chapter 6, it is applied to the outbursts occurring in the "tunnel" in Chapter 7. Outbursts that occurred in No. 26 Colliery, Glace Bay, Nova Scotia, are simulated to verify the model. A parametric analysis is performed to show the capability of the model as applied to the "tunnel" outbursts. A filled cavity model is also used to study the problem. The application of model to the outbursts occurring on a longwall face is given in Chapter 8, and the results are discussed.

In the concluding chapter (Chapter 9), the major results obtained from application of the model to both the "tunnel" case and longwall face case are summarized. The advantages and the limitations of the model are discussed. Some recommendations for further development of the model are also considered in Chapter 10.

Seven appendix chapters are included in this thesis. In Appendix A, a revised general method for analysis of geometrically altered structures is introduced in more detailed context. The patch test conducted on the finite element program, as revised for the model is considered in Appendix B. The computer programs for the model are described in Appendix C, and the data files for the sample run referred to in Chapter 6 are included in Appendix D. Appendix E shows the longitudinal and cross sections plotted from insitu observation for #36 and #37 outbursts at No. 26 Colliery. In Appendix F and G, the graphical representations of the stabilized cavity and the infinite cavity resulting from outburst modeling for the "tunnel" case from the empty cavity model, and the filled cavity model, are presented respectively.

Chapter II

INTRODUCTION TO OUTBURSTS

The term "dynamic phenomena" in mines is used to give a collective description of all the sudden, violent ejection or movements of geomaterials into an underground mining opening in a mining environment, with or without emission of gases or other substances such as water. These phenomena are distinguished by their high speed and violent effects from other underground structural failures, such as coal squeezing, loosening or partial fracturing of rocks around an opening, instability of the walls and roofs, as well as the convergence of roof-to-floor. Because of these features, dynamic failures have presented very perplexing problems in underground mining for over a century since coal outbursts were first recorded in a Belgian mine in 1847. They still defy reasonable explanation and complete solution to the present day.

With the development of mining technologies in the past century, dynamic phenomena in mines have been alleviated to some extent, though the intensity of events has increased because of deeper mining operations, as the shallower minerals have been consumed. The damage resulting from the phenomena has increased as larger scale and the higher productivity mines have been developed. Fatal casualties, serious injuries, destructive damage to the mining facilities and structures, and even partial or complete closure of mines have been continuously reported in the literature.

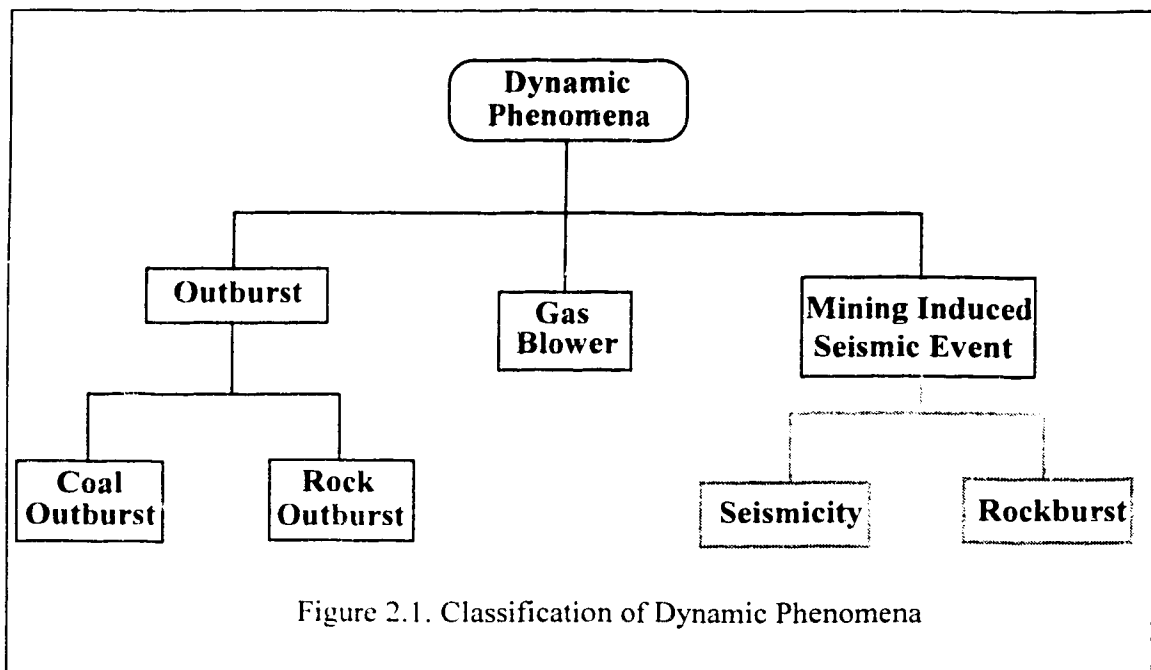
The forms of manifestation of the phenomenon have also diversified as more complex operations have been implemented in underground mining workings. A large magnitude ($M_j=4.5$) mining induced seismic event was reported at the Lubin copper mine in Poland on March 24, 1977, although fortunately, it caused only minor underground damage. Ten years later, on June 20, 1987, a seismic event ($M_j=4.3$) struck the same mine. It was combined with a large rockburst causing four fatalities and eleven injuries among the thirty miners working in the area; it also caused extensive underground damage within a radius of about 800 meters (GIBOWICZ, 1988). Many other rockburst cases can also be found in the literature and this phenomenon is getting more and more attention from researchers these days. Occasionally, a gas blower (gas-outburst) has been reported threatening underground mining safety, which presents another dynamic event (HARGRAVES, 1984).

To combat these challenges from nature, investigations and research have been extensively carried out in various countries where the problem has hindered mining

production. Through these world wide efforts, some substantial improvements have been made both in understanding and in prevention of the phenomena.

2.1. Classification of Dynamic Phenomena in Mines

Case histories of the dynamic phenomena in mines indicate that no two are alike because many factors have been considered responsible for their occurrences. As knowledge accumulates, various classifications have been established for different purposes. For example, the classification depends on whether the events occurred in rock drivages, caved longwall faces, stowed rising longwalls or the gate roads in the coal seams. In order to model an outburst, the following classification has been developed for the mechanisms responsible for the dynamic phenomena. The scheme of the classification is graphically shown in Fig. 2.1. A key factor in that the term "outburst", either in coal or in rock, involves the active participation of the gas in its mechanism.



2.1.1. Definition and classification of outbursts

Hargraves defines an instantaneous outburst of coal and gas as the violent ejection of coal and gas away from freshly exposed coal in mining, when either in breaking into or in the development of the seam. This definition basically refers only to underground coal

mining production. In fact, other underground mining activities, such as potash and salt mining, may also experience a similar violent ejection of rocks and different gases, rather than coal and gases. As a matter of fact, even in coal mines, ejection may occur in the rocks overlying or underlying the coal seam in the drivages or access gates such as the case reported at No. 26 Colliery, Nova Scotia in Canada (ASTON, 1985). With the same projection action in different materials accompanied by gas release, the same mechanism has been involved. This has led to categorizing them all under the same group by the term "instantaneous outburst" or "outburst" in brief. Hargraves' definition of an instantaneous outburst of coal and gas can, therefore, be revised as **the violent ejection of geomaterials around a mine opening and the gases retained in them, away from the freshly exposed face in a mining operation** for outburst definition. This definition is important for this thesis because it establishes a sound base for the communication, and, most of all, it defines the working domain of the thesis, which is a sub-domain of the whole field of dynamic phenomena in mines.

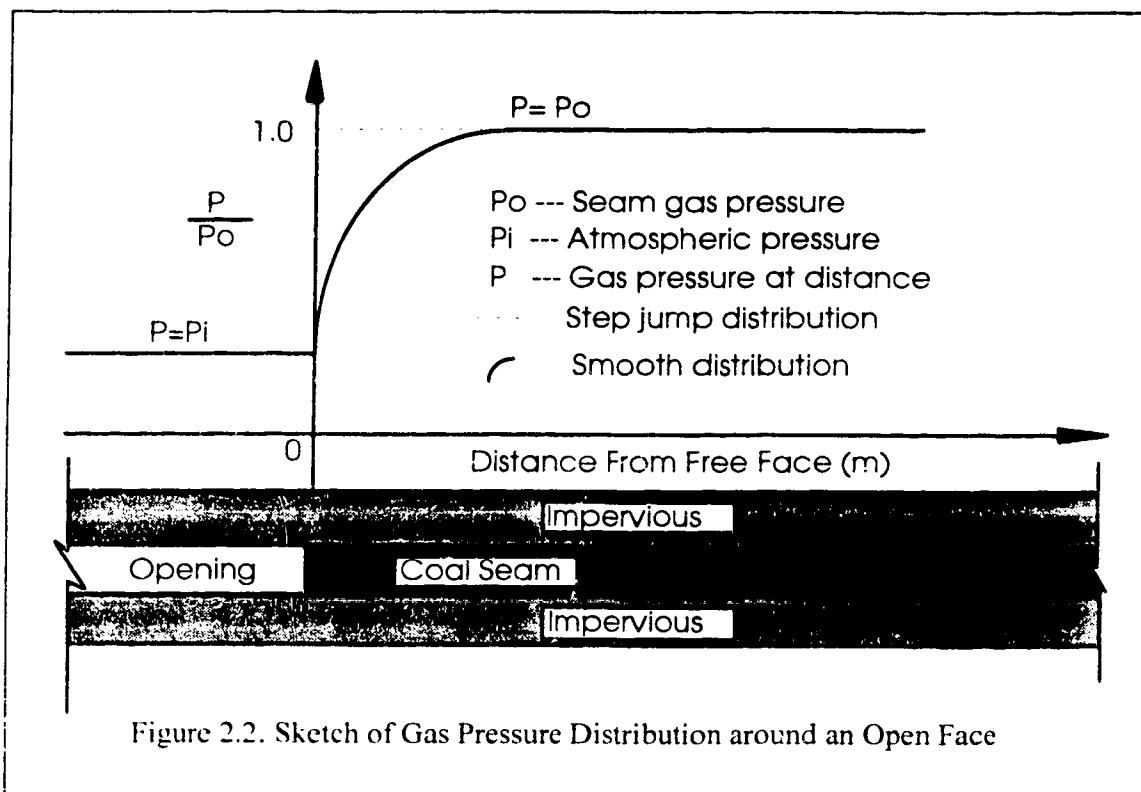
An outburst of coal and gas and that of rock and gas are categorized under the same group of the division, although they should be clearly distinguished by the differences between coal and rock with the carriage and the transport of the retained gas. It is this difference that leads the sub-division of the outbursts, as shown in Fig. 2.1; i.e., the coal outburst and the rock outburst.

In a coal seam, it is generally accepted that the gas contained exists in three phases: free gas within cracks, fissures and pores, or a liquid layer of gases sorbed on the interior surface of fissures and pores, and a molecular state dispersed between the coal molecules. Experimental investigations show that approximately 90%-95% of total methane content is held in the sorbed liquid phase (BARKER-READ, 1984; ETTINGER, 1975; SHUL'MAN, 1975). The amount of methane retained in the sorbed phase seldom exceeds 57 m³/ton at normal temperature and pressure. Therefore, the maximum methane content would not exceed 57 m³/ton for the total gas in a coal seam (PATCHING, 1970).

The flow of these retained gases through the coal seam is basically governed by two mechanisms. A flow seeps through the fissure and fracture system and the molecules of the sorbed gas diffuse through the micro-structure (CURL, 1978). The gas pressure, an important factor to cause tensile failure and the source of sufficient energy to expel the broken rocks in an outburst is, therefore, usually related to the flow gradient, which is assumed to be distributed smoothly from the open face at atmospheric pressure to an original gas pressure as shown in Fig. 2.2.

In contrast to the coal seam, rocks retain the gas only in the free gas state in the pores and fractures, and have no ability to sorb the gas. The amount of the gas retained in

rock, therefore, is much less than that in a coal seam. As a result of the consolidation during formation of the rocks, the gas in pores was pressurized to a relatively high level, for example, 2.8 MPa to 7.9 MPa as estimated by Aston and Cain (ASTON, 1985). This high pressurized gas is usually trapped and sealed in isolated pores or fractures which are assumed being randomly distributed in the stratum. The flow of this trapped gas in rock becomes very difficult, even though a fracture system has been well developed in the rock mass (Cain, 1984). The gas pressure is then distributed in a form of a step jump at the periphery of an opening as shown in Fig. 2.2. Occasionally, high pressurized gas pockets exist in the rock masses (MAHTAB, 1982), increasing the likelihood of an outburst occurrence.



It is this difference in gas flow that has complicated the problem, leading to the separate research into two phenomena. Through the studies reported here, however, it is believed that this difference only produces different boundary and initial conditions, while the same mechanism has been involved in both coal and rock outbursts. Therefore, outbursts as a sub-category of dynamic phenomena in mines could be treated as an entity from a modeling point of view.

2.1.2. Mining induced seismic activities

Mining induced seismic activities (seismic events, seismicity and tremors) indicate a sudden movement of the geomaterials in the earth's crust, resulting from release of strain energy due to the activities of the mining operation. To cause a seismic event, the fracture criterion for the rock mass must be satisfied and an excess energy will be poured into the system from the surrounding rocks.

In the second international symposium on rockbursts and seismicity in mines held in 1988, Gibowicz, in a review of the modern seismicity research work, pointed out that two aspects have characterized seismic occurrences. "Firstly, an increasing number of large seismic events corresponding to increasing depth and extent of mining operations; secondly, an erratic behavior of rock bursts in a sense that they do not follow any clear-cut lines which would imply that a specific seismic event in a given situation would become a rockburst. Large tremors don't necessary generate rockbursts and often small seismic events are associated with considerable underground damage" (GIBOWICZ, 1988). This statement explains the diversity of seismic activities and their links to rockbursts. No general rules have been established to describe seismic events by a few selected parameters, although great effort has been put into the research. However, some qualitative evaluations have been widely accepted.

A broad range of mine induced seismic mechanisms and proposals to prevent these events have been published in the literature. From the studies, two general points have been widely accepted for mine induced seismicity. Two main types of mine tremors are almost universally observed and are directly connected with the mining operation. The first one of the two is the tremor associated with the formation of fractures at stoop faces, and the second is one which is associated with the movement on major geological discontinuities. The other point worth noting is that mine seismicity is strongly affected by local geology and tectonics, that is, affected by non-homogeneities, discontinuities and the interactions between mining, lithostatic and residual tectonic stresses on a local and the regional scale.

According to Gibowicz (GIBOWICZ, 1988) and Salamon (SALAMON, 1983), rockbursts represent only a small sub-set of mining induced seismicity. Salamon argued that "virtually no systematic research has been done to elucidate the basis of setting apart those seismic events which become rockbursts from those which do not". However, from the mechanistic point of view, seismic events are essentially the result of brittle shear

failure, resembling an earthquake (WONG, 1988), while rockbursts can be caused by any form of failure (shear, tensile or compressive).

Rockbursts can be further classified depending on countries, mines and the nature of the occurrence. Phillips (PHILLIPS, 1944; PHILLIPS, 1948) made a classification of a pressure-burst and a shock-burst, based on the loading speed and conditions. Other classifications include seam burst, roof burst and floor burst depending on the place where the failure takes place; ring burst, shear burst and pillar burst depending on the stress state and the failure mechanism.

A rockburst is considered as an instantaneously explosive release of rock strain energy outwards from rib or face exposed to a mining opening, without significant gas emission. Study and research have revealed that the fundamental mechanism for a rockburst relies on the sudden, brittle failure of rock due to high stresses, although some other failure mechanisms have also been investigated. Four major independent factors contribute to the occurrence of a rockburst. They are the ability of rock to store strain energy; regional or local geological characteristics; the physical and mechanical properties of the rocks and the mining plan and design (layout of mining operation etc.). Some similarities are shared between the coal or rock outbursts and the rockbursts as both of them are a result of the high stress state around an opening. This fact suggests that it may be possible to analyze the two distinct phenomena by using the same approach, but different criteria.

2.1.3. Gas-outburst (Blower)

This catastrophic event in mines may not be relevant to this thesis, although it is also a dynamic phenomenon in mines. For the sake of completeness, only a very brief introduction of the concept will be made below.

A gas-outburst (blower) presents a hazard with a great (and perhaps prolonged) discharge of gas from the coal or rock mass without the projection of solid material (HARGRAVES, 1984). A geological fault is the usual location for such a gas blower, and the blower may sometimes be accompanied by water and sludge. Solid materials, if any, are carried out in suspension. No solid disintegration happens in a gas blower.

A gas-outburst can only occur if there exists a large amount of gases under very high pressure and a fracture or a fissure system which channels these gases to the open air without damaging the integrity of the rock mass. A gas-outburst can be very dangerous sometimes, because its dynamic force can destroy mining facilities and dust or gases may

suffocate workers at the site. In addition, it has the potential to explode and cause a fire underground. This phenomenon has been reported only in coal mines.

2.2. Historical Review of Outbursts

Among the dynamic phenomena in mines, the outburst is one of the oldest and most frequently encountered subset. It has been recognized for over a century since the Belgium mines started to record their events in 1847. Many investigations and much research have been carried out on the subject, continuing to the present day, as deeper mines and more extensive mining operations create a greater chance for an outburst. In order to have a better understanding of the phenomenon, it is worthwhile making a historical review of the occurrences and the combat of the events.

2.2.1. Outbursts in Europe

In the course of the mining industry development, Europe started to face the challenge of the outbursts at the end of the last century. Fortunately, in the beginning outbursts were scattered in only a few locations in unusual coal fields and under exceptional geological conditions (RICE, 1931). After a serious of outbursts happened in the Agrappe mine of Belgium in 1879, more attention was paid to this violently destructive phenomenon because of a large number of miners being killed. Now, unfortunately, the outbursts have spread to almost every country where the mining industry has been developed.

Belgium:

In the period between 1847 and 1908, a total of 357 outbursts occurred because of the complex geological structure of the coal measures in this country. Fifty one of these resulted in fatalities causing, in all, the death of 447 workers (VANDELOISE, 1966). This includes the catastrophe at the Agroppe mine in 1879, in this event 121 miners were killed. In the ten years from 1956 to 1966, 130 outbursts happened in Belgium mines; six deaths were reported in the period 1959-1964. The two largest outbursts during this period were those which happened during the sinking of a shaft, when 1,600 tons of coal were ejected on one occasion and 1,200 ton on the other. With such a high intensity of outbursts occurring in this country, coal mining was greatly affected. Few reports have

been found in the literature since that period, because most, if not all the mines have closed.

The structure of the coal, the pressure of gas in the seam and the stress state were considered as the original factors causing so many outbursts in this country. On the basis of understanding these factors, a classification of coal seams was proposed according to the rate of release of the methane from the coal. This index was then used to predict the occurrence of the outbursts.

Shotfiring and large bore hole drilling, either in combination or conducted individually in order to relieve gas pressure and rock stress, were the two major measures taken to prevent outbursts. These actions were reported as being efficient and effective.

Germany:

Compared with other countries in Europe that have faced the outburst problems, the former East Germany experienced outbursts considerably later, because of the later beginning of the mining activities (potash mining) and the later reaching sufficient depth (copper-slate mining). Only rock outbursts were observed in the East Germany's mining history, while both rock and coal outbursts have been observed in West Germany. The frequency and intensity of the occurrence of rock outbursts in East Germany were one of the greatest in the world during that period. The world record ejection amount during outbursting is held by the Menzengraben mine with 100,000 tons in 1953. Approximately 10,000 rock outbursts occurred in the 70 years before 1965 in the Werra potash mining district (DORFELT, 1966).

The most mines significantly affected by rock outbursts were located in the potash mining fields of Werra and "Sudharz" (Southern Harz). The violence of the outbursts in this district was very impressive; 3,700 tons salt and 50,000 m³ gas were ejected in Kaiseroda II/III mine in 1938, which suffocated 11 miners who had withdrawn to another level before shot firing triggered the outburst. This event stopped the mining advance for about half a year afterwards. The case already mentioned in Menzengraben in 1953 was much worse, when even the surface facilities were damaged to some extent. It resulted in a 3 month shutdown of the mine. In the Southern Harz potash field, rock outbursts have become of importance only since 1950. One hundred thirty three outbursts occurred before 1965, each with more than 100 tons of salt ejection.

The copper-slate mining areas of Mansfeld and Sangerhausen syncline also had a high risk of rock outbursts. Sudden rock outbursts usually occurred in sandstone with the emission of nitrogen gas. The intensity of occurrence of rock outbursts in copper-slate

mines was not as high as in potash mines. Less than 100 events occurred and only 20 of them had an ejection of over 100 tons before 1965. During this period, the most serious rock outburst was in 1933: 1,500 tons of sandstone were ejected and 17 persons were poisoned by gas, but fortunately most of them recovered (DORFELT, 1966).

In the bituminous coal mines in West Germany, 213 coal outbursts have been recorded over the 80 years from 1903-1982, of which 189 have occurred since 1972. The locations of the outbursts were concentrated in #53, #54 and #59 coal seams of Innbenburen Ostfeld, Ruhr and Aachen coalfields. The most severe coal outburst took place on August 2, 1981, during the development of an in-seam roadway in coal seam #53; 750 tons coal and 21,240 m³ gas were ejected and 8 miners were killed.

After suffering so much from outbursts, German mining engineers were mobilized to combat this challenge. The recognition of locations liable to the outbursts allowed the engineers to minimize the effects detrimental to safety and economy. Methods to predict the right time and the right place of outbursts were attempted. In 1962, the first technically controlled salt-gas outburst was triggered. This was considered to be a very important development, because it meant that a better understanding of the mechanisms causing the outbursts was obtained and the practical methods to combat the phenomenon were developed. The combination of the prediction of outburst locations and the application of a complete protective system by systematically triggering and technically controlling outbursts not only avoided the accidents and the considerable expenses for destruction, but also made it possible to reduce the normal production costs by assisting the production of the high grade salt.

United Kingdom:

Coal outbursts occurring in U.K. were characterized by very fine coal rapidly ejected from the coal body, accompanied by the emission of a large volume of gases. The incidence of the outburst was mainly confined to the north-western part of the anthracite field in South Wales. The remainder of the anthracite field was affected to a lesser extent and only in isolated pockets. A few coal outbursts also occurred in other coal fields, but they usually were small in size and were of less importance.

The largest coal outburst took place at Cwendraeth Valley mine in 1971 during the excavation of a development entry heading, in which 400 tons of fine coal were ejected and 60,000 m³ gas was emitted.

France:

France was one of the countries which were most affected by outbursts. A most spectacular coal outburst was recorded at the Richard Colliery in the Cevennes Basin, at a depth of 800 m in 1938, with 1,270 tones coal ejected and 400,000 m³ of CH₄ emitted. At the Rioux Shaft in the Isere, an outburst with CO₂ at 200 m depth trapped 8 miners at the bottom of the mine (HARGRAVES, 1983). At Merlebach Colliery, 6 sandstone and gas outbursts occurred at a depth of 1250 m during the drivage of an access-way in virgin ground. Two more outbursts again occurred in 1986.

The pre-cursors of the outbursts had been actively sought as a warning to take cautious actions during the mining (GOLDER ASSOCIATES, 1987). Drilling relief holes was considered as an effective method of protection. It was most effective in cross-cuts and coal mass between roads, but was less effective for the face outbursts (HARGRAVES, 1966).

Poland:

Some Lower Silesian collieries and some salt mines in Poland were subjected to the hazards of outbursts. The first occurrence was in 1894, and there were over 1,000 events recorded before 1964, including some catastrophes (MAHNER, 1966).

In 1981, there were only 2 outbursts of rock and carbon dioxide, but both of them were very serious. The events took place at a depth of 550 m in an exploratory cross-cut driven toward an old mined-out field, in which 1,840 tones of rock with 20,000 m³ of CO₂ were ejected the first time, and 1,300 tones of rock and 13,000 m³ of CO₂ in the second ejection in the same drivage (GOLDER ASSOCIATES, 1987).

The incidence of the outbursts was related to the gas permeability of a series of seam layers, the tectonics, the viscosity of the coal and the depth of the seams. A clear relationship between outbursts and the type of working was recognized.

Introduction of improved mining methods was attempted to reduce the outburst occurrence in development openings. Special labor safety regulations were laid down to protect people from being injured. In outburst prone sections, coal was broken exclusively by blasting, and shock blasting was used to relieve high rock pressure whenever it was possible.

Hungary:

Coal outbursts have been experienced in the coal field of Pecs situated in the southern part of Hungary. The first occurrence was recorded at Pecs Collieries on 12 Dec., 1894. It was followed by a second occurrence on the next day at the same place, which caused two fatalities. These two outbursts were the first of a total of 500 outbursts prior to 1964, which increasingly hampered the mining operations and reduced the production. On 4 Nov. 1957, at a depth of 480 m in the Istvan mine, an outburst initiated after 36 hours of an inducer shotfiring, which ejected 1,400 tons of coal and 273,00 m³ of methane. Due to the warning system and excellent work of the mine rescue team, no fatalities occurred. In September, 1960, another outburst struck the mine, 957 tons of coal and 181,000 m³ methane were discharged and 4 lives lost at the working face (SZIRTES, 1964).

The delay of outbursts after inducer shotfiring mainly originated from the unique Hungarian geological conditions. As the inducer shots demanded high costs and had other disadvantages, a perforation technique was introduced to the mine as a prevention measure. Due to the application of this technique, the incidence of outbursts was reduced to a very low level compared to the situation before its introduction.

Soviet Union:

A total of 7 coal basins and 89 mines had been affected by the outbursts in the former USSR according to the statistics in 1962. From 1946 to 1962, the outbursts in USSR totaled 1137. The highest frequency of the outbursts happened in the Donbass Basin; 1,250 outbursts had been registered before 1940, and they still present serious problems. The causes have been attributed to the complex geological structures of the basin, the presence of a large number of regional and local faults, variations in the mechanical properties of the coal and the adjacent rock, the thickness of the seams, the relatively high gas content of the seams, the great depth of working and the resultant high initial rock pressure (LIDIN, 1964). The Donbass Basin area has also experienced rock outbursts since 1950, when the depth of the coal workings reached 700 m. Almost every event was initiated by blasting. The rock ejections averaged 220 tones per ejection and were up to 3,500 tones in some cases. Up to Jan. 1983, over 3,400 rock outbursts in total had been recorded in 22 mines in the Donbass area (GOLDER ASSOCIATES, 1987).

Preventive measures were taken either to remove the gas from the parent material or to localize the outbursts in space and time. The measures were based on the principles

of relieving rock pressure and gas pressure in the vicinity of exposures, eliminating local stress concentrations, increasing the strength of coal, employing development out of the seam, discontinuing concussive blasting, manless extraction, and arresting the outbursts by barricades.

Bulgaria:

Outbursts first occurred in 1933 at the western end of the Balkan coalfield in Bulgaria. From then on, they began to develop and extend to the center and gradually spread in an eastern direction. A total of 93 events were recorded before 1964, of which 28% were estimated to be rockbursts. During this period, the most violent outburst occurred in the driving of a heading to uncover the seams. The maximum ejection of coal was 320 tons. The frequency and intensity of the outbursts in this country were relatively insignificant, but their fairly shallow depth is noteworthy, for instance, from 139 m to 210 m below the surface.

The essential causes of the outbursts were the existence of hard rock with high compressive resistance in the roof and floor of an outburst prone seam, the composite structure, the high methane pressure and the tectonic disturbance. The preventive measures of extracting protective seams, drilling pilot holes, correctly planning working layouts and limiting the advance rate proved to be highly successful.

Czechoslovakia:

The coal mines in the former Czechoslovakia have experienced only mild coal outbursts. The largest recorded was a 110 ton rock ejection and, on average, 18 ton rock was ejected per outburst prior to 1963. The first occurrence was in 1894 and totally 451 outbursts were estimated to have occurred in the mainly affected Ostrava-Karvina Coal Basin, which is the Czechoslovakian part of the Upper Silesian Coal Basin, to 1984. Three coal outbursts were recorded in another coal basin and, in addition, three rock outbursts occurred at the same mine during that period (PAUL, 1983; CZECHOSLOVAKIA, 1964).

Routine and local prediction methods were recommended by the Coal Research Institute of Ostrava-Radvanice for outburst prone zones. De-stress drilling and canmouflet blasting were the two frequently used preventive methods, while water infusion and other measures were also applied in some instances.

Yugoslavia:

In the Saka Basin of Yugoslavia, the coal mines have experienced both coal outbursts and rock outbursts. Coal outbursts usually occurred in the faulted zones of the coal seams, while the rock outbursts happened in development roadways for new production zones.

2.2.2. Outbursts in Northern America

Canada:

In Canada, only coal mines have been affected by the outbursts, but both coal and rock outbursts were observed. Most coal outbursts have been reported from three districts in western Canada: the Nanaimo district of Vancouver Island, the Coal Creek and Morrissy district in the Crowsnest area of Southeastern British Columbia and the Canmore district near Banff in Alberta. The earliest outburst occurring in Canada was recorded during the first decade of the century in the Crowsnest area. The most serious outburst happened in 1904 at the Carbonado Colliery, following the mine shut down two weeks later; 3,500 tons coal and 60,000 to 140,000 m³ gas were ejected, asphyxiating 14 miners. Hundreds of outbursts had been reported before 1964 (PATCHING, 1966).

In eastern Canada, the Sydney coalfield of Nova Scotia began to face rock outburst problems as the coal mining went to a deeper level. In the period from 1977 to 1984, 37 rock outbursts were recorded in the development of headings at No. 26 Colliery. The final two major events were so serious that the development of the main deep was halted until a method of control could be implemented. These two events ejected 450 m³ of sandstone and 3,950 m³ of methane.

To combat the hazards, the geological complexity, the material properties and the gas characteristics were studied extensively in an attempt to find some prediction criteria. The controlling methods applied in European mines were tested in outburst prone mines, and only shot induced blasting became standard practice in Canmore mines for a period. Rock outburst problems are anticipated in the Phalen mine of the Sydney coal field.

U.S.A.:

Coal outbursts have not been significant in coal mining history in the U.S.A. The report of the cases could go back to 1915. Three outbursts occurred in Pennsylvania,

including a notable event in Knickerbocker mine in Aug. 1908, which damaged mining equipment and suffocated 7 miners. The most recent outburst occurred in 1985 when 6 longwall face coal outbursts were recorded in Dutch Creek #1 mine.

In Louisiana salt mines the rock outbursts presented a significant hazard to lives or even loss of the mine itself (should the outburst cavity provide a connection to a reservoir of water or hydrocarbons). The importance of rock outbursts in Louisiana salt mines was highlighted on June 8, 1979 at the Belle Ise Mine. Five miners were killed and widespread damage was reported in the mine. The rock outburst problem in the country was relatively new, no significant reports were found before the beginning of the 1970's.

2.2.3. Outbursts In Asia

China:

In China, outbursts have been limited to coal mines and they have caused very significant problems as high gas content coal seams have been extracted widely in the country. Incomplete statistical data show that 9845 outbursts were recorded at 205 sites during the period from 1950 to 1981. Of these, 69 events were considered serious and ejected over a few thousand tons of coal. The coal fields mostly affected by outbursts are Zhongliangshan, Tianfu, Naton, Songchao, Beipiao, Beisha, Luoping, Liuzhi, Shuicheng, Jixi, Huanan. Most of these coal fields are located in Sichuan and Huainan Province. There is no data available on fatalities.

Extraction of the releasing seam (liberation seam) is one of the measures successfully applied in 26% of mines where the outbursts have been present. The other prevention methods, such as hydraulic pre-fracturing, controlled firing and borehole drilling, have been adopted in the rest of the affected mines.

Japan:

Outbursts have occurred in Japan since 1925, the frequency of occurrence increasing over the years with deeper mining and due to increasing rates of extraction. The cases recorded up to 1964 were estimated to be about 1,000, concentrated in Hokkaido and Kyushu districts, especially the Sorachi area. The largest coal outburst in Japanese coal mining history occurred in Oct. 1981, at Yubari-Shin Colliery in Hokkaido district. The outburst poured out 5,000 tones coal and emitted 500,000 m³ gas and suffocated 93 miners. The mine was closed after this fatal catastrophe.

To try to combat the hazards of outbursts, various investigations and research have been conducted and various theories were proposed to explain the experiences. The relationship between index Δp and the occurrence of outbursts provided a basic measure useful for prediction. (The index Δp is the pressure increase due to desorption of 3 g of methane saturated coal at atmospheric pressure, with a given particle size, placed in an evacuated chamber.) Safety measures include drilling boreholes and firing inducer shots, with the aim of degassing and destressing the coal seams. Improved conditions were reported as a result of these measures.

2.2.4. Outbursts in Australia

The two major Australian Black Coal Basins, the Sydney Basin, N.S.W. and the Bowen Basin, Queensland, both of Permian Age, have experienced outbursts. The documented events can be traced back to 1895 at the Metropolitan Colliery in the Sydney Basin. Several hundreds of significant outbursts had been recorded during the period up to 1954. The Leichardt occurrence was regarded as the largest outburst in this country; it ejected 500 tons coal and a large amount of methane.

1954 marked the beginning of research into the phenomenon in this country. The initial main impetus of the research was to mine safely as an immediate requirement and to develop some safe means of continuous mining as the long term objective. Under these guidelines, inducer shotfiring was introduced to all Australian mines, although the other preventive measures have also been applied in some circumstances.

2.3. Hazards Of Outbursts In Mines

Outbursts have always been considered hazardous. Injury and death have always been associated with the occurrence of outbursts regardless of prevention efforts. The characteristics of uncertain time and place of occurrence and the violent nature make it very difficult, even impossible, for mining engineers to provide adequate protection.

Once the outbursts initiate, injuries and casualties are almost inevitable. The broken rock flying with high momentum may injure or even cause the death. The powerful impulsive wave transmitted in air can also seriously injure people. The emission of fine coal dust or other dust may blind and suffocate people. The gases accompanying the ejection of solids may asphyxiate victims. A methane explosion hazard may be created by the release of methane from the coal mass. As a result of these effects, mining production may be seriously reduced and a mine may be forced to close.

In addition to the hazards to personnel, outbursts may cause considerable destruction to underground structures and facilities. As a result of an outburst, the working opening or the heading space may be strewn with broken material for tens of meters. The cavities created in the rock mass may result in exceeding the planned layout of the working, which, in turn, requires extra support materials and work to be repaired. Broken rock ejected with large energy can damage equipment and facilities near the working place. Because of the disturbance to the air flows by the gases released during outbursting, the ventilation system may be disrupted and the main fan may even shut down or be forced to reverse. The force of the air rush can blow equipment and temporary or permanent support out of the working opening for several tens of meters. This can lead to a considerable deterioration in work safety conditions, a retardation in the rate of driving of workings and a considerable increase of the cost for rehabilitation.

For a mine with methane, an outburst may create possible explosion and fire hazards underground. The most spectacular outburst that caused fire in underground mines may be the one that happened at Richard Colliery in Cevennes Basin of France. About five minutes after an outburst, there was a violent rush of air at the collar of the downcast shaft, quickly followed by heavy fumes and dust and a great flame. The flame was as high as 60 meters over the collar for a hour and it was only extinguished after 7 hours.

2.4. Studies and Research on Outbursts

The purposes of study and research on outbursts are to understand the mechanisms, to identify the prediction criteria and to find preventive measures. In these three areas, much progress has been made, some of which is briefly discussed below.

2.4.1. Understanding of mechanisms

Understanding the mechanisms of the outburst process underlies all research work. Clear and precise definition of the mechanism will provide very valuable guidance both in prediction and prevention. Many theories exist to explain the mechanisms of the outbursts as their occurrences have never been the same from one place to another. Each theory may explain certain manifestations of outbursts, but does not necessarily explain the others.

Gray (GRAY, 1980) stated " the failure may be brought about totally by material stress combinations exceeding the strength of the coal and without the effect of gas at one

extreme to the other extreme whereby internal gas pressure is sufficient to exceed the tensile strength of the coal in an unconfined state." According to the definition in the beginning of this thesis, Gray's statement confused the rock burst and outburst. When Gray spoke about one extreme without the effect of gas, he was referring to the rock bursts or bumps rather than an outburst. But the concept he used in the statement might have grasped the essence of the mechanism for an outburst. Hargraves emphasized the role of gas in outbursts, and also he pointed out that "the aspects which set outbursts apart from rockbursts or bumps are not only the inevitable gas component, but also the geometry of the places where they occur; rockbursts occur predominantly in the size reduction of stress laden pillars and instantaneous outbursts in the exposure of virgin, gassy coal in development." It is thus clear that the combination of the effect of gas pressure and field stress may dominate the causes for initiation of outbursts.

Incorporating this concept, Barron (BARRON, 1991) defined an outburst as the failure of rock due to excessive pore fluid (gas) pressure. He stated that if the effective stress exceeds the tensile strength of the rock, the rock shatters, completely destroying its structure and the resulting particles are expelled by the energy contained in the high pressure gas.

On the basis of the effective stress concept, the other phenomena described in the literature, such as the presence of faults and intrusions, the abnormal geological structures and fabrics, the increase of abutment pressure due to various reasons, the acceleration of face advance, the sudden exposure of virgin rocks, the depth of outburst location and gas content, can all be seen as the factors which increase the effective stress or reduce the tensile strength, and will increase the outburst proneness of rock mass or coal seams, but they are not the essential causes of the initiation of the outbursts.

As a supplement to the theoretical conclusions extracted from practical observations, laboratory experiments allow further examining the physical mechanisms and for verification of the theories. Laboratory reproduction of an outburst was achieved by the work of Skochinsky in 1953; a number of other experiments have been conducted since that time. Strong support for the theoretical assumptions have been obtained from this experimental work.

2.4.2. Prediction of events

Predicting the place and the time outbursts occur is a necessary step to protection and prevention. It also constitutes an important objective of outburst study and research. At the beginning, the predictions were made by identifying the increasing of frequency of

noises within the coal. Now, more comprehensive devices to measure the stress, gas and coal characteristics have been invented and the predictive capability has been greatly improved (HARGRAVES, 1993).

Two aspects are usually considered in prediction. Firstly, the regional and local predictions try to establish the proneness of seams and workings to the outbursts. Many factors were recognized and associated with the proneness. The factors in terms of coal and gas relationship were summarized by Hargraves (HARGRAVES, 1983) as the following:

- (a). presence in seam of gas in suitable quantity,
- (b). appreciable depth of cover,
- (c). local faulting, and partial crushing of coal at faults,
- (d). residual or current tectonic forces,
- (e). contortions of the seam, also variations in thickness.
- (f). steep dip of the seam,
- (g). intrusion of the seam by dikes,
- (h). low moisture content of coal,
- (i). coal of low permeability to passage of gas,
- (j). working the seam in a manner which does not allow the satisfactory escape of sorbed gas.

Besides these factors, coal seams with a higher rank can be more liable to an outburst. The vitrinite content in coal has great influence on the proneness. In some European countries, the Δp index of coal determined by laboratory tests is used to indicate the relative proneness of a coal seam (HARGRAVES, 1983).

While the regional and the local prediction can indicate where the outburst may occur, day to day prediction is required to warn workers in sufficient time to allow them to reach a safe refuge. The seismic activities before the coming event have been constantly considered as an indicator since prediction was first attempted. Initially miners only used their ears to identify the approaching event and experience was required for the predictions. With the development of technologies, various kinds of seismic detectors have been applied as a sensitive monitor of the seismic activity. Some research work has been reported to be very successful in particular circumstances, but more comprehensive prediction criteria and more sophisticated devices must be incorporated before accurate prediction can be realized. For example, Mid Continental Resources (VARLEY, 1986).

has monitored stress change, gas pressure, cutting produced along drilling, and squeezing of the coal in their program of coal outburst investigations.

2.4.3. Prevention and control measures

Prevention and control of outbursts are the final objective of the study and research. Through about a century's efforts, many empirical prevention measures have been developed and they worked very well practically and some control methods have also been invented.

For prevention of the outbursts, an adequate mining method and geometry must be adopted to avoid forming a narrow working space. The proper extraction sequence can reduce the ground pressure around the openings and eliminate the gravity influence. Reduction of the advance rate in longwall mining helps to alleviate the proneness to outburst. Seam de-stressing to below the burst point may secure the workings from an outburst. As the stress level needed to cause an outburst is still uncertain, the de-stressing techniques used are somewhat arbitrary. Under-cutting, large diameter hole drilling and perforation are practical methods used for release of the concentrated stresses. They are very effective in some instances. Seam gas pre-drainage can improve the safety conditions. A well known de-gassing method is the extraction of protective seams. For those coal seams without a protective seam available, pre-drainage holes from the surface can be drilled for gas release. Hydrofracturing underground can increase the permeability of the rock mass or coal seams to allow and to force the retained gases out of the mother body. Water infusion has been applied a lot in some European countries to release the gas pressure and to increase the moisture content, for reduction of the proneness to outbursts.

2.5. Scope of the Thesis

As discussed above, the research and study of outbursts include three main areas which have been developed individually to different levels. This thesis will focus on only two of them, i.e. understanding the mechanisms and predicting outbursts. Developing an outburst model will substantiate these goals. Through modeling, the mechanism postulated can be checked against the results of field observations and the prediction may be attempted from the results. In order to establish the model, the characteristics and mechanisms of the outbursts in past literature will be discussed in the next chapter and the models proposed in the past will be introduced and discussed.

Chapter III

CHARACTERISTICS OF OUTBURSTS AND THE THEORIES

Compared to the other dynamic phenomena discussed in chapter II, outbursts have always been more complex and more dangerous. The overwhelming violent nature can bring about many more injuries and give rise to very serious damage in underground mines. The prediction of the occurrence of the outbursts has always presented a general problem, although some local successes have been achieved. Hargraves (HARGRAVES, 1980) considered the outbursts a more complex stress phenomenon than the rockburst or the bump because the involvement of gas essentially changed its characteristics.

3.1. Factors Affecting Outbursts

The complex features of the outbursts are reflected in the influencing factors for the proneness and the occurrence. A large number of these factors have been discussed in the past literature. They may be significant locally, but not generally applicable to all the cases. Some of them played the dominant role in one case history, but might be trivial in others. Exceptional cases always exist, even in one coal field. Because of this fact, non of these factors are generally applicable for all cases.

3.1.1. The factors influencing outbursts

The physical and chemical interactions between coal and gas have no doubt contributed to the proneness to outburst, although it has not yet been fully understood. Sorption may trap a large portion of the gas in the liquid phase which can be released quickly after initiation of an outburst. In most cases, the gas volume measured after bursting and the gas pressure in the coal seam do not abide by the simple Boyle's Law relationship. The gas volume released can reach as high as 20 times of the coal volume, which can not be accounted for only by the physical contraction of the gas (HARGRAVES, 1958). Some chemical process must be involved. The energy released by this process has not yet been quantitatively established, but it must be very substantial to mobilize such a violent occurrence.

In addition to the gas volume and pressure, the coal strength can, theoretically, be reduced by the sorption. However, the experiments conducted by Ates (ATES, 1987)

suggested that no significant reduction of strength was observed from tests on Highvale coal with CO₂ pressurized up to 3.45 (MPa). This may imply that the reduction is too small to be identified with the given experimental device or the theoretical concept is invalid.

The physical and chemical interaction of coal and gas may also be visualized in the permeation process. The natural permeation of mixed gases through coal seams and coal samples results in change of composition, both in time and in distance, with perhaps a molecular sieve analogy. The gas composition in a coal seam has been found to influence the proneness to an outburst. The seams containing carbon dioxide (CO₂) are much more prone than seams containing methane (CH₄). The seams with CO₂ also exhibit greater violence after initiation (HARGRAVES, 1983).

It has been pointed out (HARGRAVES, 1983; SHEPHERD, 1981) that the higher the coal rank the more prone it is to an outburst. This is concluded from miners experience of finding that some particular coal is prone to bursting, as well as through the laboratory tests to determine the indexes Δp and the mean maximum reflectance value (R_0 max) for all vitrinite. Δp is implicitly related to the coal rank, as high rank coal always has a high desorption rate of CH₄ or CO₂. In European practice, Δp has almost become the standard indicator of the coal outbursts. $\Delta p \geq 15$ has been found to be potentially dangerous in Belgium practice (VANDELOISE, 1964). In other countries, the number found may be different, but it is related to outburst proneness.

R_0 is one of the most important characteristics in defining the rank of coal, although many other parameters have also been used. In Australian experience, all extensively mined seams with $R_0 \geq 1.10$ have been outburst prone. There have been no coal outbursts recorded with $R_0 \leq 1.00$. The rank of coal may also be correlated to the strength and the mechanical behavior of coal. The higher the vitrinite content, the more brittle the coal. The elastic properties of coal are quite different with the change of the coal rank. A high rank coal may also have higher sorption capacity for gas because the internal surface area of the coal is greater. The gas volume contained in the coal is larger because of greater adsorption and greater porosity.

The depth of mining has been considered as an important contributing factor to outbursts. It determines the stress level of the working area due to the superincumbent load and lateral confinement. It is generally accepted that the rank of coal increases with the depth following Hilts' Law (STACH, 1975). It has been found that 200 m is an adequate minimum limit for outbursts to occur unless some abnormal conditions arise. The frequency and violence of outbursts increases beyond this depth, but a few reports indicated the opposite conclusion (LAMA, 1968; NORRIS, 1958; KOWING, 1977).

When the depth further increases both occurrence and violence lessen. This relief may be due to the change of the characteristics of the rock. It is known that rocks become more ductile at a greater depth. It is this ductility which reduces the proneness to outburst and the violence after initiation.

Szirtes compared the frequency and intensity of outbursts at three different locations in Hungarian collieries. He found that the frequency and intensity were lowest at longwall faces, moderate in the drivage of headings in a seam and greatest in cross measure drift workings as a coal seam was approached. This finding seems to prevail worldwide. Hargraves examined the situation in Australian mines and found that outbursts were virtually absent in coal pillars. Pillars of dimensions up to 50m were often naturally drained of gas prior to extraction and were not outburst prone. Headings were generally the most prone place, with the dimension of the heading being related to the proneness. A small width of the heading tends to be more dangerous. The geometry of the heading may change the likelihood of outbursting. The overall geometry of the mining layout also seems having an effect on proneness. A working heading under the abutment pressure built up by adjacent workings tends to increase the proneness. After comparing the outbursts in advancing longwall panels, Szirtes found that the distance between the entry development and the longwall gate end is critical to control of outbursts. The frequency and intensity were lower when this distance was less than 5m or greater than 30m, and reach maximum at a value of 20 m.

The direction of the working is important in an outburst prone zone, especially in dipping seams. It has been reported that a dipping coal seam is more prone to burst than a flat seam. The rate of advance of the working place may increase the proneness to outburst. In USSR practice, Karagodin et al pointed out that the safe rate of advance varied between 0.5-1.0 meters per hour. The rheological properties of rock and coal are partially responsible for the delay; the gas flow in coal seam and the delaying effect of desorption are the other reasons.

Geological abnormalities may increase the risk of an outburst. Geological structures such as faults, sills, dykes and cleats have all been considered as factors influencing outbursts. Shepherd (SHEPHERD et al, 1981) has made a study of Australian outbursts and statistically related them to different geological structures. In the southern coal field of N. S. W., outbursts have been associated with disturbed or soft coal, dykes and faults. Two fatal outbursts in 1925 and in 1954 occurred in the vicinity of the faults. It was recorded high outburst frequency in road ways not necessarily on a fault, but where a normal fault terminated. At West Cliff colliery, the outbursts only occurred in the vicinity of strike-slip faults; normal faults in the area were not outburst prone. Outbursts

at Corrimal colliery were associated with a small dyke, lenses of 'sooty' coal at the roof and vertical planes containing a 100-450 mm thick 'sooty' band within a zone of crushed coal. In the Bowen basin of Queensland, all outbursts happened on faults which are characterized by thrust as well as strike-slip and normal faults. A severe outburst (400 tons of coal and an even greater tonnage of rock) occurred at the intersection of a thrust and a normal fault with vertical displacements of 3.6m and 0.7-1.4m respectively.

Ujihira and Hashimoto (UJIHIRA, 1976) investigated outbursts in the Ishikani coal field, Japan, and related them to three major geological factors: the presence of faults, the number of seams in a specific vertical section and the number of thick seams present. They also identified a large number of faults associated with outbursts. Cis et al (CIS, 1964) defined the outbursts in the Welbrzych coal field, Poland, as 'zonal' or 'dispersed' and 'compact' types. They related the 'zonal' or 'dispersed' type to geological structures, but not the 'compact' outbursts. Wilson (WILSON, 1931) and Stutzer (STUTZER, 1936) sketched an outburst cavity map for those outbursts in coal mines; it indicated that minor structures might determine the outburst cavity size and shape. Observations in Belgium and France suggested that they might occur in the region close to the hinge zones of reclined or recumbent folds and along faults, especially thrusts. Patching (PATCHING, 1966) found that outbursts in Canmore field in Canada were usually associated with structural abnormalities, while Hargraves (HARGRAVES, 1959) reported two outbursts in the same coal field related to some roof packers, probably a minor fold and a fault of unspecified type. The outbursts in the Nanaimo area were related to deformed coal pinched by rolls, coal ply structure, folding and crushed coals. Outbursts in the #26 colliery, Nova Scotia, have been closely associated with sandstone channels in the roof overlying the coal seam.

Coal micro-structure has been investigated to find its relationship to the outbursts. The pioneer work was done by Farmer and Pooley (FARMER, 1967). After they closely examined the anthracites of the Gwendraeth Valley in west Wales, U.K., they found that a basic molecular structure of anthracite comprises a condensed aromatic ring formation, a number of condensed molecules forming a basic structural unit. The outburst coal is interspersed with thin layers of clay mineral, dividing the anthracite into discrete particles. Each particle related the structural form of the anthracite unit and ranges in size from 1 μ to 30 μ . The thin layer of clay and the weak inter-molecular bonding facilitate the breakage of coal when subject to stress change. Dynamic failure along the boundaries creates a void into which gas is released and which mobilizes to pulverize the coal. The disintegration of coal can be accelerated by continuing desorption of gas and be moved by the energy released from pressurized gas. This micro-mechanism has also been examined

by Wu Jun at Fushun Research Branch, Central Coal Mining Research Institute in P.R.C. (Wu, 1987). By using a MPV-compact microscope and JSM-35c SEM, Wu studied the outburst prone coal from Huainan and Beipiao coal fields and found some micro-markers. The outburst coal possesses a random distribution of macerals with notable disturbances in the original sedimentation. A variety of micro-fractures, micro-fissures and other micro-structures were identified in this study. He also found the thin clay layers in the coal. He concluded that the origin of outburst prone coal is closely related to the matrix of coal and depositional geology.

As discussed above, many factors have been considered to be contributors to outbursts. To the author, there exists one key question why almost all control methods, despite all these influencing factors, in mechanism fall into the two categories of either reducing the gas pressure and/or decreasing the insitu stress levels. By continuing to explore this question, it is believed probable that a more reasonable explanation is that the gas pressure and the insitu stress field together with the strength characteristics are the primary factors to cause the outbursts. The other factors discussed before are considered as the physical or the chemical "additives" to these three primary factors. With the action of these secondary factors, the gas pressure or the stress field in the area become more sensitive to initiate an outburst through the increased magnitude or the altered directions. If this is so, the influence of stress, gas and strength properties on the outbursts should be carefully examined in order to fully understand these primary factors.

3.1.2. Stresses

Most outbursts occur beyond some critical depth, and in the blind ends of development roadways driving into solid coal. High stress concentration around the end can be easily formed under these conditions. The role of the stress conditions must be evaluated to understand the outburst mechanism.

In the mining environment, the insitu stresses are composed of the original field stresses and the mining induced stresses. The field stresses are related to the gravity and the tectonic activities. The weight of the overburden will build up the vertical stress which is usually one of the three principal stresses. This suggests that the depth of the seam becomes one of the influencing factors. If geological disturbances have been significant in the area, the vertical stress may be determined not only by the overburden but also by structural anomalies. In some instances, the vertical stress may become twice as high as that due to gravity alone, while in other instances it may be less. The geological conditions in the area must be incorporated when considering this field stress component.

component. The horizontal stresses in the field may result from the Poisson's lateral effect in the most ideal conditions. However, usually they depend more on the tectonic activities and geological features in the area. The horizontal stresses may easily become greater than that caused only by Poisson's effect. The geological structures can also lead to significantly different horizontal stresses; they must be taken into account when evaluating the field stresses. The presence of faults indicates that the region has undergone major tectonic activity which, in turn, indicate the disturbance of field stresses. The faults can act as a stress "filter" which will transmit compressive stress, change the shear stress magnitude according to the friction properties of the fault plane and be unable to transmit any tensile stress. The best evidence of the influence of faults on the adjacent stress state is the two studies in the Colorado School of Mines' experimental mine (SHEPHERD, 1981). After an entry was driven towards and through a low angle normal fault, they measured the stress change on either side of the fault. It was found that the compressive stresses in the foot wall were three times higher than the stresses in the hanging wall. In another experiment, the geological structures, gneissic foliation in this particular study, controlled the orientation of the insitu stress field and the magnitude of stresses. Therefore the geological factors which have been discussed in the previous section are intrinsically the causes for different field stress distributions and stress states.

Mining activity relieves the lateral constraints on the adjacent rock mass, leading to a redistribution of the original stress field. The stress state around a mining excavation can be altered both in terms of magnitude and direction. Some studies have revealed that mining activities may trigger the release of stored tectonic strain energy, so that the field stresses are distorted in that area. This changed stress is called mining induced stress. It is this stress change that brings forth various forms of failure of rock, which have been under mechanical equilibrium in the original stress field. The mining induced stresses are directly induced by mining activities. The geometry, size and direction of excavation, depth, overall layout of the mine plan and the excavation rate have been considered as the key factors. The abutment pressure built up by mining activity is one prominent example of mining induced stresses. Many outbursts have been reported occurring in abutments. The effect of gravity in seams with different inclination varies according to the friction characteristics of the seam interface. This may be why the rise side of a dipping seam was more prone to outbursts; mining to the rise is sometimes prohibited because of this, and also assist in the expulsion of fragments.

3.1.3. Gas pressure

By definition gas has to be accounted for when considering outbursts, although many other violent failures may not involve a gas component, as previously discussed in section 2.1. In past investigations, the gas content and chemical properties have been addressed, while in most cases of outbursts, the gas pressure has not been seriously considered as a major factor. Little, and inaccurate, gas pressure data can be found in the literature. Very few serious gas pressure measurements have been made, even in the most outburst prone mines. This situation may be caused either by the difficulties involved in the measurement or the lack of recognition of the importance of the gas pressure in outbursts. In the author's opinion, the gas pressure should be treated very carefully and be considered a prime factor in outburst problems. Gas pressure measurement techniques have to be adopted in those high outburst prone mines to establish a more complete and reliable data base for research.

The important role of gas pressure in an outburst process can be understood in two aspects. Firstly, it acts as an additional stress component in tension in the host rock/coal which contains the gas before the initiation of the outburst. The gas pressure acting in the host rock/coal is analogous to the water acting in soil. The effective stress concept can be adopted to describe its mechanical effects. Failure of the rock/coal only takes place under the combined action of the original field stresses and the gas pressure forces. Secondly, it acts as a motive force to accelerate the detached rock/coal and transport it. When the gas is compressed from the atmospheric pressure to a higher pressure, it will store a large amount of energy. This potential energy will be released when the gas expands. For the ideal gas it requires 3.9×10^5 J of energy to compress 1 m^3 gas at 1 atm. (approx. 1 MPa) to 50 atm. (approx. 5.0 MPa). If a seam contains 13 m^3 of gas per ton of coal, at 50 atm. (5.0 MPa) it will potentially release 5.1×10^6 J of energy per ton of coal, which is sufficient to move considerable volumes of coal upon rapid release.

There is still some uncertainty about the role of sorbed gas in the coal seam for an outburst, although it has been widely accepted that the desorbed gas will cause a more severe outburst. However, whether the sorbed gas desorbs as a result of an outburst or is the cause of an outburst is still an arguable question. The representative theory that supports the "cause" argument has been proposed by Litwiniszyn (LITWINISZYN, 1986). In his theory, the outbursts are considered as the result of the adsorbed gas changing its physical state from the liquid phase to the free gas phase. In addition, many people (ETTINGER, 1957) believe that adsorbed gas can reduce the strength of coal, and thereby, facilitate the failure of the coal mass. Ates (ATES, 1987) conducted a series of

experiments on Canadian coal and an Australian coal in order to investigate this assumption. The results of these experiments showed that no significant strength reduction was obtained for either coal. In the author's opinion, the following explanation for the role of adsorbed gas may be more conceivable.

The desorption of the adsorbed gas in coal seam starts after the initiation of an outburst. Because of the breakage of intact coal during outbursting, the gas pressure in micro-voids and cracks drops abruptly, disturbing the original physical-chemical equilibrium of the gas in these confined spaces. This disturbance creates the condition for desorption and if the desorption rate is higher than the space expansion rate, the desorbed gas will exert forces on the coal solid and break it further or accelerate the detached coal. In this condition, the sorbed gas will be an additional factor for the outburst sequence. On the other hand, the desorbed gas may not worsen the process but merely increase the amount of gas emitted into the workings. During the process of the gas expansion, it will adsorb the heat from the surrounding environment, causing a temperature drop. The decrease of the temperature in outburst workings has been observed in many instances (LITWINISZYN, 1986). Therefore, the role of sorbed gas is primarily passive initially but becomes active later in the process. This explanation tends to clarify the influence of the sorbed gas in coal and its role in the mechanism.

3.1.4. Mechanical properties

If we accept that the outbursts are only a mechanical phenomenon, the mechanical properties will have to be accounted for in the proneness to outburst. The strength properties will control the condition for failure, the constitutive relationship of the rock/coal mass will govern the stress redistribution after a mining operation disturbs the original equilibrium. Studies show that the coal usually has relatively low elastic modulus and high Poisson's ratio. However, when confined in the field, it can sustain very high stresses. When the lateral confinement is released, the coal can easily be stressed to failure to initiate an outburst. Pomeroy (POMEROY, 1956) studied the creep behavior of anthracite and revealed that it exhibited little or no creep. He concluded that the lack of creep might result in the breaking strength of anthracite being more readily exceeded, so that the proneness to outburst increases. The vitrinite content will determine the brittleness of the coal; brittle coal is more prone to outburst, according to his report. Outbursts usually take place in the weaker coal, so the low strength coal may be more prone than the high strength coal. The coal rank has been associated with the proneness of the seam, so does the strength of the coal. The fact that the coal has been stressed to

failure when an outburst occurs can be proved by the microscopic examination of the outburst coal. Such examination reveals various fracture modes such as network fracture, wall fracture, wave fracture etc., which indicates clearly the rupture of the coal in an outburst.

3.2 Mechanisms and Theories

Mechanisms and theories to explain the initiation of an outburst have been studied extensively by many researchers around the world. Over about one century, a total of 114 theories and hypotheses have been proposed and subjected to a critical analysis, according to the statistics made by Pieczuk in 1969, cited in Cyrul's paper (CYRUL, 1992). Since that time, a number of new theories and models have been published such as those of Barron, Paterson, Litwiniszyn, etc.. Because of the complex character of the outbursts, the theories, the hypotheses and the models tend either to describe one aspect or one phase of the outburst process, or to formulate very complex unusable solutions which are mainly qualitative in nature. Reviewing the past literature, the dominant causes for the outbursts have been reported differently, depending on the experiences of the researcher. In general, gas dominant, stress dominant, gas and stress combination, and geological structure dominant theories can be identified clearly.

3.2.1. Gas dominant theories

There have been a number of models which attribute the main cause of outburst to the gas content in rock/coal. Although the stress effect may also be taken into the consideration, it only makes a secondary contribution to initiation of outbursts. In the model it will not actually be used in calculation and analysis.

The most representative model is that proposed by L. Paterson. In his outburst model, he pointed out that there exist body forces in the coal equal to the pressure gradient of the flowing gas when gas is released from coal. He basically assumes that these body forces cause the structural failure of coal when they exceed the coal strength. Based on this assumption, a gas flow description and the strength of the coal have been derived and solved to result in a crescent shape of tensile failure region which represents the cavity created by the outbursts. The key concept of the model is the gas pressure gradient. The body forces are derived directly from this gradient, which initiates the outburst. The effect of a pre-existing stress field due to overburden may also be incorporated in the model, but has not yet been done successfully.

From the observations, Khristianovich and Salyanik (KHRISTIANOVICH, 1983) draw the conclusion that sudden outbursts were caused by the presence of free gas in coal. Their study revealed that the outbursts could not initiate without free gas. Based on this discovery, they advanced another theory for outbursts. They assumed that upon destressing in the direction of excavation face, a swarm of penny shaped cracks would form at some distance inside of the host coal with a thick zone of yield coal left in front. The free gas would then fill the penny shaped cracks and exert some tension forces on the inside surfaces. The resultant force from all the cracks tends to propel the yielded wall outwards; an outburst will initiate if this force can overcome the resistance. Being supported by this model, Khristianovich and Salyanik concluded that the free gas played the decisive role in an outburst.

Gray (GRAY, 1980) calculated the potential energy released from the gas and the strain energy released from the coal mass during outbursting, respectively. He found that the coal strain energy is much smaller than the gas potential energy in ideal conditions. Although the estimation could not be very accurate in absolute terms, the results highlighted the relative significance of gas versus the coal mass in connection with outbursts. According to his calculations, it is obvious that the outbursts should be a predominantly gas caused phenomenon.

The gas dominant doctrine does not exclude the effect of field stresses. As in both the Paterson and Khristianovich models, the contribution of the field stresses is also mentioned. Paterson has attempted to incorporate the pre-existing stresses due to the overburden in his simulation. Khristianovich did not calculate the influence of field stresses in his model, but he addressed destressing as a prerequisite for the model.

3.2.2. Stress dominant theories

In contrast to the gas dominant theories, some researchers emphasized the effect of field stresses. They attributed an outburst to a predominantly stress related phenomenon. They believed that it was the field stresses, or more precisely, the stress changes due to mining activity which disintegrated the rock/coal around the exposed working face. The release of the strain energy stored in gas and rock/coal impelled the broken rock/coal into the workings to initiate the outbursts.

Revalor et al (REVALOR, 1985) have assumed that the breakage of rock/coal in outbursts is caused by the insitu mechanical stresses; the free gas contained in sandstone and the decrease of their mechanical strength are aggravating factors. This hypothesis has been based on their observations of the breakage modes of rock among the rock outbursts

in the Lorrain collieries in France. According to this assumption, they measured the virgin stress states in situ by use of flat jacks, overcoring and hydro-fracturing methods. The in-situ measurement showed that the major and minor principle stresses lay in the horizontal plane and the intermediate principle stress was vertical. After analysis of measurements, they believed that the rock outbursts were caused by mechanical stresses (mainly tensile stresses) in a direct relation to the sudden release of confinement due to blasting. This state of stress was aggravated by gas contained in the rock, permitting the propagation of the breakage. The situation may also be aggravated by local conditions because of local heterogeneity.

3.2.3. Gas and stress combination doctrine

The majority of past researchers have tried to explain outbursts as a phenomenon of the gas and stress in combined action. Among the theories, Khoroshun, Hiramatsu, and Kullman and Barron's model are the most representative. Khoroshun assumed that the outburst medium is a gas-bearing massif with a solid skeleton of rock/coal. In this study, he derived equations describing the coupled processes of deformation of a gas-bearing porous medium and of gas filtration, with the coefficients in these equations defined as functions of mechanical solid and gaseous phases as well as the geometrical parameters of the structure. Hiramatsu analyzed the fracturing features of the penny shaped minute pores filled with pressurized gas under the stresses of σ_1 , σ_2 and σ_3 , and found the conditions under which compressive and tensile fracture would take place. It was believed that these conditions were necessary and sufficient to initiate an outburst. Kullman, has developed a numerical model using the boundary element method, to couple stresses and gas pressure to simulate an outburst. The model calculated the stress state of the rock mass due to the mining excavation by directly superimposing gas pressure on the original stresses (the stress distribution was obtained by only considering the field stresses). An iterative spalling mechanism was assumed and a numerical solution was obtained. In these models, the key point they all assumed was that the failure of the rock mass was due to the combined effects of field stresses and gas pressure, i.e. effective stresses, rather than due to only one of them, as assumed in gas or stress dominant theories. They are, therefore, intuitively more comprehensive. Further discussion of these models will be found in the next chapter.

3.2.4. Geological structure theories

A notable theory of outbursts is the one proposed by Shepherd (SHEPHERD, 1980). In his publications, he reviewed the role of geological structures in connection with the coal and gas outbursts and concluded that the majority of Australian outbursts occurrences were located at sites in or adjacent to a coal seam where at least one of the important factors was the pre-mining geological structure. Therefore, he tried to associate the initiation of an outburst to the particular types of geological structure. Unfortunately, his effort has not brought much success. His research only substantiates that the geological structure can be an important factor in outbursts, and no practically applicable prediction can be based on the results.

3.2.5. Summary

Among the four doctrines, the gas dominant, stress dominant and geological structure theories have put undue emphasis on one aspect of the problem. The gas dominant doctrine lays emphasis on the gas pressure, while stress doctrine considers only the contribution of field stresses. The geological structure doctrine has only superficially addressed the phenomenon of the outbursts. The gas and stress combination doctrine has taken account of two key factors for outbursts. It gives a more comprehensive and reasonable explanation of the outburst mechanism. Unfortunately, the models based on this doctrine all possess one or other weakness, which has devalued the use of the models to solve the problem. However, as a doctrine to elucidate the mechanism, the gas and stress combination theories are more acceptable.

3.3. Analysis Methods

The analytical methods used to consider the outburst problem have developed along with the development of the mining industry. After careful historic review, three stages may be clearly identified, although they may not be strictly demarcated from each other. An approximate outline for each stage could be distinguished on the basis of the time.

3.3.1. Descriptive and experimental stage

In the early days of the development prior to the 1960's, people only recorded the outburst phenomenon from the description of the survivors who had to recall the accident after undergoing the psychological shock. Some of the descriptions were superstitious. Most of the reports at this stage described the visible and/or audible impression of the events. Even in the more academic publications, the scholars could only summarize the descriptions and make a few intuitive deductions. The milestone for this stage was the specialized conferences held in 1964 and in 1966.

During this period a number of practical techniques were developed to prevent, or at least minimise, the occurrence of outbursts. These techniques included volley blasting, controlled inducing of outbursts by shot firing, gas drainage, hydro-fracturing, water infusion and stress relief hole drilling. These technologies met with mixed success in different regions.

3.3.2. Qualitative and quantitative stage

In the 1970's and early 80's, as more and more events occurred around the world, people in industry put more effort into the investigations and the problem also attracted much professional interest. Base on the accumulated knowledge from the first stage and on up-dated information, experts attempted to standardize the procedures for prediction and prevention of outbursts. Some qualitative and quantitative measures had come to light. In Europe, several indexes (such as the Δp index) were further refined to identify the seams which were outburst prone. Mathematical relations were established to define the relation between coal physical and mechanical factors and outbursts. Some laboratory experiments were conducted with the intention of defining a more realistic mechanism to explain the phenomenon. Most theories and models developed in this period form the basis of the models used today.

The technologies for control and prevention, first invented in the late 1950's and 1960's were further refined and were still in use. The combating of outbursts at this stage was more controlled and guided by research results. The intensity and violence of events in this period were greater due to deeper mining operations, but the toll of victims was reduced because of the progress.

3.3.3. Numerical computer aided analysis

With the introduction of computer technology to the world, numerical computations have become a more and more powerful tool for engineering usage. Nowadays, the ability of computer to solve geotechnical problems is gaining wide acknowledgment. In the early 80's, Paterson applied this modern technology to the outburst problem. Later, Kullman introduced another outburst model to the world. If outbursts are a mechanically related problem, then computer modeling should provide a sound approach to tackle the problem.

Chapter IV

MODELING OF OUTBURSTS

Outburst modeling has always been considered a useful potential tool to achieve the objectives of understanding the mechanisms and for predicting outbursts. A model must be established on the basis of understanding the mechanism. On the other hand, results from the model can be checked to verify whether the mechanism has been correctly interpreted. A fundamentally sound model will predict an outburst efficiently. In the past literature a number of models have been proposed, but there has been a considerable dispute between them. However, the value of modeling seems to have been widely agreed and accepted.

4.1. Purposes of Outburst Modeling

An ideal outburst model must have the capability to account for the initiation mechanism and the ejection/transport phases (FARMER, 1967); the transient effects, namely, the audible and the micro seismic noise, the instability of the face and the temperature decrease (SHEPHERD, 1981); the gas pressure gradient, the stress distribution and the failure criterion (PATERSON, 1986); and finally, the mechanism whereby an outburst ceases (BARRON, 1990). In the literature, however, most models proposed have only taken into account some of the above aspects, because it is difficult to handle all these factors mathematically.

4.2. Models Proposed in the Literature

The outburst modeling is usually divided in two main domains, with one considering a rock outburst and the other for a coal outburst. This classification is naturally based on the material for which the model was developed. In order to clearly understand the mechanism on which models have been based, they can also be divided into energy balance and mechanical failure models (SHEPHERD, 1981). This latter classification is used to organize this discussion for the clarification of the pertinent mechanism.

4.2.1. Energy balance models

This set of models have been proposed and developed according to the balance analysis between the energy stored in rock and gas before an outburst occurs and the energy released during the outburst. In general, if the energy stored in the undisturbed system is large enough to overcome the energy required for breaking solid material and transporting the broken material a certain distance, an outburst may happen provided that an appropriate triggering mechanism is invoked.

Karagodin's Model (KARAGODIN, 1983):

Through complex analytical studies and laboratory research on rock outbursts in the mines of the Donbass Basin, USSR, Karagodin defined an outburst as a process of self-sustaining fracturing of a gas-saturated rock mass. He suggested an energy condition for the occurrence of an outburst. The condition was determined by the ratio between the quantity of potential energy stored by the elastic deformation of the rock mass, which was released by the mechanical fracturing process, and the amount of the work put into breaking it.

The potential energy of the elastic deformation (u) has been found as a function of the stress state, for example, the vertical stress (γH), the elasticity (ν, E) and rheological properties of rock (χ, β) and time (t) by Zorin (ZORIN, 1978) as follows:

$$u = \frac{(\gamma H)^2}{2E_0} A - \frac{(\gamma H)^2}{2E_0} \left\{ \frac{N}{\beta_1} \left[1 - e^{-\frac{t^{1-a}}{\tau^{1-a}}} \right] + \frac{B}{\beta - k_1} \left[1 - e^{-\frac{t^{1-a}}{\tau^{1-a}} \gamma^{(1-b)}} \right] - \frac{M}{\beta_1 - k_1} \left[1 - e^{-\frac{t^{1-a}}{\tau^{1-a}} (1-a)} \right] \right\} \quad (4.1)$$

where,

$$\beta_1 = \frac{1}{\tau^{1-a}}; \quad k_1 = \frac{a}{\tau^{1-a}}; \quad a = \frac{E_0 - E_\infty}{E}; \quad b = \frac{a(1-2\nu_0)}{2(1-\nu_0)}. \quad (4.2)$$

while,

E_∞ is the stable modulus of elasticity;

τ is the relaxation time;

A, B, N, M are constants expressed through the elastic and rheological parameters.

By analyzing the above formula, Karagodin realized that the occurrence of an outburst was directly related to the rheological property of rock. He suggested that with 'instant' rock breakage (e.g. blasting, $t \rightarrow 0$) and high elastic properties of the rock, the potential energy of elastic deformation of the rock mass released will be at a maximum while, with an increase in time ($t \rightarrow \infty$), the specific potential energy decreases through relaxation of stresses governed by the rheological properties of the rocks. If a rock outburst is to initiate, the rate of fracturing of the rock mass should be such that the specific potential energy of elastic deformation of the rock mass released should exceed the amount of work put into fracturing the rock. Clearly, the mathematical interpretation of this statement should be as:

$$u > W_f$$

where W_f is the work put into fracturing the rock. This inequality provided a quantitative evaluation for the rock outburst occurrence, i.e., if $u > W_f$, a rock outburst is likely to occur. According to the principles derived from this model, the drill and blast method was changed to a rotary tunneling machine to slow down the rate of rock breakage in the Donbass mine and it has succeeded in stopping rock outbursts. However, care must be taken when considering a change from drill and blast methods to tunnel boring. Drill and blast methods tend to trigger outbursts at a time when no miners are present, while tunnel boring, although theoretically safer, could be more dangerous in practice because miners are present throughout the operation.

Although this model has been proven effective as a guide to prevention of rock outbursts in the Donbass mines, it can not be seen as a practical model. The most important weakness of this model is that the gas energy has not been considered, even though Karagodin did realize the influence of gas impregnated in the sandstone. The parameters in the elastic deformation energy equation (4.1.) are difficult to define in practice. Consequently it is unlikely to apply the expression even as a qualitative index.

Litwiniszyn's Model (LITWINISZYN, 1985):

This model assumes that the potential outburst material consists of a solid skeleton and a system of pores with different topology, dimensions and geometry. The large sized pores are filled with gas, for example, methane; while the gas inside the small size pores undergoes capillary condensation to form the liquid phase. Therefore, the

potential outburst material is comprised of a solid, liquid and gas, and is a three phase medium.

When considering a sudden outburst in such a medium, Litwiniszyn makes a postulation that there exists an interface which separates the undisturbed three phase medium from the debris and large volume of gas resulting from an outburst. This interface continuously moves into the three phase medium at a rapid speed, resembling a shock wave front. By analyzing the conservation conditions of the mass, energy and momentum before and behind this interface, Litwiniszyn deduces a quasi-linear system of hyperbolic differential equations for the stress, velocity and mass. In one dimension, these equations have been solved by incorporating proper boundary and initial conditions. The solution indicated the formation of a shock wave with a "catastrophic gradient". This shock wave, however, must be a rarefaction shock wave in order to result in an outburst. Research has shown that in a medium with negative second derivatives of the isoentropes only the rarefaction shock wave occurs. Litwiniszyn realized that this condition applied to an outburst, during which a phase transformation is taking place.

It is concluded, therefore, that a rarefaction shock wave can occur in the assumed three phase medium. Within the region of such a shock wave, a "jump-like" or "step" change in the state of the stress occurs. If the interval of the stress in which the phase transformation of the medium takes place is contained within the interval of the jump-like change of stress of the shock wave, a phase transformation occurs in the medium. In a rarefaction shock wave, the skeleton of the medium is destroyed and an outburst is initiated.

This model has discussed the process of an outburst with strictly logical deduction and strong mathematical support. It provides a theory for understanding the mechanism of a rock and a hard coal outburst. The complex mathematical formulations of the problem tend to obscure the clarification of mechanism involved in an outburst. It may present a perplexing challenge to solve the equations in higher dimensions. The model has been questioned and considered inappropriate by Paterson (PATERSON, 1986). He argues that although the model is based on outburst occurring in salt and metalliferous mines, it does not explain how the three phases can be formed as gas does not exist in an adsorbed state in these materials. The origin of the shock waves have not been considered, nor has the rapid attenuation of shock waves in coal. Furthermore, the difference between an adsorbed liquid like layer and liquid state should be distinguished.

Litwiniszyn's model poses an interesting and original concept for the outburst mechanism. However, in its present form it is hardly usable, since the mathematical function has an extremely complex form and has only been applied in a one-dimensional

problem. In the author's opinion, further development of the approach is likely to be particularly difficult and unrewarding.

4.2.2. Mechanical failure models

Mechanical failure models have been proposed on the basis of analyzing the condition of in situ stresses and gas pressure and incorporating some failure criteria under the given conditions. One of the most important advantages of these models is their straightforward mechanical concepts and the simple mathematical processes involved in the models. With continuous effort put into these models, it is likely to produce more realistic and applicable model to meet the needs of the industrial applications.

Gray's Model (GRAY, 1980):

Gray has investigated the outburst phenomenon in Australian mines. Based on these studies, he has given a theoretically possible initiation condition and suggested a subsequent propagation mechanism. He believes that an outburst is the failure of coal and the ejection of the failed coal by stored potential energy which is converted to the kinetic form and is associated with release of the seam gas.

Two exclusively gas induced coal failure mechanisms have been identified from his investigations, they are the tensile failure of unconfined coal and the "piping" effect of sheared material. The tensile failure occurs when gas pressure exceeds the tensile strength of solid coal. This mechanism is usually controlled by structural weakness in the coal mass. When sufficient drainage paths have been opened and the gas pressures have dropped, the failure ceases. The piping failure mechanism is appropriately applied to mylonite zones which have the soil type structures. This failure is fundamentally analogous to tensile failure, but rather than controlled by structural weakness, it excavates its own openings as the gas flows into the new cavity.

These are two extreme situations in practice. In more general cases, however, gas pressure and in situ stress are combined to act as a whole. From the effective stress concept, Gray suggests a failure criterion and points out that the pore pressure may decrease the shear strength of the coal because the gas pressure offsets a part of the normal stress in the Mohr-Coulomb strength expression improved by Skempton. According to Gray's viewpoint, when gas pressure exceeds the normal in situ stress, tensile failure may then take place instead of shearing.

After the failure is initiated, by whichever of the mechanisms above, the severity of the outbursts is directly related to the energy released from both compressed gas and the coal/rock stored strain energy. This release of the potential energy accelerates particles of coal or rock. The surrounding rock mass may be accelerated, too. The release is realized by either adiabatic or isothermal expansion according to the speed of desorption of adsorbed gas. In both conditions, the amount of the energy may be calculated theoretically, if the necessary parameters are given.

With the proposed theory, an endeavor has been made to calculate both gas strain energy and coal strain energy for the outbursts in Bowen No. 2 mine and Leichardt Colliery in Australia by Gray. In absolute terms, the estimates are not very accurate, but the calculations highlight the relative importance of the gas and coal/rock contributions for the occurrence of an outburst. The results substantiate the leading role of gas pressure. It suggests that degassing can alleviate the severity of an outburst very effectively. This conclusion has been proved by the practices in Leichardt Colliery.

One of the most valuable aspects of this model is the great effort contributed to the quantitative calculation of gas and coal/rock energy release during an outburst. According to Gray's calculation, the total gas strain energy released for Leichardt Colliery's December 1, 1978, outburst is 219 (MJ), which is well beyond the estimated actual coal/rock strain energy releases of magnitude 20-30 (MJ).

However, the method to calculate the kinematic energy required to eject broken materials has not been given in the model. This leaves the energy criterion undefined, as a matter of fact, this calculation could be very difficult unless significant simplifications are incorporated. This reason causes the model to be less applicable from a quantitative point of view. The gas expansion process involved in gas energy release is very difficult to predict before an outburst occurs. The choice between an adiabatic and an isothermal state, therefore, becomes uncertain for the prediction. The mechanism by which an outburst ceases has not been properly addressed in the model.

Hiramatsu's Model (HIRAMATSU, 1983):

By investigating the mechanism of coal outbursts occurring in Japanese coal mines, Hiramatsu et al. proposes a model for the coal outburst. It is found that the phenomenon of an outburst can be explained by assuming mechanical failure of the coal mass under the combined action of rock stress and gas pressure.

The model postulates that penny shaped pores are distributed randomly in the coal mass. A very high gas pressure exerts a force on the inner surfaces of the pores. It is

assumed that this internal force, combined with the insitu stresses, fractures the tip of the pores. This causes the initiation of an outburst. According to the model, the tip of the pores can be fractured both by compression and tension. Different criteria are produced by applying the extension of the Griffith's fracture theory to a penny shaped pores in three dimensions, and incorporating internal gas pressure developed by Mizuta (HIRAMATSU, 1983). It is argued that the presence of high gas pressure in the pores is essential to the initiation of an outburst; with low gas pressure, the outburst may not necessarily take place even if the concentrated stress around crack tip is higher than the strength of the coal mass.

By applying the model, some of the features of coal outburst are easy to explain, such as, outbursts are apt to occur in geologically disturbed areas, in poor and weak coal layers and in areas where gas extraction in advance of driving gate roads is insufficient. The large amount of finely crushed coal is considered being caused by the presence of high gas pressure. The pre-mining of one coal seam may prevent outbursts in other coal seams as the high gas pressure is partially drained.

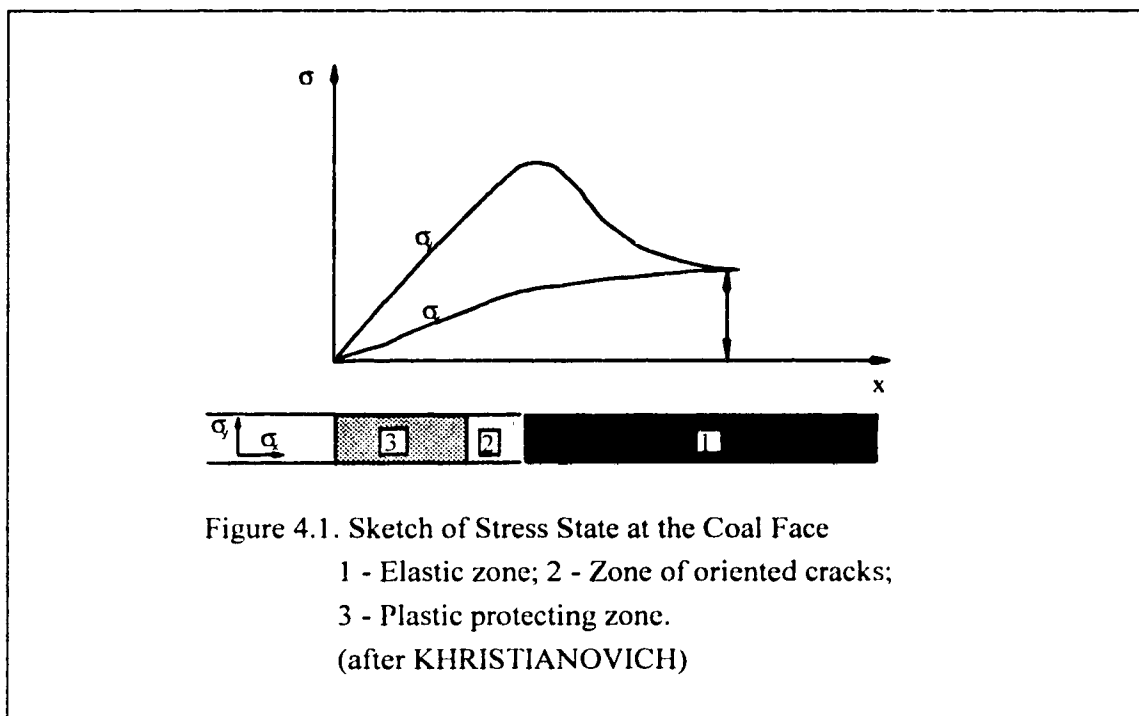
Although the authors have emphasized the vital role of gas pressure for the initiation of an outburst and indicated that high pressure is required to completely fracture the coal mass, they have only provided a quantitative criterion for fracturing penny shaped pores, leaving the evaluation of gas pressure in coal seam undetermined. High gas pressure only serves as a descriptive criterion, it is not applicable as a quantitative assessment. Moreover, Hoek (STAGG, 1979) has pointed out that, in compression conditions, the pore tip fracturing may be stabilized when the propagating cracks get oriented in the major principle stress direction. Therefore, the initiation of the fracturing does not necessarily indicate the failure of a material. This model, based only on the condition of whether or not a crack tip may start to fracture, does not give a very convincing explanation of the initiation of an outburst.

Kristianovich's Model (KHRISTIANOVICH, 1983):

The model assumes that the outburst potential material comprises many tiny penny shaped cracks filled with gas. The distribution of the cracks is sufficiently random and the intensity of the cracks is low enough so that they can be treated as isolated from each other.

In each crack, there exists a certain gas pressure, and this gas pressure is believed to be as high as the in-situ stress. The growth of a single gas-filled penny shaped crack (with constant gas content) has been investigated by Kovalenko (KOVALENKO, 1980).

It is shown that upon release of the confining stress in one direction, the original cracks may grow only if the cracks have a certain initial radius. The cracks will stabilize at a certain size. It is also found that the volume and cross sectional area will increase due to the release of confining stresses, but the gas pressure in the pore will decrease. The study has revealed the most significant fact that the differential modulus of elasticity (defined as the coefficient in differential relationship between stress and strain) in the direction orthogonal to the cracks will change. As cracks grow in the major principle stress direction, the modulus will drop suddenly. The compliance of this fractured material becomes intermediate between its original value in undisturbed state and that of the gas in the pore. The material then changes to a kind of anisotropic sponge with oriented cracks filled with pressurized gas. It is this sponge material that forms a layer acting as a piston on the restricting wall (formed by material in plastic state between free face and the sponge layer) parallel to cracks (ref. Fig. 4.1). If the force exerted by this "piston" is large enough to overcome the restricting resistance of the plastic layer, an outburst is initiated.



After the initiation of the outburst, it is a dynamic process in which spalling, crushing and fracturing waves are accompanied by an outburst wave. The spalling wave is induced when the elastic unloading (tension) wave is transmitted into the coal mass and

reflected to the free face from some reflector with almost doubled magnitude amplification of the stress level if the impedance matching is appropriate (from a low impedance material to a high one). The high tensile force formed spalls the coal from original coal body. A crushing wave starts propagating from the exposed surface by this spalling disturbance. In the crushing wave, a rapid dynamic stress relief creates very high stress gradient causing layer-by-layer breaking away and crushing coal into very fine particles, allowing complete evolution of the free gas. The crushing wave continuously transforms into the outburst wave in which the fractured coal is accelerated by compressed gas. When the gas in pores pushes the coal out, a fracturing wave starts to propagate in the split. The fracturing wave will engender a crushing wave and the alternating process of spalling coal and crushing can carry on to eject a large volume of crushed coal and gas until some mechanism arises which stops the process.

Khristianovich's model describes a mechanism of initiation of an outburst and the dynamic process during outburst. From the concept of the model, it is found that degassing the "sponge" layer is very effective for preventing an outburst.

Although some mathematical development is involved in the determination of characteristics of the model, it is unable to achieve a quantitative evaluation. The post initiation dynamic process is particularly qualitative, the calculation of the waves involved is impossible. No mechanism is discussed in the model to stop an outburst once it is initiated. For practical application, the model must be improved.

Khoroshun's model (KHOROSHUN, 1984):

This model assumes that an outburst near an underground mine excavation results from a loss of bearing capacity of rock mass under the mine pressure and the interstitial gas pressure. A chain reaction can continue once the process is started and develop into an outburst involving the creation of a large cavity in the vicinity of the excavation.

In this model, the key foundation is laid on the coupled equations pertaining to the mechanics of a saturated porous media. The theory of the saturated porous medium has been established by Khoroshun in 1976. The coupled process of deformation of a gas-saturated porous medium and of gas filtration can be described by the physical equilibrium, gas filtration equilibrium, material constitutive equation and Cauchy's strain-deformation definitions mathematically, as follows:

$$\sigma_{ij,i} + F_i^1 = 0 \quad (4.3)$$

$$P_{,ii} - F_i^2 = \frac{(a_1 \dot{P} + a_2 \dot{\epsilon}_{,rr})}{c_2 k} \quad (4.4)$$

$$\sigma_{ij} = \lambda_1^* \epsilon_{,rr} \delta_{ij} + 2\mu \epsilon_{ij}^* - \beta^* P \delta_{ij} \quad (4.5)$$

$$\epsilon_{ij} = \frac{(u_{i,j} + u_{j,i})}{2} \quad (4.6)$$

Where, σ_{ij} , ϵ_{ij} and u_i are macro-stresses, macro-strain and macro-displacements in the "skeleton-gas" system respectively; P is gas pressure in pores; F_i^1 is the body force acting on the "skeleton-gas" system; F_i^2 is the force acting on the gas from the skeleton. C_2 is the volume concentration of pores, k is the gas filtration coefficient and λ^* , μ^* , β^* , a_1 , a_2 are effective "skeleton-gas" system constants defined by the bulk shear modulus (compression), bulk compression modulus of gas and C_2 .

The stresses in solid phase σ_{ij}^1 are related to the macro-stresses and interstitial pressure as:

$$\sigma_{ij}^1 = \frac{\sigma_{ij}}{C_1} + \frac{C_2 P \delta_{ij}}{C_1} \quad (C_1 + C_2 = 1) \quad (4.7)$$

By solving the above equations under the proper boundary conditions, although it is very difficult and the most complex mathematics have to be used, the distributions of macro-stresses (σ_{ij}) and solid phase stresses (σ_{ij}^1) can be obtained. Khoroshun has solved two special boundaries - spherical and oblate ellipsoid excavations, and closed form solutions have been obtained.

On another hand, the model assumes that the strength of a gas-saturated rock mass is determined by the strength of its solid phase only. According to some other research, this strength should take the following formulation:

$$F \equiv \left(\frac{\sigma_{ij}^1}{\sigma_c^1}\right)^2 + \left[\left(\frac{1}{\sigma_t^1}\right)^2 - \left(\frac{1}{\sigma_c^1}\right)^2\right] (\sigma_{\max}^1)^2 = 1 \quad (4.8)$$

Where, σ_{\max}^1 is the maximum tensile stress in the solid phase, σ_c^1 is the compressive strength of the solid phase, σ_t^1 is the tensile strength of the solid phase.

Based on the above numerical calculations of the stress distribution and the solid phase strength around an underground opening, Khoroshun has explained the mechanism

of the ejection of coal and gas as follows: When the interstitial pressure is sufficiently high, at some distance from an opening where there exists a zone of tensile radial stress in the solid phase and the function F reaches the ultimate value, fracture of the solid skeleton and ejection of the inner layer of the rock mass will occur. As a result, this process forms a cavity, and the process will continue on the basis of this new established boundary. Thus a chain of fracture and ejection events happen with gas released from pores carrying fragments of solid phase into the void created.

This model has set up only the criterion to identify the initiation of an outburst, no numerical consideration has been given to transportation of the fractured rock. Therefore, the model may be suitable for application when gravity can clean the debris spalled from the host rock. In Khoroshun's research work, only two closed form solutions have been presented. Even these simple situations have invoked the most complex mathematical methods and very complicated functions have been used to express the stress distributions. The derivation of closed form solutions for any but the simplest shape of excavation poses an extreme mathematical problem. This suggests that a much better approach would be to solve such problem numerically using the finite element method. With the advantages of the finite element method, the problem may be solved much more easily and for more complex boundary conditions. Although a test calculation with the model has been done, the model still lacks the support from practical application, and the verification also presents a problem. Many parameters required in the calculation limit the practical application of the model due to the difficulty in measuring these parameters in the field.

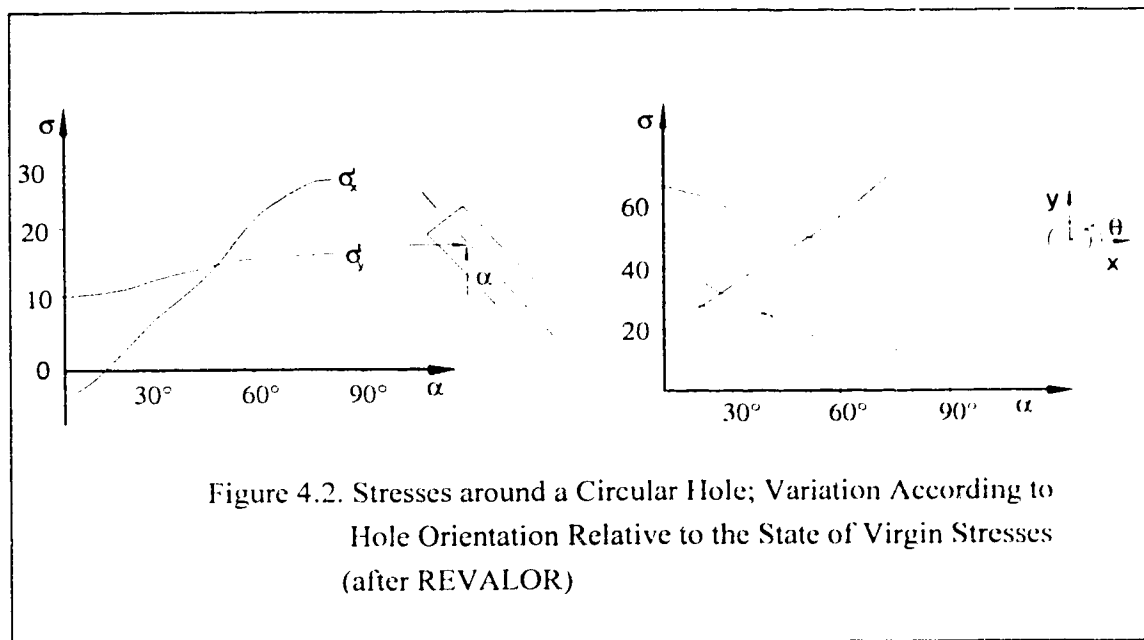
The basis for this model is much sounder than previous ones described. In the author's opinion, adapting the concepts to finite element solution might be a worthwhile development that could lead to a more practical model.

Revalor's model (REVALOR, 1985):

Based on the outburst experiences in the Vonters mine of the Lorraine collieries in North East France, Revalor et al made a hypothesis on the process of the breakage associated with an outburst that occurred in a conglomerate sandstone (slightly shaly). They believed that the outbursts occurring in the sandstone saturated with firedamp were caused by mechanical stress (i.e. tensile stresses) in direct relation to the sudden release of confinement brought by the blast. This state of stress was aggravated by the gas, permitting the propagation of the breakage. It might also be aggravated by local

conditions (higher natural stresses or gas pressure, lower strength of rock) due to local heterogeneity noted by the structural and the geological analysis.

According to Revalor et al, this hypothesis was substantiated by the calculations of the stress states around a circular gallery of 2.5 m radius. On the side of the gallery, Hiramatsu's solution (HIRAMATSU, 1968) was adopted for a section behind the face of drivage. For the central zone of the drivage face, the calculations similar to the Bonnechere's research work (BONNECHERE, 1971) were conducted to obtain an approximate solution. For different orientation of the gallery relative to the major principle stress, the two types of calculations were carried out by Revalor et al. The results showed that on the surface of the drivage face, tensile stresses with magnitude as high as -3.5 MPa could be developed in horizontal direction when the ratio of anisotropy of in situ stresses σ_1/σ_3 was greater than 1.8, while the gallery headed in a particular direction relative to the horizontal major principle stress (ref. Fig 4.2). These calculations were backed up by several field observations, according to Revalor et al.



Because of this, it was concluded that the orientation of the roadway relative to the in-situ principal stresses was most significant for the occurrence of an outburst and the outburst was initiated from the drivage face. As the tensile stress on the drivage face appeared as an axial stress tending to curve the face towards the void created by a blast, it

was believed that a concave face might suppress these tensile stresses. The violent failure nature of an outburst was attributed to the sudden establishment of these tensile stresses.

In this model, the tensile stress distribution and material anisotropic properties are addressed and taken into consideration numerically. The effect of the gas pressure has only been considered as an aggravating factor and has not been taken into account in numerical calculations. The model does not consider the transportation of the fragments and the mechanism for ceasing an outburst.

Paterson's model (PATERSON, 1985):

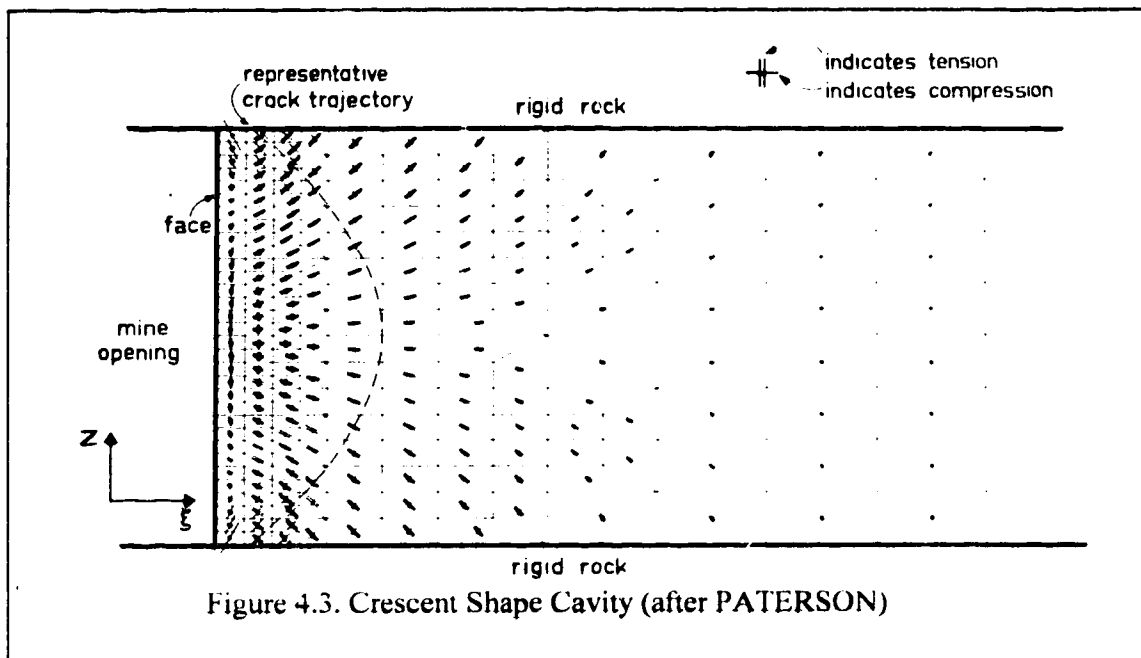
This is a theoretical model for gas and coal outburst in underground coal mines. The model can explain quantitatively why the factors such as high advance rate, low permeability, low strength (mylonite or fractured rock) or low joint strength, great depth and large pre-existing stresses tend to increase the occurrence of outbursts, although the field verification of the model is difficult in practice. Nevertheless, this research provides us with a first calculable model based on the simple field parameters.

The basic assumption of the model is that an outburst is the structural failure of coal due to excess stress resulting from body forces associated with the gas pressure gradients (similar to the seepage flow formed in a soil mass while water flows in it). When formulating the model, the flow of gas, the stress expression and the failure criterion have been considered one by one. If the simultaneous flow of gas and water is of concern, King and Ertakin's equations (KING, 1984) in the numerical simulation of degasification of coal seams can be used. By neglecting the pressure of water and assuming that Darcy's law holds the equation can be simplified. The stress state descriptions are usually formulated by the equilibrium conditions, providing that the gas pressure serves as a body force potential in the equations. The failure criterion adopted by the model is the Mohr-Coulomb function with a tensile cut-off. This is considered to be as good as any other failure descriptions at present due to a paucity of data on coal. For an outburst to happen, the tensile failure must be present and is the predominant failure mode.

With above theory about the model, a simple one dimension flow condition has been numerically solved for a longwall mining face between a rigid roof and floor by use of a non-linear finite element program. To simplify the problem, only the force resulting from gas gradients has been used as the body force. The results have predicted a crescent shape crack zone in which the tensile failure predominates. This crescent zone is believed to be the simulation of the cavity formed by an outburst (ref. Fig. 4.3). From a theoretical

point of view, the model has the potential to work in three dimension without further improvement.

This model gives a very useful mechanism, however, it is too general to be practical. The input parameters required for the calculation are so numerous, such as coal permeability k , coal density D , gas pore pressure p , gas viscosity μ and porosity of coal ϕ , and the back analysis has not been carried out due to lack of field data. In general terms, it can explain the effects of influencing parameters but to be of use, some simplifications must be made for a given situation, thus making it site specific.



Golder Associates Model (GOLDER, 1987):

Golder associates proposed a descriptive model mechanism in 1987. The essential contents for their model mechanism are listed below.

The change in stress state from triaxial to biaxial loading at the free face of an underground opening was considered to be the likely cause of tensile stresses leading to the initiation of rock fracture.

Blasting gives a rapid reduction in the confinement of the burst prone material. This, in turn, mobilizes a gas pressure gradient because the stress change due to blasting occurs more rapidly than dissipation of the gas pressure. Blasting may also superimpose tensile stresses on the static stress field.

Gas pressure also play a major role in the initiation of the outburst due to the effective stress effect. The intense fish scale fracturing in the cavity perimeter is evidence of breakage in tension along the stress trajectory around the outburst cavity.

The outburst terminates when (a) the cavity extends to a geological contact where non-outburst prone material is present; (b) an equilibrium stress condition is reached; (c) the outburst is choked by the debris creating a back pressure sufficient to stabilize the cavity.

This descriptive model is very similar to that proposed in this thesis, but they place more emphasis on the influence of the dynamic effects of blasting stresses. Unfortunately they made virtually no attempt to mathematically formulate the descriptive model.

Barron and Kullman's model (BARRON, 1991):

In this model, it is assumed that an outburst is the result of the failure of rock due to excessive pore fluid (gas) pressure. If the effective stresses calculated by superimposing gas pressure directly to the virgin *in-situ* stresses, exceeds the tensile strength of the rock, the rock shatters completely destroying its structure and the fragments are expelled away from the host rock by the energy contained in the high gas pressure. This results in the formation of a cavity, an excavation of greater size and new shape. If the gas pressure is insufficient to cause the tensile failure, but shear strength is exceeded, it is assumed that this rock remains in place but is now fractured. These fractures facilitate the gas escape from the rock, producing a gas pressure gradient in the sheared rock around the cavity.

A spalling mechanism has been assumed to simulate an outburst. As the failure criterion has been satisfied and the fracture and expelling process has been completed, the new cavity changes in size and the shape, in turn, altering the stress distribution around the opening. For this new shape cavity, the superimposition of gas pressure and failure criterion are applied again and the iteration can carry on until either a stable cavity (i.e. no tensile failure occurs) is formed or it become evident that the spalling process will carry on forever. These "instantaneous series of static events" are, therefore, simplified to an analogy with the dynamic destruction process experienced during an outburst.

A computer program, formed by a combination of two separate programs, has been edited to fulfill the model. The first program is a commercially available boundary element program which calculates the distribution of stresses around an opening with necessary material properties and boundary conditions. The second program is a post

processor for the first program which superimposes the gas pressure directly on the resultant stress distribution and judges the stability of the opening according to the previous calculations. The identified tensile failed rock is expelled and the sheared rock remains in place with no gas pressure contained. The new cavity shape, then, becomes the new input for the first program and the iteration carries on (ref. Fig. 4.4).

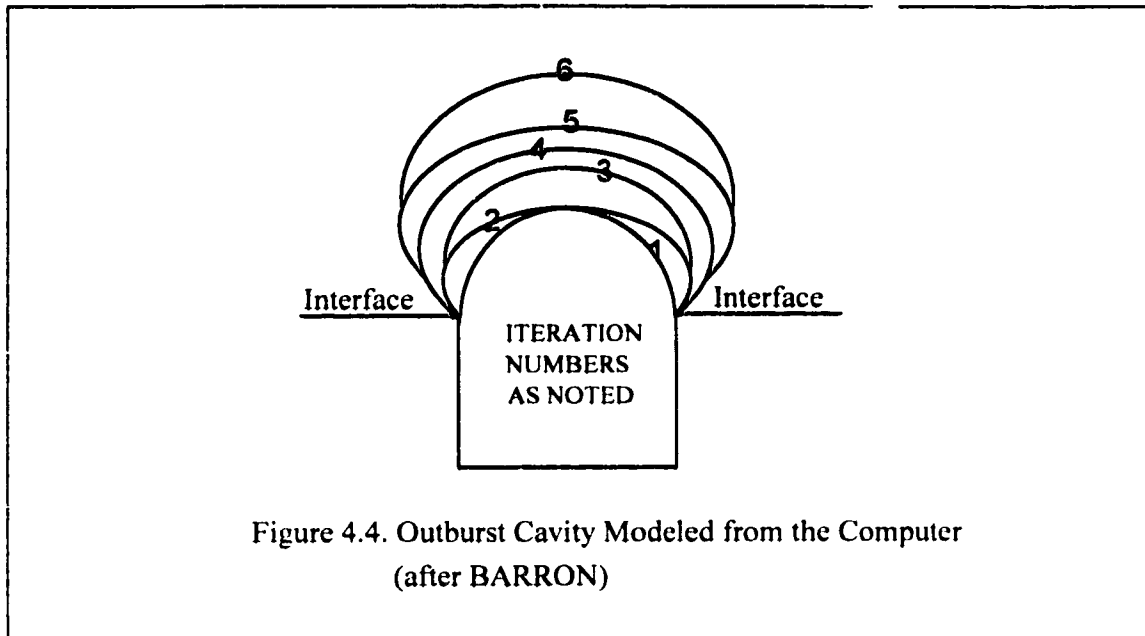


Figure 4.4. Outburst Cavity Modeled from the Computer
(after BARRON)

As this model is based on the boundary element method, the limitations from this method reflect directly in the model. For example, the gas pressure can only be superimposed on the in-situ stresses. This means that the gas pressure only becomes a reductive factor to the strength of coal, not a body force as it should be. The limitation of the materials to be dealt with by boundary element method reduces the capability of the model to handle more complex stratigraphic rock mass, which is usually the situation for coal deposit.

4.3. Discussions

As discussed in above section, each model proposed has its own advantages and disadvantages. This is because the models have been mostly developed from the local experiences with the outbursts. As the factors for the formation of an outburst have been identified differently from place to place, most models can only be utilized in local

practice, and are not likely to be adapted to the other practices. This localized application reflects that the mechanism which has been postulated in the models has only been tailored to the local manifestation of the outbursts.

Some models attempt to solve the problem quantitatively, but the parameters required in the model calculation are numerous and complex. This prohibits the practical application in real life, because the acquisition of these complicated parameters may be either uneconomic or difficult technically. In practice, the measurements of the properties, even if economically and technically possible, are always accompanied by various experimental errors. Koragodin's model calls for the rheological properties of the rock mass and Khoroshun's model needs the gas filtration coefficient and a number of effective "skeleton-gas" system constants. These parameters could be very difficult, at least, and very uneconomical to acquire in practice. Paterson's numerical model depends on more than ten parameters, in addition to the conventional material elastic and strength properties.

The energy balance theory can explain the mechanism of the outbursts excellently in terms of physical concept, but it is very unrealistic to be quantified. Not to mention the calculation of the energy stored in gas and rock, the energy required to break the rock and to move the broken rock, and the trivial components such as the energy transformed to the sound, vibration wave and temperature etc. are very difficult to define quantitatively in the state of present science. In fact, they may not even possible, so that the governing inequality in 4.2.1 section is crippled by the undetermined W_f term. Therefore, it is far from practical application of the theory to solve the outburst problems.

Although many models have appreciated the dual influence of the field stresses and gas pressure, only one of the two factors is participating in the calculations whenever the model operates. Revalor's model only counts for the effect of field stresses, and Khristianovich's model only concerns the gas pressure influence. Barron and Kullman's model has been able to account for the dual contribution of the field stresses and the gas pressure into the calculation, but the following drawbacks prevent it from being a practically valuable model.

The most significant disadvantage of the model is that the modeling process operates subjectively. The spalling mechanism postulated in the model has been designated to a manual manipulation by use of the mouse to define the newly formed cavity boundary on the computer screen. This manual operation introduces strong human subjective control to the results and brings in the physical errors at the same time. The reproducibility of the results from the model, then, is poor, especially from different operators. The reliability of the model is, therefore suspect.

The limitations of the boundary element method have been passed on to the model. When calculating the stress distribution, the gas pressure in the rock should be treated as the internal force or body force. The BEM can not fulfill such a function so that the gas pressure has to be superimposed directly onto the stress distribution calculated from the field stresses in the model. The replacement of the methodology for the stress calculation may lead to the incorrect outputs, and unreliable final results drawn from the model. The limit of number of material layers which could be dealt with in the BEM prescribes the number of materials used in the model. For a real situation, the model at least has to handle three materials, hanging wall, foot wall and gas bearing layer in order to realize the simulation. The simplified simulation, for example two layers of material, may miss out some results which can be revealed by a more realistic simulation. The material behavior must be linear elastic if BEM is in use. By imposing this assumption to the model, the capability of the model will be undoubtedly reduced and the correctness of the results from modeling is suspected.

In the summary, although many of the models have been developed in the course of past study, none of them can be considered satisfactory for practical use. A more advanced model is still the pursuit of the academic world and as well as industrial sector.

Chapter V STATEMENT OF THE PROBLEM

Outbursts have imposed a serious problem on underground mining operations for more than a century. During this period, researchers have made continual efforts to seek solutions to this challenging problem. Much experience and knowledge have accumulated through the joint efforts of the industrial and academic sectors. As a very important study tool, the establishment of an outburst model has been constantly pursued in the research because it can substantiate the mechanism, help prediction attempts and provide a solid basis for evaluating preventative and protection measures. Many models have been put forward for such purposes. The models discussed in section 4.2 are the most representative of them. Despite the number of models proposed in the past, the pursuit of a more generalized and the more practical model still continues as a major objective of rock mechanics research.

5.1 Statement of the Problem

The fundamental objective of this research work is to establish an effective 2-D numerical outburst model that is able to account for the influence of two essential factors, field stresses and gas pressure, and to incorporate the material strength to allow the economic and practical simulation. The achievement of this objective requires the clear elucidation of the mechanism and assumptions for the model. The model will be based on a numerical computational system. A computer program is developed to incorporate this numerical calculation into the assumed model.

Based on the developed model, the thesis will demonstrate its applications to two major cases, the development entry and the long-wall face, in which outbursts have frequently taken place. The model will be tested against the case history of the outbursts in the development entries at #26 Colliery of Sydney, Nova Scotia, Canada. The model will be able to calculate the conditions under which the outbursts took place. It also estimates the consequences of the outbursts and determines the conditions under which an outburst terminates. These results from the model will assist engineers in attempting to predict an outburst, and in evaluating measures to prevent and protect from outbursts.

5.2 Scope of Thesis

The thesis will be restricted to the following two defined scopes, although the potential of the model is not limited by these restrictions.

The model will be developed in two dimensional space, i.e., to create a 2-D model. For practical applications, the model will be best suited to the long-wall face case. Application to the development entry case will induce some error because of the "end effect" where the face proximity is ignored in a two dimensional representation of the development entry. These effects reduce rapidly as the distance from the end face increases.

The model will only be applied to the condition of the development entry and long-wall face situation. However, it is these two situations in which most reported outbursts have been observed. The model has the potential to be applied to other many situations in which a two dimensional representation is a reasonable approximation of any geometry.

Chapter VI DERIVATION OF THE MODEL

The finite element model for the outbursts will be described in this chapter. The model will be formulated mathematically, based on the assumptions made regarding the postulated outburst mechanism. The model procedure will be introduced while programming of the model is explained briefly.

6.1 Description of the Outbursts

As a hazardous phenomenon in underground mining environment, an outburst has been explained as a rapid ejection of broken rock from the rock massive to the mining opening. The ejection is violent in nature, with the volume of broken rock ranging from several tons to a thousand tons. The ejection must be accompanied by the release of gas or gases. The volume of gas at atmospheric pressure is usually very large compared to the rock volume. The gas expands during the outburst, causing a rush of gas through the underground opening network, disturbing the designed ventilation system and sometimes leading to the main fan shutting down.

From a mechanistic point of view, the outbursts can be considered to be the result of mechanical failure of rock due to the combined effects of field stresses and pore gas pressure. The contribution from each propelling source may vary depending on the insitu mechanical conditions. If the effective stress exceeds the tensile strength of the rock, the rock fails in tension and spalls from the host rock. The detached rock is further broken in tension to very small debris or may be completely shattered by the gas pressure destroying its structure, resulting in very fine particles. Whether the detached rock will be disintegrated or pulverized depends on the rock characteristics, coal is likely easier to pulverize than other rocks. The expanding gas will transport the debris or the coal powder. If the rock is easily broken, the excess energy will be larger, and in turn, the broken material will be transported a larger distance. Furthermore, the smaller the rock particles, the farther they can be transported. In reality, the breaking and transportation process may not strictly follow the sequence as described here, but may happen simultaneously and facilitate each other.

In past literature, the terms "sudden" or "instantaneous" are frequently used to describe the outburst process. This is because the superficially violent manifestation

misleads the observers and investigators. In fact, the bursting process can never occur instantaneously. The process continues over a time period from a fraction of a second to a few seconds or even longer. During this period, the above described spalling repeats. The elapsed time may depend on the rock rheological properties and the loading environment. The spalling process continues until some "stopping" mechanism is invoked to cease the outburst, leaving a cavity of a specific size.

This tensile failure and gas transporting spalling mechanism may be partially substantiated by the core dishing phenomenon during the drilling in an outburst zone. If the rock has a higher tensile strength, a thicker disk forms. The weaker the rock, the thinner the disk. In the high stress concentrated zone, expulsion of the powder speeds up dramatically due to the increase of the tensile failure in the bore hole. The dishing and powder expulsion resembles the failure modes of outbursts. Excessively high tensile stress will shatter the weak coal and the gas will transport the pulverized coal powder.

The role of shear failure in the outburst mechanism is not as obvious as tensile failure in the outburst process. Further investigations are strongly recommended in order to clarify role of shear in the whole outburst process. Nevertheless, the "onion skin" texture left behind on the surface of the cavity wall after termination of outbursts implies the effects of the shear failure. According to the experiences from outbursts at #26 colliery, it was found that the sandstone with such a texture was very weak compared to the intact material. This observation may suggest that the sandstone has sheared during the bursting, but remained in the place without being spalled out. This is the best information on shear failure in the outburst process so far observed.

Briefly, the previous discussions can be summarized to describe the outburst mechanism as:

- An outburst is a stress failure phenomenon.
- Effective stresses may be adopted to describe the stress system.
- Two basic failure modes (tensile and shear) are both observed in the outburst process; while tensile failure disintegrates intact rock, shear failure weakens rock and may cause some disintegration (to be proved in practice).
 - Gas pressure acts as transportation tool, in addition to being one component of effective stresses.
 - The combined effects of field stresses and gas pressure breaks and /or pulverizes the rock.
 - A rapid spalling process is in effect, which leads to progressive failure.
 - Stable conditions must be achieved before an outburst terminates.

6.2 Selection of the Numerical Method:

Since the outbursts can be explained by a stress failure concept, the stress analysis approach may be considered to solve the problem. Closed form solution and the computational methods constitute the major methodologies in modern stress analysis. The closed form solutions usually give very complicated expressions for the stress and displacement distribution even for a very simple and basic geometry of excavation and are unable to solve more complex conditions such as non-homogeneity and non-linear constitutive behavior of the rock mass. The recent rapid development of the electronic computer and computing technologies has allowed powerful numerical methods to become more practical and affordable for general engineering application. Therefore, numerical analysis for the stress is selected for this research.

Numerical computation includes the finite difference method (FDM), the finite element method (FEM), the boundary element method (BEM), the distinct element method (DEM) and the hybrid computational schemes formed by combinations of the above methods (HCS). Each method has certain advantages and disadvantages as well as limitations, although the sophisticated user may overcome the disadvantages and blur the differences. To achieve the most efficient calculations and to serve the most suitable tool for modeling this specific problem, a proper selection should be carried out from amongst these methods.

FDM has been a traditional approach for numerical solutions of differential equations. This method is well developed and there is abundant technical knowledge of its use. The most significant disadvantage for this method, however, lies in the difficulty arising when handling the boundary conditions for regions containing irregular holes or excavations. Because of this inconvenience, it is not usually used for underground excavation stress analysis. So, FDM is not selected for this model.

BEM was used to establish the Kullman and Barron model. The problems with this model are mostly associated with the drawbacks of the BEM as discussed in section 4.3. The most important drawback is the difficulty to handle the nonlinear, non-homogeneous and anisotropic material. It is also inconvenient to deal with the spalling process as assumed in the model. The definition of the new boundary of the cavity presented major difficulties in the Kullman and Barron model. Therefore, it was not selected for this study.

DEM is basically designed to treat the rock mass as assemblages of distinct rock blocks. The emphasis is placed on the rigid movement of the rock blocks, although the block deformations have begun to be incorporated into current analyses. It is most

suitable for applications in a heavily jointed rock mass. One major disadvantage of this method, which prohibits its use here is that it is not possible to deal with the gas pressure as internal force.

FEM has been developed to a relatively more sophisticated phase, and its flexibility for dealing with nonlinear, non homogeneity and anisotropic behavior has made it the most popular method for underground excavation analysis. The technique of removing elements from the system during calculation is applicable to the spalling mechanism as postulated in the model. The method has been extensively verified in numerous case studies for variety of engineering problems. The source code is conveniently accessible and the pre-processor and the post-processor have been developed for easy preparation of input data and for clear presentation of output data. So, it is selected to develop this model.

Theoretically speaking, a hybrid computational scheme from amongst FEM, BEM and DEM might be the most ideal analysis means for the problem confronted in this study. However, the difficulty in effectively incorporating the spalling process prohibits the utilization of the scheme.

6.3 Model Assumptions

The mechanism of the outbursts has been assumed in section 6.1 and the model is chosen to be built on the finite element method. In order to formulate the mathematical framework of the model, a number of postulates have to be stated. The following assumptions form the basis of the model:

- 1). Small deformation is assumed to prevail throughout the system, allowing the application of the finite element method code to the model.
- 2). The rock simulated in the model follows a perfect elasto-plastic constitutive relationship. The plastic deformations beyond the yield strength abide by the associated flow rule developed by Reyes and Deere (REYES, 1966), while Drucker-Prager's generalized failure criterion (DRUCKER, 1952) determines yield condition.
- 3). The effective stress concept is adopted to describe the combined effects of the field stresses and gas pressure, and to define all failure criteria used in the model.
- 4). The elements representing the rock failed in tensile mode (tensile failed elements) are "removed" from system in each cycle of spalling process, leaving a geometrically altered boundary for next cycle of the spalling.

5). The elements representing the rock failed in shear mode (sheared elements) "remain" in the place for the current cycle, but are de-gassed instantaneously in the next cycle.

6). The spalling process is simulated by the reiterations of the cycles and only stops when a stable boundary shape is formed or it is apparent that the spalling will continue indefinitely.

The first assumption implies that the model is able to handle the discontinuities, non-homogeneous and anisotropic material provided that the input data has been properly prepared. For a large deformation system, a special formulation for FEM must be used and a special set of procedures to realize FEM has to be incorporated. In this research, the large deformation is not the major concern of the study. As an approximation, the geotechnical problem in rock is conventionally treated as a small strain problem.

Assumption 2). prescribes the rock properties dealt with by the model. As it is well known, rock behavior can differ from one place to another, varying from linear elastic to nonlinear plastic with strain hardening or softening post failure behavior. The perfect elasto-plastic relation has been selected to describe the stress-strain relationship before and after yielding for the model because it well represents the characteristics of soft rock, such as coal, shale and weak sandstone, etc., in which the outbursts have mostly taken place. In addition, the parameters required in Drucker-Prager's yield criterion and Reyes-Deere's stress strain relation can be practically extracted from experiment relatively simply and inexpensively.

As previously discussed, the failure of rock during outbursting is caused by the combined effects of field stresses and gas pressure. The effective stress concept may quantify this effect as a first approximation. However, the difference must be noted between a water-soil system and gas-solid medium. The gas is highly compressible while the water is usually assumed incompressible. As a result, the solid skeleton of rock in gas-solid medium is much stronger and more stable than the soil-grain assemblage in water-soil system. The theoretical formulation of the relationship associated with the deformation for the gas-solid medium was extensively discussed by Khoroshun (KHOROSHUN, 1976; KHOROSHUN, 1981; KHOROSHUN, 1984). The mathematical expression of the relation was very complex to be incorporated into FEM. However, the effective stress concept is relatively easy to be considered by FEM.

Assumptions 4). and 5). are made on basis of the postulated outburst mechanism, and play a major role in the formulation of the model. The computational realization of these two assumptions forms the major task in establishing this model. Although needing

additional proof from practice, a lot of evidence indicates that the tensile failure mode is predominant during outbursting, while shear failure may also occur. The straightforward tensile failure criterion is used to quantify the assumption 4). The tensile strength of the rock can be obtained by any standard tests, though preference is given to the Brazilian test. When the rock shears, it is assumed that the gas contained in this part of the rock is degassed. The shear strength of the rock is determined by the generalized Drucker-Prager criterion.

A spalling process is covered in assumption 6). The process is considered to be an "instantaneous" series of static events. As the tensile failed rock spalls and is removed, it forms a cavity, changing the boundary geometry of previous excavation. The size and the shape of the excavation will alter the stress distribution around the excavation simultaneously. This newly formed stress distribution becomes the starting point for the next iteration.

6.4 Mathematical Derivation of the Model

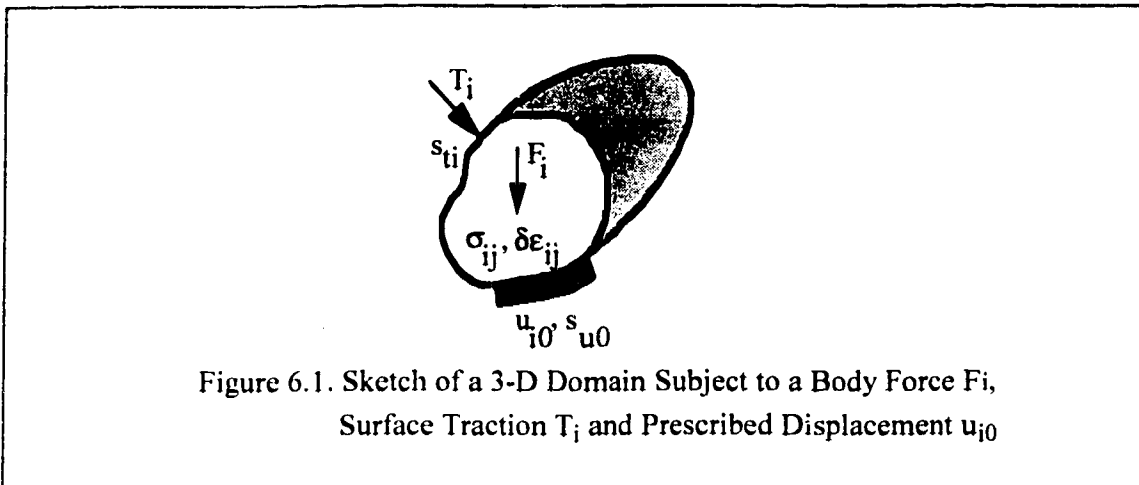
In this section, the mathematical formulation of the model suitable for numerical solution by the FEM will be developed on basis of the above assumptions. Removal of the broken rock and degassing of the sheared rock in the spalling process will be quantitatively incorporated into the FEM formulation.

6.4.1 Generalized formulation of FEM analysis

To calculate the effective stress distribution in an irregular domain by FEM, the basic equations must be first derived. Many techniques exist to formulate the equations. These techniques include the method of weighted residuals, the principle of minimum potential energy and the principle of virtual work (or virtual displacement), etc. When analyzing the stress distribution around geotechnical structures, the principle of virtual work provides a straightforward and effective method to obtain the basic equations.

Fig. 6.1 illustrates a general three dimensional irregular domain, on which a body force F_j is subjected together with prescribed displacement u_{j0} over the surface s_{u0} ; the boundary traction T_j is exerted over the remaining surface s_{tj} . Under such a system, the principle of virtual work states that

"The equilibrium of the body requires that any kinematically admissible displacement field imposed on the body, the total internal virtual work is equal to the total external virtual work."



The mathematical interpretation of such a statement can be expressed as following equation:

$$\int_V \delta \epsilon_{ij} \sigma_{ij} dv = \int_V \delta u_i F_i dv + \int_S \delta u_i T_i ds \quad (6.1)$$

Where \int_V , \int_S indicate integration over the entire body and portion of the surface subjected to traction respectively, δu_i is the "kinematically admissible displacement field" (virtual displacement imposed on the body), while $\delta \epsilon_{ij}$ represents the associated virtual strain field distributed over the whole body. The left term in Eq. (6.1) calculates the virtual work done by the internal stresses σ_{ij} , and the right first and the second term in equation express the virtual work done by the external body force F_i and traction T_i . The sum of the right side of the equation computes the total virtual work done by external forces.

The FEM requires discretization of the whole domain into an assemblage of finite small interacting elements as shown in Fig. 6.2. For this discretized domain, the principle of virtual work can be applied to each element and the summation of each element gives the discretized form of Eq. (6.1):

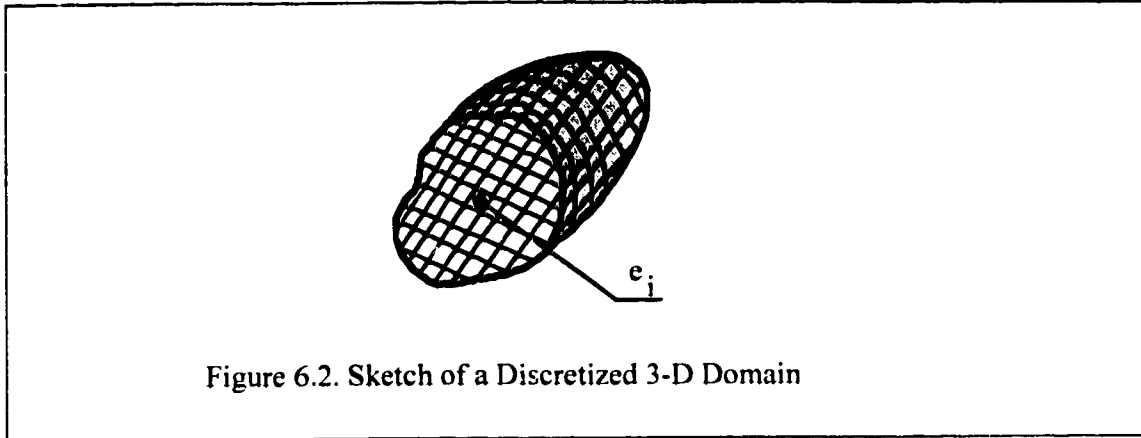


Figure 6.2. Sketch of a Discretized 3-D Domain

$$\sum_{n=1}^{ele} \int_{V_c} \delta \epsilon_{ij} \sigma_{ij} dv = \sum_{n=1}^{ele} \int_{V_c} \delta u_i F_i dv + \sum_{n=1}^{ele} \int_{S_c} \delta u_i T_i ds \quad (6.2)$$

where, $\sum_{n=1}^{ele}$ summarizes all the elements discretized in the domain. In Eq. (6.1) and Eq. (6.2), σ_{ij} represent total stress tensor. According to the effective stress concept, in terms of effective stress and gas pressure the total stress can be expressed in tensor form as the following:

$$\sigma_{ij} = \sigma'_{ij} + p \Delta_{ij} \quad (6.3)$$

Where, σ'_{ij} - effective stress tensor;

p - pore gas pressure,

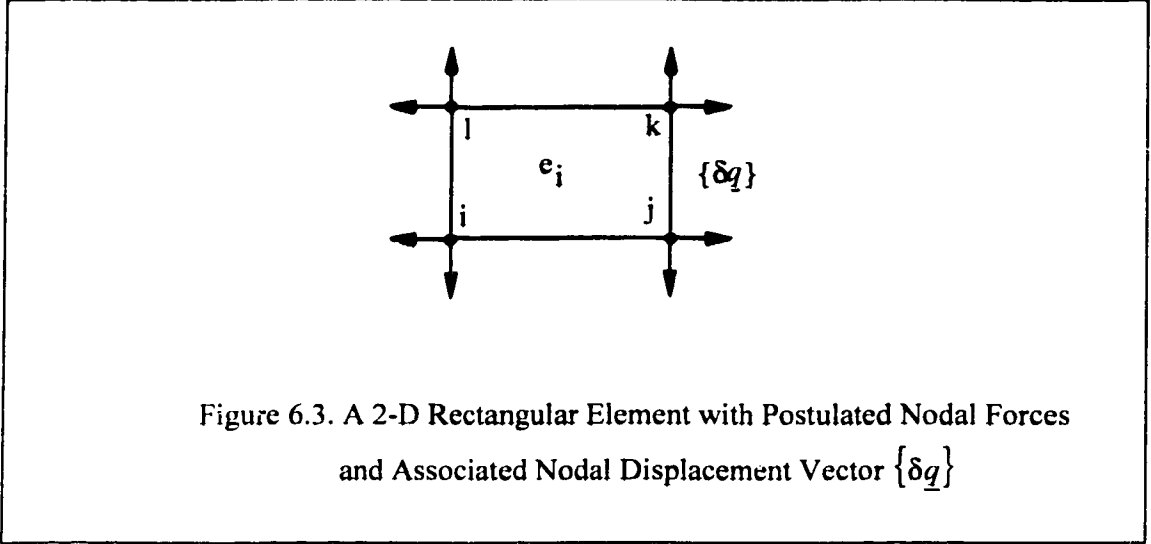
Δ_{ij} - Keronecker delta (or substitution tensor);

$$\Delta_{ij} = \begin{cases} 1 & i = j \\ 0 & i \neq j \end{cases}$$

Substituting Eq. (6.3) into Eq.(6.2) and adjusting the terms, gives:

$$\sum_{n=1}^{ele} \int_{V_c} \delta \epsilon_{ij} \sigma'_{ij} dv = \sum_{n=1}^{ele} \int_{V_c} \delta u_i F_i dv + \sum_{n=1}^{ele} \int_{S_c} \delta u_i T_i ds - \sum_{n=1}^{ele} \int_{V_c} \delta \epsilon_{ij} p \Delta_{ij} dv \quad (6.4)$$

Now let us examine each particular element such as a 2-D rectangular element shown in Fig. 6.3, which is defined by four corner nodes i, j, k and l. For such an element a set of nodal forces $\{Q\}'_e$ are defined associated with the nodal displacements $\langle \underline{q} \rangle$ so that:



$$\langle \delta \underline{q} \rangle \{Q\}'_e = \int_{V_e} \delta \epsilon_{ij} \sigma'_{ij} dv \quad (6.5)$$

Now let us define a set of forces $\{P_b\}$ associated with $\langle \underline{q} \rangle$ such that they do the same work as the distributed body forces. It is mathematically expressed as:

$$\langle \delta \underline{q} \rangle \{P_b\}_e = \int_{V_e} \delta u_i F_i dv \quad (6.6)$$

Similarly for traction and gas pressure, we may obtain:

$$\langle \delta \underline{q} \rangle \{P_t\}_e = \int_{S_e} \delta u_i T_i ds \quad (6.7)$$

$$\langle \delta \underline{q} \rangle \{P_{gp}\}_e = \int_{V_e} \delta \epsilon_{ij} p \Delta_{ij} dv \quad (6.8)$$

Where in equations (6.5)-(6.6):

$\{Q\}'_e$ - nodal force vector associated with effective stress tensor;

$\{P_b\}_e$ - nodal force vector associated with body forces;

$\{P_t\}_e$ - nodal force vector associated with traction on the surface;

$\{P_{gp}\}_e$ - nodal force vector associated with pore gas pressure.

Putting Eqs. (6.5)-(6.8) into Eq. (6.4) will result in:

$$\sum_{n=1}^{ele} \langle \delta \underline{q} \rangle \{Q\}'_e = \sum_{n=1}^{ele} \langle \delta \underline{q} \rangle \{P_b\}_e + \sum_{n=1}^{ele} \langle \delta \underline{q} \rangle \{P_t\}_e + \sum_{n=1}^{ele} \langle \delta \underline{q} \rangle \{P_{gp}\}_e \quad (6.9)$$

Since $\langle \delta \underline{q} \rangle$ is an arbitrary permissible displacement vector, Eq.(6.9) requires:

$$\sum_{n=1}^{ele} \{Q\}'_e = \sum_{n=1}^{ele} \{P_b\}_e + \sum_{n=1}^{ele} \{P_t\}_e + \sum_{n=1}^{ele} \{P_{sp}\}_e \quad (6.10)$$

$$\text{or} \quad \{Q\}' = \{R\} \quad (6.11)$$

Equation (6.10) or (6.11) is the governing equation of the finite element method for the domain with pore gas pressure. To find each term in Eq. (6.10), let us consider plane stress and plain strain problems. For these two problems, the stress and the strain tensor can be expressed in vector form as:

$$\begin{aligned} \sigma'_{ij} &\Rightarrow \{\sigma'\} = \langle \sigma'_x, \sigma'_y, \tau'_{xy} \rangle^T \quad [\sigma'_z = \mu(\sigma'_x + \sigma'_y) \text{ for plane strain problem}] \\ \epsilon_{ij} &\Rightarrow \{\epsilon\} = \langle \epsilon_x, \epsilon_y, \gamma_{xy} \rangle^T \quad [\epsilon_z = 0 \text{ for plane strain}] \\ \Delta_{ij} &\Rightarrow \langle L \rangle = \langle 1, 1, 0 \rangle \quad [i=1,2; j=1,2] \end{aligned}$$

In order to define the strain vector in an element $\{\epsilon\}$ with the nodal displacement vector $\langle \underline{q} \rangle$, a displacement vector in the element $\{\bar{q}\}$ and a shape function matrix $[N]$ are assumed such that:

$$\{\bar{q}\} = \begin{bmatrix} \langle N \rangle_1 \\ \langle N \rangle_2 \end{bmatrix} \begin{Bmatrix} u \\ v \end{Bmatrix} = [N] \{q\}_e \quad (6.12)$$

Where $\langle N \rangle_1$ and $\langle N \rangle_2$ are the shape functions associated with nodal displacement vector u and v in x and y directions respectively. By taking variational form of Eq. (6.12), it gives:

$$\{\delta \bar{q}\} = \{\delta u, \delta v\} = [N] \{\delta \underline{q}\}_e \quad (6.13)$$

According to the well-know relations

$$\{\boldsymbol{\varepsilon}\} = \begin{Bmatrix} \varepsilon_x \\ \varepsilon_y \\ \varepsilon_{xy} \end{Bmatrix} = \begin{Bmatrix} \frac{\partial u}{\partial x} \\ \frac{\partial v}{\partial y} \\ \frac{\partial u}{\partial y} + \frac{\partial v}{\partial x} \end{Bmatrix}, \quad (6.14)$$

it gives

$$\{\boldsymbol{\varepsilon}\} = \begin{Bmatrix} \frac{\partial \langle N \rangle_1}{\partial x} \\ \frac{\partial \langle N \rangle_2}{\partial y} \\ \frac{\partial \langle N \rangle_1}{\partial y} + \frac{\partial \langle N \rangle_2}{\partial x} \end{Bmatrix} \begin{Bmatrix} u \\ v \end{Bmatrix} = [\mathbf{B}] \{ \underline{q} \}_e \quad (6.15).$$

Where, $[\mathbf{B}]$ is called the B-matrix, and the virtual incremental $\{\delta \boldsymbol{\varepsilon}\}$ can be obtained from this relation as:

$$\{\delta \boldsymbol{\varepsilon}\} = [\mathbf{B}] \{ \delta \underline{q} \}_e \quad (6.16)$$

In terms of effective stresses and by considering Eq. (6.16), the constitutive relationship can be generally expressed in the following form:

$$\{\boldsymbol{\sigma}'\} = [\mathbf{c}'] \{\boldsymbol{\varepsilon}\} = [\mathbf{c}'] [\mathbf{B}] \{ \underline{q} \}_e \quad (6.17)$$

with $[\mathbf{c}']$ represents the material constant matrix in terms of effective stresses.

If relations (6.13), (6.16) and (6.17) apply into the Eq.(6.4) and Δ_{ij} is substituted by definition $\langle L \rangle^T$, it will produce:

$$\sum_{n=1}^{ele} \int_{V_e} [\mathbf{B}] \{ \delta \underline{q} \}_e [\mathbf{c}'] [\mathbf{B}] \{ \underline{q} \}_e dv = \sum_{n=1}^{ele} \int_{V_e} [\mathbf{N}] \{ \delta \underline{q} \}_e \{ F_i \} dv + \sum_{n=1}^{ele} \int_{S_e} [\mathbf{N}] \{ \delta \underline{q} \}_e \{ T_i \} ds - \sum_{n=1}^{ele} \int_{V_e} [\mathbf{B}] \{ \delta \underline{q} \}_e p \{ L \} dv$$

Rearranging the above equation, gives:

$$\sum_{n=1}^{ele} \langle \delta \underline{q} \rangle_e \int_{V_e} [\mathbf{B}]^T [\mathbf{c}'] [\mathbf{B}] dv \{ \underline{q} \}_e = \sum_{n=1}^{ele} \langle \delta \underline{q} \rangle_e \int_{V_e} [\mathbf{N}]^T \{ F_i \} dv + \sum_{n=1}^{ele} \langle \delta \underline{q} \rangle_e \int_{S_e} [\mathbf{N}]^T \{ T_i \} ds - \sum_{n=1}^{ele} \langle \delta \underline{q} \rangle_e \int_{V_e} [\mathbf{B}]^T p \{ L \} dv$$

Since $\langle \delta \underline{q} \rangle_e$ is an arbitrary displacement vector, the above equation leads to:

$$\sum_{n=1}^{ele} \int_{V_e} [\mathbf{B}]^T [\mathbf{c}'] [\mathbf{B}] dV \{ \delta \underline{q} \}_e = \sum_{n=1}^{ele} \int_{V_e} [\mathbf{N}]^T \{ \mathbf{F}_i \} dV + \sum_{n=1}^{ele} \int_{S_e} [\mathbf{N}]^T \{ \mathbf{T}_i \} dS - \sum_{n=1}^{ele} \int_{V_e} [\mathbf{B}]^T p \{ \mathbf{L} \} dV$$

By comparing this equation with Eq. (6.10), following relations can be obtained:

$$\{ \mathbf{Q}' \}_e = \int_{V_e} [\mathbf{B}]^T [\mathbf{c}'] [\mathbf{B}] dV \{ \underline{q} \}_e \quad (6.18)$$

$$\{ \mathbf{P}_b \}_e = \int_{V_e} [\mathbf{N}]^T \{ \mathbf{F}_i \} dV \quad (6.19)$$

$$\{ \mathbf{P}_t \}_e = \int_{S_e} [\mathbf{N}]^T \{ \mathbf{T}_i \} dS \quad (6.20)$$

$$\{ \mathbf{P}_{gp} \}_e = \int_{V_e} [\mathbf{B}]^T p \{ \mathbf{L} \} dV \quad (6.21)$$

$$\text{If denoting } \int_{V_e} [\mathbf{B}]^T [\mathbf{c}'] [\mathbf{B}] dV \text{ as } [\mathbf{k}]_e, \text{ i.e., } [\mathbf{k}]_e = \int_{V_e} [\mathbf{B}]^T [\mathbf{c}'] [\mathbf{B}] dV \quad (6.22),$$

Eq. (18) can be rewritten as:

$$\{ \mathbf{Q}' \}_e = [\mathbf{k}]_e \{ \underline{q} \}_e \quad (6.23)$$

Therefore, Eq. (6.10) becomes:

$$\sum_{n=1}^{ele} [\mathbf{k}]_e \{ \underline{q} \}_e = \sum_{n=1}^{ele} \left[\int_{V_e} [\mathbf{N}]^T \{ \mathbf{F}_i \} dV + \int_{S_e} [\mathbf{N}]^T \{ \mathbf{T}_i \} dS + \int_{V_e} [\mathbf{B}]^T p \{ \mathbf{L} \} dV \right] \quad (6.24)$$

Where, $[\mathbf{k}]_e$ is the stiffness of the element; $\sum_{n=1}^{ele} [\mathbf{k}]_e$ assembles the element stiffness into global stiffness of the system $[\mathbf{K}]$.

And, so does the displacement vector:

$$\sum_{n=1}^{ele} \{ \underline{q} \}_e = \{ \underline{q} \}.$$

By assuming left side expression to be denoted by $\{ \mathbf{R} \}$, Eq. (6.24) can be written as:

$$[K]\{q\}=\{R\} \quad (6.25)$$

This equation represents the governing equation of the finite element method as Eq. (6.11). The stiffness matrix $[K]$ can be assembled from the matrix $[k]_e$ which is calculated from Eq. (6.22), so can be the load vector $\{R\}$ from Eq. (6.19) - (6.21). The unknown global displacement vector $\{q\}$ can be obtained from solving equations (6.25).

In formulating the above FEM equations, no material behavior has been specified. The calculations, then, are valid for any material. Reyes and Deere developed the $[c]$ matrix for perfect elasto-plastic behavior of a Mohr-Coulomb type material. The matrix form of stress-strain relationship is expressed as follows:

$$\begin{Bmatrix} \dot{\sigma}_{11} \\ \dot{\sigma}_{22} \\ \dot{\sigma}_{12} \end{Bmatrix} = 2G \begin{bmatrix} c_{11} & c_{12} & c_{13} \\ c_{21} & c_{22} & c_{23} \\ c_{31} & c_{32} & c_{33} \end{bmatrix} \begin{Bmatrix} \dot{\epsilon}_{11} \\ \dot{\epsilon}_{22} \\ \dot{\epsilon}_{12} \end{Bmatrix} \quad (6.26)$$

where, $\dot{\epsilon}$ denotes incremental quantities. The elements in the constitutive matrix are defined by:

$$\left. \begin{aligned} c_{11} &= 1 - h_2 - h_1 \sigma_{11} - h_3 \sigma_{11}^2 \\ c_{22} &= 1 - h_2 - 2h_1 \sigma_{22} - h_3 \sigma_{22}^2 \\ c_{33} &= \frac{1}{2} - h_3 \sigma_{12}^2 \\ c_{12} &= c_{21} = -h_2 - h_1 \sigma_{11} - h_1 \sigma_{22} - h_3 \sigma_{11} \sigma_{22} \\ c_{13} &= c_{31} = -h_1 \sigma_{12} - h_3 \sigma_{12} \sigma_{11} \\ c_{23} &= c_{32} = -h_1 \sigma_{12} - h_3 \sigma_{12} \sigma_{22} \end{aligned} \right\} \quad (6.27)$$

and,

$$h_1 = \frac{\frac{3}{2} \alpha \frac{K}{G} - \frac{\sigma_{kk}}{6\sqrt{J_2}}}{\sqrt{J_2} \left(1 + 9\alpha^2 \frac{K}{G} \right)}$$

$$h_2 = \frac{\left(\alpha - \frac{\sigma_{kk}}{6\sqrt{J_2}} \right) \left(32 \frac{K}{G} - \frac{\sigma_{kk}}{3\sqrt{J_2}} \right)}{\left(1 - 9\alpha^2 \frac{K}{G} \right)} - \frac{3\nu f K}{\sqrt{J_2}} \frac{1}{E \left(1 - 9\alpha^2 \frac{K}{G} \right)}$$

$$h_3 = \frac{1}{2\sqrt{J_2} \left(1 + 9\alpha^2 \frac{K}{G} \right)}$$

where, $J_2 = \frac{1}{2} S_{ij} S_{ij}$ ($S_{ij} = \sigma_{ij} - \frac{\sigma_{kk}}{3}$)

and, $f = \alpha \frac{\sigma_{kk}}{3} + \sqrt{J_2}$

$$\alpha = \frac{\tan \phi}{\sqrt{9 + 12 \tan^2 \phi}}$$

$$K = \frac{E}{3(1-2\mu)} \quad (K - \text{bulk modulus})$$

$$G = \frac{E}{2(1+\mu)} \quad (G - \text{shear modulus})$$

ϕ - angle of internal friction,

μ - Poisson's ratio,

E - Young's modulus.

As it may be seen, the terms in the matrix are no longer constant. The current stress state has its influence so that the incremental stress and strain relationship has to be considered in the analysis.

6.4.2 Incremental analysis:

Because the material dealt with by the model is assumed to be non-linear, the incremental approach is adopted to the FEM analysis. In the incremental analysis, the

loads, stresses and displacements for any incremental step can be written as $\{R_n\}$, $\{\sigma_n\}$ and $\{q_n\}$. Then, $\{\sigma_n\}$ and $\{q_n\}$ can be regarded as the initial stresses and displacements for the next loading increment. Thus the matrix form of the governing equation (6.11) is expressed in:

$$[K_{n+1}]\{q_{n+1}-q_n\} = [K_{n+1}]\{\Delta q_n\} = \{\Delta R_n\} \quad (6.28)$$

Where, $\Delta R_n = \sum_{n=1}^{ele} [\{\Delta P_b\} + \{\Delta P_t\} + \{\Delta P_{gp}\}]$ and $\{\Delta P_b\}$, $\{\Delta P_t\}$ and $\{\Delta P_{gp}\}$ are the increments of the respective external loading.

In nonlinear analysis, the stiffness depends on stress state and has to be re-evaluated at small increments of load starting from the previously determined conditions. For the perfect elasto-plastic nonlinear material, however, the whole external loading is applied at once in the first cycle, by assuming all elements to be elastic to begin with. As the problem is non-linear, the solution may not be correct if the stress state exceeds the strength of the material. In this case, a stepwise linear relationship between yielding of one element to another one is assumed for the analysis. This is assumed not to cause any significant error. The difference resulting from the linear handling of the problem in first cycle will be adjusted within the element system until it reduces to a tolerable range.

The adjustment process is illustrated in Fig. 6.4. In the stress space O, point A represents the initial stress state and C point represents the final stress state in an element

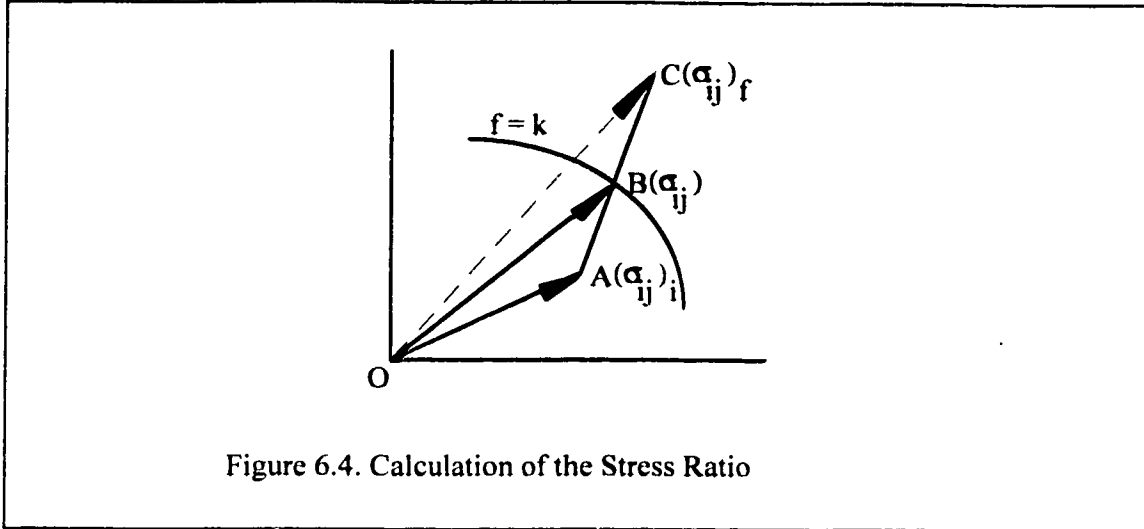
for one particular step in the calculation. The curve $f=k$ ($k = \frac{3c}{\sqrt{9+12 \tan^2 \phi}}$, c is cohesion

and ϕ is internal friction angle) in the space is the yielding surface specified. For those elements that begin to yield in this loading cycle, \overline{AC} meets the surface of $f=k$ at point B. According to the elasto-plastic behavior assigned to the material, loading up to point C is not permissible. The maximum loading the element can sustain is that represented by the points on the curve and as soon as the loading reaches the curve, it should stay on the curve. From Fig. 6.4, the extra loading \overline{BC} has to be removed from this element. To accomplish this removal, the so called "stress ratio" (s_r) is calculated as follows:

$$\text{Let} \quad s_r = \frac{|\overline{AB}|}{|\overline{AC}|} \quad (6.29);$$

$$\text{note} \quad |\overline{OA}| = (\sigma_y)_i; \quad |\overline{OB}| = \sigma_y$$

and $|\overline{OC}| = (\sigma_{ij})_f$.



To evaluate s_r , it is known from Fig. 6.4 and Eq. (6.29):

$$\overline{AC} = \overline{OC} - \overline{OA}$$

$$|\overline{AC}| = |\overline{OC}| - |\overline{OA}| = (\sigma_{ij})_f - (\sigma_{ij})_i \quad (6.30)$$

$$\overline{OB} = \overline{OA} + \overline{AB}$$

$$|\overline{OB}| = \sigma_{ij} = |\overline{OA}| + |\overline{AB}| = |\overline{OA}| + s_r |\overline{AC}| = (\sigma_{ij})_i + s_r [(\sigma_{ij})_f - (\sigma_{ij})_i] \quad (6.31)$$

$$\sigma_{ij} = (\sigma_{ij})_i (1 - s_r) + (\sigma_{ij})_f \quad (6.32)$$

As the point B must stay on the curve $f=k$, it requires:

$$f[\sigma_{ij}] = f[(\sigma_{ij})_i (1 - s_r) + (\sigma_{ij})_f] = k \quad (6.33)$$

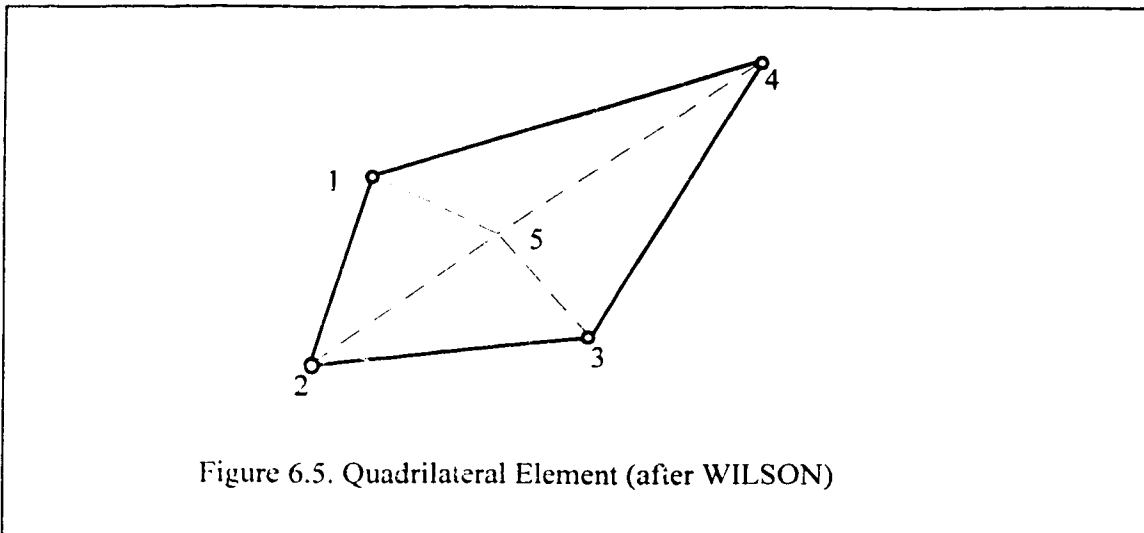
Solving Eq. (6.33) for s_r , s_r is used to scale down the stress state and the displacement field in the element onto the yielding surface. This s_r is calculated for each element in the whole system. The element that has the farthest distance from the surface (refer Fig. 6.4), indicates the worst exceeding of the stress state and will receive the minimum value of the stress ratio. If the stresses and displacements for all elements in the

system are proportionally reduced by this minimum ratio, then the stresses and strains at the point where the system has its first element just enter the plastic region from purely elastic system is defined.

In the next step, the element/elements having the minimum stress ratio will be assumed plastic. As the plastic flow constitutive relation is defined by Eq. (6.26), the stiffness matrix is calculated, and Eq. (6.28) is solved to obtain the displacement increments. This procedure will repeat again and again until the system has balanced to within a tolerable range: the cumulated stresses and strains produce the final results of the analysis.

6.4.3 Finite element method

In this analysis, the finite element has been formulated on basis of Wilson's quadrilateral element (WILSON, 1965). The typical quadrilateral element is composed of four triangular elements as illustrated in Fig. 6.5. The stiffness and B matrix of the element are calculated from those of the four triangular elements. This transformation between triangular and quadrilateral elements is conducted as follows:



From the governing equation (6.25), the matrix formula is rewritten as:

$$\begin{Bmatrix} R_a \\ R_b \end{Bmatrix} = \begin{bmatrix} K_{aa} & K_{ab} \\ K_{ba} & K_{bb} \end{bmatrix} \begin{Bmatrix} q_a \\ q_b \end{Bmatrix} \quad (6.34)$$

Where \underline{q}_a , R_a are associated with point 1-4, while \underline{q}_b , R_b with point 5. Expanding Eq. (6.34) produces:

$$\{R_a\}=[K_{aa}]\{\underline{q}_a\}+[K_{ab}]\{\underline{q}_b\} \quad (6.35)$$

$$\{R_b\}=[K_{ba}]\{\underline{q}_a\}+[K_{bb}]\{\underline{q}_b\} \quad (6.36)$$

Solving Eq. (6.36) for displacement vector $\{\underline{q}_b\}$ gives:

$$\{\underline{q}_b\}=[K_{bb}]^{-1}\{R_b\}-[K_{bb}]^{-1}[K_{ba}]\{\underline{q}_a\} \quad (6.37)$$

Substituting Eq. (6.37) into Eq. (6.35) yields:

$$\begin{aligned} \{R_a\} &= [K_{aa}]\{\underline{q}_a\} + [K_{ab}]([K_{bb}]^{-1}\{R_b\} - [K_{bb}]^{-1}[K_{ba}]\{\underline{q}_a\}) \\ &= ([K_{aa}] - [K_{ab}][K_{bb}]^{-1}[K_{ba}])\{\underline{q}_a\} + [K_{ab}][K_{bb}]^{-1}\{R_b\} \end{aligned} \quad (6.38)$$

Since $\{R_b\}$ can be selected to equal zero, we may obtain the stiffness of the quadrilateral element $[K]$ as:

$$[K] = [K_{aa}] - [K_{ab}][K_{bb}]^{-1}[K_{ba}] \quad (6.39)$$

B-matrix transformation can be realized as follows:

$$\begin{Bmatrix} R_a \\ R_b \end{Bmatrix} = \begin{bmatrix} B_a \\ B_b \end{bmatrix} \{\sigma\} \quad (6.40)$$

Similarly,

$$\{R_a\} = [B_a]\{\sigma\} \quad (6.41)$$

$$\{R_b\} = [B_b]\{\sigma\} \quad (6.42)$$

From Eq. (6.38) and considering Eq. (6.39), (6.41) and (6.42),

$$[K]\{\underline{q}_a\} = \{R_a\} - [K_{ab}][K_{bb}]^{-1}\{R_b\}$$

$$\begin{aligned}
 &= [B_a] \{ \sigma \} - [K_{ab}] [K_{bb}]^{-1} [B_b] \{ \sigma \} \\
 &= ([B_a] - [K_{ab}] [K_{bb}]^{-1} [B_b]) \{ \sigma \}
 \end{aligned} \tag{6.43}$$

Considering the relation $[K] \{ q \} = [B] \{ \sigma \}$, Eq. (6.43) produces the B-matrix of the quadrilateral element:

$$[B] = [B_a] - [K_{ab}] [K_{bb}]^{-1} [B_b] \tag{6.44}$$

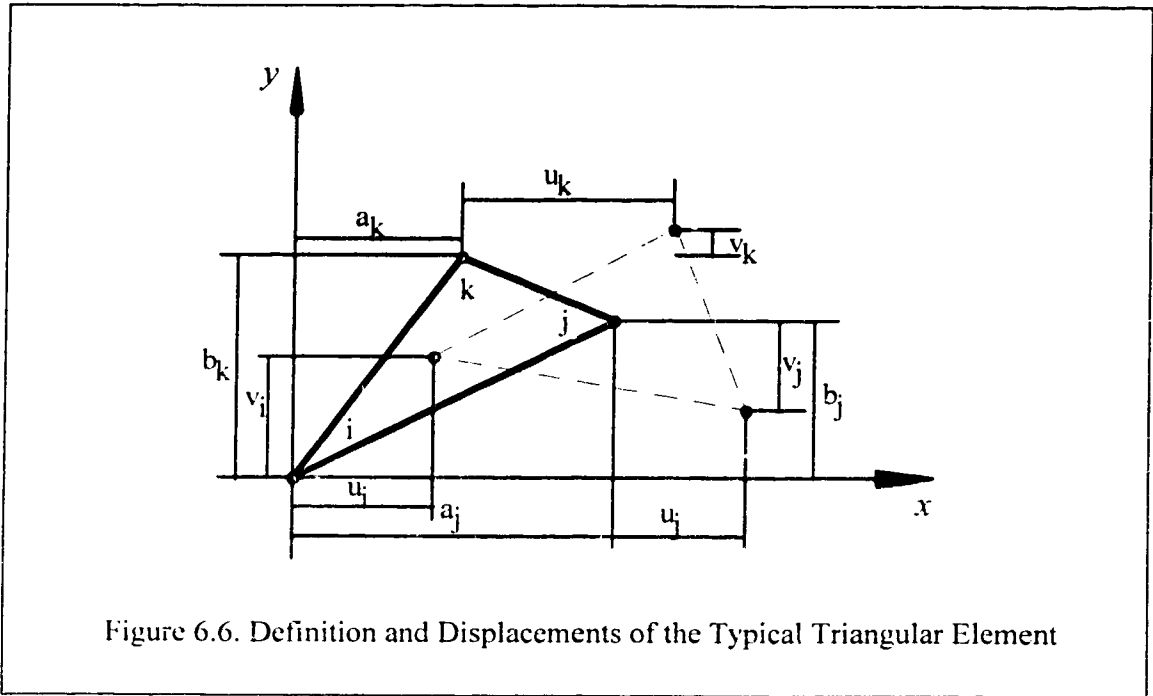


Figure 6.6. Definition and Displacements of the Typical Triangular Element

The formulation of typical triangular element was given by Wilson (WILSON, 1963). For the element with assumed displacement pattern as shown in Fig. 6.6, the B-matrix of the element can be defined as:

$$[B] = \frac{1}{a_i b_k - a_k b_i} \begin{bmatrix} b_i - b_k & 0 & b_k & 0 & -b_j & 0 \\ 0 & a_k - a_i & 0 & -a_k & 0 & a_j \\ a_k - a_i & b_j - b_k & -a_k & b_k & a_i & b_j \end{bmatrix} \tag{6.45}$$

The stiffness of the element, then, can be readily evaluated according to the following matrix expression:

$$[K]_e = [B][c][B]^T \quad (6.46)$$

Where $[c]$ is the same as defined previously.

6.4.4 Gas pressure consideration in FEM

In this model, the gas pressure within the specific strata is assumed to be uniformly distributed throughout the strata. The gas pressure p in Eq. (6.16), therefore, does not vary with the position in the strata. At the periphery of the excavation, the gas pressure changes abruptly from atmospheric to the insitu gas pressure (refer to Fig. 3.2). If the stratum is sheared, it is assumed that the gas will escape from it instantaneously and there is no gas pressure in the shear zone. After specifying a pre-existing shear zone or resulting the shear zone from the previous calculation, the step distribution of the gas pressure moves towards the inside of the strata.

Based on the assumption of the gas pressure distribution described above, there are two aspects about the gas pressure to be considered in FEM formulation of the model. One aspect is concerned with the gas pressure as one component of the effective stresses while calculating the stress distribution around the opening. In fact, this aspect has been completed during generalized formulation of the governing equation in section 6.1.1. From Eq. (6.16), the gas pressure, in terms of the effective stress concept, can be readily treated as an extra loading term. It can be evaluated by Eq. (6.21) which is rewritten here for the sake of the clarity:

$$\{P_{gp}\}_e = \int_{V_e} [B]^T p \{L\} dV.$$

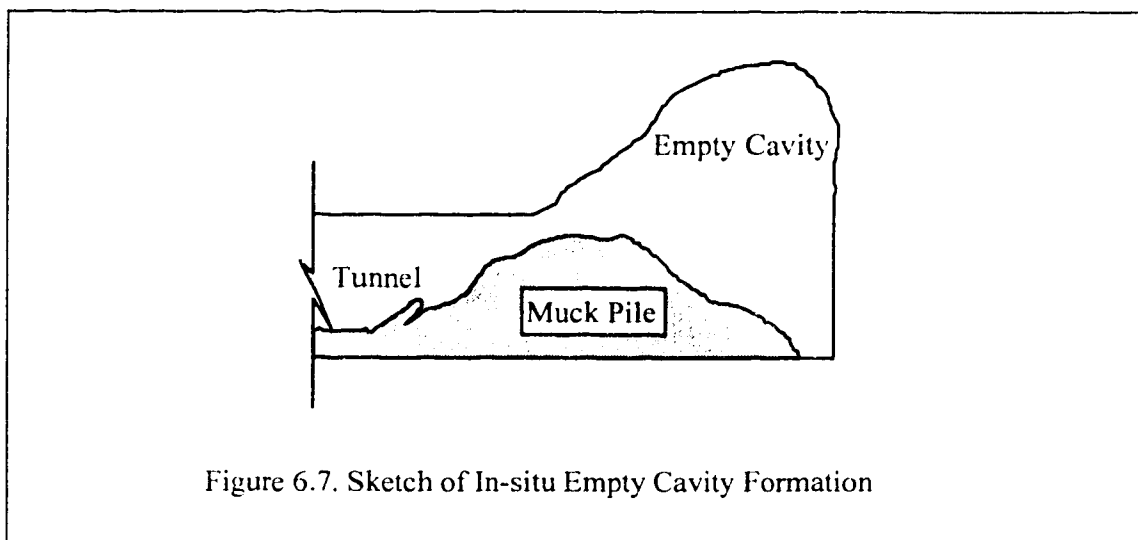
Another aspect for handling of the gas pressure in the model relates to the degassing process assumed. This consideration will be given to the sheared zones, i.e., those elements failed in shear mode. Experience and experiments have shown that the permeability of intact rock will increase as it fails in shear. The flow of the gas in these zones will be much easier. The model assumes that instantaneous degassing in these zones occurs. This instantaneously degassing is simulated mathematically by applying an equal but opposite gas pressure loading to those sheared elements in the next iteration. The loading forces, therefore, can be readily calculated as follows:

$$\{P_{gp}\}_e = \int_{V_e} [B]^T (-\rho)\{L\}dv \quad (6.47)$$

These nodal forces, together with those resulting from removing the tensile failed elements, will act as the external forces for next iteration.

6.4.5 "Excavation" of the material

According to assumption 4). in section 6.3, the tensile failed elements should be removed from the system. The observations of the outbursts in situ reveal that there are basically two physical processes involved in association with the failed rock being removed. In most cases, the rock failed in tension may receive very high energy of motion transmitted from high potential energy stored in compressed gas and from the strained solid rock such as elastic energy. It is this energy that transports the broken rock for some distance before it piles up in the open space available. In addition, gravity may also contribute to the transportation. The broken rock, therefore, piles up a distance away from the spalling surface and provides virtually no support to it. This situation can be schematically illustrated in Fig. 6.7.



In contrast to this situation, the broken rock may not obtain enough energy to be transmitted far from the spalling surface. It will quickly pile up at the front of the spalling surface and provide back support to it. The sketch of this situation is illustrated in Fig.

6.8. Strictly speaking, this situation is more fictitious than reality. Even though the broken rock piles up right in front of the surface, the back support can be trivial. When considering the "choke up" case reported by Gray (GRAY, 1981) and other discussions about the factors bringing about the end of an outburst event (GOLDER ASSOCIATES, 1987), this filled cavity formation may describe some extreme situations in situ.

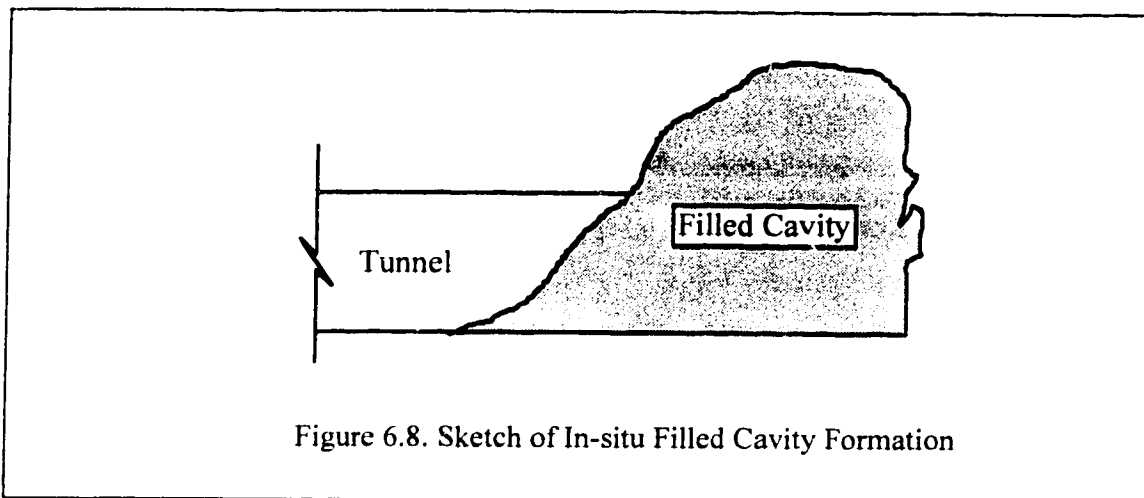


Figure 6.8. Sketch of In-situ Filled Cavity Formation

Any situation between previous two base mechanisms may happen in practice. In fact, they are more likely to take place in one process. At the beginning of the spalling, the broken rock is transported away and does not give any back support. As the spalling progresses, previously piled up rock restrains the further transportation of the spalled rock. Due to the swelling of the rock, the empty space between spalling surface and muck pile is filled up rapidly until the mechanism shown in Fig. 6.8. becomes effective and "chokes up" the outburst. However, this transition process imposes some difficulties on mathematical and numerical simulation because of unpredictable condition to control the transition. The two base mechanisms simplify the problem and make it possible to simulate numerically.

There are many approaches to achieve "excavation" of certain elements from the element system with finite element method generally. In order to simulate the above two described base mechanisms by one program, the model adopts the approach of reducing the Young's modulus of the "removed" elements to a very low value or to a specific prescribed value. The procedures of simulation follow the general method for analysis of geometrically altered structures revised by Ghaboussi and Pechold (GHABOUSSI, 1984).

According to the analysis method, if \bar{P} expresses the nodal external load vector and \bar{I} is the internal resisting force vector that can be computed from element stresses as:

$$\bar{I} = \sum_{i=1}^{ele} L_i^T \int_V B_i^T \sigma_i dv \quad (6.48).$$

The residual load vector \bar{R} can be calculated as:

$$\bar{R} = \bar{P} - \bar{I} \quad (6.49)$$

When the elements and their associated external loads and internal stresses are removed from the element system at the beginning of increment n , the standard nonlinear formulation of FEM will apply as long as the load vector is modified appropriately to take account of the initial disturbance and inequilibrium due to altering the system. This modified residual load vector \bar{R}_n^* can be computed by:

$$\bar{R}_n^* = \bar{P}_{n-1} - \bar{I}_{n-1}^* \quad (6.50)$$

Where, \bar{P}_{n-1} indicates all the effects of external loads at increment $n-1$, which is regarded as unchanged when the system geometrically changed at the beginning of increment n . \bar{I}_{n-1}^* is assembled from elements' contributions computed from stresses σ_{n-1} existing at the end of increment $n-1$ as Eq. (6.48). It counts for the change because the elements removed from system will no longer contribute to the internal resisting force vector. The load vector, revised by removing elements, therefore, can be expressed as:

$$\bar{R}_n = \Delta \bar{P} + \bar{R}_n^* = \bar{P}_n - \bar{P}_{n-1} + \bar{P}_{n-1} - \bar{I}_{n-1}^* = \bar{P}_n - \bar{I}_{n-1}^* \quad (6.51)$$

Particularly in this model, \bar{P}_n will be zero because the elements are removed only after the system has been equilibrated and the tensile failed elements have been selected. Denoting \bar{I}_{n-1} to the internal nodal force vector without removing the elements, and \bar{I}_{n-1}^* to the internal nodal force vector after removing the elements, then, \bar{I}_{n-1}^* is obtained from:

$$\bar{I}_{n-1}^* = \bar{I}_{n-1} - \bar{I}_{n-1} \quad (6.52)$$

The mathematically detailed derivation of the general method for geometrically altered structure is provided in Appendix A.

Another problem for the geometrically altered structure is concerned with the "deactivation" or "activation" of element in the system. This model only involves "deactivation". In the beginning of this section, the removal of elements from the system is designed by assuming a very small Young's modulus for the empty cavity situation and by assuming a particular small Young's modulus for the filled cavity situation. A very small Young's modulus will result in very small stresses or very large strains in an element, because the stiffness of the element is always proportional to this value. Therefore, instead of totally disassembling the element's contribution, the element to be deactivated is assigned a specific Young's modulus, very small or a specific value. The contribution from the deactivated element has not been omitted from the assembly of the governing equations, but is controlled by the given Young's modulus, so that the contribution becomes so trivial as to be ignored, or can be controlled. The stiffness matrix in the governing equation will be calculated in each iteration.

6.5 Model Operation

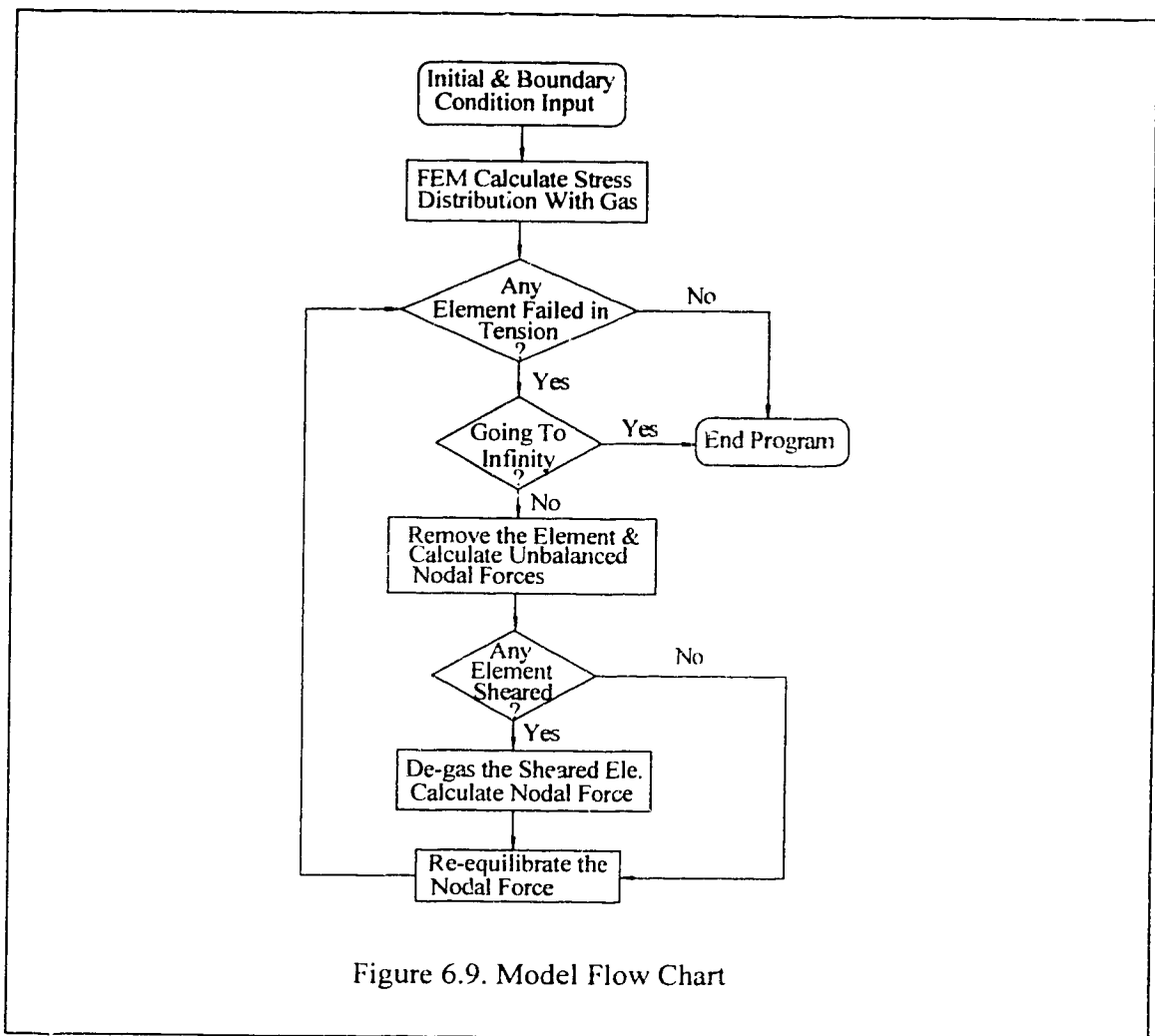
The model may operate on any computer, except that the pre-processor and post-processor only operate on IBM personal computer compatible machines. A large capacity computer is preferred to run the model because a fine mesh arrangement for the gas contained rock leads to more reliable results. The present program is designed to handle 1,500 elements, thus matches the upper limit for the pre-processor and post-processor. The model itself can easily be expanded to handle more elements and only limited by what the pre-processor and post-processor can deal with. The preparation of input data and interpretation of output data without assistance of pre-processor and post-processor can be time consuming and confusing.

6.5.1 Model sequence

The model is composed of three parts: the pre-processor, FEM model program and the post-processor. The three programs can execute individually or by using a batch job arrangement. The pre-processor and the post processor will be introduced briefly in next section, while the FEM model program is described below.

Fig. 6.9 shows the simplified logical flow diagram for FEM model program. There are two distinct functional package program subroutines fulfilling every task in the

diagram. One package realizes the calculation of the finite element method. The mathematical formulations incorporated in this program follow the discussion in the previous section. The program is able to handle the gas pressure for effective stress calculation under any given conditions. A patch test has been conducted to validate this program as shown in Appendix B. The second package of the program routines functions by identifying the elements failed in shear and tension and in retaining or removing them accordingly. The incorporation of the degassing sheared elements and the removing of tensile failed elements into the FEM program has been mathematically formulated previously.



The shear failure criterion is an inherent consideration of FEM program (assuming that a yield element has been sheared). The failure criterion for tension uses the direct comparison of the stress and strength (i.e., $\sigma_3 \leq \sigma_t$, σ_3 is the minor principle stress and σ_t is the tensile strength of the rock). Alternating between these two packages accomplishes the modeling process. The logic flow diagrams for these two programs are listed in Appendix C. The modeling is carried out by following the steps:

1). The given required boundary conditions, external loading conditions and gas pressure information are prepared as input data; and the revised FEM program is used to calculate the stress distribution around the initial underground excavation.

2). Each element is then examined to test whether it has failed in tension, in shear or has not yet failed. If no element has failed in tension within the gas bearing stratum, the program terminates, either not initiating an outburst or stabilizing at some specific size cavity. Otherwise, the program carries on to the next step.

3). Those elements failing in tension are "removed". This change in geometry of the study domain causes a redistribution of stresses that can be computed by the general method (Eq. 6.51) in the next iteration. Those elements failing in shear (yielded) are degassed. The resulting external loading forces computed from Eq. (6.47) will also participate in calculation in the next iteration.

4). The nodal forces induced from "removing" and "degassing" elements, calculated from Eq. (6.51) and Eq. (6.47), unbalances the forces in the element system. FEM program iterates to re-equilibrate these unbalanced forces so as to produce the redistributed stress field around the new cavity formed through the spalling. The spalling includes both removing and degassing processes in this context.

5). Step 2), 3) and 4) successively iterate until it terminates at a stabilized cavity or is deemed to carry on indefinitely.

The final result from the modeling, therefore, falls in one of the following three categories:

- 1). outburst not initiating (program terminates at first iteration);
- 2). forming a stabilized cavity (program ends after more than one iteration);
- 3). outburst carrying on indefinitely (program ends after many iterations).

These three results accommodate all possible consequences of an outburst in practice. The third result can be interpreted as the situation that the outburst can not cease if no other mechanisms are introduced by the given field conditions, such as the change of lithology.

6.5.2 Inputs for the model

There are two direct input data files prepared for the FEM model; one of them can be prepared through the pre-processor, while the other one is prepared manually. To start the modeling, three data files should be initiated, which contain element information for tensile and shear failure and the information of the nodal points currently removed.

One of the direct input data files, FEOMPIN.DAT, includes all information for conventional FEM program. This file comes from the pre-processor that is composed of two programs, "MSHGEN" and "EPFEC". MSHGEN is a mesh generator that produces finite element output data, which can be graphically expressed and edited by "SAP2D" and "MSHPLT" that are part of the pre-processor. The input data for MSHGEN is GENIN.DAT; the output data is GENOUT.DAT. Program EPFEC merges the finite element information with other material information to produce FEMOPIN.DAT. Samples of the format for these files are found in Appendix D.

Another direct input data file contains the insitu gas pressure information. This file is prepared manually. The format of this file is illustrated in Appendix D.

Three data files to be initiated are TENFAL.DAT, PLTFAL.DAT and FNPRM.DAT which can be initiated simply (refer to Appendix D). The relations among all input data files and between programs can be clearly explained in Fig. 6.10.

6.5.3 Output from the model

Two files output from the modeling in each iteration; they are FEOMPRT.DAT and EPFEOUT.DAT. The file FEOMPRT.DAT is a printing file which lists all results of the FEM calculations. The latter file is used as the input file for the post-processor which may graphically present the results for this iteration. The iterations the model may execute depend on the given conditions. The model is designed to retain all results from each iteration so that the post-processor can plot them out to show the progressive spalling process. Both print output and graphical output can be found in Appendix D as an example.

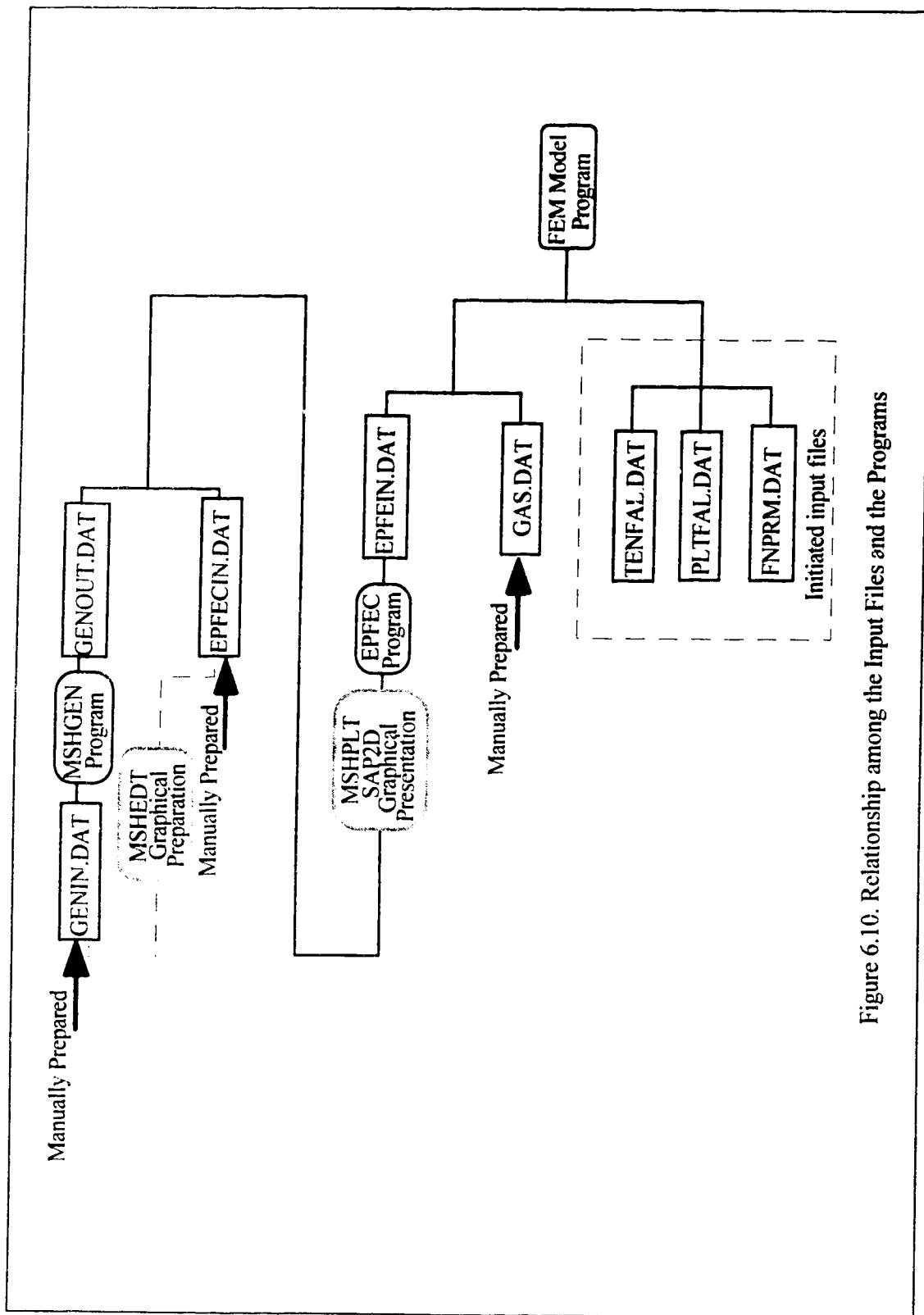


Figure 6.10. Relationship among the Input Files and the Programs

6.6 Sample Run Of Model

This sample run of the model makes use of one of its applications to the entry development given in next chapter. It is used here to demonstrate the procedure in running the whole model. The first step is to analyze the available information. The analysis should define the cross-sectional shape of the heading. The area within the rock mass around the excavation is then selected for division into a number of interconnected model zones which are required by pre-processor for proper discretization. A large area is not required since the only region of interest is where the gas bearing stratum is exposed to or near to the opening, provided that the influence of boundary restraints on the stress distribution is properly considered. The input data files then are prepared and the pre-processor is applied to output the input data file for the model. The program FEOMP.EXE that integrates the FEM program and the general method program is executed to start the simulation. After the simulations are completed, the post-processor can be used to present results graphically. All results are numerically recorded in output file FEOMPRT.DAT. Sample files are given and explained in Appendix D.

Chapter VII

APPLICATION OF MODEL TO A DEVELOPMENT ENTRY

From the review of outburst occurrences through out the world, it is known that the majority of outbursts occur in development entries in coal mines, usually at the entry headings which are driven into the virgin rock containing gas. The application of the model to this scenario, therefore, is obviously important for validation of the model and for practical usage. However, most case histories lack the detailed information and necessary data to allow them to be modeled. The last two outbursts at No. 26 Colliery are exceptions, as the mine first mapped the cavities formed and a series of investigations associated with the outbursts have been carried out. The data for application of the model are available. Because of this, these two outbursts will be used as cases to test the validation of the model.

7.1 Introduction to Outbursts in No. 26 Colliery

The outburst events at No. 26 Colliery started in the summer of 1977 when the workings reached a depth of 700 meters below the sea level. Since that time, 37 outbursts had been described as rock outbursts. Shortly after these outbursts, a fire caused the closure of the mine in April 1984. During this period, the frequency and intensity of outbursts increased with the depth. Prior to June 1983, gas was neither detected, tested nor recorded after the rock outbursts. In the later events, however, a large volume of gas was detected after each initiation. The detailed characteristics of each outburst from No. 26 Colliery were summarized in Table A.1 of his thesis by Kullman (KULLMAN, 1989) and also reported by Golder Associates (GOLDER, 1987).

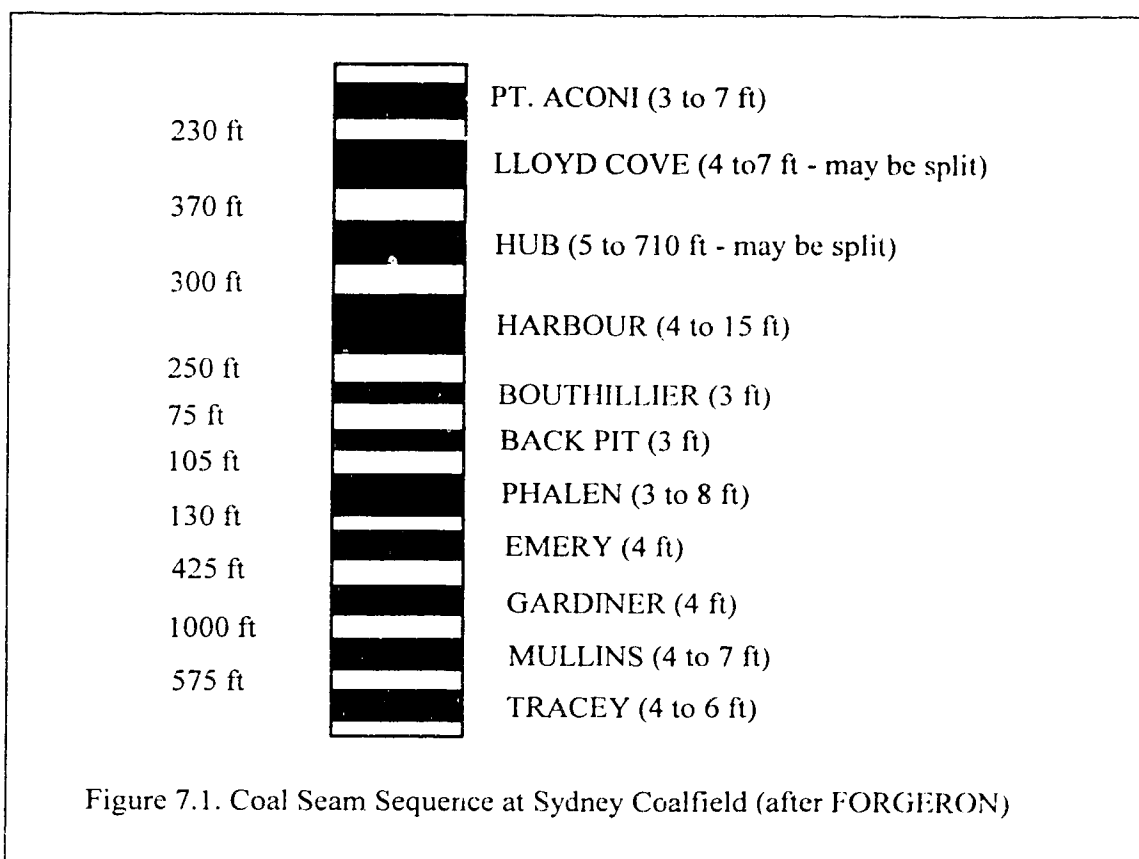
The outbursts occurred exclusively in the development entries when driven into virgin coal where the sandstone erosion channel was located within 2.5 meters above the top of the coal seam. The bursting formation was invariably sandstone, sometimes with siltstone inter-beds. The failure face exposed within the outburst cavities was typical of a surface resulting from shear failure. The failed material was generally pulverized or in small flakes, leaving an "onion skin" texture within the cavity.

The outburst problem in the mine became a subject of considerable practical and research interest at that time because of the influence on the mine itself and the possible significance to the other operating mines or future mines in the Sydney Coalfield as they

would reach similar depths where the similar conditions might be encountered. Field and laboratory data related to the outburst events were collected and compiled by both CBDC (Cape Breton Development Corporation) and CANMET (Canada Center for Mineral and Energy Technology). This information and data will serve as the basis of this modeling application.

7.1.1 Geological features related to outbursts

The Sydney coal field is located in Nova Scotia along the northern coastline of Cape Breton island. It consists of the on-land and near-shore portion of a submarine carboniferous Basin. Eleven coal seams have been identified in the field, while six of them are considered to be economically minable. Fig. 7.1 depicts the sequence of the eleven seams. All these seams dip gently under the Atlantic Ocean. The coal field has hardly been disturbed tectonically. The major faults have little effect on mining operations.



#1B/26 Colliery was one of oldest coal mines operating in the Coalfield. It was developed in the Phalen seam at the beginning of mining. The Harbour seam was developed later and was worked until the mine closed. Presently, the Phalen mine is the only one in operation as a close neighbor mine to No. 26 Colliery after the Lingan mine was flooded last year. The Phalen mine is about to reach the same depth as No. 26 colliery where outbursts took place. As similar conditions may be encountered, outbursts might be expected in the mine. This has resulted in the initiation of a program to monitor the possible rock outbursts by the Cape Breton Coal Research Center, CANMET. Modeling of No. 26 Colliery's outbursts has obviously great significance for Phalen mining operation.

The major geological feature related to outbursts at No. 26 Colliery was the sandstone Paleo-river channels developed within the seams and in close proximity. It is believed that the sandstone intrusions are an infilled Paleo-river which eroded and migrated across the alluvial plain sometime shortly after the deposition of peat. The presence of the channels in the Coalfield is unpredictable before they are encountered in mining operations. Five of these sandstone channels were identified during the life of No. 26 Colliery operations. Outbursts were recorded at each of these locations. Because of the limited width of these channels, the integrity of roof strata above the seam has been destroyed completely where an intrusion appears. The interface between this sandstone channel and siltstone or mudstone formations always constitutes a weak bedding plane along which rock immediately separates when coal is removed.

7.1.2 Mining operation at No. 26 Colliery

All outbursts occurred in the Harbour seam, which was mined by the longwall advancing face method. The longwalls advanced in the strike direction and were serviced by rib gate roads. Full caving was allowed in the gob area. Development roadways, usually including deeps, gate roads and coal face developments, were driven by the drill and blast method and supported by various sized arches. These entries were all driven in the coal seam. The floor of entries was consistent with the floor of the coal seam, while the roof usually intruded into the immediate hanging wall of coal seam. The outbursts occurred in those places where the sandstone became the direct hanging wall or was in close proximity. All but one outburst were initiated after shot firing. One rock outburst took place when workers were preparing the heading for firing.

7.1.3 Geotechnical properties of rocks

Laboratory tests on rock cores from No. 26 Colliery were undertaken in the Rock Mechanics Laboratory of MRL, CANMET. The uniaxial and triaxial compressive strength of sandstone and siltstone were determined and the Young's modulae were calculated. Two sets of tests on the different borehole cores were carried out by CANMET and by Golder Associates. Core from borehole D-164 was retrieved from the 14 south coal roadway after the occurrence of the last two outbursts, and was tested in laboratory by CANMET. The rocks from the core were tested to measure tensile strength (by Brazilian test), uniaxial compressive strength, elastic modulus and Poisson's ratio. In early 1985, another borehole D-165 was drilled in vicinity of D-164 and tested to determine:

1. the behavior of rock under dynamic loading (stress change) around underground openings;
2. the effect of pore gas pressure on the rock strength and mode of failure under various stress conditions;
3. the failure behavior under very fast stress changes.

Rock Strength and Deformation Properties

Table 7.1

Rock Type (data source)	σ_c (MPa)	σ_t (MPa)	E (GPa)	μ	γ (Mg/m ³)	η (%)	k(g) (mdarcy)
SANDSTONE (CANMET)	59.3	7.7-8.0	16.5	0.09	N.A.	0.8	0.01
SANDSTONE (Golder Associates Report No. 841- 1287 and 831- 1296)	49.0	N.A.	13.1-17.5	0.2	2.6	2	N.A.
SANDSTONE (Aston and Cain, 1985)	60-100	2.6-8.0	12.0-20.0	0.09-0.28	N.A.	4.5-5.5	0.02
SILTSTONE (CANMET)	82.3	N.A.	25.8	N.A.	2.7	N.A.	N.A.

Notes: σ_c =Uniaxial compressive strength μ =Poisson's ratio σ_t =Tensile strength γ =Bulk density

E=Young's modulus

 η =Porosity

k(g)=Gas permeability

In addition to these tests done on core retrieved directly from No. 26 Colliery, many laboratory experiments were conducted on the specimens collected from the neighboring mines, such as Lingan mine. The data of strength and deformation properties from the work by CANMET and Golder Associates Ltd. are presented in Table 7.1.

The coal properties are available but were ignored in the model because, in the model, the coal seam was replaced by siltstone and siltstone properties were used. This replacement of the coal seam by siltstone demands some explanation.

In the field, it was only the overlying sandstone which contained high pressure gas. Although the coal seam contained some gas, it was not under high pressure. Further, no outburst or other failure occurred in the coal around the entries. Hence, it was believed that as long as no failure occurred in the coal, the model would be a good representation of the field situation. By replacing the coal seam with siltstone, the model could be simplified (reducing the number of different material from 3 to 2 and speeding up convergence). It was thought that this should not have a major effect on the results because all failures were confined to the sandstone due to the presence of the high pressure gas.

7.1.4 In situ gas properties

The data and information about the gas contained in the sandstone are relatively limited for No. 26 Colliery. At the beginning, gas was completely ignored in observation and recorded unintentionally. Substantial volumes of gas released from outbursts were detected between 1981-1984. The gas pressure in the sandstone was investigated by different methods. Due to the low permeability of the sandstone formation, reliable data has not been obtained. Estimation can only provide a guide line for application in the model.

Constant head permeability tests on sandstone were conducted by CANMET (GORSKI, 1984). The permeability of the sandstone is approximately 500 nano-darcies and even lower for the siltstone. With such a low permeability, it is very difficult technically to measure the gas pressure directly in situ.

Nevertheless, one test for gas pressure measurement was conducted from a borehole in No. 26 colliery (GALLANT, 1985). The in situ measurement took place in the coal pillar separating the main and belt development deeps at the deepest extent of the workings. The bore hole, drilled parallel to the main deeps and intersected with 0.56 m sandstone, was installed with a packer system. Installation was done immediately after

completion of drilling. Two inflatable glands sealed a bore hole section in the sandstone and was pressurized to 7.93 MPa. This sealed chamber was then left to equalize with the in situ strata pressure. After 5 days, there was no discernible pressure increase in the test chamber. Nitrogen was then injected into the sealed chamber to hasten equilibrium condition after the previous frustration due to very low permeability of sandstone. The chamber was pressurized to 3.45 MPa. Eight days after initial pressurization, the pressure in the chamber decreased to 2.62 MPa before a 2.76 MPa pressure was observed on 17th day. Throughout the remaining test period (test ended on 45th day after packer installation) this pressure remained constant. This equilibrium pressure of 2.76 MPa obtained from this test approximated quasi-steady state condition, whereby the volume of gas lost by leakage along the seal equaled the volume of gas released by the strata. It is believed that this gas pressure represents the minimum strata gas pressure.

Shortly after this in situ test, Aston (ASTON, 1985) undertook a back analysis to get a theoretical estimation from the obtained data from the last two outburst events. The analysis used the general gas and Darcy equations to calculate the in situ gas pressure. It estimated a gas pressure of 4.6 MPa and 39.1 MPa respectively for events No. 36 and 37. Aston and Cain (ASTON, 1985) worked out the gas pressure value of 7.9 MPa by using the hydrostatic water column, a reservoir engineering "rule of thumb". According to the discussion between the engineer of Golder Associates Ltd. and the officials of the Nova Scotia Department of Mines and Energy, the correlation appeared to be 10.7 KPa/meter of depth (GOLDER ASSOCIATES, 1987). This will give a gas pressure of 8.5 MPa at a depth of 790 m, according to the "rule of thumb". Paterson (PATERSON, 1986) proposed a general correlation of 23 KPa/meter of depth below the surface to evaluate the initial gas pressure. By applying this correlation, a 18 MPa initial gas pressure can be obtained for the mine 790 m below the surface.

By assuming errors that inevitably occurred in the in situ test and the estimations made above, Aston and Cain (ASTON, 1985) stated that the most likely range of values for the gas pressure in No. 26 Colliery would be 2.8 MPa to 7.9 MPa. In this modeling application, this value range is assumed.

7.1.5 In situ field stresses

Some in situ stress measurements were carried out by the overcoring method in vicinity of the last two outbursts. Three boreholes were used. Two of them were drilled in the siltstone formation above the coal seam, one penetrated into the sandstone that overlay this siltstone formation. US Bureau of Mines (USBM) deformation gauges were

installed, 120° apart in radial direction, to measure borehole deformation during overcoring. The cores retrieved from these boreholes were tested in laboratory to determine the elastic modulus of the rocks. The field stresses calculated from the tests are listed in the table 7.2.

In Situ Stresses from Overcoring Tests Table 7.2

Stress Components	Magnitude (MPa)	Orientation	
		Bearing	Dip (up)
σ_x	23.31	E-W	Horizontal
σ_y	24.98	N-S	Horizontal
σ_z	25.27	Vertical	
σ_1	26.30	Due west	-25°
σ_2	23.20	N82°W	64°
σ_3	24.05	N9°E	-13°

Kullman (KULLMAN, 1989) found a number of reasons to question the above results from in situ tests. Due to the influence of roadway opening, the stress disturbance became the source for the error as the tested area did not reach the original stress region. A boundary element program was used to simulate the testing condition. It gave the re-evaluated original stresses as:

$$\sigma_1 = \sigma_x = 26.3 \text{ (MPa)}$$

$$\sigma_3 = \sigma_y = 24.0 \text{ (MPa)}$$

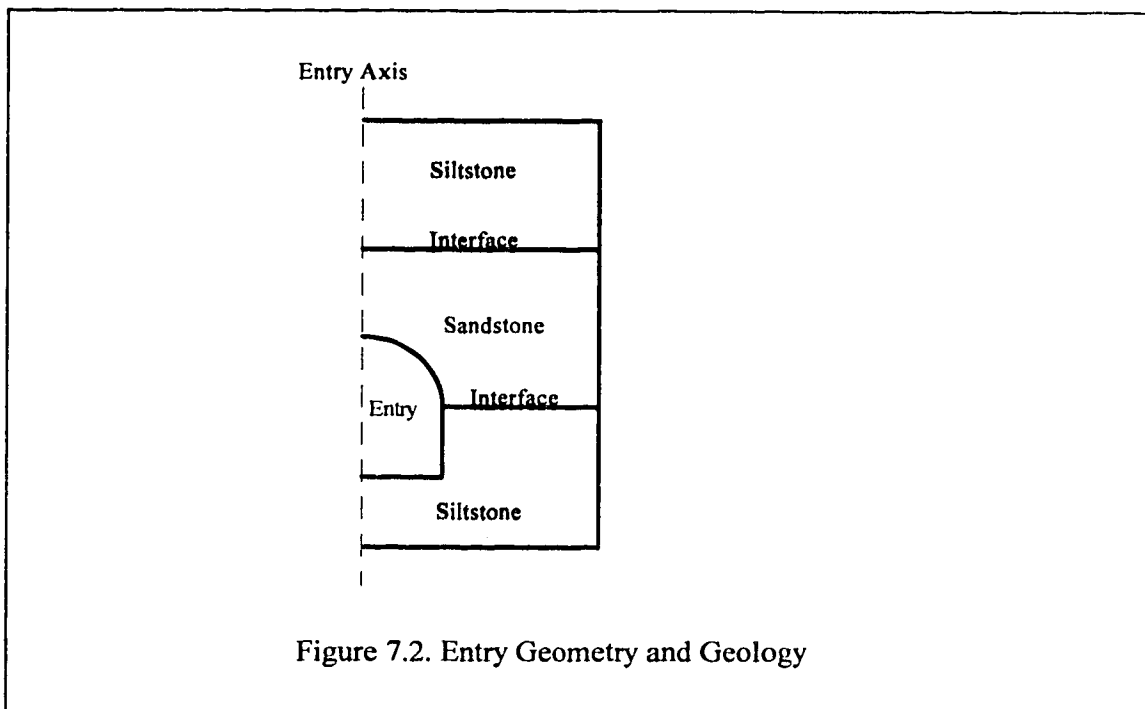
where, x and y are the horizontal and vertical direction. The stress ratio between the two principle stresses is in accordance with the in situ test results, but the orientation has been altered. Considering the other questionable factors, the horizontal and vertical stresses are assumed to be 25 MPa and 23 MPa for last two outbursts in No. 26 Colliery.

7.2 Initial Conditions for the Modeling

Based on the above data obtained from various sources, the initial conditions are postulated for the model applications. This is because the determinate solution requires specific value of inputs while some of the tests gave a range of values. Some conditions have to be numerically interpreted so that they can be used as input data, such as the exposed area of sandstone to the entry opening.

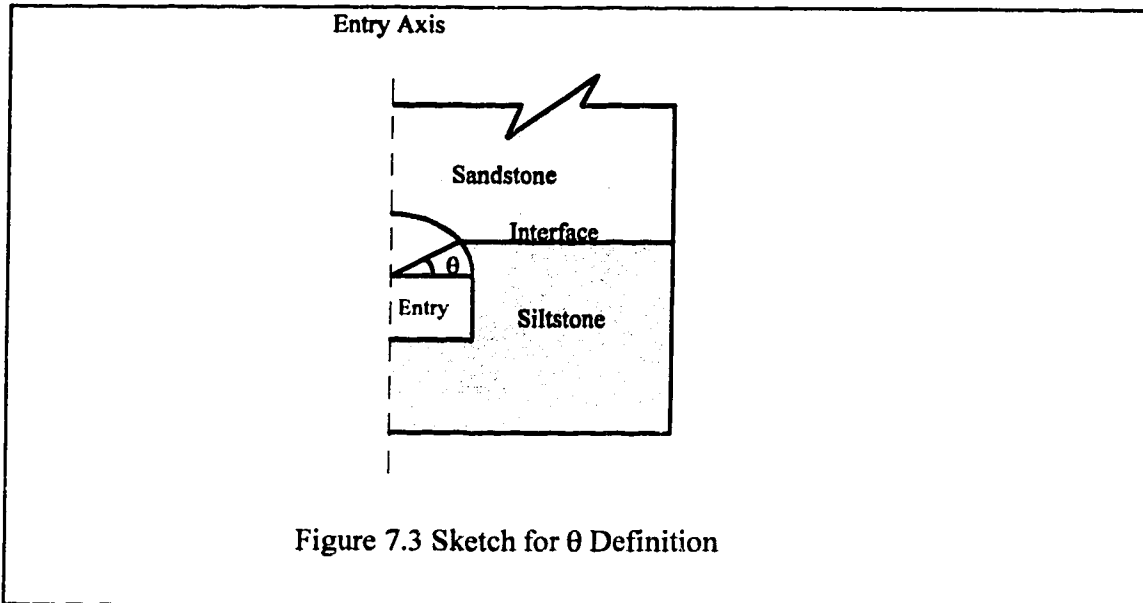
In No. 26 Colliery, the entry in which outbursts took place was always driven in the coal seam with the floor following that of the coal seam. The underlying formation below the coal seam is siltstone. Wherever the outbursts took place, sandstone was

present in the roof strata. The sandstone channel may directly overlie the coal seam, but frequently siltstone partings lie between the coal seam and the sandstone channel. The sandstone channel thickness varies in a range that was difficult to determine before outbursting. On top of sandstone channel a massive siltstone was found over all the mining zone. This geological layout has been simplified as shown in Fig. 7.2. The coal seam is replaced by siltstone so that the entry is located in siltstone, with the crown penetrating into the sandstone which, in turn, is overlaid directly by the siltstone. The model was, therefore, composed only of siltstone and sandstone. The entry geometry was simplified to be composed of a rectangular excavation at the bottom and a semi-circular shape of excavation at the top part. The entry width is 4.5 m and the wall height is 2.0 m. The semi-circle has a radius of 2.25 m. The simplified geometry of the entry, and geology around it are sketched in Fig. 7.2.



To simulate the situation where the sandstone is not fully exposed to the entry width, a so-called "exposure angle" is defined as shown in Fig. 7.3. When the angle (θ) varies from 0° to 90° , the sandstone area exposed to the entry changes from full entry width to very small until it is completely unexposed when $\theta = 0^\circ$.

The modeling area was selected as 30 m wide and 60 m high. Since the entry is symmetrical about the entry axis, only half of the layout will be studied in the modeling application. The boundary condition is set up as a typical plane strain symmetrical problem. A stress field, with a given stress ratio, is applied uniformly along the right and top side while proper restraints are set along the left and bottom side of the selected modeling area.



The elasto-plastic properties and rock strength parameters assumed in the modeling application are listed in Table 7.3 on the basis of in situ measurements and laboratory tests. The friction angle and cohesion of the rocks are derived from the triaxial strength test data collected by Kullman. Hoek & Brown's constants m and s were determined by the least squares solution of Hoek and Brown by Kullman.

Elasto-Plastic Properties and Strength Parameters of the Rock Table 7.3

Elasto-plastic properties	Young's Modulus E (GPa)	Poisons Ratio μ	Friction Angle ϕ ($^{\circ}$)	Cohesion c (MPa)
Siltstone	26.15	0.36	35	20
Sandstone	18.5	0.18	30	18
Strength parameters	Uniaxial Strength σ_c (MPa)	Tensile Strength σ_t (MPa)	H&B Const m	H&B Const. s
Siltstone	50.5	-11.4	4.2	1.0
Sandstone	48.4	-2.9	14.9	1.0

With above postulated conditions, the model was first applied to the last two outbursts at No. 26 colliery for verification. A set of parametric analyses were then conducted to investigate the influence of various parameters on outburst initiation and propagation. Through these analyses, the model is further tested by the reasonable results obtained from model. The results may then be used to attempt prediction, and to assist in evaluating the preventive measures.

7.3 Verification of the Model against In Situ Observation

The cavity formed in the last two outbursts at No. 26 Colliery was mapped in longitudinal direction and at ten cross sections. Fig. 7.4 exhibits the longitudinal and cross sections selected for verification. Three cross sections were selected for this purpose because they have different areas of sandstone exposed over the crown of the entry. The mapping was done when the cavity was repaired with timber cribbing support. This cavity, therefore, had stabilized itself at that time, and it is called a "stabilized cavity". These cavity maps allow the verification to be realized by comparison with the model results.

Under the initial conditions postulated in the previous section, a stress ratio of 1.1, representing the in situ measurement, was used to simulate the stress field with vertical stress of 23 MPa and horizontal stress of 25 MPa. The exposed area of sandstone to the entry opening was controlled by the exposure angle defined in previous section. The conditions for the modeling were specified as following:

Modeling area:	60 m (high) × 30 m (wide);
Geology in area:	refer to Fig. 7.2;
Entry geometry:	4.5 m (wide), 2.0 m (wall height), 2.25 m (radius of semicircle);
Stress field:	$\sigma_v=23$ (MPa) $\sigma_h=25$ (MPa);
Stress ratio:	1.1;
Sandstone height above the crown:	3.8 m (12.5 ft);
Sandstone and siltstone properties and strength:	refer to Table 7.3;
Exposure angle:	$\theta=0^\circ, 25^\circ, 45^\circ$;
Gas pressure:	3.0 (3.4) MPa (determined by trial runs).

A number of trial runs were conducted for each exposure angle by using different gas pressures and the stabilized cavity resulting from modeling was compared with that from the selected cross sections. Those modeling results, one from each exposure angle

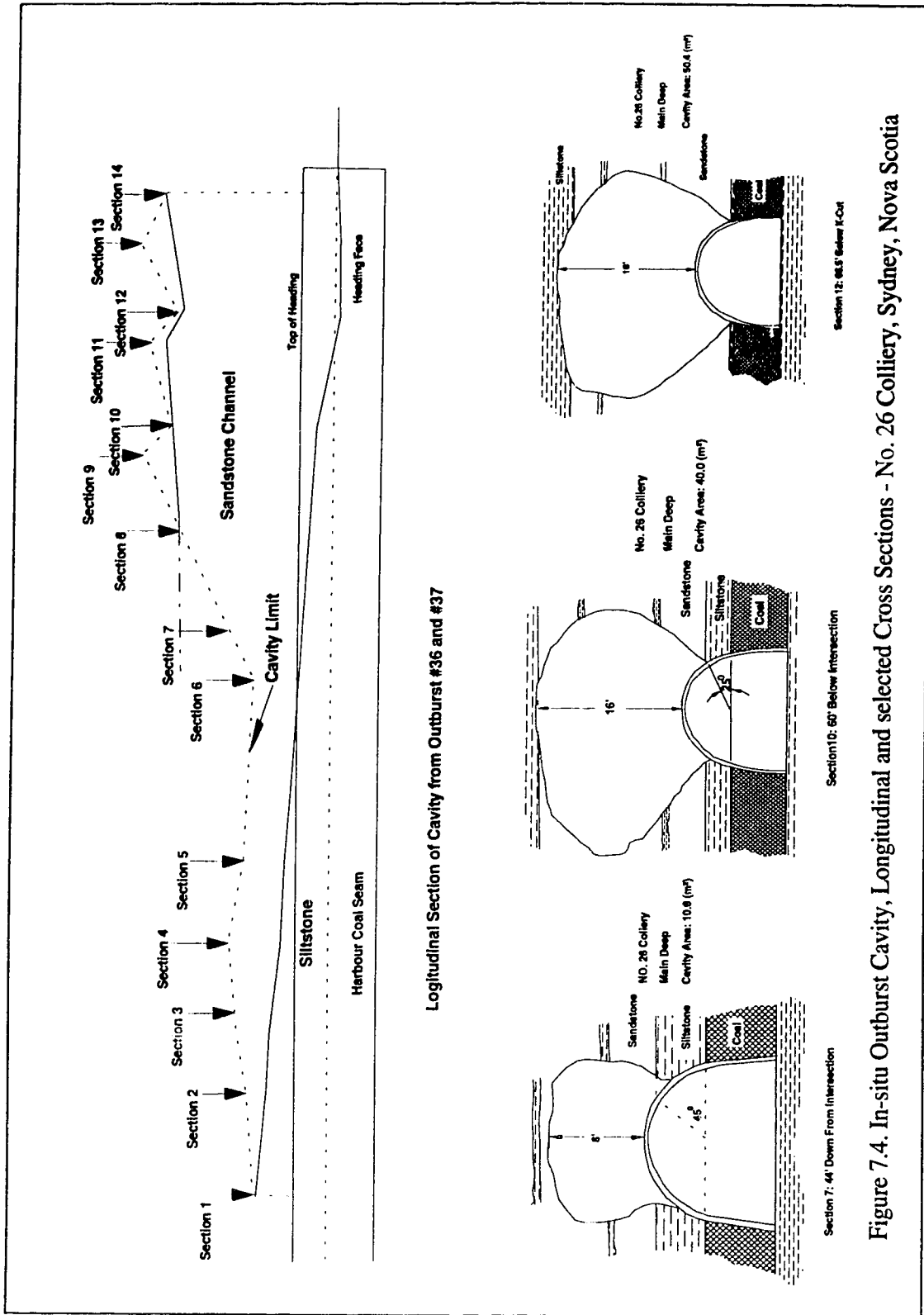
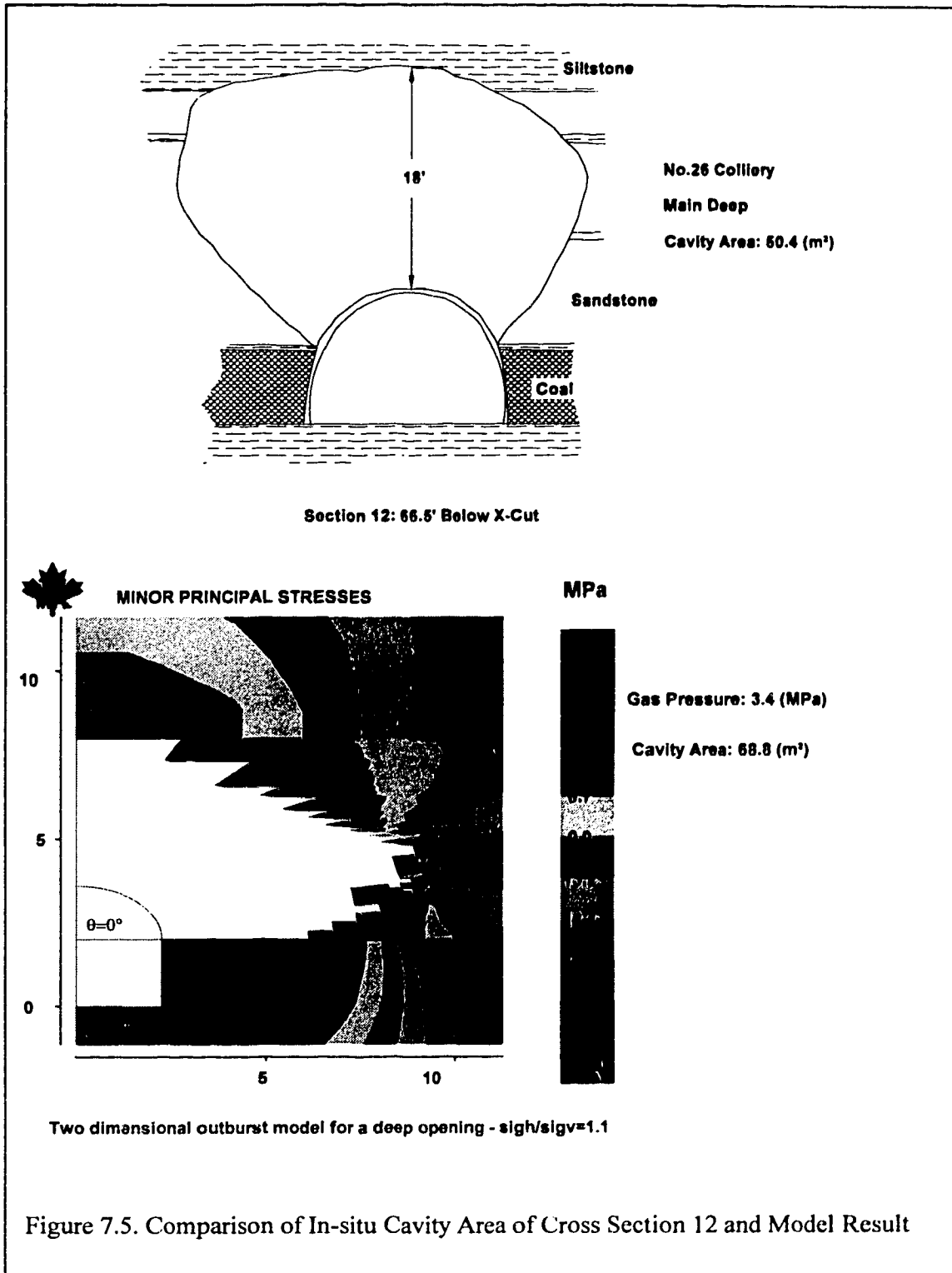


Figure 7.4. In-situ Outburst Cavity, Longitudinal and selected Cross Sections - No. 26 Colliery, Sydney, Nova Scotia



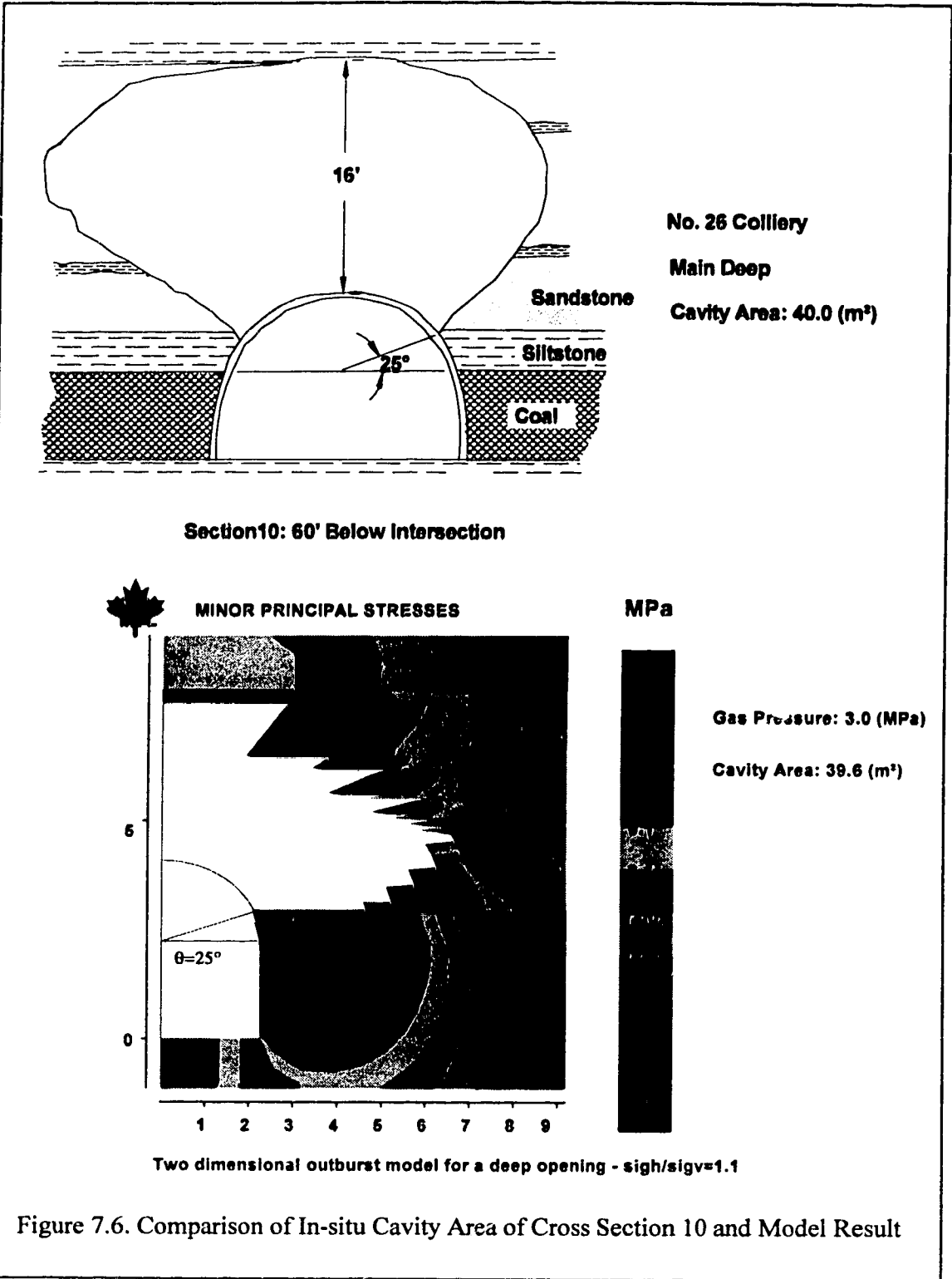
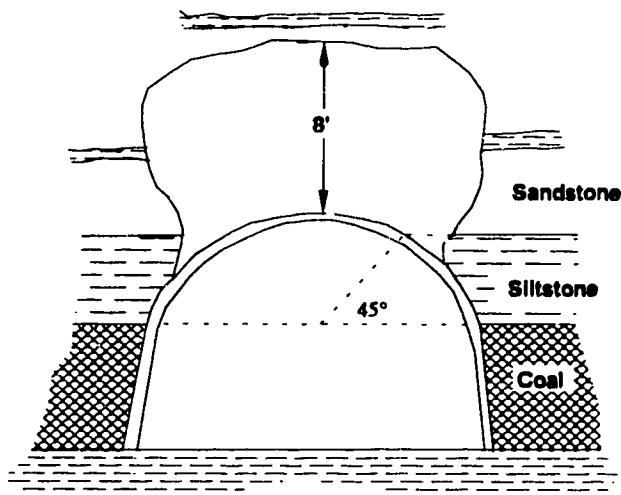
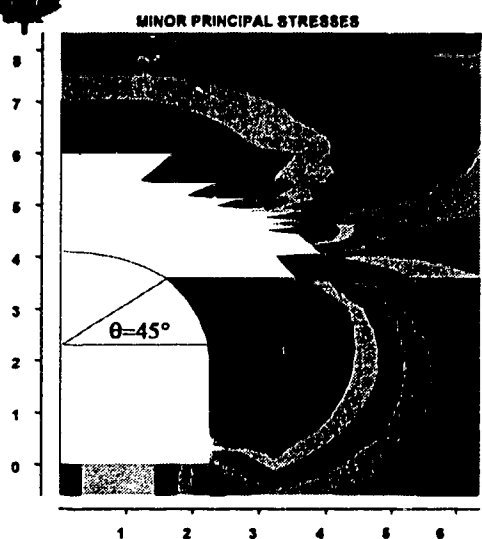


Figure 7.6. Comparison of In-situ Cavity Area of Cross Section 10 and Model Result



NO. 26 Collery
Main Deep
Cavity Area: 10.8 (m²)

Section 7: 44' Down From Intersection



MPa



Gas Pressure: 3.0 (MPa)
Cavity Area: 12.2 (m²)

Two dimensional outburst model for a deep opening - $\sigma_{gh}/\sigma_{gv}=1.1$

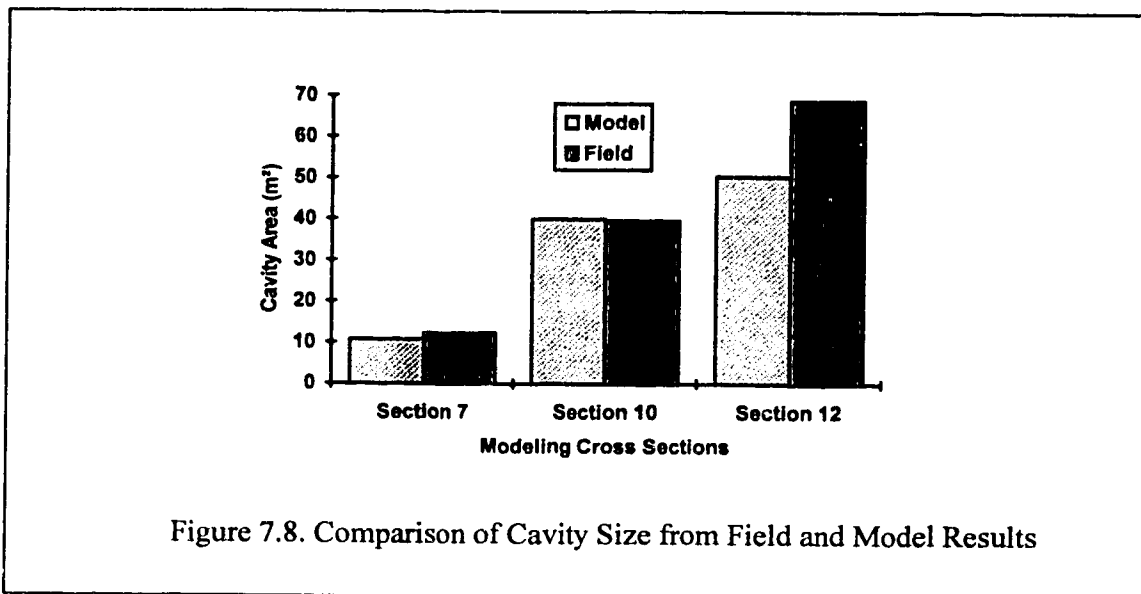
Figure 7.7. Comparison of In-situ Cavity Area of Cross Section 7 and Model Result

trial run, which appear both to match the in situ cavity size and to have the same gas pressure were identified. The comparison between the modeling results and the selected in situ cross sections is shown in Fig. 7.5 - 7.7.

After examining Fig. 7.5-7.7, the verification of the numerical model against in situ observation is discussed below.

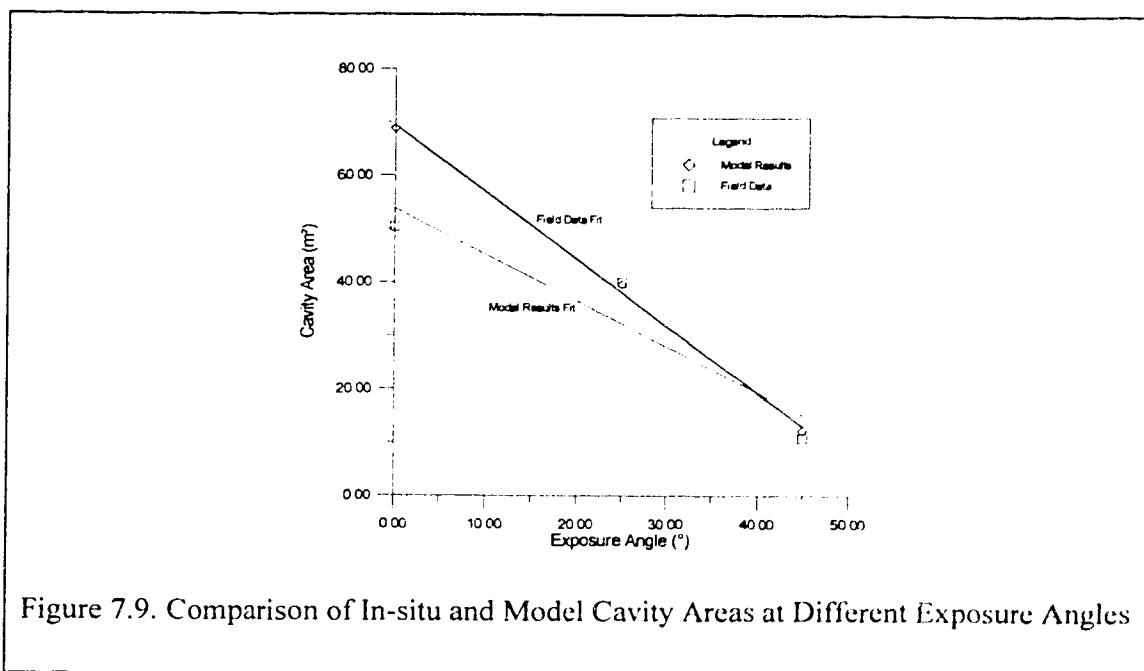
The model finds that the outbursts occurred when gas pressure was given approximate values of 3.0 MPa. In modeling cross section 7 and 10, the results from gas pressure of 3.0 MPa are the ones most closely comparable to the in situ cavity data. Sandstone in these two sections is not fully exposed to the entry opening. The exposure angles for section 7 and 10 are 45° and 25° respectively. Modeling for section 12, however, gives a gas pressure of 3.4 MPa. In the trial runs for this condition, it is the smallest gas pressure that can induce an outburst. By slightly decreasing (by a decrement of 0.1 MPa) this gas pressure, no outburst is initiated in the model. The gas pressures of both these magnitudes fit into the range that Aston and Cain estimated as the most likely for the last two outbursts at No. 26 Colliery.

The cavity sizes obtained from the numerical model agree approximately with those measured by engineers in the mine. Areas of the cavity resulting from modeling for section 12 and 7 are 36.5% and 13% higher, and 1% lower for section 10 modeling. The error may be caused by the modeling as well as the in situ measurement. In engineering measurement, this is quite acceptable. The cavity sizes from field and model results are compared in Fig. 7.8.



The shape of the cavity from modeling is generally comparable with the observation as shown in Fig. 7.5-7.7. All three cavities tend to be elliptical with the major axis lying in horizontal direction which coincides with that of major principle stress. The growth of the cavity corresponds to that of the real cavity. The cavity top of section 12 reached the overlying siltstone, so did the modeled cavity. For section 10, a very thin layer of sandstone was left in top of the cavity from modeling while the in situ cavity top just touched the overlying siltstone. A layer of sandstone was left on top of cavity in both the model and in reality for section 7. These similarities of the cavity shape and growth are encouraging for verification purposes.

The sandstone area exposed to the entry opening depends on the thickness of siltstone layer lying between coal seam and sandstone channel and has a major influence on the cavity size. The less the exposed area of sandstone to the entry opening, the smaller the cavity size. This tendency can be clearly observed both from modeling results and from the in situ observation as it is clearly shown in Fig. 7.9.



From observing Fig. 7.5-7.7 and the discussions above, it is concluded that the model results agree quite well with the measurement data from outburst cavities in the field. The cavity size, cavity shape and cavity growth showed substantial similarity

between modeling and reality. Conditions postulated in the modeling follow closely the site testing data and information collected from field. All these indicate that the spalling mechanism of the outbursts, inherent in this model, may offer a viable explanation for the outburst mechanism. Thus, a practical model is, now, available for numerical analysis of the outburst phenomenon.

7.4 Parametric Analysis

After verification with the outbursts in No. 26 Colliery, the model is now ready to investigate the sensitivity of the outbursts to the change in a number of factors under different conditions. This exercise aims to test a number of factors which are responsible for outburst initiation and its consequences, and to establish certain relationships between these factors and the behavior of an outburst. The analysis done here will demonstrate, to some extent, the ability of the model to better explain aspects arising from the outburst phenomenon.

A systematically designed set of conditions will be tested in this parametric analysis. Two major aspects of an outburst are considered. The outburst initiation, always being of research interest, will be studied first. The consequences of an outburst, the process after initiation until termination of the outburst, will be investigated afterwards. Previous reviews of the factors influencing an outburst have shown that there are many influencing parameters. It would be a very time-consuming effort to examine all of them with this model. Only those factors which have direct impact on the outburst behavior in association with the model calculation will be addressed here. These factors include stress ratio, sandstone height (sandstone thickness above the crown of the entry), exposure angle (an indirect measure of sandstone area exposed to the entry opening - referring to the definition in section 7.2) and gas pressure.

7.4.1 Outburst initiation

The gas pressure required to initiate an outburst has constantly been an important topic when considering the outburst problem. This model was used to study this initiation problem of the outbursts. A series of conditions were specified for this purpose, and they are summarized below:

Modeling area:	60 m (high) × 30 m (wide);
Geology in area:	refer to Fig. 7.2;
Entry geometry:	4.5 m (wide), 2.0 m (wall height), 2.25 m (radius of semicircle);

Stress field:	$\sigma_v = 25$ (MPa):
Stress ratio:	0.5, 1.1, 2.0;
Sandstone height:	2.8, 3.8, 7.8, 11.8, 15.8 m;
Sandstone and siltstone properties and strength:	refer to Table 7.3;
Exposure angle:	$\theta = 0^\circ, 25^\circ, 45^\circ, 65^\circ$.

These conditions can be combined into a number of sets of conditions by changing the stress ratio (k_0), sandstone height (t) and exposure angle (θ), such as given by: $k_0=0.5$; $t=3.8$; $\theta=0^\circ$. The other conditions were kept unchanged at all times. For each set of conditions, the input data files were prepared accordingly. A gas pressure was applied on a trial and error basis to find the minimum value to cause tensile failure around boundary of the entry. This gas pressure, then, was assumed to be the initiation gas pressure.

Some confusion was experienced during running the program and deciding the initiation gas pressure when only one or a few elements failed in tension and were removed before the spalling process terminates. In such cases, it is unreasonable to interpret the event as an outburst. To pinpoint the initiation gas pressure in a consistent manner, a "rule of thumb" was established that at least the first row of elements must be removed before the event could be count as outburst. This kind of dilemma, however, only happened in a few cases when sandstone height was smallest (2.8 m) and the stress ratio was high (2.0). In such a condition, elements around the boundary of the entry changed to a very flat rectangular shape. It is known that such an element may cause errors in the stresses calculated from FEM. The simulation completed in such conditions, then, is questionable. For the sake of completeness of analysis, the results are still included. Since such cases were few, they should not affect the general conclusions drawn from the results.

Another fact to be mentioned here is the difficulty of controlling the element size in the sandstone zone. When discretizing the zone, a constant grid scheme was used for simplifying input data preparation. Alteration of the sandstone height changed the element size in the zone. The exposure angle also contributed slightly to this variation of the size. According to the tests on the model with different element sizes, it was shown that the results can be affected. Again, this was assumed not to influence the conclusions in a great deal.

The modeling results are listed in Table 7.4. Fig. 7.10, 7.11 and 7.12 plot these results in 3-D which is intended to clearly illustrate the general pattern of the relationship between initiation gas pressure and sandstone height as well as exposure angle. The data

The Initiation Gas Pressure Under Different Conditions Table 7.4

Stress Ratio=0.5									
t=2.8 m		t=3.8 m		t=7.8 m		t=11.8 m		t=15.8 m	
Pg (MPa)	A (m ²)	Pg (MPa)	A (m ²)	Pg (MPa)	A (m ²)	Pg (MPa)	A (m ²)	Pg (MPa)	A (m ²)
$\theta=0^\circ$									
2.3	0	2.6	0	3.3	0	2.6	0	4	0
2.4	43.6	2.7	50.4	3.4	212.8	2.7	50.4	4.1	To infinity
$\theta=25^\circ$									
1.7	0	1.5	0	1.7	0	1.5	0	2.2	0
2	19	1.6	12.4	1.8	2.2	1.6	12.4	2.3	2.8
$\theta=45^\circ$									
2.2	0	2.2	0	2.2	0	2.2	0	2	0
2.3	5	2.3	14.6	2.3	14.8	2.3	14.6	2.1	1.8
$\theta=65^\circ$									
3.9	0	2.5	0	3.1	0	2.5	0	3.9	0
4.2	3.8	2.6	3.6	3.2	29.2	2.6	3.6	4	1.4
Stress Ratio=1.1									
t=2.8 m		t=3.8 m		t=7.8 m		t=11.8 m		t=15.8 m	
Pg (MPa)	A (m ²)	Pg (MPa)	A (m ²)	Pg (MPa)	A (m ²)	Pg (MPa)	A (m ²)	Pg (MPa)	A (m ²)
$\theta=0^\circ$									
2.9	0	3.2	0	4.3	0	4.4	0	4.5	0
3.4	63	3.4	68.8	4.4	275.4	4.5	420.6	4.6	To infinity
$\theta=25^\circ$									
2.3	0	1.7	0	2.5	0	2.7	0	2.8	0
2.4	24	1.8	5.2	2.6	102.8	2.8	9.6	2.9	78.4
$\theta=45^\circ$									
2.2	0	2	0	2	0	2.5	0	2.5	0
2.3	4.4	2.1	7	2.1	3.8	2.6	1.6	2.6	1.8
$\theta=65^\circ$									
3.9	0	3.7	0	3.8	0	4	0	3.3	0
4.2	3.8	3.8	4.6	3.9	3.2	4.1	10	3.4	6.4
Stress Ratio=2.0									
t=2.8 m		t=3.8 m		t=7.8 m		t=11.8 m		t=15.8 m	
Pg (MPa)	A (m ²)	Pg (MPa)	A (m ²)	Pg (MPa)	A (m ²)	Pg (MPa)	A (m ²)	Pg (MPa)	A (m ²)
$\theta=0^\circ$									
3.8	0	3.9	0	4.6	0	5.4	0	5.3	0
4	2	4	57.6	4.7	To infinity	5.5	To infinity	5.4	3
$\theta=25^\circ$									
1.4	0	1.9	0	2.2	0	2.9	0	3.1	0
1.5	6.2	2	10.6	2.3	4.4	3	2.7	3.2	2
$\theta=45^\circ$									
2	0	3.8	0	3.4	0	3.5	0	3.8	0
2.1	2.2	4	18.2	3.5	7.5	3.6	9.4	3.9	3.6
$\theta=65^\circ$									
2.3	0	4.3	0	2.7	0	3	0	3.4	0
2.5	6.8	4.4	2	2.8	1.8	3.2	2.6	3.5	6.4

Notes: θ - exposure angle;

t - sandstone height;

Pg - initial gas pressure;

A - cavity size (0 indicates no outburst initiated)

("To infinity" indicates the infinity spalling process).

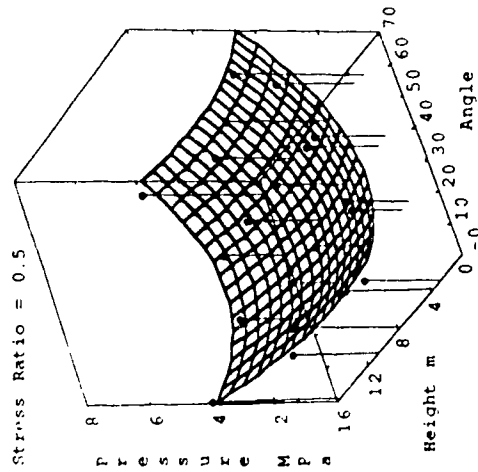


Figure 7.10. 3-D Plot of Initiation Gas Pressure vs. Sandstone Height and Exposure Angle for Stress Ratio 0.5

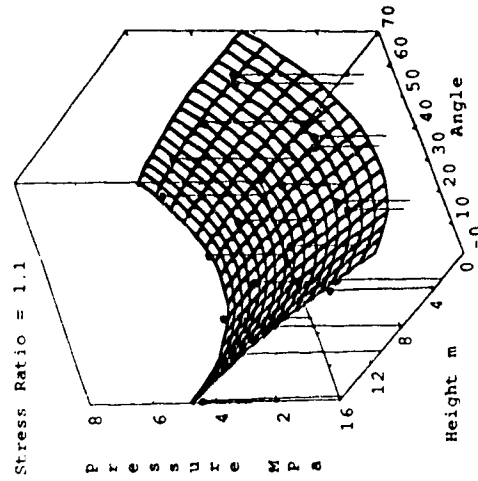


Figure 7.11. 3-D Plot of Initiation Gas Pressure vs. Sandstone Height and Exposure Angle for Stress Ratio 1.1

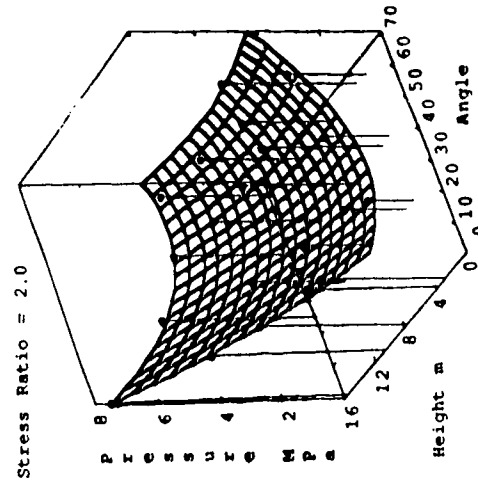
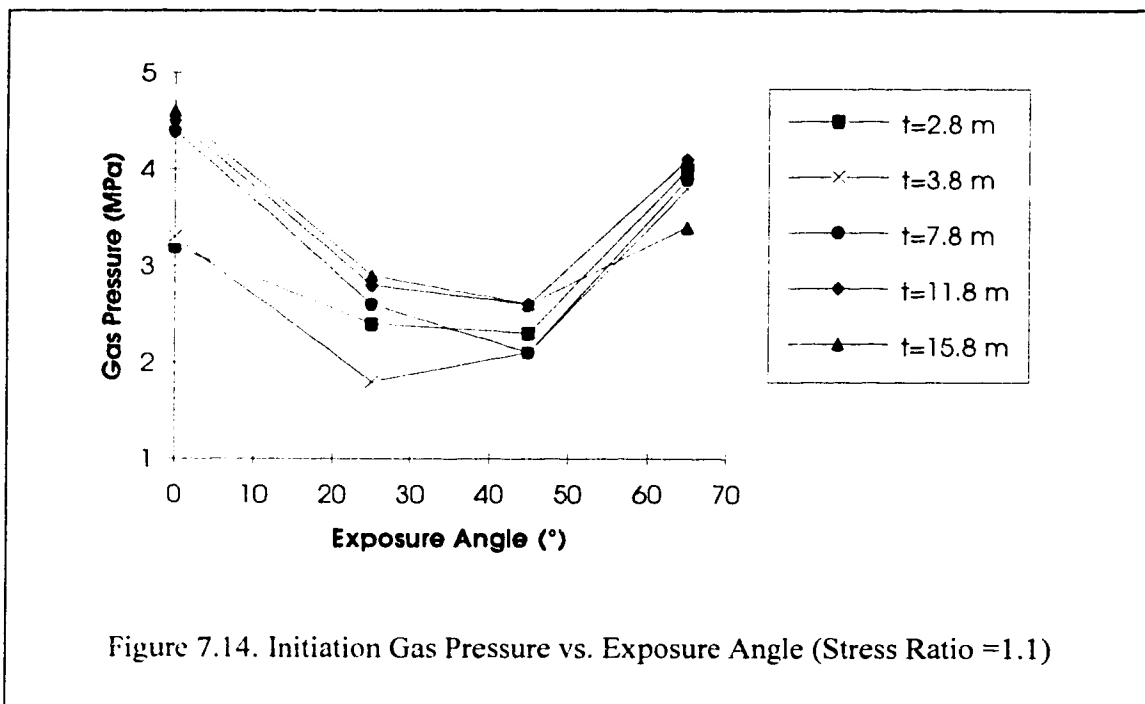
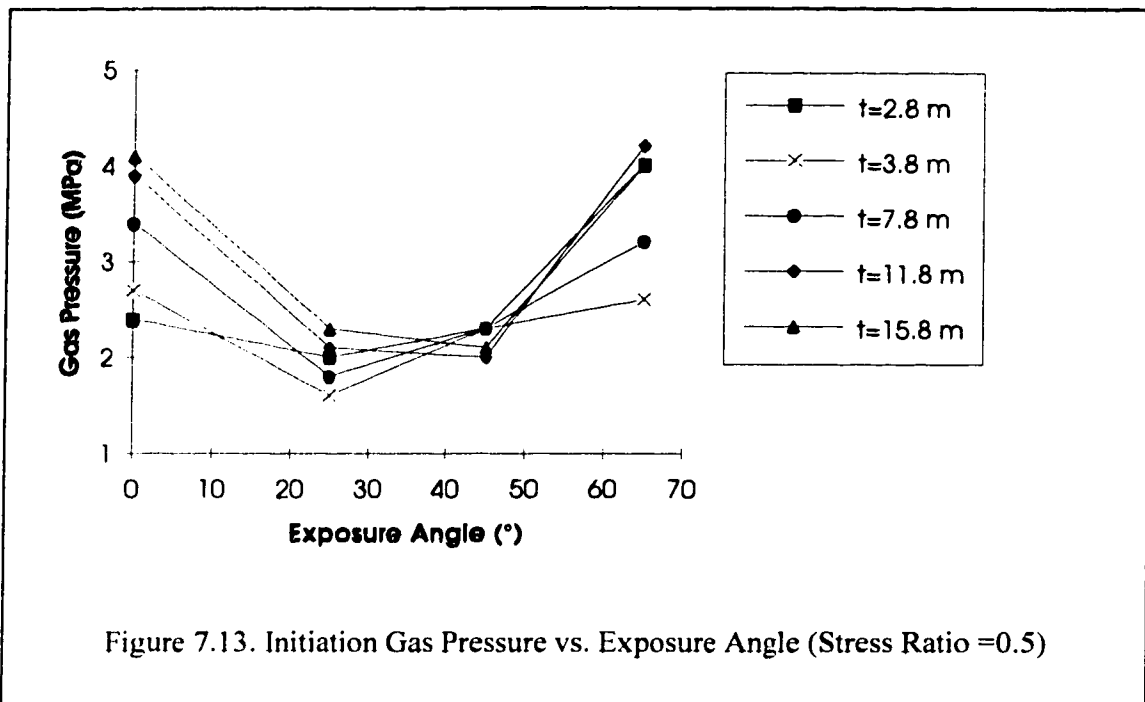
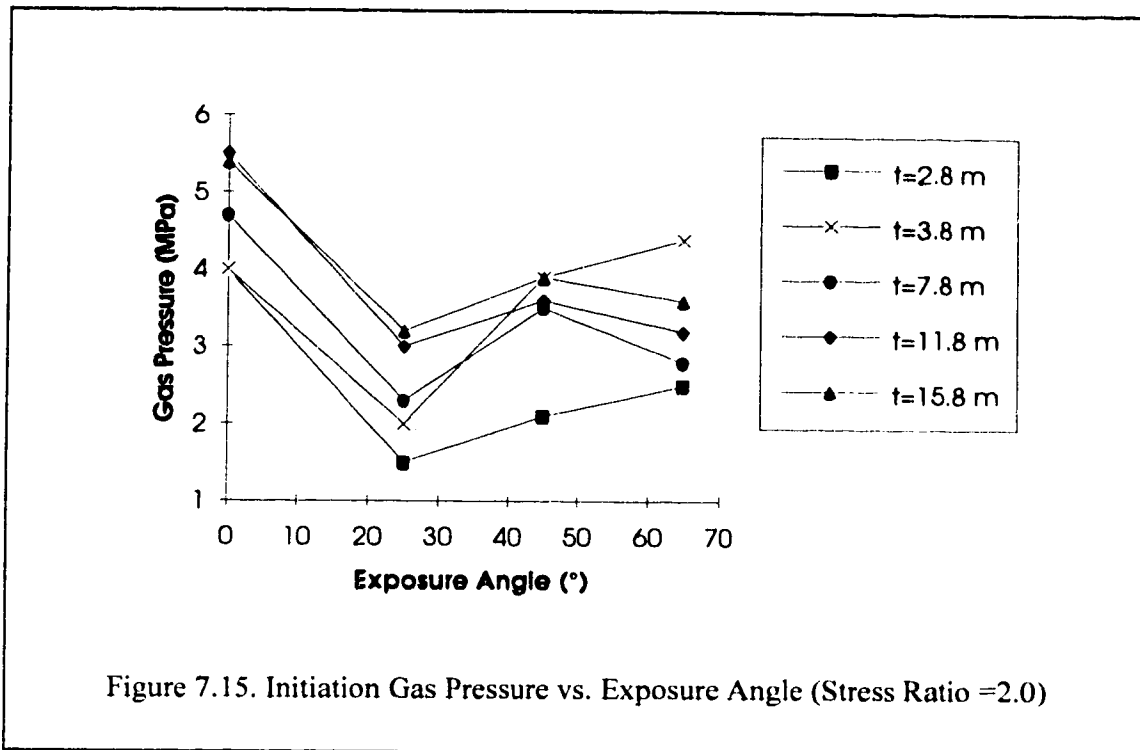


Figure 7.12. 3-D Plot of Initiation Gas Pressure vs. Sandstone Height and Exposure Angle for Stress Ratio 2.0





are fitted by a quadratic surface in the graphs to reveal the general tendency of the relationship. Each graph accommodates the results from one of the three different stress ratios. Corresponding to each 3-D graph of Figs. 7.10, 7.11, 7.12, the 2-D representations for the initiation gas pressure and exposure angle are shown in Fig. 7.13-7.15 to demonstrate the significant relationship between the two variables.

From these graphs, the following tentative conclusions can be drawn:

1. Sandstone height has less influence on the gas pressure needed to initiate an outburst than does the exposure angle, under the same stress ratio. The initiation gas pressure decreases slightly with the decrease of sandstone height at a constant exposure angle. In the modeling, as the grid intensity was fixed for the sandstone zone, the element size in the zone changed when changing sandstone height. This fact may have partially contributed to this weak relationship between the two variables.

2. Exposure angle changes the gas pressure necessary for outburst initiation. Under the same stress ratio, the gas pressure versus exposure angle graphs (refer to Fig. 7.13-7.15) can be approximately described with quadratic relation. There is a minimum gas pressure at which an outburst can initiate and this minimum occurs when exposure angle lies in the range of 25° to 45°. The sandstone height does not affect this relationship.

3. Stress ratio has a slight influence on the gas pressure required to initiate an outburst. It is difficult to find a general correlation between the two factors. Each individual case should be analyzed since the results showed, indeed, the difference for different stress ratio.

This exercise of identifying the gas pressure required to initiate an outburst has proved that the model is able to determine numerically the initiation gas pressure for a given set of conditions. The model provides a theoretical approach to assist in the prediction of an outburst. It may also be used as a numerical tool for an engineer to evaluate preventive measure for outbursts. This is demonstrated by some trial runs conducted, as described below.

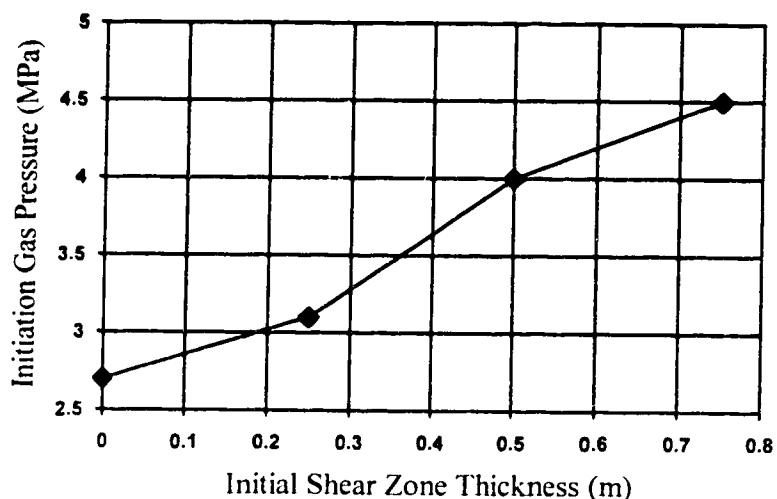


Figure 7.16. Initiation Gas Pressure vs. Initial Shear Zone Thickness

In these runs, an initial shear zone was specified along the boundary of the entry excavation. The shear zone could be the result of the blasting, or of deliberately creating it manually by hydrofracturing, or by controlled blasting for the purpose of outburst prevention. By altering the thickness of the defined shear zone, the model has produced different initiation gas pressures. The correlation between shear zone thickness and gas pressure required to initiate outburst is shown in Fig. 7.16. This set of results were obtained under conditions given by: $\theta=0^\circ$, $t=15.8$ m and $k_0=0.5$. The figure 7.16 shows that when shear zone gets thicker the initiation gas pressure increases. For a specific site,

the gas pressure in strata has a specific value. From the model, a particular shear zone thickness can be found at which no outburst would be initiated. If a gas release program was designed for prevention of outbursts, the model could be used to find the required extent of the release zone.

7.4.2 Gas pressure influence on outburst consequences

After the initiation of an outburst, the model can produce two consequences. In a limited range of gas pressure, a stabilized cavity can be formed provided that the conditions are adequate. By further increasing the gas pressure, the model will eventually result in an infinite cavity, i.e. the spalling process is deemed to carry on indefinitely. Both consequences are closely related to the gas pressure for a given set of conditions. In general, the gas pressure has an influence not only on outburst initiation (as discussed in the previous section) but also on the stabilized cavity size and infinite spalling process. This section will address the influence of the gas pressure cavity development after the initiation of an outburst.

A set of runs were set up to investigate this aspect. Conditions for the model were the same as those set in the previous section except that only 2.8 m, 3.8 m and 15.8 m sandstone heights were tested. From the established initiation gas pressure, the gas pressure was increased with an arbitrary increment while the other conditions were held constant. The maximum gas pressure tested was 20.0 MPa.

Some stabilized cavities and some infinite cavities are graphically illustrated in Appendix F. The infinite cavity was obtained from the last iteration in execution of the program, when the spalling process was deemed to carry on indefinitely. Results derived from all runs are listed in Table 7.5, 7.6 and 7.7 for each of the three different stress ratios. The data in each table are plotted in a graph with vertical axis representing size of cavity and horizontal axis for gas pressure. These graphs are shown in Fig. 7.17-7.25. Each of the 3 graphs represents the results for the specific sandstone height considered. The dashed line at top of each graph indicates the infinite cavity.

In Fig. 7.17-7.19, zero cavity sizes are plotted. These points represent the situation when an outburst is just on the brink of initiation. Slightly increasing gas pressure (usually by a magnitude of 0.1 MPa) triggers the outbursts. In Fig. 7.20-7.25, no such zero data are plotted, in order to avoid the confusion on the graph (and the gas initiation pressure have been discussed in the previous section).

From the graphs in Appendix F and Fig. 7.17-7.25, the following two conclusions can be drawn:

Cavity Size Results from the Model Runs Table 7.5

Stress Ratio = 0.5					
t=15.8 (m)		t=3.8 (m)		t=2.8 (m)	
Pg (MPa)	A (m ²)	Pg (MPa)	A (m ²)	Pg (MPa)	A (m ²)
$\theta=0^\circ$					
4	0	2.7	50.4	2.4	43.6
4.1	To infinity	4	88	5	71
		10	150.8	10	106.2
		20	To infinity	20	To infinity
$\theta=25^\circ$					
2.2	0	1.6	12.4	2	19
2.3	2.8	5	51.6	5	35.2
3	3.4	10	118	10	56.8
5	To infinity	20	To infinity	20	To infinity
$\theta=45^\circ$					
2	0	2.3	14.6	2.3	5
2.1	1.8	5	41.4	2.5	7.2
2.5	2.2	10	69.6	5	24.4
3.5	2.4	20	To infinity	10	42.8
4.5	To infinity			20	To infinity
$\theta=65^\circ$					
3.9	0	2.6	3.6	4.2	3.8
4	1.4	5	18.6	5	5.4
4.5	To infinity	10	54.2	10	33.4
		20	To infinity	20	To infinity

Notes: t - Sandstone height;

Pg - Gas pressure in strata;

θ - Exposure angle;

A - Stabilized cavity size (0 indicates no outburst initiation)

("To infinity" indicates infinite cavity).

Cavity Size Results from the Model Runs Table 7.6

Stress Ratio = 1.1					
t=15.8 (m)		t=3.8 (m)		t=2.8 (m)	
Pg (MPa)	A (m ²)	Pg (MPa)	A (m ²)	Pg (MPa)	A (m ²)
$\theta=0^\circ$					
4.5	0	3.4	68.8	3.4	63
4.6	to infinity	4.4	98.2	4.9	69.2
		5	108.8	12	91.8
		6	123.8	20	157.8
		9	149.8		
		12	168.6		
		20	To infinity		
$\theta=25^\circ$					
2.8	0	1.8	5.2	2.4	24
2.9	78.4	3	39.6	3	26.4
5	627.8	4	57.2	4	29
10	760	10	102.2	10	66.4
20	To infinity	20	151.2	20	102.8
$\theta=45^\circ$					
2.5	0	2.1	7	2.3	4.4
2.6	1.8	2.5	11.6	5	16.2
3	2.4	3	12.2	10	36.2
3.5	380	4	31.6	20	80.2
5	519.8	20	113.8		
10	639.4				
20	To infinity				
$\theta=65^\circ$					
3.3	0	3.8	4.6	4.2	3.8
3.4	6.4	4	5	10	23
10	597.6	10	41.8	20	43.6
20	To infinity	20	92.6		

Notes: t - Sandstone height;

Pg - Gas pressure in strata;

θ - Exposure angle;

A - Stabilized cavity size (0 indicates no outburst initiation)

("To infinity" indicates infinite cavity).

Cavity Size Results from the Model Runs Table 7.7

Stress Ratio = 2.0					
t=15.8 (m)		t=3.8 (m)		t=2.8 (m)	
Pg (MPa)	A (m ²)	Pg (MPa)	A (m ²)	Pg (MPa)	A (m ²)
$\theta=0^\circ$					
5.3	0	4	57.6	4	2
5.4	3	5	80.8	5	50.8
7.5	3	10	110	10	82.2
10	To infinity	20	171.4	20	116.4
$\theta=25^\circ$					
3.1	0	2	10.6	1.5	6.2
3.2	2	5	41.6	5	21.8
5	2	10	80.4	10	57.4
10	529.4	20	120.4	20	87.4
20	To infinity				
$\theta=45^\circ$					
3.8	0	4	18.2	2.1	2.2
3.9	3.6	5	38.2	5	17.8
5	9.2	10	51.4	10	38.4
10	490.2	20	89	20	55.8
20	To infinity				
$\theta=65^\circ$					
3.4	0	4.4	2	2.5	6.8
3.6	6.4	10	17	4.5	5
5	21	20	73.8	10	12
10	485.2			20	36
20	To infinity				

Notes: t - Sandstone height;

Pg - Gas pressure in strata;

θ - Exposure angle;

A - Stabilized cavity size (0 indicates no outburst initiation)

("To infinity" indicates infinite cavity).

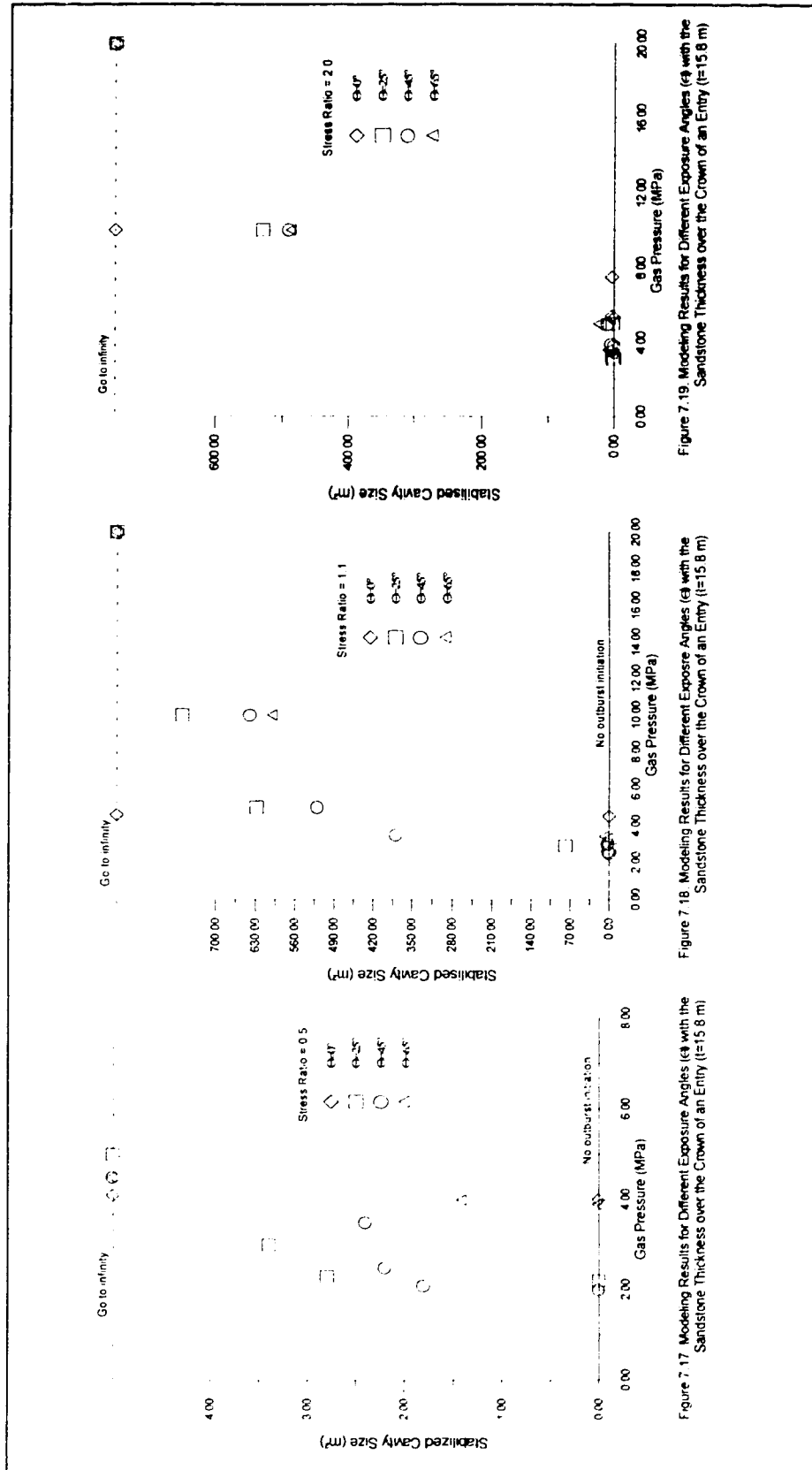


Figure 7.17 Modeling Results for Different Exposure Angles (0° with the Sandstone Thickness over the Crown of an Entry (i=15.8 m))

Figure 7.18 Modeling Results for Different Exposure Angles (0° with the Sandstone Thickness over the Crown of an Entry (i=15.8 m))

Figure 7.19 Modeling Results for Different Exposure Angles (0° with the Sandstone Thickness over the Crown of an Entry (i=15.8 m))

Go to infinity

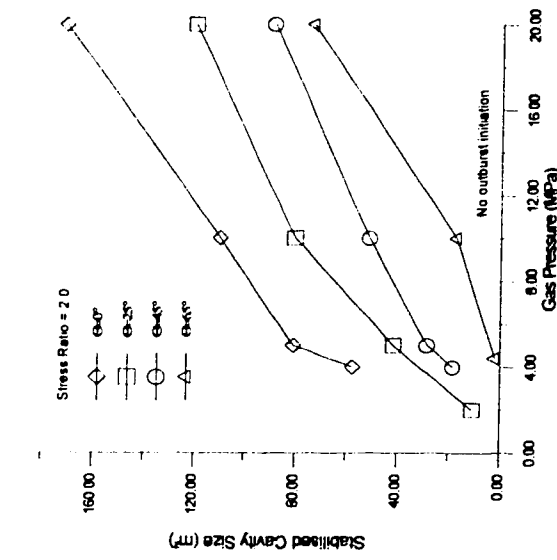


Figure 7.20. Modeling Results for Different Exposure Angles (α) with the Sandstone Thickness over the Crown of an Entry ($t=3.8$ m)

Go to infinity

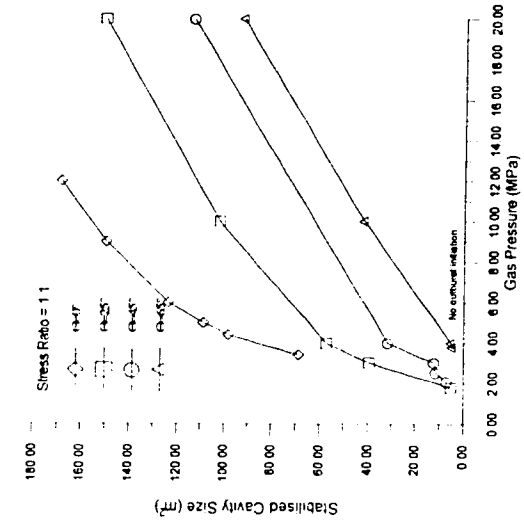


Figure 7.21. Modeling Results for Different Exposure Angles (α) with the Sandstone Thickness over the Crown of an Entry ($t=3.8$ m)

Go to infinity

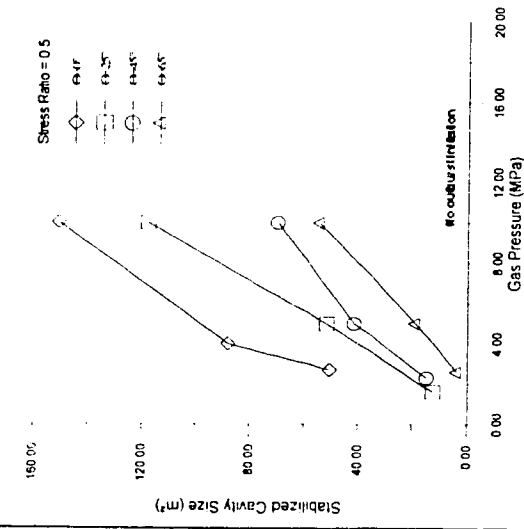


Figure 7.22. Modeling Results for Different Exposure Angles (α) with the Sandstone Thickness over the Crown of an Entry ($t=3.8$ m)

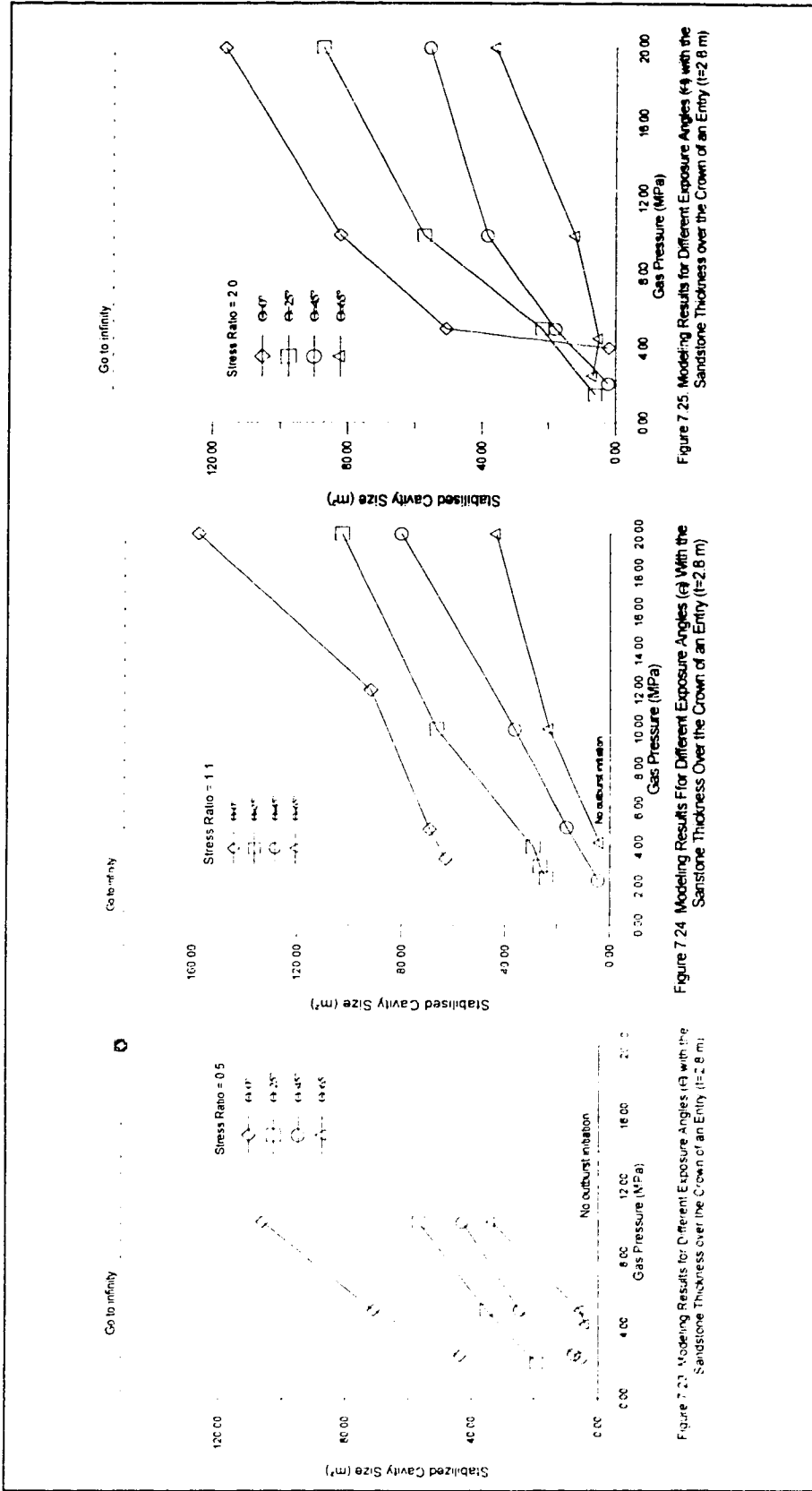


Figure 7.23 Modeling Results for Different Exposure Angles (α) with the Sandstone Thickness over the Crown of an Entry (t=2.8 m)

Figure 7.24 Modeling Results for Different Exposure Angles (α) with the Sandstone Thickness over the Crown of an Entry (t=2.8 m)

Figure 7.25 Modeling Results for Different Exposure Angles (α) with the Sandstone Thickness over the Crown of an Entry (t=2.8 m)

1. The stabilized cavity size increases with the gas pressure at constant exposure angle. There always exists a gas pressure which is large enough to cause an infinite cavity, although it has not been reached for some cases in this exercise. In some extreme cases, no stabilized cavity forms. In other cases, no intermediate cavity can be produced, the stabilized cavity either becomes very small ($< 10 \text{ m}^2$) or develops to a very large cavity ($> 400 \text{ m}^2$). These two situations happen when sandstone height is relatively high (refer to Fig. 7.17-7.19).

2. The stabilized cavity (refer to Appendix F) always tends to grow into an elliptic shape. The long axis of this ellipse lies in the direction of the major principle stress. In a given field stress, it is known that an elliptic opening oriented in the same manner is most stable. With such a geometry, the stresses distribute smoothly around the cavity, eliminating possible tensile stress and stress concentrations. Therefore, the spalling process, based on the tensile failure, can be terminated by solely changing the shape of the cavity due to this favorable stress condition. For a given stress field, a high enough gas pressure will break such equilibrium condition and always induce tensile stress along the periphery of newly excavated cavity, exceeding the tensile strength of the rock. As a result, the spalling process continues until some other mechanism is invoked, such as change in lithology or the gas pressure drops.

The first conclusion about the gas pressure influence is only good as a general guide line when gas pressure is considered to be a major cause for an outburst. Individual cases must be examined in practical application, because so many factors are included in the model. As matter as fact, some of them are significant and they will be discussed in the following sections.

7.4.3 Influence of sandstone height

Section 7.4.1 discussed the effect of sandstone height on the initiation of an outburst and showed that it was an almost negligible factor. However, the sandstone height has a substantial influence on the subsequent development of the outburst cavity, as it is indicated from modeling results given below.

For the convenience of comparison, Fig. 7.17-7.25 in pages 112-114 have been rearranged in pages 116-118. Each page contains the graphs with different sandstone heights under the same stress ratio. The significant influence on post initiation behavior of the outbursts can be clearly observed from these graphs. Cavity size and stability are closely dependent on the sandstone height.

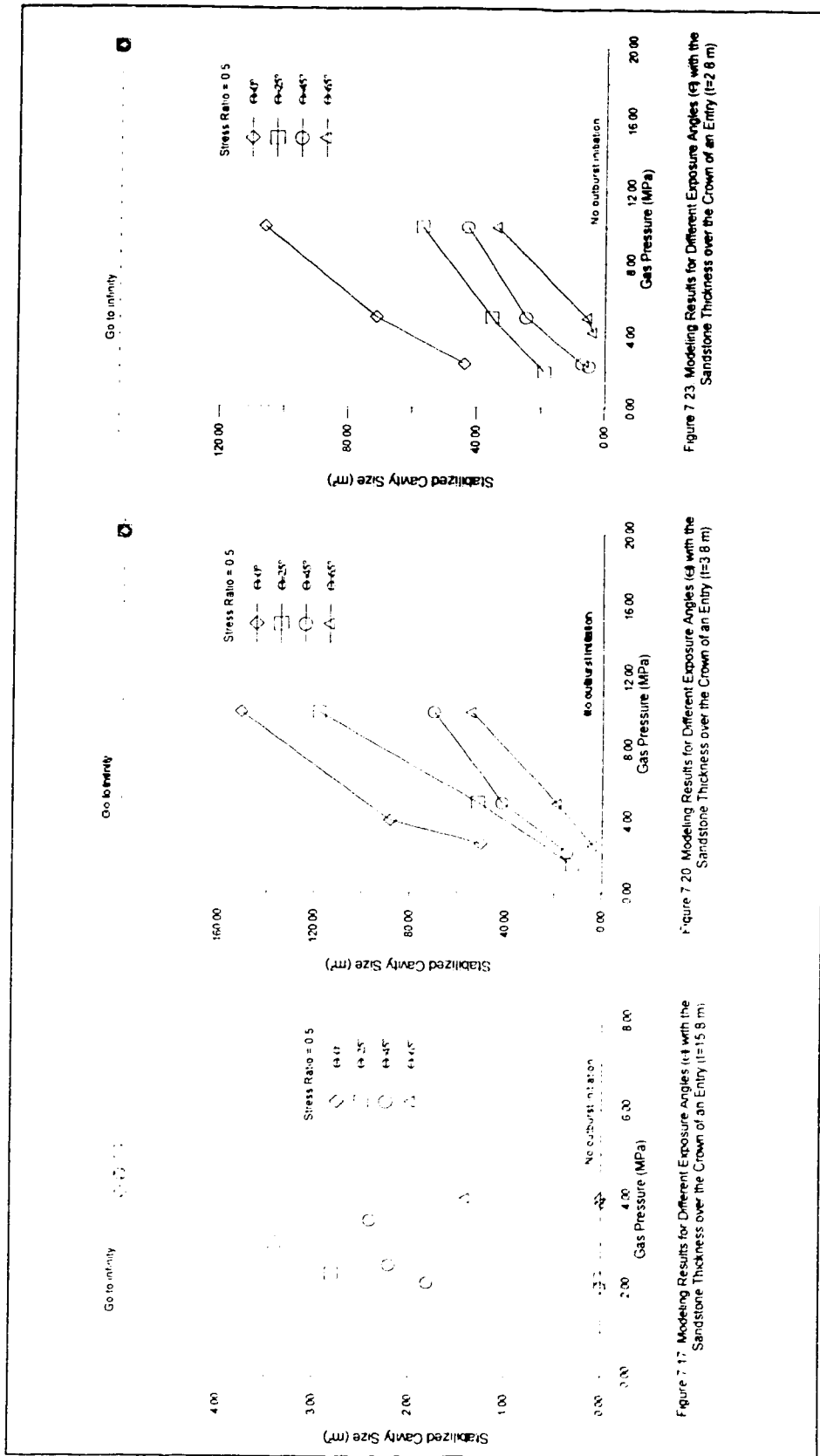


Figure 7.17 Modeling Results for Different Exposure Angles (15 with the Sandstone Thickness over the Crown of an Entry (l=15.8 m))

Figure 7.20 Modeling Results for Different Exposure Angles (38 with the Sandstone Thickness over the Crown of an Entry (l=3.8 m))

Figure 7.23 Modeling Results for Different Exposure Angles (28 with the Sandstone Thickness over the Crown of an Entry (l=2.8 m))

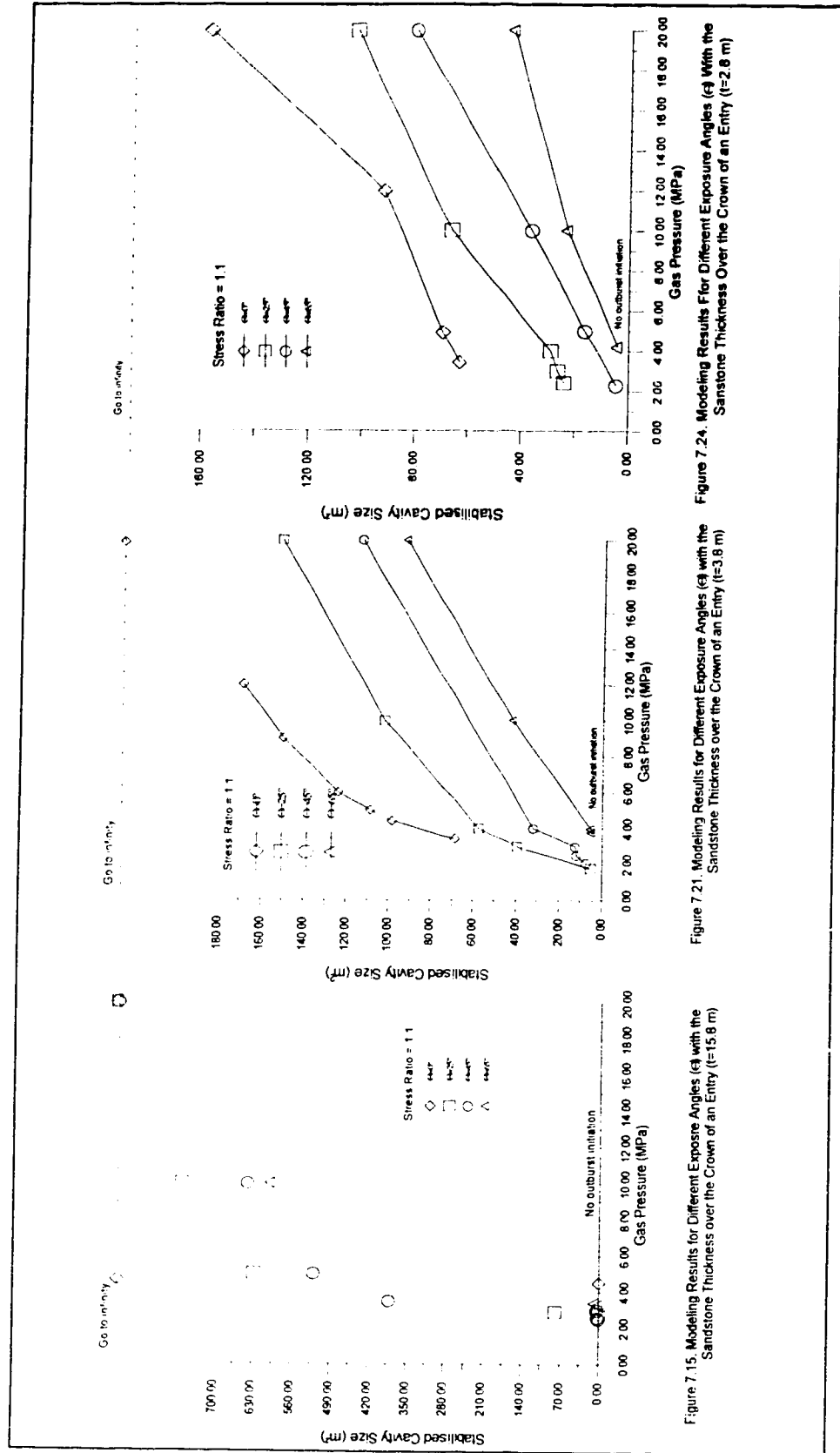
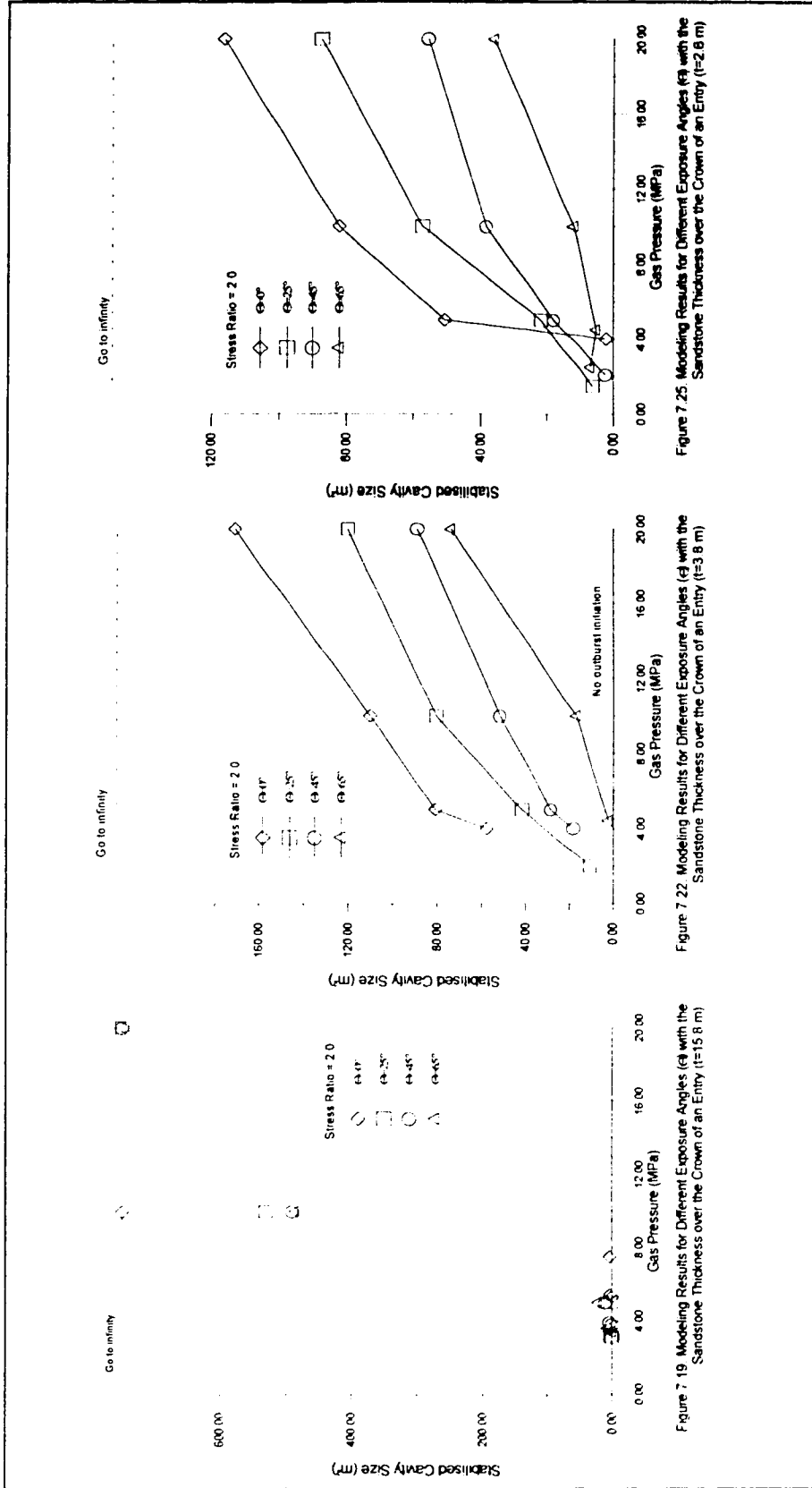


Figure 7.15. Modelling Results for Different Exposure Angles (α) with the Sandstone Thickness over the Crown of an Entry ($t=15.8\text{ m}$)

Figure 7.21. Modelling Results for Different Exposure Angles (α) with the Sandstone Thickness over the Crown of an Entry ($t=3.8\text{ m}$)

Figure 7.24. Modelling Results for Different Exposure Angles (α) with the Sandstone Thickness over the Crown of an Entry ($t=2.8\text{ m}$)



Go to infinity

Go to infinity

Go to infinity

Figure 7.19 Modeling Results for Different Exposure Angles (α) with the Sandstone Thickness over the Crown of an Entry ($t=15.8$ m)

Figure 7.22 Modeling Results for Different Exposure Angles (α) with the Sandstone Thickness over the Crown of an Entry ($t=3.8$ m)

Figure 7.25 Modeling Results for Different Exposure Angles (α) with the Sandstone Thickness over the Crown of an Entry ($t=2.8$ m)

The difference between the results from the 15.8 m sandstone height and 3.8 m, 2.8 m heights are obvious from the graphs on each page. When the sandstone height is 15.8 m, the outbursts stabilize at either a very small size or, with the same magnitude increase of gas pressure as those of 3.8 m and 2.8 m cases, the cavity size become very large and until it goes to infinity. In an extreme, a few cases with exposure angle of zero show that it is either completely stable (no outburst initiated) or totally unstable (infinity cavity forms). Once the outburst initiates, there is no intermediate cavity that can be formed for such a sandstone height. Considering that this sandstone height is relatively high compared to the whole dimension of the modeling area, the behavior described here may be representative of all the situations with a thicker sandstone formation.

From Fig. 7.17, the gas pressure range to form a stabilized cavity is much smaller than that of the other two sandstone heights, although this is dubious in the cases shown in Fig. 7.18 and 7.19. This trend seems to be maintained for the case of sandstone height 3.8m and 2.8m.

A different pattern of the cavity size distribution is shown in Fig. 7.20-7.25 when the sandstone height is reduced to 3.8 m and 2.8 m. A series of increasingly larger intermediate size stable cavities occur within a gas pressure range before an infinity cavity is achieved. When the sandstone height is smaller, the stabilized cavity size gets smaller, provided that the other conditions are kept unchanged. It is clear that the sandstone height has a controlling influence on whether or not an outburst will terminate in a stabilized cavity.

7.4.4 Exposure angle and stress ratio influences

Exposure angle (θ) represents the area of sandstone exposed in the entry. Examining Fig 7.17-7.25 again, it is seen that the exposure angle will also influence the post initiation behavior of an outburst. When $\theta=0^\circ$ and $t=15.8$ m (refer to Fig. 7.17-7.19 in pages 112-114), for each of three stress ratios, as soon as the outburst is initiated the cavity size goes to infinity. This does not apply to the cases with the other exposure angles.

For the sandstone height 3.8 m and 2.8 m, Fig. 7.19-7.25 clearly illustrate that the stabilized cavity size increases with decrease of the exposure angle. This same tendency also applies to 15.8 m sandstone height except in the case when $\theta=0^\circ$.

The general conclusion drawn for exposure angle influence is that the area of sandstone exposed in the entry roof has a substantial influence on the resulting cavity size: the larger the exposed area, the larger is the stabilized cavity size.

Field stress ratio appears to control whether the outburst will proceed rapidly to an infinite cavity at a lower or a higher gas pressure. For the sandstone height of 15.8 m (Fig. 7.17-7.19), the cavity size goes to infinity before the gas pressure reaches 6.0 MPa for all exposure angles, when stress ratio is 0.5. Under the same conditions, the other two stress ratios, 1.1 and 2.0, require that the gas pressures at least exceed 10.0 MPa before an infinite cavity can be obtained. Two exceptional cases are those when exposure angle equals zero. When stress ratio equals 1.1, the gas pressure less than 4.0 MPa sends the cavity to infinity (refer to Fig. 7.18). The gas pressure required to cause an infinite cavity for stress ratio of 2.0 exceeds, at least, 7.0 MPa (refer to Fig. 7.19). Fig 7.20-7.22 show the cavity size for the sandstone height 3.8 m with the three different stress ratios. The cavity sizes go to infinity for all angles when 0.5 stress ratio is used in modeling. For the stress ratio value of 1.1, only the exposure angle $\theta=0^\circ$ case achieves an infinite cavity at a gas pressure 20.0 MPa, while none of the cavities go to infinity at a gas pressure of 20.0 MPa when stress ratio changes to 2.0. The similar trend can be observed for sandstone height 2.8 m as exhibited in Fig. 7.23-7.25.

7.4.5 Influence of stress level

A few tentative runs were carried out to investigate the influence of stress level. The results from the modeling are plotted in the following figure.

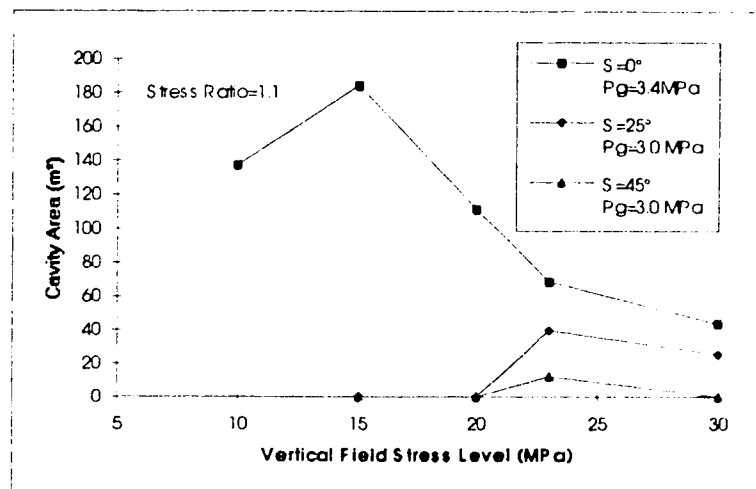


Figure 7.26. Field Stress Level Effects on the Outbursts

In the figure, zero value of cavity area means no outburst initiation. The constant gas pressure remained unchanged for each exposure angle. For $\theta=0^\circ$, the cavity sizes increase with the increase of the vertical stress level before σ_v reaches 15 MPa. After σ_v passes this point, the size decreases with increase of the stress level. The test run for $\sigma_v=5$ MPa indicated that the spalling process would go to infinity. This is probably because the unchanged gas pressure is relatively too high. Theoretically speaking, gas pressure should increase with the depth and, perhaps, be directly related to stress level.

For $\theta=25^\circ$ and 45° , there is no outburst initiated when $\sigma_v < 20$ MPa. The maximum cavity size is achieved around the stress level 25 MPa. The bilinear relationship between the cavity size and the stress level is clearly illustrated in the figure.

7.5 Filled Cavity Modeling

The exercises on the numerical modeling have so far been limited to the empty cavity situation as it was illustrated in section 6.4.5. In such a situation, the rock failed in tension is "completely" removed from the cavity and provides no back support. The aim of these test runs, however, was to model an outburst in a situation where the cavity is not emptied, but remains filled with the broken rock which provides a confining pressure to the inside of the cavity (refer to Fig. 6.8). This model resembles the practical 'choke up' outburst as reported in the literature. As discussed in section 6.4.5, it is simulated by assigning a specified Young's modulus to the broken rock in the cavity which is lower than that of the unbroken rock.

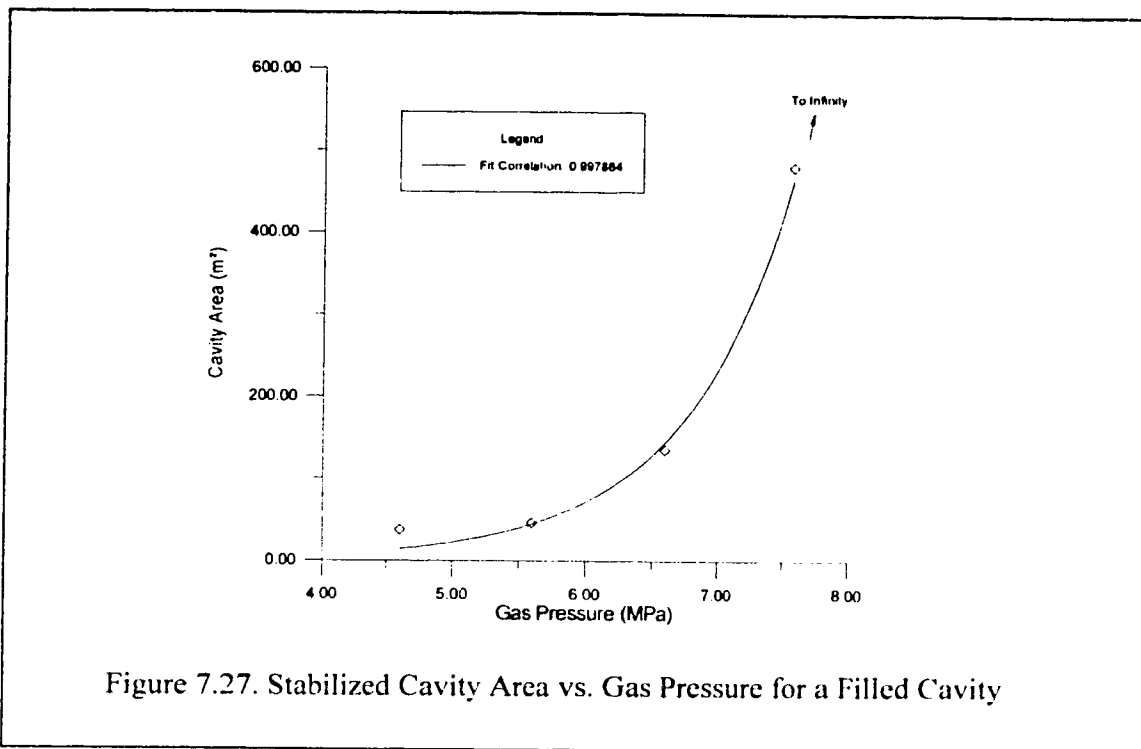
The conditions for the model are basically the same as used in the parametric study. Only a stress ratio 0.5, exposure angle 0° and sandstone height of 15.8 m were tested against the gas pressure.

Gas Pressure Influence on Cavity Size for Filled Cavity Table 7.8

Gas Pressure(MPa)	4.6	5.6	6.6	7.6	9.6
Stabilized Cavity Size (m ²)	37.0	45.8	135.0	480.4	To Infinity

The cavity development was investigated for a modulus ratio (E_u/E_b) of 18.5, where E_u is the Young's modulus of unbroken rock and E_b is that for the broken rock. Table 7.8 shows the cavity size development for a range of increasing gas pressure from 4.6 MPa to 8.6 MPa. The figures in the Appendix G show the shapes and sizes of the cavities formed after the expelling process ceased and the cavity with which the spalling

process was deemed to go to infinity. A steady increase of cavity sizes was obtained before it goes to infinity at gas pressure 8.6 MPa. This relationship is plotted in Fig. 7.27. Cavity shape formed possesses the same characteristics as discussed in the parametric study in section 7.4.2.



One factor that must be investigated for this situation is the influence of variation of the assigned value for the Young's modulus of the broken rock. This variation is directly associated with the changing E_u/E_b ratio. Preliminary investigations show that the ratio of Young's modulus between unbroken and broken rock has a significant influence on the stability of the cavities as well as on the size of the cavities, under the same other conditions. When modulus ratio is greater than 20, the results are very similar to those for the empty cavity where this modulus ratio is much higher (185000 times). When the modulus ratio lies between 1 to 20, the cavities stabilize more easily. It is also found that the size of stabilized cavity tends to increase with this ratio, assuming that the other conditions remain the same.

7.6 Discussion

In this chapter, the model established in chapter 6 has been applied to the development entry of a coal mine where the outbursts have most frequently taken place. The model was first tested against the case history of outbursts at No. 26 Colliery. It was found that the model could produce very similar results to observations in practice. As No. 26 Colliery is the only case history available for verification purposes, the model can not be said to have been fully verified.

Parametric studies were then carried out to further test the model, in addition to investigating some other pertinent aspects of outbursts. The results from these studies have shown very favorable support to the model through the similarities shared with the field observations. Field observations and model results all suggest that outburst tends to more severe (more broken material expelled) as the gas pressure increases (in the field, it is generally observed that gas pressure increases with the depth and so does the severeness of the outbursts). An outburst case was reported by Gray (GRAY, 1980) in which the cavity left by the outburst measured 21 m long, and a total of 300 m³ (400 tons) broken material was expelled. There were no field measured data to show the conditions under which this outburst took place, but it was certain that the unusual size of the cavity was related to the high gas energy (pressure). By this model it is known that when gas pressure increases beyond a certain magnitude, the spalling process tends to continue to infinity. A very large (deep) cavity may form and the outburst terminates due to some other mechanisms (such as broken material "choking" it). The results from analysis of the influence of sandstone height and exposure angles are also similar to the observations in the field.

The parametric studies also revealed some interesting trends that can be utilized in prevention measures. The most obvious example is the study of the pre-existing shear zone. Other factors discussed in the chapter may also be used as the guide lines for the prevention. For example, the exposure angle can be adjusted by changing the position of entry in the formations to minimize the possibility of outburst initiation. As matter as fact, the model has included many factors, such as rock strength, rock deformation properties, formation geology, etc.. Sensible application of the model to investigate the factors involved may eventually generate a preventive plan for a mine to avoid the harm from the outbursts.

7.7 Summary

From above applications of the model and the discussions, several interesting points can be concluded as below.

1. The model has been verified by comparison with the outbursts at No. 26 Colliery. This verification is strengthened by the following parametric analysis.

2. The initiation gas pressure study shows that the gas pressure required to initiate an outburst is more sensitive to exposure angle than sandstone height and field stress ratio. A minimum gas pressure occurs at exposure angle ranging between 25° and 45°.

3. Cavity size left after cessation of an outburst is greatly influenced by the gas pressure contained in the formation. The gas pressure increases the cavity size until it goes to infinity. A stabilized cavity tends to become an elliptical shape in all conditions, with the major axis oriented in the direction of the major principle stress.

4. Sandstone height, associated with the formation thickness in which the gas is contained, controls whether the outburst can be stabilized, while exposure angle will influence the stabilized cavity size. The thinner the gas containing formation, the easier it is for the outburst to stabilize. The larger the exposure angle, the smaller will be the stabilized cavity size.

5. Stress ratio does not show regulated influence on the outbursts, but it is, indeed, an influencing factor. Kullman's results on the bilinear relationship between the initiation gas pressure and field stress ratio (KULLMAN, 1989) may apply to a particular set of conditions. Stress levels show certain pattern of influence on the stabilized cavity size. A bilinear relation is clearly illustrated.

6. The filled cavity model indicates that the cavity may stabilize an outburst more easily. The influence of gas pressure on the cavity size with a filled cavity model is similar to that summarized in conclusion three above. The Young's modulus ratio has a significant contribution to the stability of the cavity formed by the outbursts.

7. The model can be used to attempt a prediction, as well to assess preventive measures for a particular situation. As many factors have been involved in the model, which are directly or indirectly responsible for the outburst phenomenon, the application of the model to specific cases may be more useful than doing "general" analysis with the model. However, care must be exercised when applying the model results to assessment of the real mining situation. In particular, it is believed that the model is better used to make comparison of the relative merits of two mining schemes, rather than relying on the absolute values.

Chapter VIII

APPLICATION TO LONGWALL FACE

Outbursts have taken place on longwall faces, but have rarely been reported in the literature. A few cases have been mentioned for mines in European countries. Most cases found in the literature have provided very little, if any, usable data for this modeling application. In 1982, a number of outbursts occurred at Dutch Creek #1 coal mine which belonged to Mid-Continent Resource (MCR), Pitkin county, Colorado, U.S.A.. Varley reported this case history in a paper (VARLEY,1986) which contained almost enough information for the model application. This information is the most detailed that has been found by reviewing the literature and it will be used in this application. Additional data needed in the model was derived from other relevant resources.

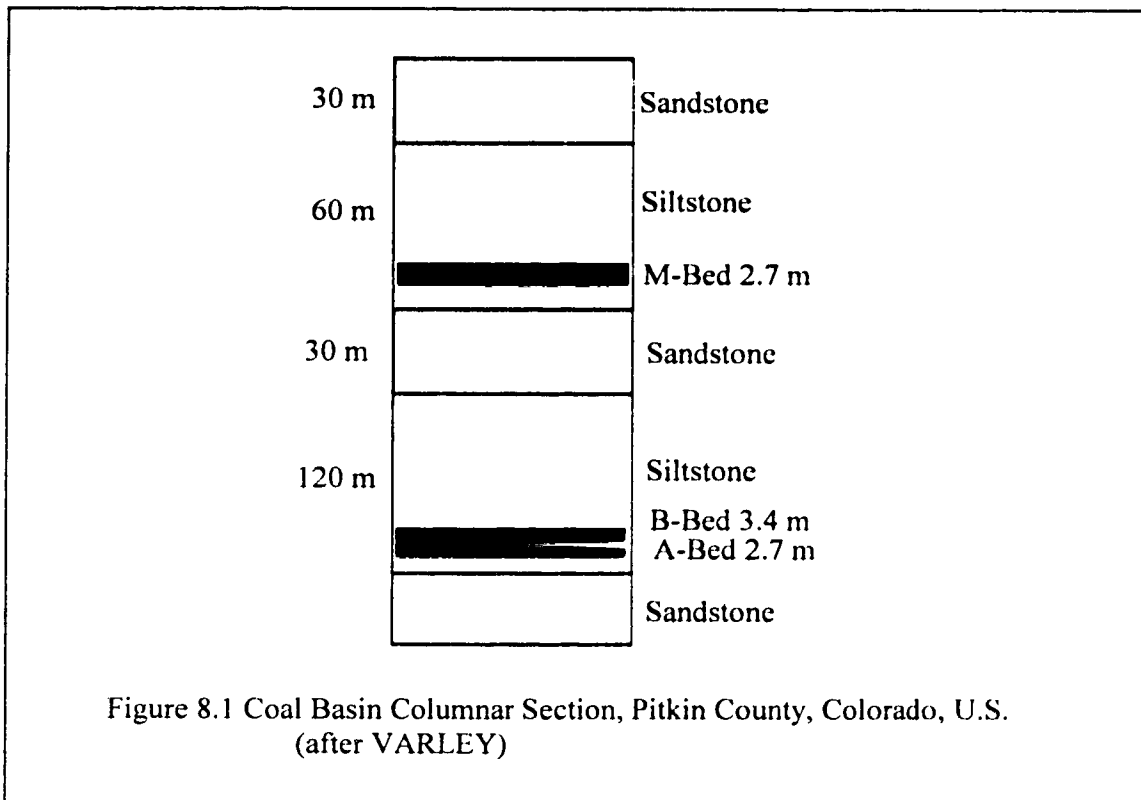
8.1 Statement of the Problem

Compared to outbursts occurring in entries, outbursts on longwall faces always happen in the coal seam, which usually is the major gas bearing strata. Due to the difference of the working face layout, the geometry of the model for longwall face outbursts will be different from that of the entry model. As the longwall face width is relatively much longer than the longwall face height, plane strain conditions can best represent of the stress conditions on the cross sections of the central portion of the longwall. The two dimensional model developed in Chapter 6 will be most suitable for this condition. Field observations also reveal the differences in the development of an outburst cavity and show that, in this case, the cavity formed develops horizontally into the face and usually grows into a crescent shape.

In applying the model, these distinct features of longwall face outbursts will be incorporated as model inputs and will be examined against the model results accordingly. The object of this study is to test the application of the model to longwall face outbursts. Only the empty cavity model will be studied in this application. The outburst development will be the major subject to be examined.

8.2 Introduction to MCR outbursts

Mid-Continent Resource operated a number of mines in the pitching seams which outcrop at 3,000 m elevation in the Pitkin Coal Basin. Mining workings were at a depth of 600 m to 900 m when outbursts were recorded. There were two coal seams which were simultaneously mined at that time, the M-Bed and the B-Bed seam. The columnar section of the strata around the two seams is shown in Fig. 8.1. The thickness of the M-Bed ranges from 1.2 m to 4.6 m and that of the B-Bed ranges from 1.8 m to 4.0 m. The two seams lie 140 m to 150 m apart, with M-Bed on the top. B-Bed is underlain by 0.3 m to 2.4 m of competent shale, which is followed, in turn, by the A-Bed ranging in a thickness from 1.8 m to 3.7 m. In some area of the Coal Basin, A and B beds combine to form a 7.6 m coal seam.



Both M-Bed and B-Bed have an immediate roof of siltstone which is overlain by a sandstone formation. The immediate roof is over 50 m thick for both seams. A very thin layer of siltstone constitutes immediate floor of both beds. A thicker sandstone formation

underlies the immediate floor of the seams. The siltstone and sandstone are both described as competent and generally strong. The coal seams are generally soft and weak, having a Hardgrave index in excess of 100.

Outburst control measures were started in 1976 in the mines belonging to MCR. Dutch Creek #1 mine (one of MCR mines) began to put an advancing longwall face (LW102) into operation in late 1982. The longwall face was located in B-Bed and was 244 m wide. It was this panel that experienced outburst problems soon after start up. Table 8.1 lists the outbursts that occurred on longwall LW 102 during the life of this advancing longwall operation.

Severe Outbursts of LW 102

Table 8.1

Events	Type	Date	Location Advanced (m)	How Triggered
1	CO	1-23-83	82	mining
2	CO	2-22-83	125	mining
3	CO	2-25-83	131	mining
4	CO	3-23-83	163	mining
5	CO	4-25-83	184	mining
6	FO	4-20-83	188	mining
7	FO	9-17-83	305	blasting
8	FO	1-28-84	414	blasting/WI
9	FO	6-18-84	572	blasting/WI

Notes: CO - Outburst of coal face

FO - Outburst of floor strata

WI - Water infusion

Methane was stored in the coal seam. When outbursts took place the methane acted as a medium to transport the broken coal, almost like fluid, towards the free face. A high abutment pressure zone was detected in front of the longwall face by the monitoring program started shortly after the outbursts impeded the mining operation. According to the descriptions of these events, they obviously belong to "coal outbursts" as defined in this thesis. A control program for the panel was set up later, after a short period of suspension of the operation. The outburst control system included recognition of the outburst prone zones, prevention through mine planning and operation, monitoring the stresses in problem areas and relieving the stresses in critical areas. No uncontrolled outbursts have been recorded since the introduction of the program until the completion

of panel in March, 1986, when the longwall had advanced about 1.2 km. The events 7-9 recorded in Table 8.1 were manually controlled outbursts.

8.3 Field Data

The layout of the advancing longwall face is shown in Fig. 8.2. It is an advancing longwall with a single head gate (HG) and tail gate (TG). A hydro-mechanical support system was applied for maintaining the gate road at the working face. The coal seam extracted was B-Bed. The overburden above the workings ranged from 600 m to 900 m. The stress field at such a depth is not known for this mine. An assumption has to be made for the model application.

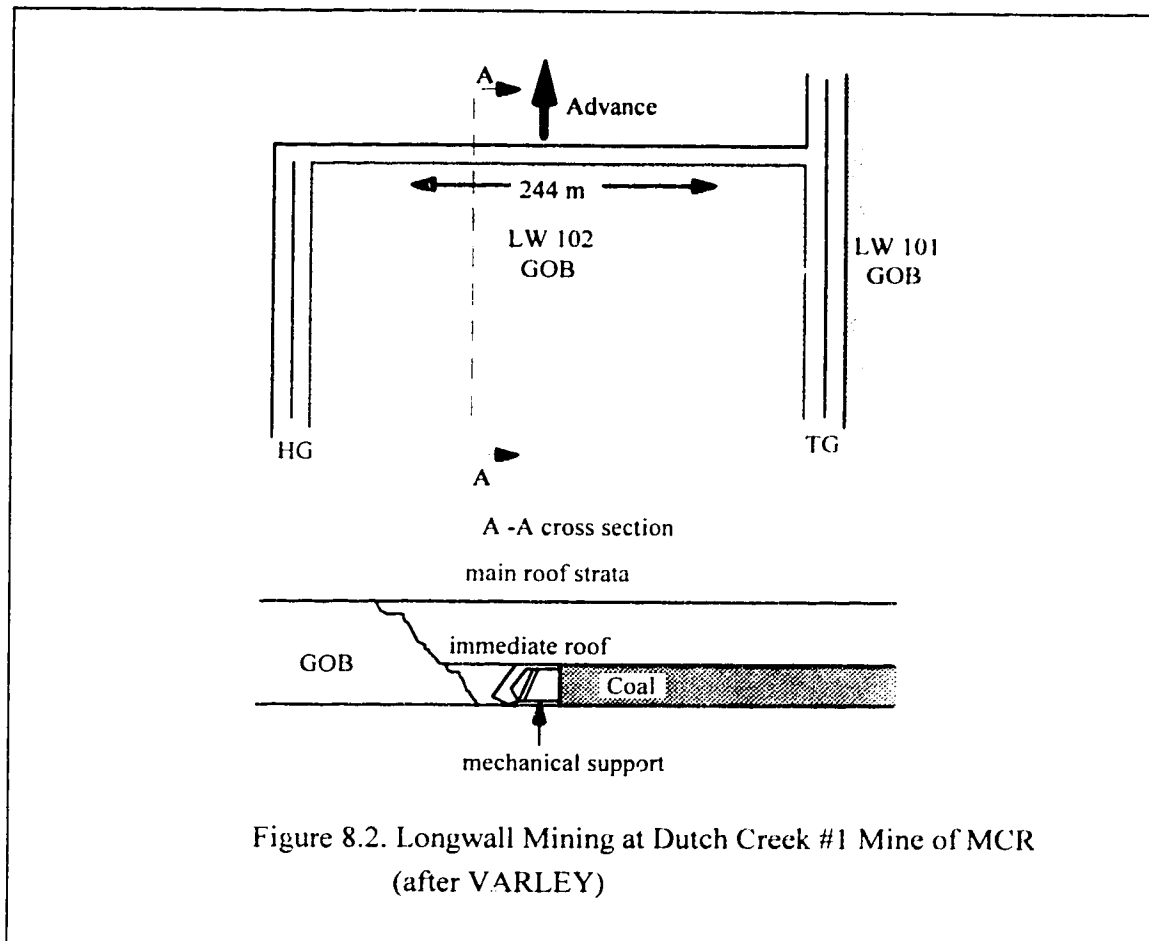


Figure 8.2. Longwall Mining at Dutch Creek #1 Mine of MCR
(after VARLEY)

The coal seam was generally soft, having an uniaxial compressive strength of 4,100 KPa to 7,600 KPa. The immediate roof and floor rock (siltstone) was generally strong with an uniaxial compressive strength of 62.0 MPa to 165.5 MPa. This is the only information about the strength and properties of coal seam and rock of strata available from Varley's paper. To achieve successful modeling, more information has to be extracted from other sources.

By searching through the literature, it was found that the mining geological settings of mines in the Southern Appalachian Basin, located in Buchanan County, VA, are similar to that of Dutch Creek #1 mine. Longwall mining has been the major productive method in these mines. The longwall panel was developed at a depth around 670 m and the coal thickness averaged 1.7 m. Dark gray shale (siltstone) composed the immediate floor and roof of the coal seam, and the main roof was a massive quartz arenite sandstone. Due to the rockburst problems in the area, many research and investigations have been carried out by U.S. Bureau of Mines. A number of data for the coal seam and surrounding rock formations have been derived which could be utilized as references.

A few NX-size boreholes were drilled into immediate roof and floor in the field investigations. Detailed lithological logs were produced from visual examination of the recovered core. Unconfined compressive and Brazilian tensile tests were performed on selected core samples, and Young's moduli and Poisson's ratios for rocks and coal material were calculated. The relevant data from these tests and calculations are extracted from the report (CAMPOLI, 1990), and are tabulated in Table 8.2.

Strength and Stiffness of Rock and Coal for Pocahontas No. 3 Coalbed Table 8.2

Rocks	σ_c (MPa)	σ_t (MPa)	E (GPa)	μ
Coal	12.5	NA	1.7-5.0	0.16-0.27
Shale	86.9-167.1	7.5-14.6	26.2-53.1	0.27-0.35
Sandstone	36.8-174.1	5.4-15.4	16.5-66.2	0.15-0.5

Notes: Coal - Common banded coal;

Shale - Dark gray shale;

Sandstone - Gray sandstone with shale streaks.

These strength and stiffness data for the strata are considered uncommonly high for coal measure rocks. Compared with the information at Dutch Creek #1 mine,

however, this coal has a 5-8 MPa higher uniaxial compressive strength while the shale and sandstone share a similar range of magnitude of uniaxial compressive strength.

8.4 Input Data for Modeling

The input data for the modeling were estimated from the above information collected from different sources. Estimation has to be made for the input data as there does not exist a complete set of data for the Dutch Creek #1 mine alone.

The modeling region was selected to be a square area, 60 m wide and 60 m high. The formation arrangement for the modeling area follows the sequence of shale (floor), coal seam, shale (immediate roof) and sandstone (main roof), which is analogous to the formation order that is revealed in the columnar section in Fig. 8.1. The thickness for each formation is given the values of 10.0 m, 2.5 m, 8.0 m and 39.5 m respectively. The coal seam is assumed to be extracted partially, leaving an open space with a specific span. The left and bottom sides of the modeling area are constrained only in the x and y direction respectively, while the right side and the top of the modeling area are all subjected to field stresses. All materials of the formation are assumed to be weightless for the gravitational loading calculation. The geology and the geometry of the modeling region and the boundary conditions are illustrated in the sketch, Fig. 8.3.

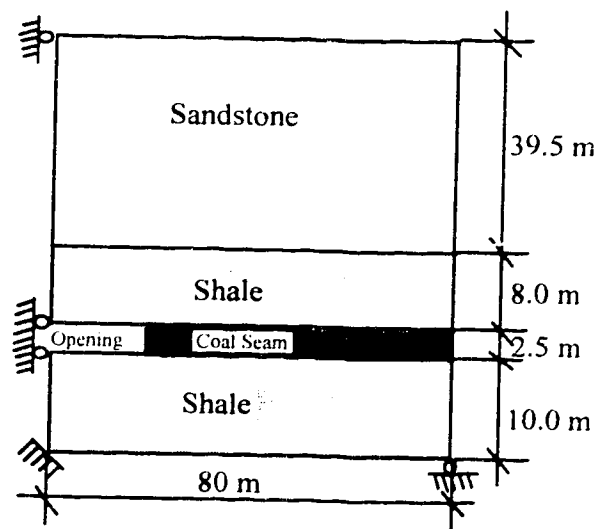


Figure 8.3. Setting-up for Longwall Modeling

Assuming 700 m overburden for the coal seam, the vertical stress can be estimated as 15 MPa if only gravitational stress is considered and if the overburden weight averages 0.021 MN/m³. Due to the relatively large depth, a stress ratio of 1.1 is assumed for the stress field in this application. The strength and property parameters of rock and coal seam are assumed according to the insitu information and estimation where the insitu information is absent. These data are tabulated in the following table.

Strength and Property Parameters of Rock and Coal for Modeling Table 8.3.

Rock	W (MN/m ³)	σ_t (MPa)	c (MPa)	ϕ (°)	E (GPa)	μ
Coal	0.015	1.00	5	30	5.0	0.27
Shale	0.025	NA	20	35	18.5	0.23
Sandstone	0.023	NA	18	32	17.0	0.25

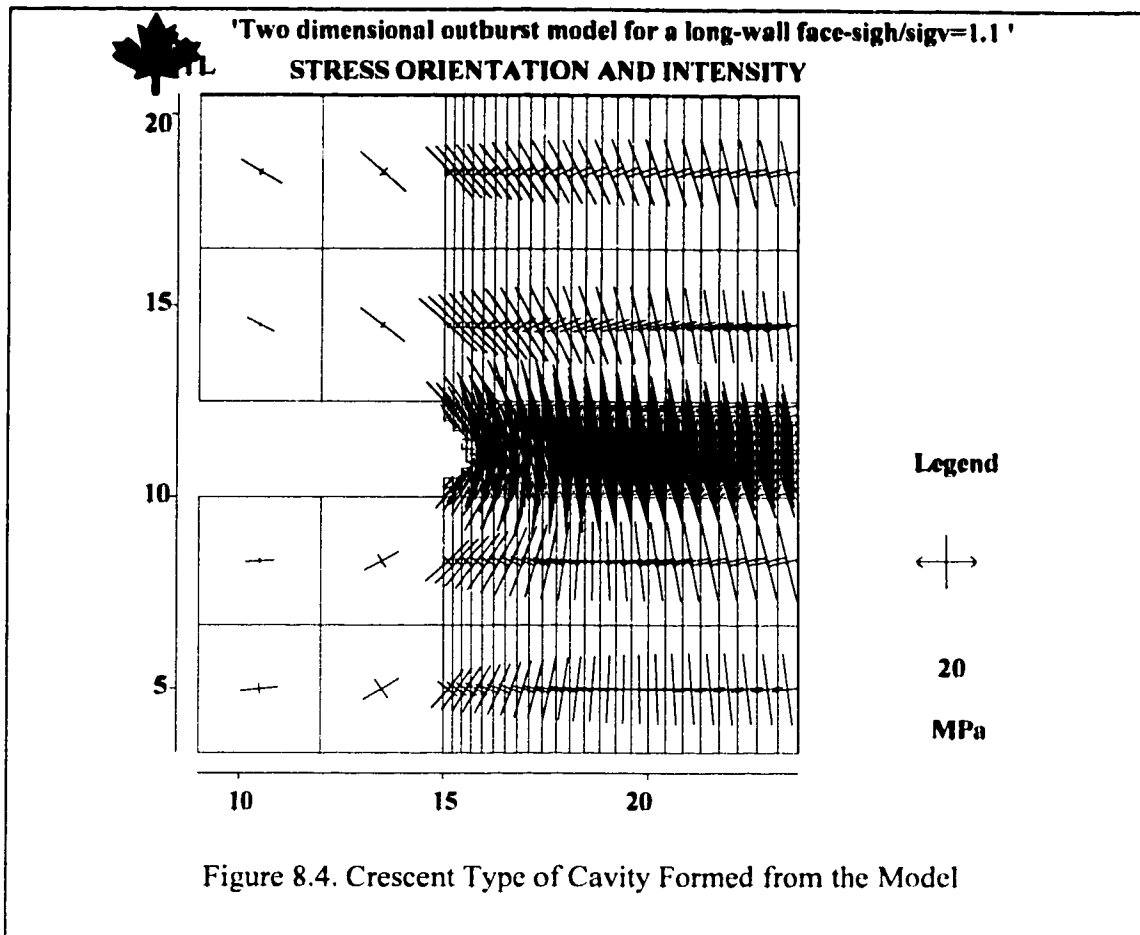
Note: NA - Not applicable.

Above data and conditions are sufficient for the model application. Because this information is only estimated, the model application can only serve as an example rather than as a true case study as was the No. 26 Colliery case. This exercise, however, will prove that this model is capable of handling the outburst problems encountered on a longwall face and, therefore, is worthwhile carrying out.

8.5 Results from the Model Application

A number of test runs of the model have been carried out under a set of different gas pressures. The span of the extraction was found not to influence the initiation of the outbursts and the development of the cavity size to any great extent. Three different spans were set up for examination. The results of all these runs have confirmed that the outbursts terminate with a crescent shape cavity being formed. Fig. 8.4 shows clearly a crescent shaped cavity which is resulted from the model run with a 15.0 m span and the 9 MPa gas pressure.

The cavity areas resulting from these preliminary runs of the model are summarized in Table 8.4. For a given span of the extraction, the cavity size formed by the outburst increases with the increase of the gas pressure. When the span increases the cavity area remains almost unchanged as shown in Fig. 8.5. Because there was no cavity size data collected in the field, the resulting cavity sizes can not be verified.



Model Results for the Cavity Formed for Longwall Face

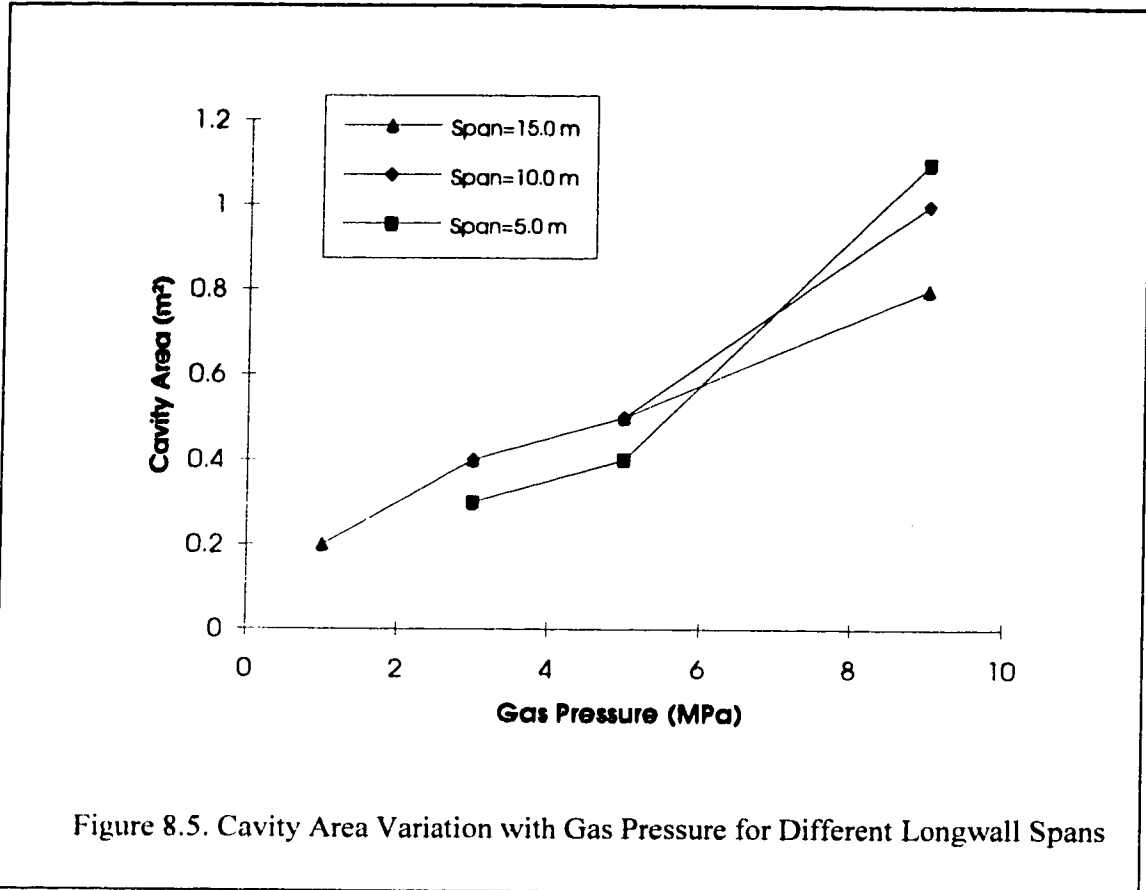
Table 8.4

Span (m)	5			10			15				
Gas pressu. (MPa)	3.0	6.0	9.0	3.0	6.0	9.0	0.5	1.0	3.0	6.0	9.0
Cavity size (m ²)	0.3	0.4	1.1	0.4	0.5	1.0	0.0	0.2	0.4	0.5	0.8

Note: Cavity size of 0.0 indicates that no outburst initiates.

The gas pressure that initiates an outburst was examined only for the 15.0 m span case. When gas pressure drops to 0.5 MPa, an outburst does not initiate. If gas pressure increases to 1.0 MPa, an outburst initiates and results in an 0.2 m² stabilized cavity. The outburst initiation gas pressure for this case, then, is estimated to lie between 0.5 MPa

and 1.0 MPa. As the cavity development is not sensitive to the span, it is assumed the initiation of the outbursts will not be greatly influenced by the change of the span.



8.6 Summary

An outburst occurring on a longwall face has been simulated with the model developed in this Chapter. The simulation conditions are approximated on the basis of the outbursts that took place at Dutch Creek #1 mine at Pitkin County, Colorado. Due to lack of the data required to conduct the simulation, other sources have to be used to estimate the input data required for the model. Therefore, this application can only serve as an example of the model application. The results of the simulation seem to be reasonable in a general sense. They show that, under the same conditions, the stabilized cavity size formed from the outburst increases with the increase of the gas pressure. This tendency has been observed in field. An initiation gas pressure was identified for the situation

when the extraction span was 15.0 m. With such a capability, the model can be useful in assisting engineers in attempting to predict an outburst. This example has shown that the model can efficiently deal with outbursts occurring on a longwall face. However, no field cavity data has been found that would allow the model to be verified.

Chapter IX CONCLUSIONS

Many models of outbursts occurring in underground mines have been proposed in the past. Most of them are descriptive in nature, or difficult to manage in an engineering manner, and are not practically workable models. The modern electronic numerical computations and computer modeling technology has opened new horizons for a break through. This model is developed on the basis of such a new starting point. It has shown that the model may be applied to practical engineering problems. The model has great potential for growth into a more sophisticated tool to assess outbursts. In particular, the following contributions can be identified and conclusions can be drawn.

9.1 Summary

- 1). This study has accomplished the goal of developing a numerical model of the outburst phenomenon.
- 2). The comparison between the model and the case history from No. 26 Colliery is successful in terms of verification. The parametric analysis also provides very strong support to this model verification. This indicates that the mechanism inherent in the model may offer a viable explanation of the true mechanism for outbursts.
- 3). Parametric studies reveal the general characteristics reported in past literature. The results show that outburst initiation, cavity development, stabilized cavity size and the stabilization of an outburst are influenced by gas pressure, sandstone height, exposure angle, stress ratio and stress level. In addition, many other factors have been considered in the model and their influences can be easily investigated with this model.
- 4). The model can be used to examine the factors involved in the model for a given set of conditions; this should help attempts to make the regional and local predictions, and to identify what remedial actions might be the most likely to succeed in minimizing or eliminating the outburst dangers.

- 5). The filled cavity model simulates the "choke up" outburst phenomenon successfully. This proves that the model is able to explain this particular cessation mechanism for an outburst, which has been reported in the past literature.
- 6). Application of the model to the outbursts occurring on a longwall face was demonstrated. The crescent shape cavity increases with the gas pressure. However, no field data was available that would allow the quantitative, rather than qualitative, verification of this application.

9.2 Model Advantages

Through the study and application of the model, following advantages have been realized:

- 1). This model is a practical tool which demands only conventional field data for execution, so that data collection is affordable by an individual mine.
- 2). The model can be easily adapted to cope with the local conditions. Because the finite element method is designed to evaluate the stress states, any material stress-strain constitutive relationship could be dealt with. Major faults or other geological features of concern could be introduced and simulated in one run.
- 3). Operation of the model is straightforward. As soon as several simple input files are prepared, the model executes automatically to produce final results graphically or in the readable data prints.
- 4). The model has a great potential for further development. It is easy to incorporate a new failure algorithm and new features concerned with the outburst phenomenon. The energy aspects of outbursts could be included in the model through a proper modification.

9.3 Model Limitations

Although good success has been achieved by this model, there are some limitations which can be summarized below.

- 1). The verification of the model still requires substantially more case histories for comparison. Until such field data is forthcoming, it will not be possible to fully verify this or any other outburst model.
- 2). The model itself is not perfect. Many modifications can be made to improve the model, such as using more a sophisticated finite element. It is this limitation that is the origin of the recommendations for further development of the model in next chapter.

Chapter X FUTURE WORK RECOMMENDED

Many recommendations are considered for the future research in this direction of solving the outburst problems. The more important ones are summarized as:

- 1). The model needs to be developed into three dimensions to accommodate the end effects of the entry face. As most outbursts occur in the development entry headings, a 3-D model could more realistically simulate the stress state for the condition.
- 2). The current model can only handle a perfect elasto-plastic material. More material constitutive relationships should be included in the program for a better performance of the model. The capability of dealing with discontinuities would also add an extra feature to the model.
- 3). A better finite element section and finite element algorithm to handle the non-linearity may speed up the execution of the model and save effort.
- 4). Attention must be paid to data collection from more case histories, for the verification purposes. Physical experiments in the laboratory are recommended as an additional support for the verification of the model.
- 5). The general studies, such as the parametric analysis conducted in this study, are recommended for the parameters such tensile strength, Young's modulus, Poisson's ratio and shear strength, etc..

REFERENCES

- ASTON, T. R. C.** (1985). Theoretical in situ strata reservoir and pore pressure calculations for material from No. 26 Colliery, N.S. Report No. 85-15 (TR), ERP/CRL CANMET.
- ASTON, T. R. C. & CAIN, P.** (1985). Gas and rock outbursts at No. 26 Colliery, Sydney coalfield, Nova Scotia - a case history. Proc. 21st Int. Conf. Safety in Mines Research Inst., Sydney, Australia, 139-146.
- ATES, Y.** (1987). The effect of sorption on strength of coal and its influence on coal outbursts. MSc. Thesis, University of Alberta.
- BARKER-READ, G. R.** (1984). The gas-dynamic behavior of Coal Measures strata with particular reference to west Wales outburst-prone seams. Ph.D. Thesis, University of Wales (Cardiff), U.K..
- BARRON, K. & KULLMANN, D.** (1990). An effective stress/strength approach to the simulation of gas induced outbursts. Special Conference: Stresses in Underground Structure: Determination, Prediction and Monitoring Ottawa, Canada.
- BARRON, K. & KULLMANN, D.** (1991). Modeling of outbursts at #26 colliery, Glace Bay, Nava Scotia: Part 2: Proposed outburst mechanism and model. Mining Science and Technology, .
- BONNECHERE, F.** (1971). Contribution a la determination de l'etat de contraintes des massifs rocheux.. Ph.D. Thesis, Universite de Liege.
- CAIN, P.** (1984). Outbursts at Number 26 Colliery. Report No. ERP/CRL 84-1(CF). CANMET.
- CIS J. et al** (1964). Outbursts of CO₂ and solids in the mines of the Lower Silesian coalfield, and methods of outburst control. Symp. on Coal and Gas Outbursts, Nimes, France. 179-193.

- CURL, S. J. (1978).** Methane prediction in coal mines. IEA Coal Research.
- CYRUL T. (1992).** A concept of prediction of rock and gas outbursts. *Geotechnical and Geological Engineering*, v. 10, 1-17.
- CZECHOSLOVAKIA P. (1964).** Coal and gas outbursts in Ostrava-Karvina coalfield. *Symp. on Coal and Gas Outbursts, Nimes, France*, 282-289.
- DORFELT, H. (1966).** Sudden outbursts of gas and rock in the mining of the GDR in relation to the safety in mines. *Intl. Congress on Sudden Outbursts of Gas and Rock Leipzig, GDR.*,
- DRUCKER, D. C. & PRAGER, W. (1952).** Soil mechanics and plastic analysis or limit design. *Q. App. Math.* v. 10, 157-165.
- ETTINGER, I. L. & LAMBA, E. G. (1957).** Gas medium in coal breaking process. *Fuel*, 36, 298-231.
- ETTINGER, I. L. & SHUL'MAN, N. V. (1975).** Distribution of methane in the pores of natural coals. *Nauka*.
- FARMER, I. W. & POOLEY, F. D. (1967).** A hypothesis to explain the occurrence of outbursts in coal, based on a study of west Wales outburst coal. *Int. J. Rock Mech. and Min. Sci.*, v. 4, 189-193.
- GALLANT, W. D. & ASTON, T. R. C. (1985).** Measurement of in situ strata gas pressure at NO. 26 Colliery, Sydney Coalfield, N.S. Report No. 85-10(TR), ERP/CRI. CANMET.
- GIBOWICZ, S. J. (1988).** The mechanism of seismic events induced by mining: - A review. *The Proc. Second Int. Symp. Rockbursts and Seismicity in Mines, Minneapolis, Minnesota, U.S.A.*, 2 - 121.

- GOLDER ASSOCIATES, (1987).** Development of an outburst model for the Sydney coalfield Cape Breton, Nova Scotia. Contract Report (DSS Contract No. 23440-6-9025). Golder Associates consulting geotechnical and mining engineers.
- GORSKI, B. (1984).** Laboratory test results of rock cores from No. 26 Colliery, Sydney Coalfield. Report No. 84-25(TR), ERP/MRL CANMET.
- GRAY, I. (1980).** The mechanism of, and energy release associated with outbursts. Symp. on Occurrence, Prediction and Control of Outbursts in Coal Mines, Southern Queensland Branch, Austr. Inst. Mining and Metall., Australia, 111-126.
- HARGRAVES, A. J. (1958).** Instantaneous outbursts of coal and gas. Proc. Australas. Inst. Min. Metall., 186, 21-72.
- HARGRAVES, A. J. (1959).** Some instantaneous outbursts of coal and gas. Qd. Govt. Min. J., 160, 695-699.
- HARGRAVES, A. J. (1966).** Occurrence, investigation and control of sudden outbursts of coal and gas in Australian mines. Intl. Cong. on Problems of Sudden Outburst of Gas and Rock Leipzig. GDR.
- HARGRAVES, A. J. (1980).** A review of instantaneous outburst data. Symp. on the Occurrence, Prediction and Control of Outbursts in Coal Mines, Southern Queensland Branch, Austra. Inst. Mining and Metall., Australia, 1-18.
- HARGRAVES, A. J. (1983).** Instantaneous outbursts of coal and gas - A review. Proc. Australas. Inst. Min. Metall., 285, 1-37.
- HARGRAVES, A. J. (1984).** Particular gas problems of Australian deep coal mining. 3rd Intl. Mine Ventilation Congress, Harrogate, England.
- HARGRAVES, A. J. (1993).** Update on instantaneous outbursts of coal and gas. Proc. Australas. Inst. Min. Metall., No2, 3-17.

- HIRAMATSU, Y. & OKA, Y.** (1968). Determination of the stress in rock unaffected by boreholes and drifts, from measured strains and deformations. *Int. J. Rock Mech. Min. Sci.*, 5, 337-353.
- HIRAMATSU, Y., SAITO, T., & ODA, N.** (1983). Studies on the mechanism of gas and coal bursts in Japanese coal mines. *Proc. the 5th Intl. Conf. on Rock Mechanics*, Melbourne, Australia, E7-10.
- KARAGODIN, L., KOLESOV, O., & BOL'SHINSKII, M.** (1983). Method of forecasting and suppression of rock and gas outbursts in Donbass. HSE Transl. No. 12025. 20th Int. Conf. Safety in Mines Research Inst., Sheffield, United Kingdom, 11pp.
- KHOROSHUN, L. P.** (1976). Saturated porous media. *Soviet Applied Mechanics* (English translation of *Prikladnagn mekhanika*), 12 (12), 1231-1237.
- KHOROSHUN, L. P. & ISRAFILOV, R. M.** (1981). *Soviet Applied Mechanics* (English translation of *Prikladnagn mekhanika*), 17 (5), 412-417.
- KHOROSHUN, L. P. & SHIKULA, E. N.** (1984). Stress state in vicinity of ellipsoidal excavation in gas-bearing massif during nonsteady gas filtration. *Soviet Applied Mechanics* (English Translation of *Prikladnaya Mekhanika*), 20 (4), 309-313.
- KHRISTIANOVICH, S. A. & SALGANNIK, R. L.** (1983). Several basic aspects of the forming of sudden outbursts of coal (rock) and gas. *Proc. the 5th Intl. Congress on Rock Mechanics*, Melbourne, E41-50.
- KING, G. R. & ERTEKIN, T.** (1984). A comparative evaluation of vertical and horizontal drainage wells for the degasification of coal seams, SPE 13091, SPE.
- KOVALENKO, Y. F.** (1980). Effective characteristics of bodies with isolated gas-filled cracks (in Russian). *Fracture wave*, Moscow: Inst. Probl. Mech. Acad. Sci. USSR, preprint 155.
- KOWING, K.** (1977). The relationship of geological structure to gas outbursts. *Gluckauf*, 113 (20), 996-999.

- LAMA, R. D.** (1968). Outbursts of gas and coal. *Colliery Engineering*, v. 45, 103-109.
- LIDIN, G. D. & FKODOT, V. V.** (1964). Control of coal and gas outbursts in mines of the USSR. *Symp. on Coal and Gas Outbursts, Nimes, France*, 228-243.
- LITWINISZYN, J.** (1985). Technical note - A model for the initiation of coal-gas outbursts. *Int. J. Rock Mech. Min. Sci. & Geomech. Abstr.*, 22 (1), 39-46.
- LITWINISZYN, J.** (1986). Remarks concerning sudden rock-and-gas mass outbursts. *Mining Science and Technology*, v. 3, 243-253.
- MAHNER, S.** (1966). Critical observations on some gas-outbursts which have occurred in recent years. *Int. Congr. on Problems of Sudden Outburst of Gas and Rock, Leipzig, GDR*.
- MAHTAB, M. A.** (1982). Geomechanical aspects of gas outbursts in Louisiana salt mines. *Bulletin of the Association Engineering Geologists*, 19 (4), 389-400.
- NORRIS, D. K.** (1958). Structural conditions in Canadian coal mines. *Bull. Geol. Surv. Can.*, v. 44, p. 55.
- PATCHING, T. H. & BOTHAM, J. C.** (1966). Occurrence, research and combating sudden outbursts of coal and gas in Canada. *Int. Congress on Sudden Outbursts of Gas and Rock: for outbursts in coal, Leipzig, GDR*, 23 (4), 327-332.
- PATCHING, T. H.** (1970). The retention and release of gas in coal - A review. *CIM Transl.*, v. 73, 328-334.
- PATERSON, L.** (1985). Technical Note - A model for outbursts in coal mines. *Int. J. Rock Mech. Min. Sci. & Geomech. Abstr.*, 23 (4), 327-332.
- PATERSON, L. & SCHLANGER, H. P.** (1985). Technical Note - A theoretical model for outbursting in coal mines. *Bull. Proc. Austras. Inst. Min. Metall.*, 290 (7), 67-69.

- PAUL, K.** (1983). Methane bursts involving the ejection of rock material. Symp. Methane Bursts Involving the Ejection of Coal or Rock. Luxembourg, GDR.
- PETUKHOV, I. M.** (1983). Theoretical principles and fundamentals of rock burst prediction and control. Proceedings of the 5th International Congress on Rock Mechanics, Melbourne, Australia, D113-120.
- PHILLIPS, W.** (1944). Rock bursts and bumps in coal mines. Trans. Inst. of Min. Eng., v. 104, 55-94.
- PHILLIPS, W.** (1948). Tectonics in mining. Colliery Eng., p. 12.
- POMEROY, C. D.** (1956). Creep in coal at room temperature. Nature, v. 178, 279-280.
- REYES, S. F. & DEERE, D. V.** (1966). Elastic-plastic analysis of underground openings by finite element method. Proc. First Congr. Int. Society of Rock Mechanics, Lisbon, 477-483.
- REVALOR, R., ARCAMONE, J., & JOSIEN, J. P.** (1985). In situ rock stress measurements in French coal mines: Relation between virgin stresses and rock bursts. 26th US Symp. on Rock Mech.: Research and Engineering Applications in Rock Masses, Rapid City, U. S. A., 1103-1112.
- RICE, G. S.** (1931). Introductory notes on origin of instantaneous outbursts of gas in certain coal mines of Europe and western Canada. Transactions of the American Institute of Mining and Metallurgical Engineers (Coal Division), 75-87.
- SALAMON, M. D. G.** (1983). Rockburst hazard and the fight for its alleviation in South Africa, in Rockburst. Prediction and Control. Symp. Proc., London, U.K., 11 - 36.
- SHEPHERD, J., RIXON, L. K., & GRIFFITHS, L.** (1981). Rock mechanics review: Outbursts and geological structures in coal mines: A review. Int. J. Rock Mech. Min. Sci. & Geomech. Abstr., v18, 267-283.

- SHUL'MAN, N. V.** (1975). The micropore structure of natural coal as a factor which determines the potential methane content of coal seams. Ph.D. Thesis, IPKON of the Academy of Science of the USSR.
- STACH, E., et al** (1975). Stach's text book of coal petrology. 2nd Edition.
- STAGG, K. G. & ZIENKIEWICZ, O. C.** (1979). Rock mechanics in engineering practice. John Wiley & Sons.
- STUTZER O.** (1936). Carbon dioxide eruptions from coal seams in Lower Silesia. *Econ. Geol.*, 31, 441-451.
- SZIRTES, L.** (1964). Problems relating to the safety and economics of shaft sinking in seams subject to gas outbursts. *Symp. on Coal and Gas Outbursts, Nimes, France*, 149-158.
- UJIHIRA M. & HASHIMOTO K.** (1976). A study of gas outbursts, geological structural conditions and effect of blasting. *J. Min. Metall. Inst. Japan*, 92(1066), 791-796 (in Japanese).
- VANDELOISE, R.** (1964). Survey of the methods of outburst control used in Belgium. *Symp. on Coal and Gas Outbursts Nimes, France*, 46-71.
- VANDELOISE, R.** (1966). Sudden outbursts of coal and methane in the Belgian coalfields - research work and methods of prevention of sudden outbursts. *Intl. Congress on Sudden Outbursts of Gas and Rock, Leipzig, GDR*.
- VARLEY, F. D.** (1986). Outburst control in underground coal mines. *Proc. 5th Confer. on Ground Control in Mines. West Virginia Univ., U.S.A.*, 249-256.
- WILSON, E. L.** (1963). Finite element method in two-dimensional problem. D. Engg. Thesis. University of California, Berkeley.
- WILSON, E. L.** (1965). Structural analysis of axisymmetric solids. *J. AIAA*, 3 (12), 2269-2274.

- WILSON, P. A. C.** (1931). Instantaneous outbursts of carbon dioxide in coal mines in Lower Silesia. *Trans. Am. Inst. Min. Metall. Engrs*, 94, 88-136.
- WONG, I. G. & MCGARR, A.** (1988). Implosional failure in mining-induced Seismicity: A critical review. *The Proc. Second Int. Symp. Rockbursts and Seismicity in Mines, Minneapolis, Minnesota, U.S.A.*, 13-28.
- WU, J.** (1987). Study on micro-structure and surface features of coal prone to outburst. *J. China Coal Society*, 40-46.
- ZORIN, A. N.** (1978). Upravleniye dinamicheskimi proyavleniyami gornogo davleniya (Controlling dynamic manifestations of mine pressure). *Nedra*, 67-73.

APPENDICES

Appendix A.

A Revised General Method for Geometrically Altered Structures

When dealing with geotechnical problems, the situation under consideration may involve major changes in the configuration of the structure due to either addition or removal of structural components. If the material behavior is inelastic, the final states of stress and deformation will be very dependent on the addition and/or the removal process. The general method is designed to determine stress and deformations resulting from major geometric alterations in structures. It incorporates the geometric alteration problem into the context of the Newton-Raphson family of solution techniques which are the major tools for nonlinear analysis. So, this method can be used to tackle the geometric non-linearity as well as the material property nonlinearities, which is the particular problem encountered in this model development. The general method is both more versatile and simpler to implement than the conventional procedure for tackling such a problem. It is this advantage that leads to the selection of this method in the development of this model.

In a system of the discretized elements in equilibrium, removal of a specific number of elements will destroy the initial equilibrium and induce a system of residual forces which will destroy the equilibrium of the system. A residual vector R is defined as

$$R = P - I \tag{A.1}$$

where, P denotes the nodal external load vector and I is the nodal internal resisting force vector calculated from element stresses σ_k as

$$I = \sum_k L_k^T \int_{V_k} B_k^T \sigma_k dV_k \tag{A.2}$$

In above equation the subscript k is an element label and the summation is over the relevant group of elements. L_k is the Boolean incidence matrix, B_k is the element strain-nodal displacement matrix and σ_k is the element stress vector. Equation (A.2) provides a

consistent relation between nodal forces and element stresses and will in many cases be evaluated by Gaussian integration.

In a standard incremental formulation for nonlinear analysis, the loads and displacements for any incremental step can be expressed as ΔP_n and ΔU_n . The incremental equilibrium equations for increment n can then be expressed, then, as

$$K_n \Delta U_n = \Delta P_n + R_n \quad (\text{A.3})$$

where, K_n is the tangent stiffness and

$$\Delta P_n = P_n - P_{n-1}; \quad R_n = P_{n-1} - I_{n-1}. \quad (\text{A.4})$$

For a system which is exactly in equilibrium, $R_n = 0$. In nonlinear analysis, the absolute value of R_n is zero to within a small tolerance.

Substituting equations (A.4) into equation (A.3), gives following equation:

$$K_n \Delta U_n = P_n - I_{n-1} \quad (\text{A.5})$$

where I_{n-1} indicates the nodal internal resisting force vector computed from the element stresses in n-1 step. P_n is the total external load applied up to the n-th step. This equation can be used at the beginning of step n as long as the load vectors are modified appropriately to include the initial disturbance in equilibrium caused by altering the structure. This disturbance can be reflected in I_{n-1}^* . I_{n-1}^* can differ from I_{n-1} due to two distinct effects: first, elements which are removed from the structure do not contribute to the internal resisting force vector and therefore do not include in I_{n-1}^* ; second, if prestressed elements are added to the structure, I_{n-1}^* contain these additional load effects, but not in I_{n-1} . With such modification, equation (A.5) can be rewritten as

$$K_n \Delta U_n = P_n - I_{n-1}^* \quad (\text{A.6})$$

where I_{n-1}^* now simply represents the effects of internal stresses in those elements which are currently active. Solution of equation (A.6) will be used to calculate the stress and strain increment in step n and, then, in turn to update the displacements, stresses and strains from step n-1 as follows:

$$U_n = U_{n-1} + \Delta U_n$$

$$\begin{aligned}\epsilon_n &= \epsilon_{n-1} + \Delta\epsilon_n \\ \sigma_n &= \sigma_{n-1} + \Delta\sigma_n\end{aligned}\tag{A.7}$$

These incremental computations are iterated until all the load is applied and the geometric alteration is terminated to produce the result.

After implementing equation (A.6) in a nonlinear analysis FEM program, the procedures of addition and/or removal for elements should be considered. "Activate" and "deactivate" procedures are designed to accomplish the addition and the removal accordingly. The stiffness assembly, the generation of external loads and the internal resisting load vector under such a scheme must reflect the appropriate geometry changes of the system. The scheme keeps the stiffness matrix, the load and displacement vector size the same throughout the analysis. Those displacements representing currently non-activated elements are simply assigned a zero value in the usual manner. The "activate" and the "deactivate" procedures are described as follows:

Activating elements. All the elements (include those elements to be added) are present in the finite element mesh at all times. But those elements to be added only make contributions to the stiffness matrix, element load vector and internal resisting force vector when they are activated at a specific stage of the program as previously planned. These contributions can be realized by simply assembling the relevant terms into the proper position in the matrix and vectors of equation (A.6), which were previously occupied by a zero value. These activated elements will perform as other "permanent" elements in the usual manner for the rest of the steps if they are not "deactivated" again later.

Deactivating elements. The procedure to deactivate elements involves exactly opposite process as activating elements. At the n th step, when the "deactivation" is planned, the contributions of the group of the elements will not be accounted for in equation (A.6), i.e., those corresponding positions in the matrix and vectors are simply reset to a value zero. These reset values are kept unchanged in the rest of the calculation until it is commanded otherwise.

The both procedures are very simple to incorporate into an existing nonlinear finite element computer program. For this particular problem in the thesis, only the "deactivate" procedure is considered. The "deactivate" elements are not planned prior to the inception of the program. They have to be calculated from the previous result. These "decision" and "deactivate" procedures continue until no more elements are calculated and decided to be removed. With such a design, the whole simulation is handled within the same general framework.

Appendix B.
Patch Test

The patch test arose historically to test non-conforming elements. By using non-conforming elements in a standard finite element formulation one is, in effect, setting the wrong virtual work expression to zero. There are missing terms that are caused by discontinuities of the virtual displacements at the inter-element boundaries. These missing terms may or may not lead to divergence from an answer or to convergence to a wrong answer.

Among all the things that patch test can do, found lately by mathematicians, it can test for consistency. An approximate numerical procedure for solving a problem is said to satisfy consistency, if the approximate model, in the FEM case, $[K]\{q\}=\{R\}$, approaches the governing differential equations in the limit. Passing of the patch test, therefore, ensures the correct solution.

The patch test has also been used as the replacement for the continuity requirement in the list of sufficient conditions for the FEM convergence. In fact, it becomes the only condition that must be satisfied; that is, the patch test is a necessary and sufficient condition for convergence, since it tests for essential (kinematics) boundary conditions and completeness requirements for the convergence. The patch test has been referred as a valuable tool for testing new FEM program and finding programming bugs.

Since a patch test is a "must" to guarantee the convergence of the FEM program, it must be done in this research for the revised FEM program given here. Now, the problem is how the test is done. There are two basic methods to do the test, i.e., the mathematical patch test and the numerical patch test. The convention prefers a numerical test. The basic idea of the test is to set up a simple problem in which the exact strain field (that is stress field) is one that the individual elements are capable of representing. The constant strain field is always selected in the standard patch test since all elements must meet the constant strain requirement.

The patch test is not just a test of the elements but of the grid. For example, some elements are found to pass in one type of grid and fail in another. To avoid a grid in which the element might just happen to pass the test, it is usual practice to use a rather irregular grid containing different element sizes and shapes.

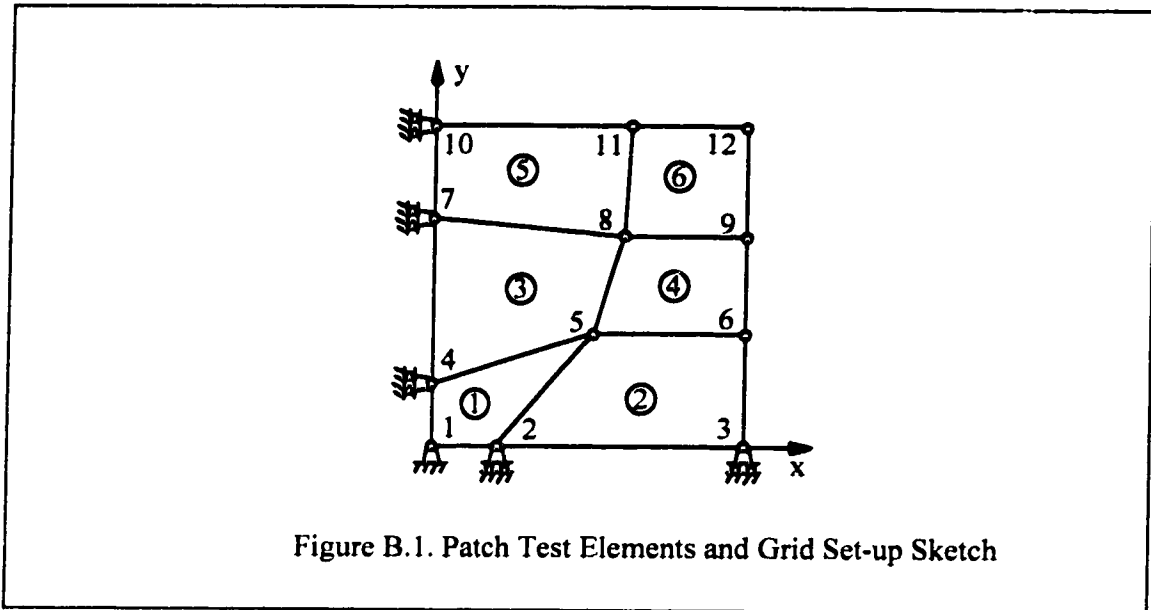


Figure B.1. Patch Test Elements and Grid Set-up Sketch

To do the patch test, set up a patch of elements as shown in Fig. B.1. The material properties are assumed to be:

Material Properties Used for Patch Tests			Table B.1
Young's Modulus (E)	Poisson's Ratio(μ)	Internal Friction Angle (ϕ)	Cohesion (c)
1.85 (GPa)	0.18	30°	10.0 (MPa)

In applying the patch test, all possible states of constant stress (strain) must be considered. For plane strain elements, constant σ_x , σ_y and σ_{xy} must be tested.

Constant σ_y :

By applying a uniformly distributed traction in y direction (refer to Fig. B.1), $T_{iy}=5$ (MPa), the closed form solution for the constant strain can be obtain as the follows.

$$\text{Given: } \sigma_x=0; \quad \sigma_y=5 \text{ (MPa);} \quad \tau_{xy}=0.$$

$$\epsilon_x = \frac{1-\mu^2}{E} \left(\sigma_x - \frac{\mu}{1-\mu} \sigma_y \right) = -\frac{0.18(1+0.18)}{0.185} \times 5 \times 10^{-5} = -5.9 \times 10^{-5}$$

$$\epsilon_y = \frac{1-\mu^2}{E} \left(\sigma_y - \frac{\mu}{1-\mu} \sigma_x \right) = \frac{1-0.18^2}{0.185} \times 5 \times 10^{-5} = 0.26 \times 10^{-3}$$

$$\gamma_{xy} = \frac{1}{G} \tau_{xy} = 0$$

The displacements of nodal points as shown in Fig. B.1, therefore, can be found in following table.

Closed Form Solution for Nodal Displacements											Table B.2	
Ele.	1	2	3	4	5	6	7	8	9	10	11	12
x (m)	0.0	0.7	3.0	0.0	1.6	3.0	0.0	2.0	3.0	0.0	2.2	3.0
y (m)	0.0	0.0	0.0	1.1	1.7	1.7	3.3	3.1	3.1	5.0	5.0	5.0
ux*	0.0	-4.1	-17.7	0.0	-9.4	-17.7	0.0	-11.8	-17.7	0.0	-12.98	-17.7
uy**	0.0	0.0	0.0	0.29	0.44	0.44	0.86	0.81	0.81	1.3	1.3	1.3

* unit is ($\times 10^{-5}$ m); ** is ($\times 10^{-3}$ m).

The finite element program results are shown in List B.1. The outputs give the "exact" nodal displacement values as closed form solution except the sign because of the opposite definition. The patch of elements is said to have passed this test.

Constant σ_x :

By applying a uniformly distributed traction in x direction, $T_{ix}=5$ (MPa), the closed form solution for the constant strain can be found as the follows.

$$\text{Given: } \sigma_x=5 \text{ (MPa); } \quad \sigma_y=0; \quad \tau_{xy}=0.$$

$$\epsilon_x = \frac{1-\mu^2}{E} \left(\sigma_x - \frac{\mu}{1-\mu} \sigma_y \right) = \frac{1-0.18^2}{0.185} \times 5 \times 10^{-5} = 0.26 \times 10^{-3}$$

$$\epsilon_y = \frac{1-\mu^2}{E} \left(\sigma_y - \frac{\mu}{1-\mu} \sigma_x \right) = -\frac{0.18(1+0.18)}{0.185} \times 5 \times 10^{-5} = -5.9 \times 10^{-5}$$

$$\gamma_{xy} = \frac{1}{G} \tau_{xy} = 0$$

The displacements of nodal points, therefore, can be determined in following table.

Ele.	1	2	3	4	5	6	7	8	9	10	11	12
x (m)	0.0	0.7	3.0	0.0	1.6	3.0	0.0	2.0	3.0	0.0	2.2	3.0
y (m)	0.0	0.0	0.0	1.1	1.7	1.7	3.3	3.1	3.1	5.0	5.0	5.0
ux*	0.0	0.18	0.78	0.0	0.42	0.78	0.0	0.52	0.78	0.0	0.57	0.78
uy**	0.0	0.0	0.0	-6.49	-10.0	-10.0	-19.47	-18.29	-18.29	-29.5	-29.5	-29.5

* unit is ($\times 10^{-3}$ m); ** is ($\times 10^{-5}$ m).

The finite element program results are obtained as List B.2. The solution is the "exact" same as the closed form solution, therefore, the patch of elements is said to have passed this test.

Pure Shear τ_{xy} :

In order to simulate the pure shear, the displacements for each node are prescribed in following table.

Ele.	1	2	3	4	5	6	7	8	9	10	11	12
x (m)	0.0	0.7	3.0	0.0	1.6	3.0	0.0	2.0	3.0	0.0	2.2	3.0
y (m)	0.0	0.0	0.0	1.1	1.7	1.7	3.3	3.1	3.1	5.0	5.0	5.0
ux*	0.0	0.0	0.0	1.54	2.38	2.38	4.62	4.34	4.34	7.0	7.0	7.0
uy	0.0	0.0	0.0	0.0	0.0	0.0	0.0	0.0	0.0	0.0	0.0	0.0

* unit is ($\times 10^{-4}$ m).

Therefore, it is given: $\epsilon_x=0$; $\epsilon_y=0$; $\gamma_{xy}=1.4 \times 10^{-4}$.

$$\sigma_x = \frac{1}{(1-2\mu)} \left(\frac{E(1-\mu)}{1+\mu} \epsilon_x - \mu(1+\mu) \epsilon_y \right) = 0$$

$$\sigma_y = \frac{1}{(1-2\mu)} \left(\frac{E(1-\mu)}{1+\mu} \epsilon_y - \mu(1+\mu) \epsilon_x \right) = 0$$

$$\tau_{xy} = G\gamma_{xy} = \frac{E}{2(1+\mu)} \gamma_{xy} = \frac{18.5 \times 10^3}{2(1+0.18)} \times 1.4 \times 10^{-4} = 1.097 \text{ (MPa)}$$

The finite element program results are shown in table B.3. The solution is the "exact" value as the closed form solution, the patch of elements is said to have passed this test.

Biaxial Loading with Gas Pressure:

In order to examine the ability of program to handle gas pressure, applying a uniformly distributed traction in x direction, $T_{ix}=2.0$ (MPa), and in y direction, $T_{iy}=5.0$ (MPa), and assuming a uniformly distributed gas pressure in the material, $P_{gp}=3.6$ (MPa), the closed form solution for the constant strain can be obtained as the follows.

$$\text{Given: } \sigma_x = -1.6 \text{ (MPa); } \quad \sigma_y = 1.4 \text{ (MPa); } \quad \tau_{xy} = 0.$$

$$\epsilon_x = \frac{1-\mu^2}{E} \left(\sigma_x - \frac{\mu}{1-\mu} \sigma_y \right) = \frac{1-0.18^2}{0.185} \times 10^{-5} \left(-1.6 - \frac{0.18}{1-0.18} \times 1.4 \right) = -1.0 \times 10^{-4}$$

$$\epsilon_y = \frac{1-\mu^2}{E} \left(\sigma_y - \frac{\mu}{1-\mu} \sigma_x \right) = \frac{1-0.18^2}{0.185} \times 10^{-5} \left(1.4 + \frac{0.18}{1-0.18} \times 1.6 \right) = 0.92 \times 10^{-4}$$

$$\gamma_{xy} = \frac{1}{G} \tau_{xy} = 0$$

The displacements of nodal points, therefore, can be determined in following table.

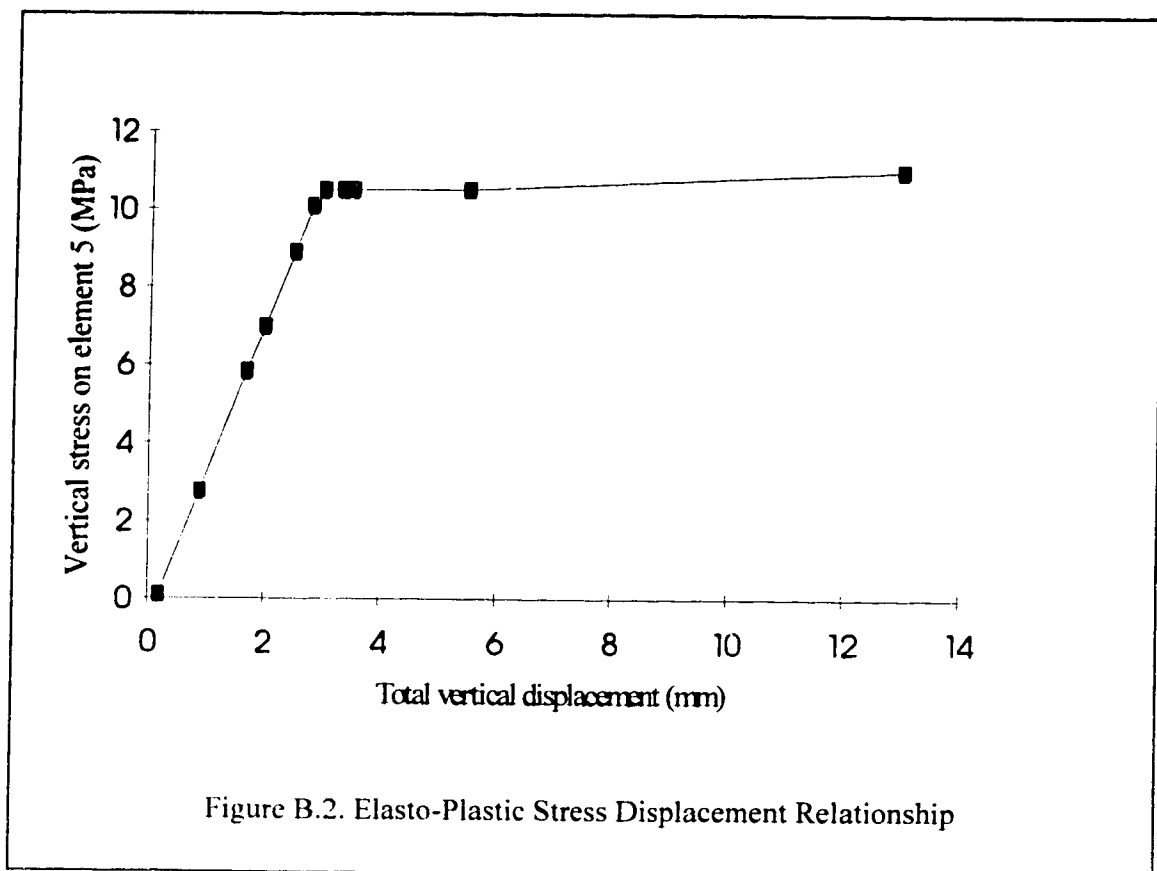
Closed Form Solution for Nodal Displacements										Table B.5		
Ele.	1	2	3	4	5	6	7	8	9	10	11	12
x (m)	0.0	0.7	3.0	0.0	1.6	3.0	0.0	2.0	3.0	0.0	2.2	3.0
y (m)	0.0	0.0	0.0	1.1	1.7	1.7	3.3	3.1	3.1	5.0	5.0	5.0
ux*	0.0	-0.7	-3.0	0.0	-1.6	-3.0	0.0	-2.0	-3.0	0.0	-2.2	-3.0
uy*	0.0	0.0	0.0	1.01	1.56	1.56	3.04	2.85	2.85	4.6	4.6	4.6

* unit is ($\times 10^{-4}$ m).

The finite element program results are shown in List B.4. They give the "exact" solution as that from closed form solution, the patch of elements is said to have passed this test.

Elasto-Plastic Constitutive Relationship:

The constitutive relationship adopted in the program can be examined by applying a set of prescribed displacements in y direction. The vertical stresses in element 5 (refer Fig. B.1) are plotted against these displacements as shown in Fig. B.2.



Conclusion

This FEM program has passed all patch tests conducted above with or without gas pressure and it has shown reasonable responses to the elasto-plastic stress and strain relationship. The program, therefore, will converge consistently. Because the elements in

the patch have irregular shape and different sizes, the solution from the FEM program will validate for any grid scheme.

List B.1 - Program Output for Constant σ_y

```

Patch test for irregular elements
NUMBER OF NODAL POINTS----- 12
NUMBER OF ELEMENTS----- 6
NUMBER OF DIFF. MATERIALS--- 4
NUMBER OF PRESSURE CARDS--- 2
X-ACCELERATION----- .0000E+00
Y-ACCELERATION----- .0000E+00
NUMBER OF APPROXIMATIONS--- 200
1 .2500E-01
COELASTIC MODULUS NU COHESION FRICTION ANGLE
.18500E+05 .18000E+00 .10000E+02 .30000E+02
2 .2700E-01
COELASTIC MODULUS NU COHESION FRICTION ANGLE
.26150E+05 .35000E+00 .20000E+02 .35000E+02
3 .2500E-01
COELASTIC MODULUS NU COHESION FRICTION ANGLE
.10000E+05 .20000E+00 .10000E+02 .20000E+02
4 .2500E-01
COELASTIC MODULUS NU COHESION FRICTION ANGLE
.10000E+05 .35000E+00 .18000E+02 .30000E+02
NODAL POINT
1 TYPE X ORIGINATE Y ORIGINATE X LOAD OR DISPLACEMENT Y LOAD OR DISPLACEMENT Z-LOAD OR DISPLACEMENT
3.00 .0000000E+00 .0000000E+00 .0000000E+00 .0000000E+00 .0000000E+00 .0000000E+00
2.00 .7000000E+00 .0000000E+00 .0000000E+00 .0000000E+00 .0000000E+00 .0000000E+00
3.00 .3000000E+01 .0000000E+00 .0000000E+00 .0000000E+00 .0000000E+00 .0000000E+00
4.00 .1600000E+01 .1100000E+01 .0000000E+00 .0000000E+00 .0000000E+00 .0000000E+00
5.00 .3000000E+01 .1700000E+01 .0000000E+00 .0000000E+00 .0000000E+00 .0000000E+00
6.00 .3000000E+01 .1700000E+01 .0000000E+00 .0000000E+00 .0000000E+00 .0000000E+00
7.00 .0000000E+00 .3300000E+01 .0000000E+00 .0000000E+00 .0000000E+00 .0000000E+00
8.00 .2000000E+01 .3100000E+01 .0000000E+00 .0000000E+00 .0000000E+00 .0000000E+00
9.00 .3000000E+01 .3100000E+01 .0000000E+00 .0000000E+00 .0000000E+00 .0000000E+00
10.00 .0000000E+00 .5000000E+01 .0000000E+00 .0000000E+00 .0000000E+00 .0000000E+00
11.00 .2200000E+01 .5000000E+01 .0000000E+00 .0000000E+00 .0000000E+00 .0000000E+00
12.00 .3000000E+01 .5000000E+01 .0000000E+00 .0000000E+00 .0000000E+00 .0000000E+00
ELEMENT NO. I J K L MATERIAL X-STRESS Y-STRESS XY-STRESS Y-LOAD OR DISPLACEMENT X-LOAD OR DISPLACEMENT Y-LOAD OR DISPLACEMENT Z-STRESS
1 1 1 2 5 4 1 .000 .000 .000 .000 .000 .000 .000
2 2 2 3 6 5 1 .000 .000 .000 .000 .000 .000 .000
3 4 5 8 7 1 .000 .000 .000 .000 .000 .000 .000
4 5 6 9 8 1 .000 .000 .000 .000 .000 .000 .000
5 7 8 11 10 1 .000 .000 .000 .000 .000 .000 .000
6 8 9 12 11 1 .000 .000 .000 .000 .000 .000 .000
PRESSURE BOUNDARY CONDITIONS
I J PRESSURE I PRESSURE J
11 10 5.000
12 11 5.000
BAND WIDTH FOR THIS DATA = 10
1 STRESSES AFTER APPROXIMATION NUMBER 1

```

EL.NO.	X	Y	X-STRESS	Y-STRESS	XY-STRESS	MAX-STRESS	MIN-STRESS	ANGLE	Z-STRESS	PLASTIC
1	.5750000E+00	.7000000E+00	.3310394E-14	-.5000000E+01	.1612245E-15	.3552714E-14	-.5000000E+01	.1850728E-14	-.9000000E+00	0
2	.2075000E+01	.8500000E+00	.2131108E-14	-.5000000E+01	.1393233E-14	.1776357E-14	-.5000000E+01	.1599320E-13	-.9000000E+00	0
3	.9000000E+00	.2300000E+01	.4581188E-14	-.5000000E+01	.1912285E-14	-.4440892E-14	-.5000000E+01	-.2195150E-13	-.9000000E+00	0
4	.2490000E+01	.2400000E+01	.3301070E-14	-.5000000E+01	.1369475E-14	-.3552714E-14	-.5000000E+01	.1572047E-13	-.9000000E+00	0
5	.1050000E+01	.4100000E+01	.3190373E-14	-.5000000E+01	.5500723E-15	.3552714E-14	-.5000000E+01	-.6314390E-14	-.9000000E+00	0
6	.2550000E+01	.4050000E+01	.5540273E-16	-.5000000E+01	.5328501E-15	.0000000E+00	-.5000000E+00	-.6116693E-14	-.9000000E+00	0

OTHE UNBALANCED LOAD AT THIS STAGE IS .000000E+00

THE RATIO FOR CORRECTION OF STORED STRESSES IS 1.0000

THE NEXT ELEMENT YIELDING IS 0
 AND THE TOTAL NUMBER OF ELEMENTS THAT CAN YIELD WITH THE LINEAR ADDITION OF TOTAL LOAD IS 0
 LOAD UP TO THIS STAGE AS A FRACTION OF TOTAL IS 1.00000

IN. P. NUMBER	UX	UY
1	.0000000E+00	.0000000E+00
2	.4018378E-04	.0000000E+00
3	.1722162E-03	.0000000E+00
4	.0000000E+00	-.2876649E-03
5	.9184865E-04	-.4445730E-03
6	.1722162E-03	-.4445730E-03
7	.0000000E+00	-.8629946E-03
8	.1148108E-03	-.8106919E-03
9	.1722162E-03	-.8106919E-03
10	.0000000E+00	-.1307568E-02
11	.1262919E-03	-.1307568E-02
12	.1722162E-03	-.1307568E-02

List B.2 - Program Output for Constant σ_x

```

Input test for irregular elements
NUMBER OF NODAL POINTS----- 12
NUMBER OF ELEMENTS----- 6
NUMBER OF DIFF. MATERIALS--- 4
NUMBER OF PRESSURE CARDS--- 3
X ACCELERATION----- .0000E+00
Y ACCELERATION----- .0000E+00
NUMBER OF APPROXIMATIONS----- 250
1 .2500E-01
ELASTIC MODULUS NU COHESION FRICTION ANGLE
1 .18500E+05 .18000E+02 .30000E+02
2 .2700E-01
ELASTIC MODULUS NU COHESION FRICTION ANGLE
3 .26150E+05 .20000E+02 .35000E+02
4 .2500E-01
ELASTIC MODULUS NU COHESION FRICTION ANGLE
5 .10000E+05 .10000E+02 .20000E+02
6 .2500E-01
ELASTIC MODULUS NU COHESION FRICTION ANGLE
7 .10000E+05 .18000E+02 .30000E+02
8 .2500E-01
ELASTIC MODULUS NU COHESION FRICTION ANGLE
9 .30000E+05 .30000E+02 .30000E+02
10 .22000E+05 .50000E+02 .50000E+02
11 .22000E+05 .50000E+02 .50000E+02
12 .30000E+05 .50000E+02 .50000E+02
ELEMENT NO. I J K L MATERIAL X-STRESS Y-STRESS XY-STRESS Z-STRESS
1 1 2 5 4 .000 .000 .000 .000
2 2 3 6 5 .000 .000 .000 .000
3 4 5 8 7 .000 .000 .000 .000
4 5 6 9 8 .000 .000 .000 .000
5 7 8 11 10 .000 .000 .000 .000
6 8 9 12 11 .000 .000 .000 .000
PRESSURE BOUNDARY CONDITIONS
I J PRESSURE I PRESSURE J
1 6 5.000 5.000
3 6 5.000 5.000
6 9 5.000 5.000
9 12 5.000 5.000
BAND WIDTH FOR THIS DATA = 10
1 STRESSES AFTER APPROXIMATION NUMBER 1
  
```

EL. NO.	X	Y	X-STRESS	Y-STRESS	XY-STRESS	MAX-STRESS	MIN-STRESS	ANGLE	Z-STRESS	PLASTIC
1	.5750000E+00	.7000000E+00	.5000000E+00	.1813003E-14	.8494374E-16	.1776357E-14	.5000000E+01	-.9015743E+02	.9000000E+00	0
2	.2075000E+01	.8500000E+00	.5000000E+00	.1589874E-14	.7960590E-15	.1776357E-14	.5000000E+01	-.9015743E+02	.9000000E+00	0
3	.9000000E+00	.2300000E+01	.5000000E+00	.1118029E-14	.4647914E-15	.8881784E-15	.5000000E+01	.9015743E+02	.9000000E+00	0
4	.2400000E+01	.2400000E+01	.5000000E+00	.1891065E-14	.5934390E-15	.1776357E-14	.5000000E+01	-.9015743E+02	.9000000E+00	0
5	.1050000E+01	.4100000E+01	.5000000E+00	.1940722E-15	.1344056E-15	.0000000E+00	.5000000E+01	-.9015743E+02	.9000000E+00	0
6	.2550000E+01	.4050000E+01	.5000000E+00	.1231762E-14	.3319338E-17	.8881784E-15	.5000000E+01	-.9015743E+02	.9000000E+00	0

0 THE UNBALANCED LOAD AT THIS STAGE IS .00000E+00

THE RATIO FOR CORRECTION OF STORED STRESSES IS 1.0000

THE NEXT ELEMENT YIELDING IS 0
 AND THE TOTAL NUMBER OF ELEMENTS THAT CAN YIELD WITH THE LINEAR ADDITION OF TOTAL LOAD IS 0
 LOAD UP TO THIS STAGE AS A FRACTION OF TOTAL IS 1.00000

IN.P. NUMBER	UX	UY
1	.0000000E+00	.0000000E+00
2	-.1830595E-03	.0000000E+00
3	-.7845405E-03	.0000000E+00
4	.0000000E+00	.6314595E-04
5	-.4184216E-03	.9758919E-04
6	-.7845405E-03	.9758919E-04
7	.0000000E+00	.1894378E-03
8	-.5230270E-03	.1779568E-03
9	-.7845405E-03	.1779568E-03
10	.0000000E+00	.2870270E-03
11	-.5753287E-03	.2870270E-03
12	-.7845405E-03	.2870270E-03

List B.3 - Program Output for Pure Shear

```

Patch test for irregular elements
NUMBER OF NODAL POINTS-----
6
NUMBER OF ELEMENTS-----
4
NUMBER OF DIFF. MATERIALS-----
1
NUMBER OF PRESSURE CAPDS-----
.0000E+00
X-ACCELERATION-----
.0000E+00
Y-ACCELERATION-----
200
NUMBER OF APPROXIMATIONS-----
1 .2500E-01
ELASTIC MODULUS
1 .18500E+05
2 .2700E-01
ELASTIC MODULUS
3 .26150E+05
4 .2500E-01
ELASTIC MODULUS
5 .10000E+05
6 .2500E-01
ELASTIC MODULUS
7 .10000E-01
8 .10000E-01
9 .10000E-01
10 .10000E-01
11 .10000E-01
12 .10000E-01
NU COHESION FRICTION ANGLE
.18000E+02 .30000E+02
NU COHESION FRICTION ANGLE
.36000E+02 .35000E+02
NU COHESION FRICTION ANGLE
.20000E+02 .20000E+02
NU COHESION FRICTION ANGLE
.35000E+02 .30000E+02
TYPE X ORDINATE Y ORDINATE X LOAD
3.00 .0000000E+00 .0000000E+00
3.00 .7000000E+00 .0000000E+00
3.00 .3000000E+01 .0000000E+00
3.00 .0000000E+00 .1100000E-01
3.00 .1600000E+01 .1700000E+01
3.00 .3000000E+01 .1700000E+01
3.00 .0000000E+00 .3300000E+01
3.00 .2000000E+01 .3100000E+01
3.00 .3000000E+01 .3100000E+01
3.00 .0000000E+00 .5000000E+01
3.00 .2200000E+01 .5000000E+01
3.00 .3000000E+01 .5000000E+01
MATERIAL X-STRESS Y-STRESS XY-STRESS Y-LOAD OR DISPLACEMENT Y-LOAD OR DISPLACEMENT PORE PRESSURE
I J K L
1 1 2 5 4 1 .000 .000 .000 .000 .000 .000
2 2 3 6 5 1 .000 .000 .000 .000 .000 .000
3 4 5 7 8 1 .000 .000 .000 .000 .000 .000
4 5 6 9 8 1 .000 .000 .000 .000 .000 .000
5 7 8 11 10 1 .000 .000 .000 .000 .000 .000
6 8 9 12 11 1 .000 .000 .000 .000 .000 .000
PRESSURE BOUNDARY CONDITIONS
I J PRESSURE I PRESSURE J
0 0 .000
BAND WIDTH FOR THIS DATA = 10
1 STRESSES AFTER APPROXIMATION NUMBER 1

```

EL.NO.	X	Y	X-STRESS	Y-STRESS	XY-STRESS	MAX-STRESS	MIN-STRESS	ANGLE	Z-STRESS	PLASTIC
1	.5750000E+00	.7000000E+00	.7098314E-16	.1558166E-16	.1097458E+01	.1097458E+01	-.1097458E+01	.4507871E+02	.1558166E-16	0
2	.2075000E+01	.8500000E+00	.1289394E-16	.2830377E-17	.1097458E+01	.1097458E+01	-.1097458E+01	.4507871E+02	-.2830377E-17	0
3	.9000000E+00	.2300000E+01	.6805874E-16	.1493972E-16	.1097458E+01	.1097458E+01	-.1097458E+01	.4507871E+02	-.1493972E-16	0
4	.2400000E+01	.2400000E+01	.1310662E-15	.2877064E-16	.1097458E+01	.1097458E+01	-.1097458E+01	.4507871E+02	-.2877064E-16	0
5	.1050000E+01	.4100000E+01	.7483803E-15	.1642786E-15	.1097458E+01	.1097458E+01	-.1097458E+01	.4507871E+02	-.1642786E-15	0
6	.2350000E+01	.4050000E+01	.3791084E-15	.8321893E-16	.1097458E+01	.1097458E+01	-.1097458E+01	.4507871E+02	.8321893E-16	0

THE RATIO FOR CORRECTION OF STORED STRESSES IS 1.0000

THE NEXT ELEMENT YIELDING IS 0
 AND THE TOTAL NUMBER OF ELEMENTS THAT CAN YIELD WITH THE LINEAR ADDITION OF TOTAL LOAD IS 0
 LOAD UP TO THIS STAGE AS A FRACTION OF TOTAL IS 1.00000

IN.P. NUMBER	UX	UY
1	.0000000E+00	.0000000E+00
2	.0000000E+00	.0000000E+00
3	.0000000E+00	.0000000E+00
4	.1540000E-03	.0000000E+00
5	.2380000E-03	.0000000E+00
6	.2380000E-03	.0000000E+00
7	.4620000E-03	.0000000E+00
8	.4340000E-03	.0000000E+00
9	.4340000E-03	.0000000E+00
10	.7000000E-03	.0000000E+00
11	.7000000E-03	.0000000E+00
12	.7000000E-03	.0000000E+00

EL.NO.	X	Y	X-STRESS	Y-STRESS	XY-STRESS	MAX-STRESS	MIN-STRESS	ANGLE	Z-STRESS	PLASTIC
1	.5750000E+00	.7000000E+00	.1600000E+00	.1400000E+01	-.6630799E-15	.1600000E+01	-.1400000E+01	.1268604E-13	.3600000E-01	0
2	.2075000E+01	.8500000E+00	.1600000E+00	.1400000E+01	.1295191E-14	.1600000E+01	-.1400000E+01	.2477959E-13	.3600000E-01	0
3	.9000000E+00	.2300000E+01	.1600000E+01	.1400000E+01	-.8499042E-15	.1600000E+01	-.1400000E+01	.1626037E-13	.3600000E-01	0
4	.2400000E+01	.2400000E+01	.1600000E+01	.1400000E+01	.5502798E-15	.1600000E+01	-.1400000E+01	.1052795E-13	.3600000E-01	0
5	.1050000E+01	.4100000E+01	.1600000E+01	.1400000E+01	-.7795112E-15	.1600000E+01	-.1400000E+01	.1491361E-13	.3600000E-01	0
6	.2550000E+01	.4050000E+01	.1600000E+01	.1400000E+01	-.7872404E-15	.1600000E+01	-.1400000E+01	.1506148E-13	.3600000E-01	0

THE RATIO FOR CORRECTION OF STORED STRESSES IS 1.0000

THE NEXT ELEMENT YIELDING IS 0
 AND THE TOTAL NUMBER OF ELEMENTS THAT CAN YIELD WITH THE LINEAR ADDITION OF TOTAL LOAD IS 0
 LOAD UP TO THIS STAGE AS A FRACTION OF TOTAL IS 1.00000

IN.P. NUMBER	UX	UY
1	.0000000E+00	.0000000E+00
2	.6983049E-04	.0000000E+00
3	.2992735E-03	.0000000E+00
4	.0000000E+00	-.1007529E-03
5	.1596125E-03	-.1557090E-03
6	.2992735E-03	-.1557090E-03
7	.0000000E+00	-.3022586E-03
8	.1995157E-03	-.2839399E-03
9	.2992735E-03	-.2839399E-03
10	.0000000E+00	-.4579676E-03
11	.2194672E-03	-.4579676E-03
12	.2992735E-03	-.4579676E-03

Appendix C.

Development of the Outburst Model Finite Element Program FEOMP

The development of the computer program is one of the major tasks in this research project. Although there are many finite element computer programs accessible for public and for research purposes, none of them could be directly used for this model development. Implementation has to be programmed to couple with the special requirements of the model, such as the gas pressure considerations and the implementation of the general method to accomplish the removal of elements failed in tension. The calculation of the tensile failed elements and the algorithm to identify the elements to be removed are programmed from scratch. This programming requires, at the same time, to work consistently with the selected finite element computer program. It is time-consuming work and took about 50% of the time for the whole project. In this appendix, a brief description of the whole program will be given. An overview of the model program will be introduced first. Program flow and algorithms are explained by subroutines.

C.1. Overview of the Program

To achieve the entire modeling, pre-processor and post-processor are adapted directly from a commercial program. FEOMP, abbreviated from Finite Element Outburst Model Program, is the core program of the whole simulation package. An overview of the program is provided in Fig. C.1. The flow chart is almost self explanatory and all subroutines in FEOMP are presented. Statements in a plane rectangular box describe the actions taken at that stage in a program flow, while a rectangle with a vertical frame represents subroutines and contains statements for the functions of the subroutine. The grey open frame encloses the comments on the flow at that point. The grey line indicates data connections and the double arrowhead heavy grey line show that the actions in the plain rectangle are completed by the relevant subroutine. The following sections will be devoted to brief description of each subroutine shown in the flow chart.

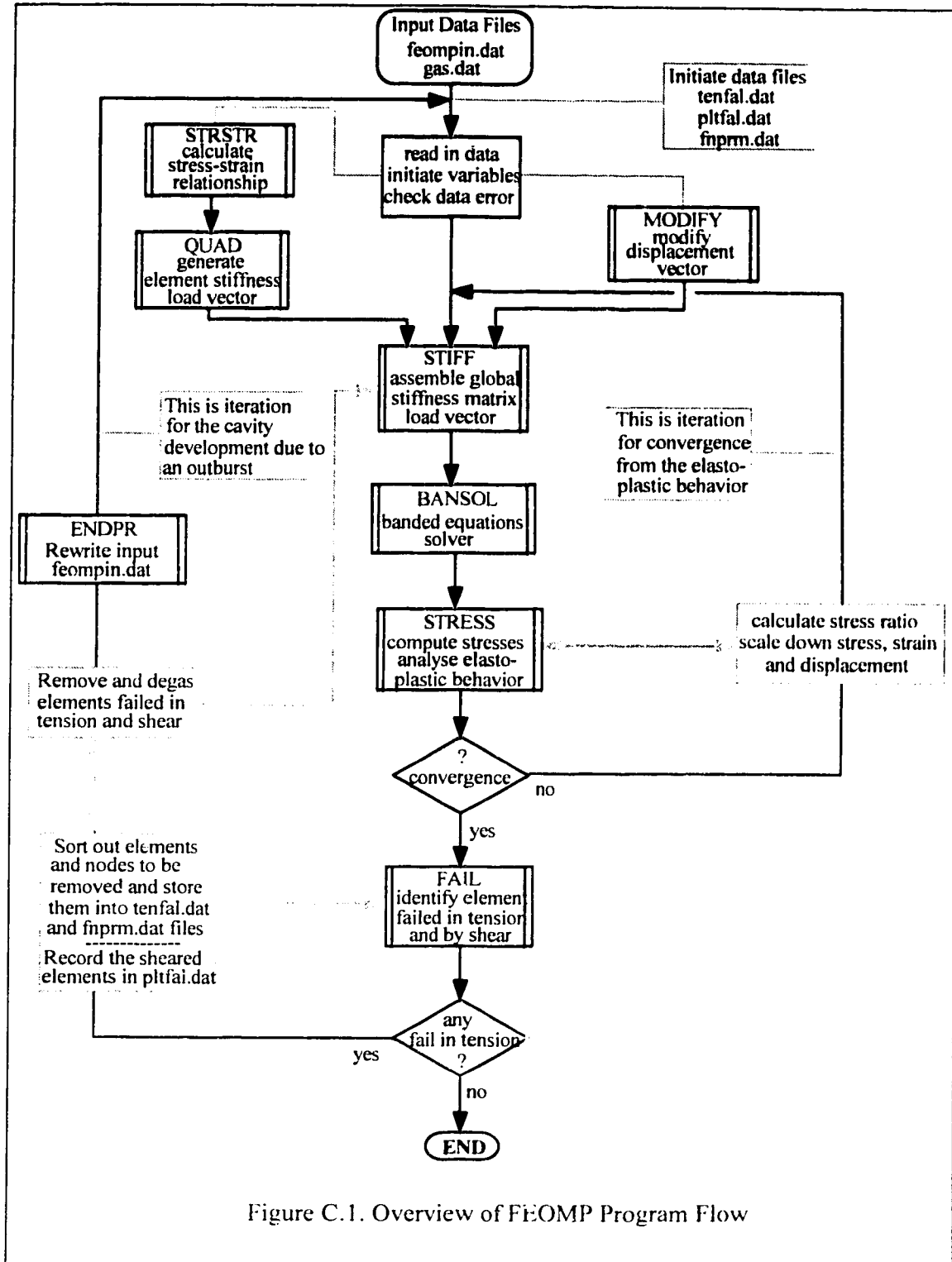


Figure C.1. Overview of FEOMP Program Flow

C.2. Subroutine STIFF

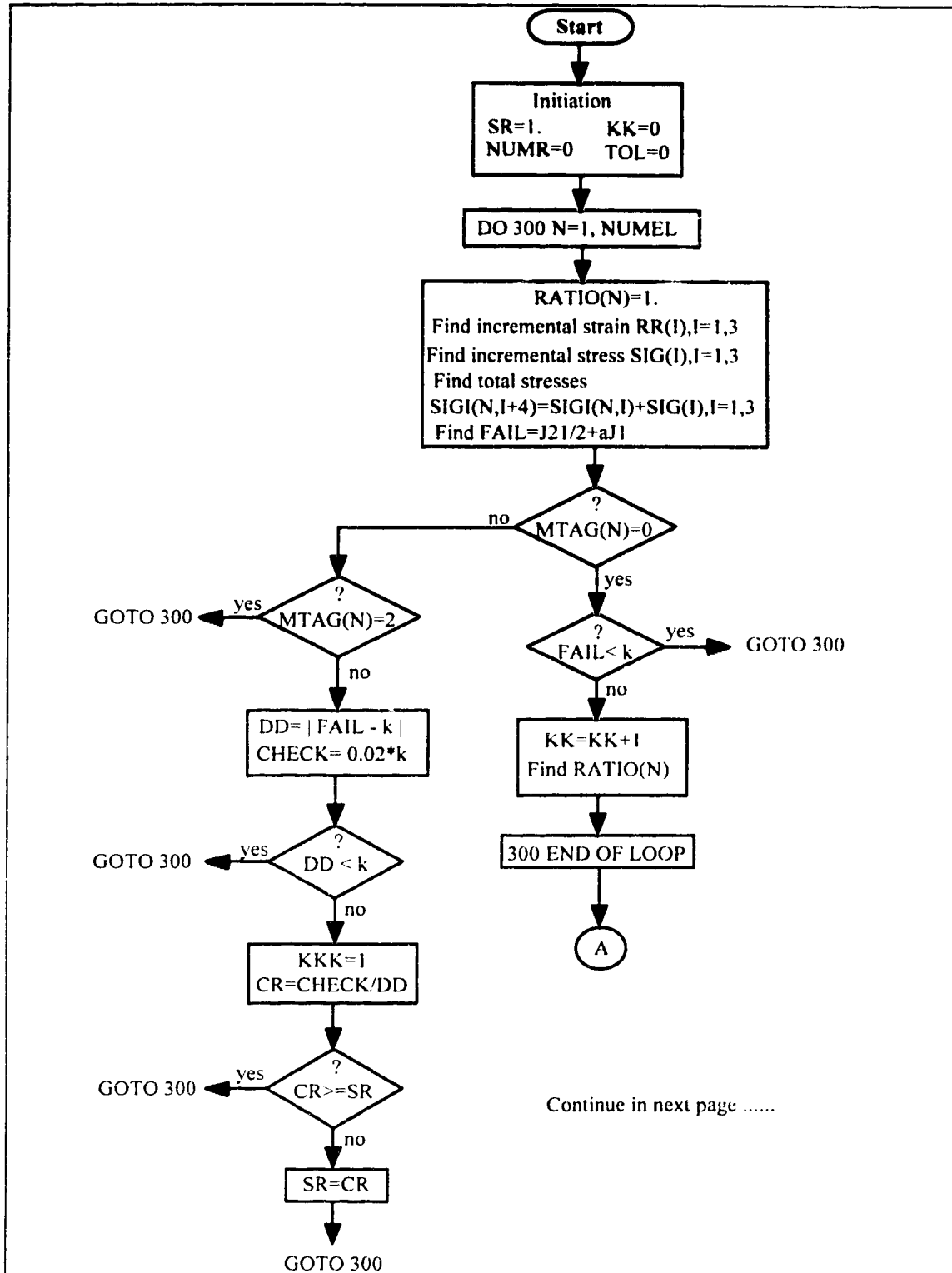
This routine is concerned with assembling the global stiffness matrix, load vector and modifying the global displacement vector according to the prescribed boundary constraints at a given incremental stage for allowing progressive failure and a geometrically altered structure. To obtain the global stiffness matrix and load vector, STIFF calls for subroutine QUAD to calculate the element stiffness matrix and element load vector. QUAD computes the displacement-strain relationship matrix [B] for the given element. It calls for subroutine STRSTR for stress-strain relationship matrix [c]. STRSTR produces the [c] matrix for either elastic element and plastic element depending on the current information of whether the element is in elastic or plastic state. With the calculated [B] and [c] matrix, QUAD generates the element stiffness [k] and computes the nodal external loads. These results are assembled in global matrix by STIFF.

STIFF finally calls for MODIFY to modify the displacement vector in equations (6.25) as presented in Chapter 6. MODIFY assigns the specific degree of freedom with the prescribed constraints, usually zero values.

The execution of subroutine STIFF, in fact, is preparing each term in equation (6.25), i.e., [K], {q} and {R} at the given stage. The equations in Eq. (6.25) will be solved in the subroutine BANSOL.

C.3. Subroutine BANSOL

This subroutine is an equation solver. After the stiffness matrix and load vector have been prepared and the displacement vector has been modified by STIFF, this solver is called to obtain the solutions. The solver uses Gaussian elimination technique for banded equations. The subroutine first triangularizes the stiffness matrix according to the elimination algorithm and then, back-substitutes through the triangular matrix to give the solution. Although the method is most straightforward, the computer memory required to solve a large set of equations may be too much for a conventional personal computer. More economical and faster equation solving techniques exist and could be readily adopted.



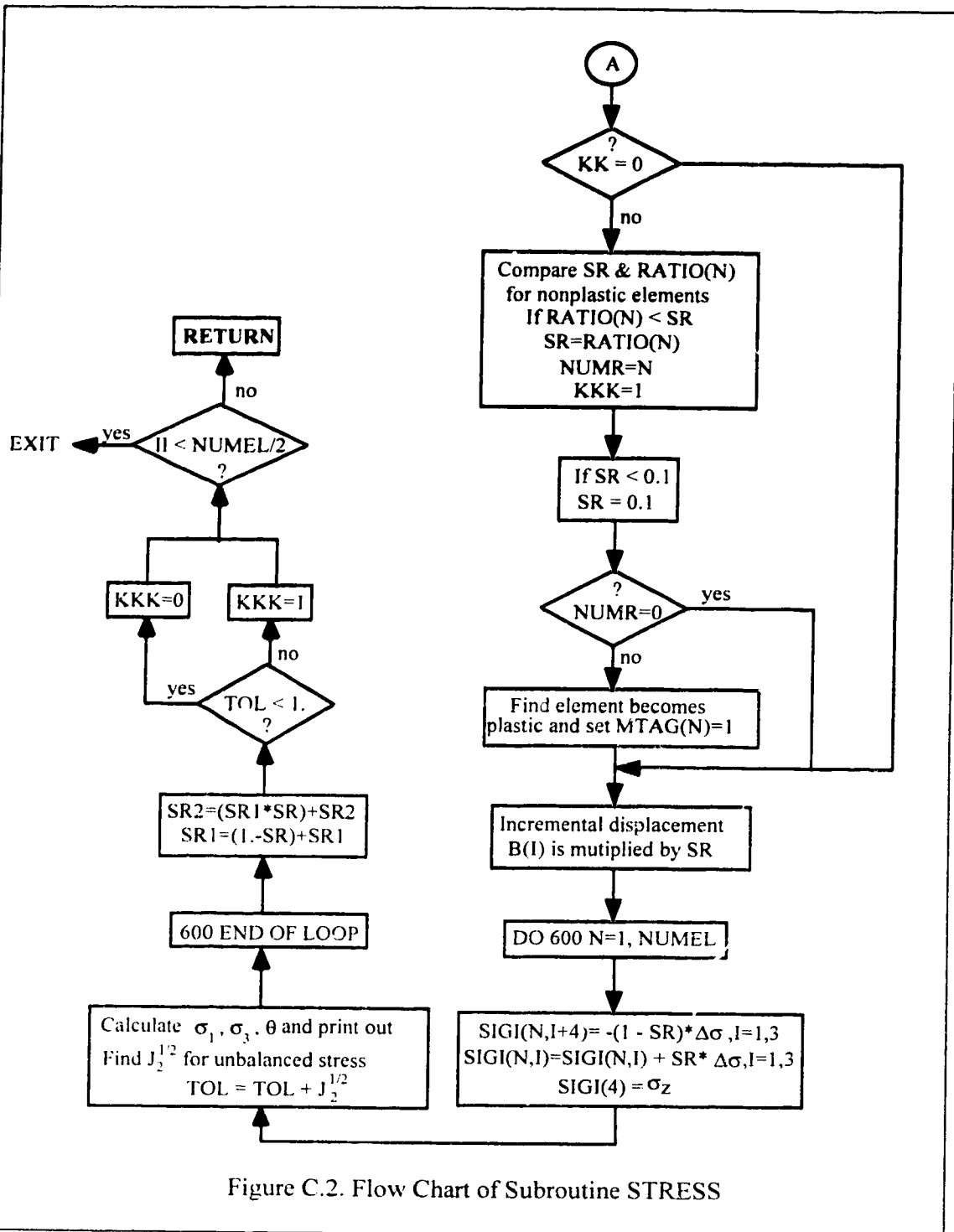


Figure C.2. Flow Chart of Subroutine STRESS

C.4. Subroutine STRESS

Progressive failure of the elastic-plastic continuum has been accounted for in this routine. The basic theory and technique employed has been introduced in Chapter 6. The logic involved in this subroutine is provided in the detailed flow diagram Fig. C.2. The important variables used in the flow chart are listed below.

SR	stress ratio
KK	number of yield element at this iteration
NUMR	last element number of yield element at this iteration
TOL	total unbalanced stress
NUMEL	total element number
RATIO(N)	stress ratio for each element
SIGI(N,I)	incremental stresses (first 4 dimensions) and total stresses (last 4 dimensions)
J_1	first stress invariant
$J_2^{1/2}$	second stress invariant
MTAG(N)	label identifying elastic and plastic element
KKK	indicator for iteration
B(I)	nodal displacement vector

C.5. Program FAIL

This routine is designed to accomplish the operation of the spalling process postulated for an outburst. The elements failed in a tensile mode are identified by a direct comparison between tensile strength and the tensile stress for an element. An algorithm is incorporated to pick out those elements to be removed. It is assumed that all the elements in front of a tensile failed element must be removed in the next iteration, regardless whether they are sheared or unfailed. This assumption simulates the expulsion mechanism found in an outburst. The discretization scheme of the finite element program is appropriately made use of in order to achieve this.

The elements failed in a shear mode are identified for degassing operation. The method is straightforward as the finite element program produces an identifier for the sheared element. To plot the configuration of the result, the nodes removed with the

element also are identified. The number of elements to be removed and degassed and that of the nodes to be removed are recorded in files in the rest of the computation.

The general method for a geometrically altered structure is incorporated to handle the removal of the selected elements. Residual forces are calculated and assembled in load vector. The elements removed are deactivated by setting another material number to the elements. This material has an approximately zero Young's modulus. The nodal forces calculated from Eq. (6.47) are assembled in its load vector to degas the selected elements. The load vector together with the rewritten input data files become the initial conditions for next iteration.

Appendix D.
Sample Run of the Model

A sample run of the model is included in this appendix. The procedures for carrying out the modeling will be followed step by step. All data files will be briefly introduced. Finally, the results of the modeling will be presented.

Preparation of input data

The simulation starts with preparation of input data files GENIN.DAT and EPFECIN.DAT. The format and definition of the files is briefly presented in Table D.1 and D.2. The sample of input data files are illustrated in List D.1 and D.2. The full documentation for preparation of these files can be found in the references (TOEWS, 1985 & Yu, 1988).

Format and Definition of GENIN.DAT File

Table D.1

Variable(s)	Variable Definition or Description	Format
Line No.1 -Problem title information:		
HEAD	72 character problem: title.	18^4
Line No. 2 - Problem control information:		
NSPNP	Total number of specified nodal points.	15
NVZONE	Total number of non-void zones.	15
NSPAN1	Total number of spans in ξ direction.	15
NSPAN2	Total number of spans in η direction.	15
NPROB	The total number of sub-problems, default value is 1.	15
NSIDNT	Identification indicator, a value of zero or blank means no identification; value 1 indicates identification; default value is 0 for most of the meshes generated.	15
Line No. 3 - Data define zone subdivisions:		
NSBDV1(1)	Array defining number of subdivisions in each zone in ξ direction.	15
Continue in next page		

Line No. 4 - Data defining zone subdivisions:												
NSBDV2(I)	Array defining number of subdivisions in each zone in η direction.	15										
Record No. 1 - Coordinates of specified nodes:												
N	Specified nodal point number.	15										
NCOD(N)	Constraint code of specified nodal point N. The table below defines the possibilities:	15										
	<table border="1"> <thead> <tr> <th><u>NCOD(N)</u></th> <th><u>Constraint at node N</u></th> </tr> </thead> <tbody> <tr> <td>0</td> <td>No constraint on displacements.</td> </tr> <tr> <td>1</td> <td>x-displacement = 0.</td> </tr> <tr> <td>2</td> <td>y-displacement = 0.</td> </tr> <tr> <td>3</td> <td>x-displacement = 0, y-displacement = 0.</td> </tr> </tbody> </table>	<u>NCOD(N)</u>	<u>Constraint at node N</u>	0	No constraint on displacements.	1	x-displacement = 0.	2	y-displacement = 0.	3	x-displacement = 0, y-displacement = 0.	
<u>NCOD(N)</u>	<u>Constraint at node N</u>											
0	No constraint on displacements.											
1	x-displacement = 0.											
2	y-displacement = 0.											
3	x-displacement = 0, y-displacement = 0.											
XSP(N)	x coordinate of node N.	*										
YSP(N)	y coordinate of node N.	*										
Data group defining non-void zones:												
N	Non-void zone number.	110										
IZ(I,N)	Nodal number defining non-void zone N.	18										
MATZ(N)	The material number associated with N non-void zone, the default value is 1.	18										
NCUT(N)	The default is zero.	15										
NUMPC	The number of sides (0-4) of non-void zone with pressure applied, i.e., a total of 'NUMPC' records defining pressure loading will follow immediately.	18										
Record No. 2. - Records defining pressure sides on zone N:												
NSIDE	The side number of zone N.	15										
P1	The pressure at node 1 of zone side 'NSIDE'.	F10.2										
P2	The pressure at node 2 of zone side 'NSIDE'.	F10.2										

Note: * indicates free format.

Format and Definition of EPFECIN.DAT File

Table D.2

Variable(s)	Variable Definition or Description	Format
Line No. 1 - Problem control information:		
MAXELR	Maximum number of elements to be removed or added.	I5
NP	Maximum number of iterations.	I5
NRES	An indicator for input initial stresses: = 0, input initial stress coefficients; initial stresses will be calculated and read in as input data. = 1, no initial stresses will be input.	I10
NMAT	Total number of different materials: NMAT = actual number of materials + 1.	I5
ACELR	Acceleration in x-direction (horizontal).	F10.2
ACELR	Acceleration in y-direction (vertical).	F10.2
SCALE	A scaling factor.	F10.2
Line No. 2 - Output print control:		
INDPRT	Output print control indicator. = 0, will print out stresses and displacements for last iteration only. = 1, will print out stresses and displacements for every iteration.	I5
Data group for material properties (there are two records for each material):		
Record No. 1		
MTYPE	Material identification number.	I5
RO	Density of material.	E15.7
Record No. 2		
E(M.1)	Young's modulus.	E15.7
E(M.2)	Poisson's ratio.	E15.7
E(M.3)	Cohesion.	E15.7
E(M.4)	Angle of internal friction.	E15.7
E(M.5)	Area of 1-D element (default zero)	E15.7
Continue in next page		

Data group defining concentrated nodal forces (two records involved):		
Record No. 1		
NUMCO	Total number of nodes where nodal forces are acting.	I5
Record No. 2		
NPC	Nodal point number.	I5
XLOAD	x-load or y-displacement.	F10.2
YLOAD	y-load or x-displacement.	F10.2
Data group defining initial stress coefficients (four records):		
Record No. 1		
AXX	Coefficient	F10.2
BXX	Coefficient	F10.2
Record No. 2		
AYY	Coefficient	F10.2
BYY	Coefficient	F10.2
Record No. 3		
AZZ	Coefficient	F10.2
BZZ	Coefficient	F10.2
Record No. 4		
AXY	Coefficient	F10.2
BXY	Coefficient	F10.2

Note: The initial stresses are assumed to be varying linearly with depth, Y.

The coefficients above are better illustrated by the following equations:

$$\sigma_{xx} = AXX + BXX \times Y$$

$$\sigma_{yy} = AYY + BYY \times Y$$

$$\sigma_{zz} = AZZ + BZZ \times Y$$

$$\sigma_{xy} = AXY + BXY \times Y$$

where, σ_{xx} , σ_{yy} , σ_{zz} and σ_{xy} are the initial stresses.

List D.1 - Sample of GENIN.DAT File

```

'Two dimensional outburst model for a deep opening - sigh/sigv=0.5 '
22 6 3 4 1 0 0
5 40 25
5 5 10 10
1 3 0. -10.
2 2 2.25 -10.
3 2 28. -10.
4 0 30. -10.
5 1 0. 0.
6 0 2.25 0.
7 0 28. 0.
8 0 30. 0.
9 0 0. 2.
10 0 2.25 2.
11 0 28. 2.
12 0 30. 2.
13 0 0. 2.
14 0 1.59099 3.59099
15 0 28. 9.5
16 0 28. 50.
17 0 0. 2.
18 1 0. 4.25
19 1 0. 9.5
20 1 0. 50.
21 0 2.079 2.861
22 0 0.861 4.0787
1 1 2 6 5 0 0 0 0 2 0 0
2 2 3 7 6 0 0 0 0 2 0 1
  2 12.5 12.5
5 6 7 11 10 0 0 0 0 2 0 1
  2 12.5 12.5
8 10 11 15 14 0 0 0 21 1 0 1
  2 12.5 12.5
11 14 15 19 18 0 0 0 22 1 0 0
12 15 16 20 19 0 0 0 0 2 0 2
  1 12.5 12.5
  2 25.0 25.0
(EOF)

```

List D. 2 - Sample of EPFECIN.DAT File

```

0 400 1 4 .00 .00 .00
0
1 .250000E-01
.185000E+05 .180000E+00 .180000E+02 .300000E+02 .000000E+00
2 .270000E-01
.261500E+05 .360000E+00 .200000E+02 .350000E+02 .000000E+00
3 .250000E-01
.100000E+05 .200000E+00 .100000E+02 .200000E+02 .000000E+00
4 .250000E-01
.010000E+00 .350000E+00 .180000E+02 .300000E+02 .000000E+00
0
*****Evaluating the stress and displacement*****
4
(EOF)

```

Above two prepared files are used as inputs for the pre-processor. The output from the pre-processor is a file called FEOMPIN.DAT which will be the input file for the main program FEOMP of the model and a sample of this file is shown below.

List D. 3 - Sample of FEOMPIN.DAT File

```

Two dimensional outburst model for a deep opening - sigh/sigv=0.5
1551 1450 4 55 0.00 0.00 200 1 1 1
0
10.2500E-01
0.1850E+050.1800E+000.1800E+020.3000E+020.0000E+00
20.2700E-01
0.2615E+050.3200E+000.2000E+020.3500E+020.0000E+00
30.2500E-01
0.1000E+050.2000E+000.1000E+020.2000E+020.0000E+00
40.2500E-01
0.1000E-010.4000E+000.1800E+020.3000E+020.0000E+00
1 3. 0.0000000E+00 -0.1000000E+02 0.0000000E+00 0.0000000E+00
2 2. 0.4500000E+00 -0.1000000E+02 0.0000000E+00 0.0000000E+00
3 2. 0.9000000E+00 -0.1000000E+02 0.0000000E+00 0.0000000E+00
4 2. 0.1350000E+01 -0.1000000E+02 0.0000000E+00 0.0000000E+00
5 2. 0.1800000E+01 -0.1000000E+02 0.0000000E+00 0.0000000E+00
.....
1547 1. 0.0000000E+00 0.4328000E+02 0.0000000E+00 0.0000000E+00
1548 1. 0.0000000E+00 0.4496000E+02 0.0000000E+00 0.0000000E+00
1549 1. 0.0000000E+00 0.4663999E+02 0.0000000E+00 0.0000000E+00
1550 1. 0.0000000E+00 0.4831999E+02 0.0000000E+00 0.0000000E+00
1551 1. 0.0000000E+00 0.5000000E+02 0.0000000E+00 0.0000000E+00

```

```

1 1 2 48 47 2 2 0.00 0.00 0.00 0.00 1.0000
2 2 3 49 48 2 2 0.00 0.00 0.00 0.00 1.0000
3 3 4 50 49 2 2 0.00 0.00 0.00 0.00 1.0000
4 4 5 51 50 2 2 0.00 0.00 0.00 0.00 1.0000
5 5 6 52 51 2 2 0.00 0.00 0.00 0.00 1.0000
.....
1445 1479 1480 1546 1545 2 2 0.00 0.00 0.00 0.00 1.0000
1446 1480 1481 1547 1546 2 2 0.00 0.00 0.00 0.00 1.0000
1447 1481 1482 1548 1547 2 2 0.00 0.00 0.00 0.00 1.0000
1448 1482 1483 1549 1548 2 2 0.00 0.00 0.00 0.00 1.0000
1449 1483 1484 1550 1549 2 2 0.00 0.00 0.00 0.00 1.0000
1450 1484 1485 1551 1550 2 2 0.00 0.00 0.00 0.00 1.0000
*****Evaluating the stress and displacement*****
1551 1450 0 55 4 0 0
46 92 0.1250000E+02 0.1250000E+02
92 138 0.1250000E+02 0.1250000E+02
138 184 0.1250000E+02 0.1250000E+02
184 230 0.1250000E+02 0.1250000E+02
230 276 0.1250000E+02 0.1250000E+02
.....
1221 1287 0.2500000E+02 0.2500000E+02
1287 1353 0.2500000E+02 0.2500000E+02
1353 1419 0.2500000E+02 0.2500000E+02
1419 1485 0.2500000E+02 0.2500000E+02
1485 1551 0.2500000E+02 0.2500000E+02
(EOF)

```

At this stage, the gas pressure data file is prepared and the intermediate files TENFAL.DAT, PLTFAL.DAT and FNPRM.DAT are initiated as in the following examples:

GAS.DAT (file name)

N $p_g(\downarrow)$ # repeat NMAT times, set $P_g = 0$ if no gas in corresponding material;
(EOF)

TENFAL.DAT (file name)

0 (\downarrow) # free format in first line of the file;
(EOF)

PLTFAL.DAT (file name)

0 (↵) # free format in first line of the file;
(EOF)

FNPRM.DAT (file name)

0 (↵) # free format in first line of the file;
(EOF)

Now, the program FEOMP can be executed in a working directory which contains following files:

GENIN.DAT
FEOMPIN.DAT
GAS.DAT
TENFAL.DAT
PLTFAL.DAT
FNPRM.DAT

Output from program FEOMP

The major output files from program FEOMP are EPFEOUT.DAT and FEOMPRT.DAT. The first file is used as input data for post-processor which will graphically express the results, while the second one contains the results for printing out. For each geometrically altered iteration, these two data files are stored in a sub-directory iterN (N indicates the number of the particular iteration). One set of such data file samples are listed in List D. 4 and D. 5. The graphical presentations of the results for each geometrically altered iteration are shown in Fig. D. 1 to Fig. D.8.

List D. 4 - Sample of EPFEOUT.DAT File

```

0 0 0 1 0 Two dimensional outburst model for a deep opening - sigh/sigv=0.5'
1 0
0 1 1576 0 Two dimensional outburst model for a deep opening - sigh/sigv=0.5'
0.0000000E+00 -0.1000000E+02
0.4500000E+00 -0.1000000E+02
0.9000000E+00 -0.1000000E+02
0.1350000E+01 -0.1000000E+02
0.1800000E+01 -0.1000000E+02
.....
0.0000000E+00 0.4520000E+02
0.0000000E+00 0.4639999E+02
0.0000000E+00 0.4759999E+02
0.0000000E+00 0.4879999E+02
0.0000000E+00 0.5000000E+02
0 2 0 0 Two dimensional outburst model for a deep opening - sigh/sigv=0.5'
0 3 0 0 Two dimensional outburst model for a deep opening - sigh/sigv=0.5'
0 4 1475 0 Two dimensional outburst model for a deep opening - sigh/sigv=0.5'
1 1 2 48 47 2 2
2 2 3 49 48 2 2
3 3 4 50 49 2 2
4 4 5 51 50 2 2
5 5 6 52 51 2 2
.....
1470 1504 1505 1571 1570 2 2
1471 1505 1506 1572 1571 2 2
1472 1506 1507 1573 1572 2 2
1473 1507 1508 1574 1573 2 2
1474 1508 1509 1575 1574 2 2
1475 1509 1510 1576 1575 2 2
.....
1 1 1443 1 Two dimensional outburst model for a deep opening - sigh/sigv=0.5'
1 1 0.0000000E+00 0.0000000E+00
2 1 -0.3705137E-03 0.0000000E+00
3 1 -0.7412657E-03 0.0000000E+00
4 1 -0.112501E-02 0.0000000E+00
5 1 -0.1484585E-02 0.0000000E+00
.....
1571 1 0.0000000E+00 -0.2098849E-02
1572 1 0.0000000E+00 -0.2063868E-02
1573 1 0.0000000E+00 -0.2032057E-02
1574 1 0.0000000E+00 -0.2003891E-02
1575 1 0.0000000E+00 -0.1979999E-02
1576 1 0.0000000E+00 -0.1961168E-02
.....
1 2 1332 1 Two dimensional outburst model for a deep opening - sigh/ginv=0.5'
1 0 0.0000000E+00 0.0000000E+00 0.0000000E+00 0.0000000E+00 0.0000000E+00 0.0000000E+00 0.0000000E+00
2 0 -3426535E+02 -1653557E+02 -1828833E+02 -5613223E-02 -1653557E+02 -3426535E+02 -5013925E+02 0.6750000E+00 -9000000E+01
3 0 -3426541E+02 -1646557E+02 -1826315E+02 -1496153E-01 -1646556E+02 -3426542E+02 -9010918E+02 0.1125000E+01 -9000000E+01

```

```

4 0 -3425095E+02-1635572E+02-1821840E+02-2229695E-01-1635569E+02-3425097E+02-9008591E+020.1575000E+01-9000000E+01
5 0 -3423982E+02-1622038E+02-1816567E+02-3720927E-01-1622030E+02-3423989E+02-9003891E+020.2025000E+01-9000000E+01
.....
1470 0 -2446095E+02-1281070E+02-1341779E+02-4503759E-01-1281052E+02-2446113E+02-8993555E+020.1400000E+010.4340000E+02
1471 0 -2421143E+02-1274036E+02-1330264E+02-4172186E-01-1274021E+02-2421158E+02-8994867E+020.1400000E+010.4460000E+02
1472 0 -2395435E+02-1267374E+02-1318611E+02-3631487E-01-1267362E+02-2395446E+02-8997266E+020.1400000E+010.4580000E+02
1473 0 -2368609E+02-1261264E+02-1306755E+02-2876726E-01-1261257E+02-2368617E+02-9000832E+020.1400000E+010.4699999E+02
1474 0 -2340298E+02-1255894E+02-1294629E+02-1904259E-01-1255890E+02-2340302E+02-9005664E+020.1400000E+010.4819999E+02
1475 0 -2310130E+02-1251451E+02-1282169E+02-7131206E-02-1251450E+02-2310130E+02-9011876E+020.1400000E+010.4940000E+02
(EOF)

```

List D.5. Sample of FEOMPRT.DAT File

```

Two dimensional outburst model for a deep opening - sigh/sgn=0.5'
NUMBER OF NODAL POINTS----- 1576
NUMBER OF ELEMENTS----- 1475
NUMBER OF DIFF MATERIALS--- 4
NUMBER OF PRESSURE CARDS--- 55
X-ACCELERATION----- 0.0000E+00
Y-ACCELERATION----- -0.1000E+01
NUMBER OF APPROXIMATIONS----- 400
10.2500E-01
0ELASTIC MODULUS      NU      COHESION  FRICTION ANGLE
0.18500E+05          0.18000E+00  0.18000E+02  0.30000E+02
20.2700E-01
0ELASTIC MODULUS      NU      COHESION  FRICTION ANGLE
0.26150E+05          0.36000E+00  0.20000E+02  0.35000E+02
30.2500E-01
0ELASTIC MODULUS      NU      COHESION  FRICTION ANGLE
0.10000E+05          0.20000E+00  0.10000E+02  0.20000E+02
40.2500E-01
0ELASTIC MODULUS      NU      COHESION  FRICTION ANGLE
0.10000E-01          0.35000E+00  0.18000E+02  0.30000E+02
NODAL POINT  TYPE  X ORDNATE  Y ORDNATE  X LOAD OR DISPLACEMENT  Y LOAD OR DISPLACEMENT  Z-LOAD OR DISPLACEMENT  PORE PRESSURE
1 3.00 0.0000000E+00 -0.1000000E+02  0.0000000E+00  0.0000000E+00  0.0000000E+00  0.0000000E+00
2 2.00 0.4500000E+00 -0.1000000E+02  0.0000000E+00  0.0000000E+00  0.0000000E+00  0.0000000E+00
3 2.00 0.9000000E+00 -0.1000000E+02  0.0000000E+00  0.0000000E+00  0.0000000E+00  0.0000000E+00
4 2.00 0.1350000E+01 -0.1000000E+02  0.0000000E+00  0.0000000E+00  0.0000000E+00  0.0000000E+00
5 2.00 0.1800000E+01 -0.1000000E+02  0.0000000E+00  0.0000000E+00  0.0000000E+00  0.0000000E+00
.....
1572 1.06 0.0000000E+00 0.4328000E+02 0.0000000E+00 0.0000000E+00 0.0000000E+00 0.0000000E+00
1573 1.00 0.0000000E+00 0.4496000E+02 0.0000000E+00 0.0000000E+00 0.0000000E+00 0.0000000E+00
1574 1.00 0.0000000E+00 0.4663999E+02 0.0000000E+00 0.0000000E+00 0.0000000E+00 0.0000000E+00
1575 1.00 0.0000000E+00 0.4831999E+02 0.0000000E+00 0.0000000E+00 0.0000000E+00 0.0000000E+00
1576 1.00 0.0000000E+00 0.5000000E+02 0.0000000E+00 0.0000000E+00 0.0000000E+00 0.0000000E+00
ELEMENT NO.  I  J  K  L  MATERIAL  X-STRESS  Y-STRESS  XY-STRESS  Z-STRESS
1 1 2 48 47 2 0.000 0.000 0.000 0.000
2 2 3 49 48 2 0.000 0.000 0.000 0.000
3 3 4 50 49 2 0.000 0.000 0.000 0.000
4 4 5 51 50 2 0.000 0.000 0.000 0.000
5 5 6 52 51 2 0.000 0.000 0.000 0.000
.....
1470 1504 1505 1571 1570 2 0.000 0.000 0.000 0.000
1471 1505 1506 1572 1571 2 0.000 0.000 0.000 0.000
1472 1506 1507 1573 1572 2 0.000 0.000 0.000 0.000
1473 1507 1508 1574 1573 2 0.000 0.000 0.000 0.000

```

1474 1508 1509 1575 1574 2 0.000 0.000 0.000
1475 1509 1510 1576 1575 2 0.000 0.000 0.000

PRESSURE BOUNDARY CONDITIONS

1 J PRESSURE: I PRESSURE: J
46 92 12.500 12.500
92 138 12.500 12.500
138 184 12.500 12.500
184 230 12.500 12.500
230 276 12.500 12.500

1246 1312 25.000 25.000
1312 1378 25.000 25.000
1378 1444 25.000 25.000
1444 1510 25.000 25.000
1510 1576 25.000 25.000

BAND WIDTH FOR THIS DATA = 136

STRESSES AFTER APPROXIMATION NUMBER 1
0THE UNBALANCED LAOD AT THIS STAGE IS 0.73018E+04

THE RATIO FOR CORRECTION OF STORED STRESSES IS 0.4669

THE NEXT ELEMENT YIELDING IS 759
AND THE TOTAL NUMBER OF ELEMENTS THAT CAN YIELD WITH THE LINEAR ADDITION OF TOTAL LOAD IS 17
LOAD UP TO THIS STAGE AS A FRACTION OF TOTAL IS 0.46687

STRESSES AFTER APPROXIMATION NUMBER 2
0THE UNBALANCED LAOD AT THIS STAGE IS 0.65517E+04

THE RATIO FOR CORRECTION OF STORED STRESSES IS 0.1000

THE NEXT ELEMENT YIELDING IS 799
AND THE TOTAL NUMBER OF ELEMENTS THAT CAN YIELD WITH THE LINEAR ADDITION OF TOTAL LOAD IS 16
LOAD UP TO THIS STAGE AS A FRACTION OF TOTAL IS 0.52019

STRESSES AFTER APPROXIMATION NUMBER 3
0THE UNBALANCED LAOD AT THIS STAGE IS 0.58984E+04

THE RATIO FOR CORRECTION OF STORED STRESSES IS 0.1000

THE NEXT ELEMENT YIELDING IS 599
AND THE TOTAL NUMBER OF ELEMENTS THAT CAN YIELD WITH THE LINEAR ADDITION OF TOTAL LOAD IS 13
LOAD UP TO THIS STAGE AS A FRACTION OF TOTAL IS 0.56817

STRESSES AFTER APPROXIMATION NUMBER 4
0THE UNBALANCED LAOD AT THIS STAGE IS 0.53051E-04

THE RATIO FOR CORRECTION OF STORED STRESSES IS 0.1000

THE NEXT ELEMENT YIELDING IS 559
 AND THE TOTAL NUMBER OF ELEMENTS THAT CAN YIELD WITH THE LINEAR ADDITION OF TOTAL LOAD IS 10
 LOAD UP TO THIS STAGE AS A FRACTION OF TOTAL IS 0.61135
 |
 STRESSES AFTER APPROXIMATION NUMBER 5
 OTHE UNBALLANCED LAOD AT THIS STAGE IS 0.477541E+04

 THE RATIO FOR CORRECTION OF STORED STRESSES IS 0.10600

 THE NEXT ELEMENT YIELDING IS 0
 AND THE TOTAL NUMBER OF ELEMENTS THAT CAN YIELD WITH THE LINEAR ADDITION OF TOTAL LOAD IS 9
 LOAD UP TO THIS STAGE AS A FRACTION OF TOTAL IS 0.65022
 |
 STRESSES AFTER APPROXIMATION NUMBER 40
 OTHE UNBALLANCED LAOD AT THIS STAGE IS 0.22329E+01

 THE RATIO FOR CORRECTION OF STORED STRESSES IS 0.2233

 THE NEXT ELEMENT YIELDING IS 0
 AND THE TOTAL NUMBER OF ELEMENTS THAT CAN YIELD WITH THE LINEAR ADDITION OF TOTAL LOAD IS 0
 LOAD UP TO THIS STAGE AS A FRACTION OF TOTAL IS 0.99983
 |
 STRESSES AFTER APPROXIMATION NUMBER 41
 OTHE UNBALLANCED LAOD AT THIS STAGE IS 0.17335E+01

 THE RATIO FOR CORRECTION OF STORED STRESSES IS 0.2233

 THE NEXT ELEMENT YIELDING IS 0
 AND THE TOTAL NUMBER OF ELEMENTS THAT CAN YIELD WITH THE LINEAR ADDITION OF TOTAL LOAD IS 0
 LOAD UP TO THIS STAGE AS A FRACTION OF TOTAL IS 0.99987
 |
 STRESSES AFTER APPROXIMATION NUMBER 42
 OTHE UNBALLANCED LAOD AT THIS STAGE IS 0.13458E+01

 THE RATIO FOR CORRECTION OF STORED STRESSES IS 0.2233

 THE NEXT ELEMENT YIELDING IS 0
 AND THE TOTAL NUMBER OF ELEMENTS THAT CAN YIELD WITH THE LINEAR ADDITION OF TOTAL LOAD IS 0
 LOAD UP TO THIS STAGE AS A FRACTION OF TOTAL IS 0.99990
 |
 STRESSES AFTER APPROXIMATION NUMBER 43
 OTHE UNBALLANCED LAOD AT THIS STAGE IS 0.10449E+01

 THE RATIO FOR CORRECTION OF STORED STRESSES IS 0.2233

 THE NEXT ELEMENT YIELDING IS 0
 AND THE TOTAL NUMBER OF ELEMENTS THAT CAN YIELD WITH THE LINEAR ADDITION OF TOTAL LOAD IS 0

LOAD UP TO THIS STAGE AS A FRACTION OF TOTAL IS 0.99992

STRESSES AFTER APPROXIMATION NUMBER 44

EL. NO.	X	Y	X-STRESS	Y-STRESS	XY-STRESS	MAX-STRESS	MIN-STRESS	ANGLE	Z-STRESS	PLASTIC
1	0.2250000E+00	-9.0000000E+01	-1.772200E+02	-3.64413E+01	-2.46928E+01	-3.644470E+01	-1.772205E+02	-9.005675E+02	-7.691946E+01	0
2	0.6750000E+00	-9.0000000E+01	-1.770577E+02	-3.726434E+01	-7.440318E+01	-3.726038E+01	-1.770617E+02	-8.985195E+02	-7.715595E+01	0
3	0.1125000E+01	-9.0000000E+01	-1.767289E+02	-3.890473E+01	-1.250363E+00	-3.889339E+01	-1.767402E+02	-8.963678E+02	-7.762810E+01	0
4	0.1575000E+01	-9.0000000E+01	-1.762257E+02	-4.136978E+01	-1.770759E+00	-4.134653E+01	-1.762489E+02	-8.940395E+02	-7.833436E+01	0
5	0.2025000E+01	-9.0000000E+01	-1.755414E+02	-4.466798E+01	-2.312050E+00	-4.462715E+01	-1.755822E+02	-8.914387E+02	-7.927537E+01	0
4450	1.480086E+02	0.2193062E+01	-6.576640E+01	-4.149572E+02	0.4946189E+01	-5.889546E+01	-4.218282E+02	7.922396E+01	-8.653025E+01	0
4460	1.544472E+02	0.2198278E+01	-6.642542E+01	-3.950551E+02	0.4921207E+01	-5.921418E+01	-4.022663E+02	8.351026E+01	-8.306649E+01	0
4470	1.608858E+02	0.2203495E+01	-6.591201E+01	-3.785144E+02	0.4744246E+01	-5.887046E+01	-3.855595E+02	8.457137E+01	-7.999675E+01	0
4480	1.673244E+02	0.2208711E+01	-6.466305E+01	-3.649088E+02	0.4485839E+01	-5.810423E+01	-3.714676E+02	8.332916E+01	-7.732294E+01	0
4490	1.737630E+02	0.2213928E+01	-6.300936E+01	-3.537376E+02	0.4185425E+01	-5.710384E+01	-3.596431E+02	8.045315E+01	-7.501446E+01	0
4500	1.802016E+02	0.2219144E+01	-6.118286E+01	-3.445368E+02	0.3864462E+01	-5.600695E+01	-3.497127E+02	7.641928E+01	-7.302954E+01	0

STRESSES AFTER APPROXIMATION NUMBER 44

EL. NO.	X	Y	X-STRESS	Y-STRESS	XY-STRESS	MAX-STRESS	MIN-STRESS	ANGLE	Z-STRESS	PLASTIC
4510	1.866402E+02	0.2224316E+01	-5.933818E+01	-3.369130E+02	0.3534277E+01	-5.490878E+01	-3.413474E+02	7.155963E+01	-7.132521E+01	0
4520	1.930789E+02	0.2229577E+01	-5.757768E+01	-3.305462E+02	0.3200262E+01	-5.387591E+01	-3.342480E+02	6.609654E+01	-6.986231E+01	0
4530	1.995175E+02	0.2234794E+01	-5.596715E+01	-3.251814E+02	0.2864209E+01	-5.295360E+01	-3.281950E+02	6.016709E+01	-6.860674E+01	0
4540	2.059560E+02	0.2240010E+01	-5.455002E+01	-3.206171E+02	0.2525670E+01	-5.217373E+01	-3.229934E+02	5.384295E+01	-6.753008E+01	0
4550	2.123946E+02	0.2245227E+01	-5.335590E+01	-3.166952E+02	0.2182659E+01	-5.155909E+01	-3.184920E+02	4.714335E+01	-6.660920E+01	0
14710	1.400000E+01	0.4243999E+02	-1.540073E+02	2.451595E+02	0.2512428E+00	-1.539381E+02	-2.452228E+02	1.580407E+01	-1.437001E+02	0
14720	1.400000E+01	0.4412060E+02	-1.556361E+02	2.472910E+02	0.2096591E+00	-1.555881E+02	-2.473389E+02	1.312010E+01	-1.450537E+02	0
14730	1.400000E+01	0.4580000E+02	-1.581183E+02	2.489735E+02	0.1648173E+00	-1.580884E+02	-2.4900033E+02	1.040745E+01	-1.465530E+02	0
14740	1.400000E+01	0.4747999E+02	-1.616625E+02	2.501626E+02	0.1137303E+00	-1.616479E+02	-2.501772E+02	7.374265E+00	-1.482570E+02	0
14750	1.400000E+01	0.4915999E+02	-1.665415E+02	2.507825E+02	0.5256000E+01	-1.665383E+02	-2.507858E+02	3.580890E+00	-1.502367E+02	0

THE RATIO FOR CORRECTION OF STORED STRESSES IS 0.2233

THE NEXT ELEMENT YIELDING IS 0

AND THE TOTAL NUMBER OF ELEMENTS THAT CAN YIELD WITH THE LINEAR ADDITION OF TOTAL LOAD IS 0

LOAD UP TO THIS STAGE AS A FRACTION OF TOTAL IS 0.99994

IN. P. NUMBER	UX	UY
1	0.000000E+00	0.000000E+00
2	-0.236327E-03	0.000000E+00
3	-0.4716876E-03	0.000000E+00
4	-0.7051098E-03	0.000000E+00
5	-0.9356108E-03	0.000000E+00

1571 0.00000000E+00 -0.5012628E-01
1572 0.00000000E+00 -0.5101043E-01
1573 0.00000000E+00 -0.5190175E-01
1574 0.00000000E+00 -0.5279488E-01
1575 0.00000000E+00 -0.5368356E-01
1576 0.00000000E+00 -0.5456020E-01
(EOF)

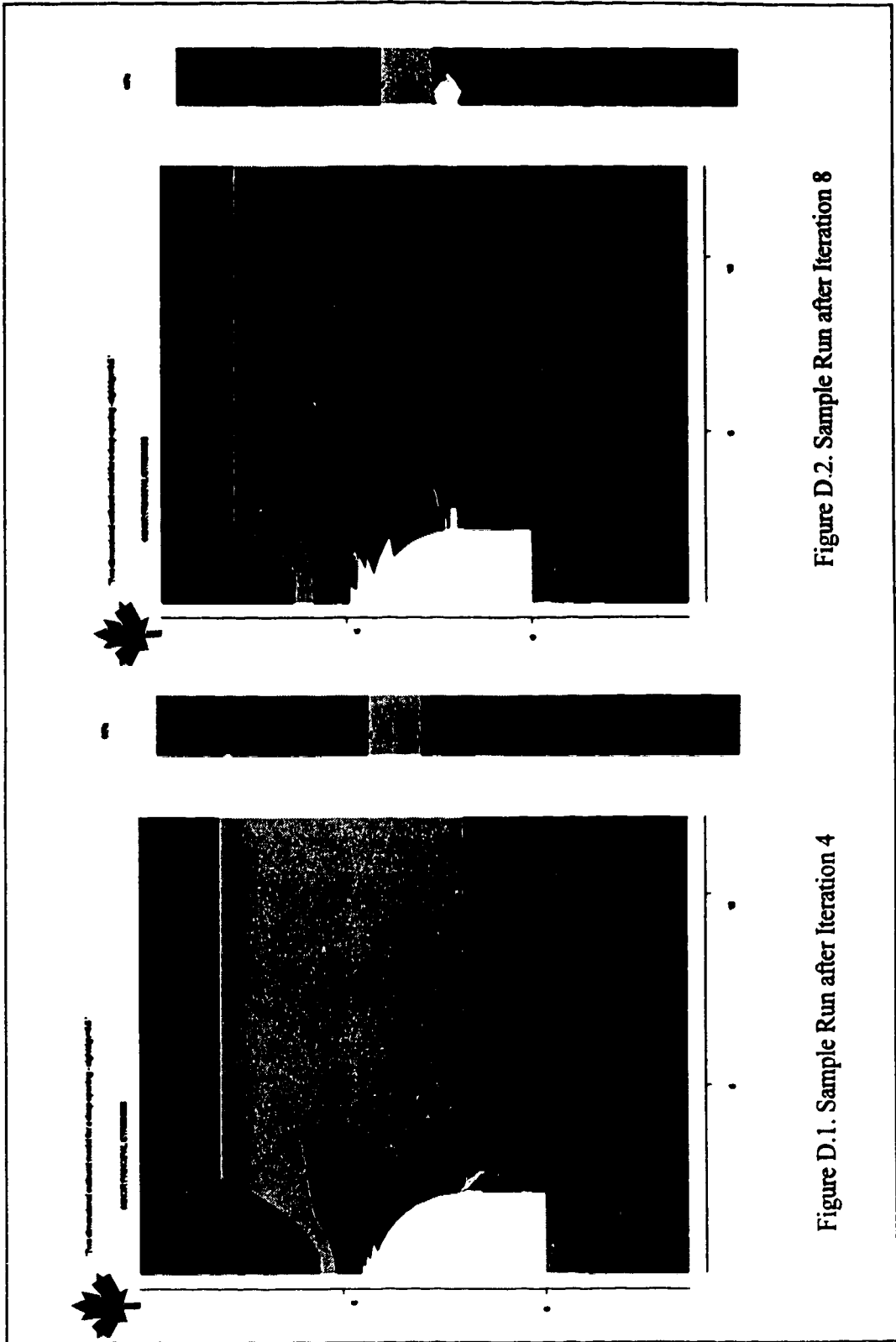


Figure D.2. Sample Run after Iteration 8

Figure D.1. Sample Run after Iteration 4

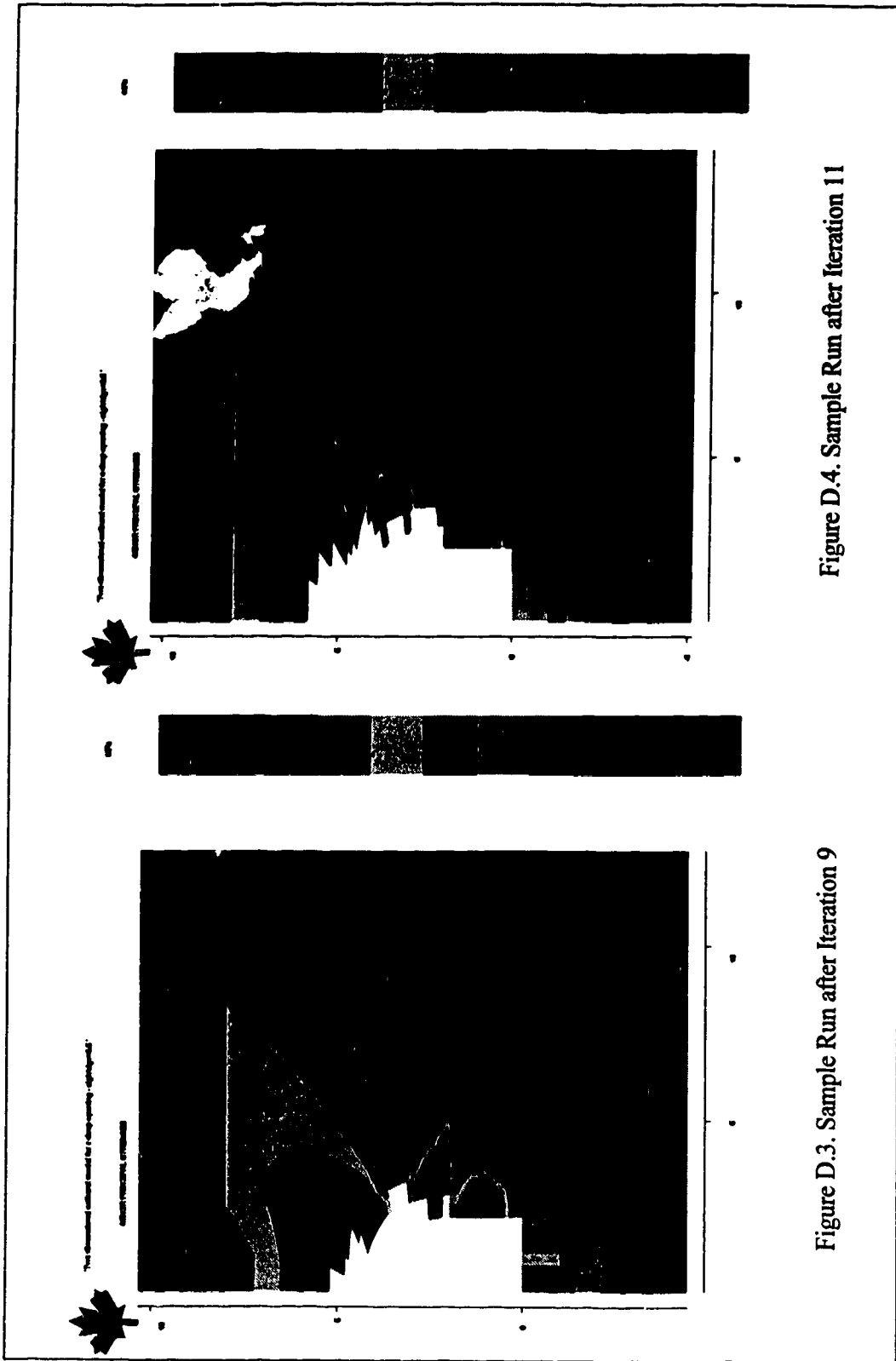


Figure D.4. Sample Run after Iteration 11

Figure D.3. Sample Run after Iteration 9

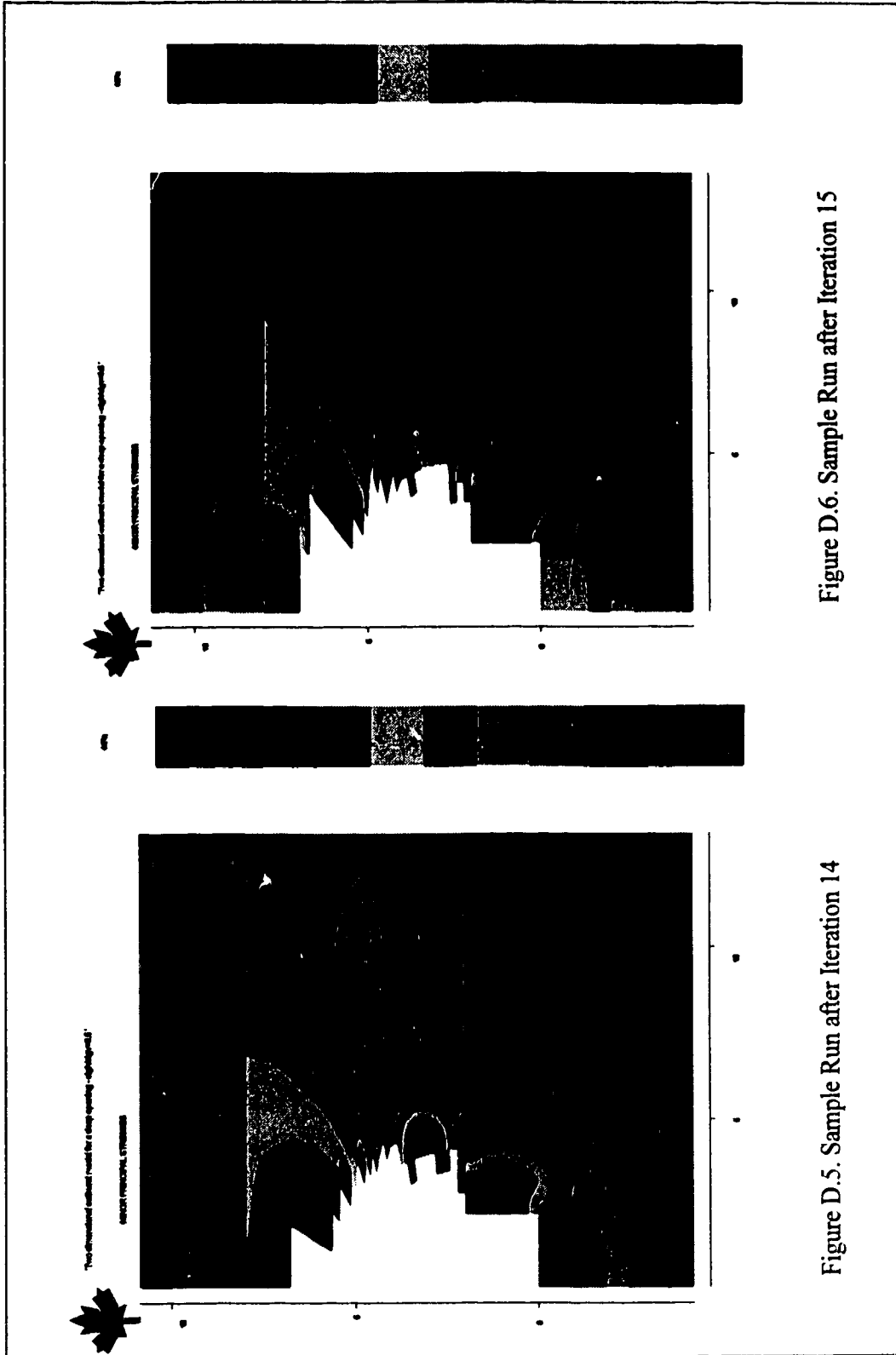


Figure D.6. Sample Run after Iteration 15

Figure D.5. Sample Run after Iteration 14

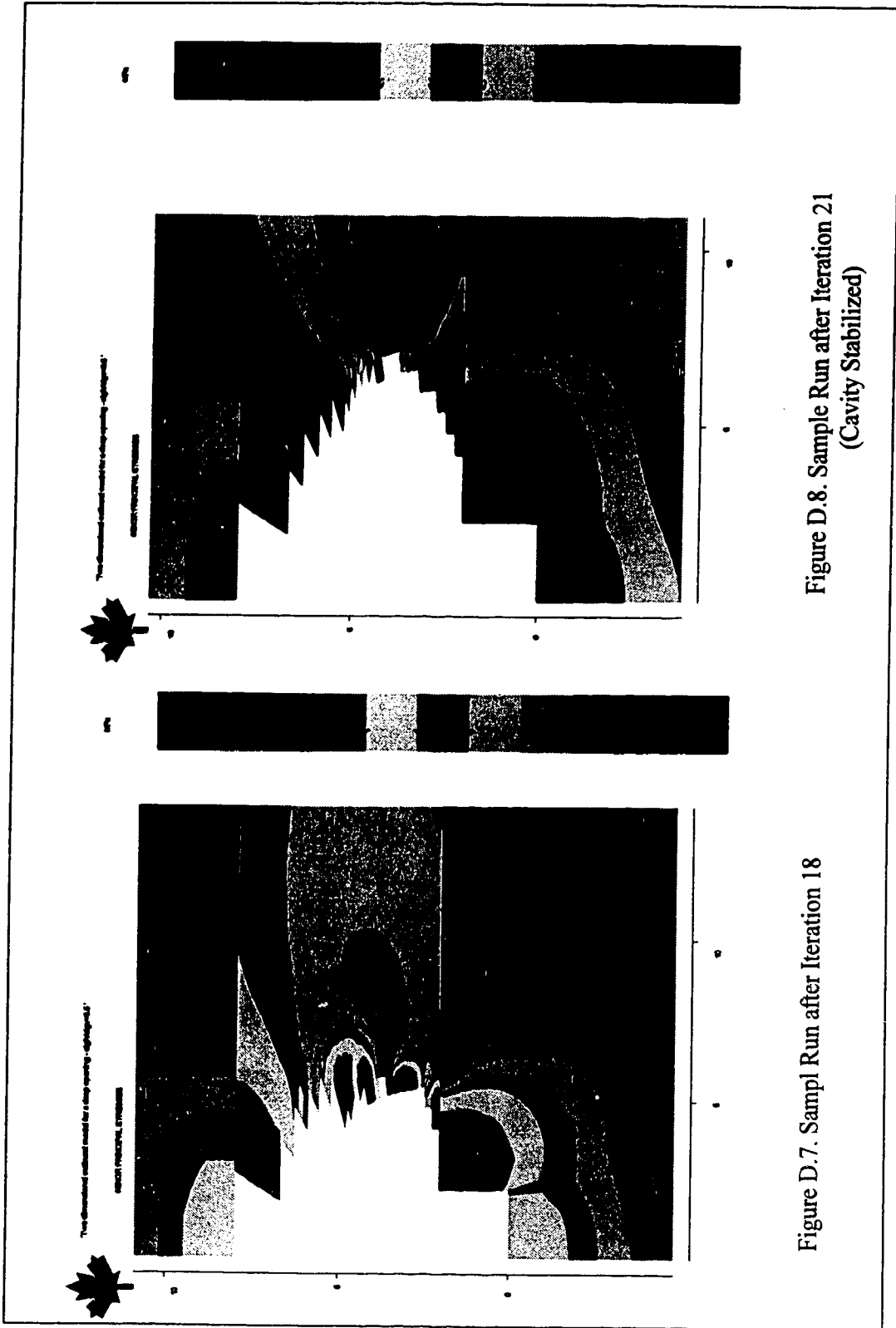


Figure D.8. Sample Run after Iteration 21
(Cavity Stabilized)

Figure D.7. Sample Run after Iteration 18

Appendix E.
Cavity Shape and Size of #36 and #37 Outbursts

The longitudinal section of the cavity produced by outbursts #36 and #37 at No. 26 Colliery, Nova Scotia is illustrated in Fig. E.1. The cross sections for this cavity are presented in Fig. E.2-E.15.

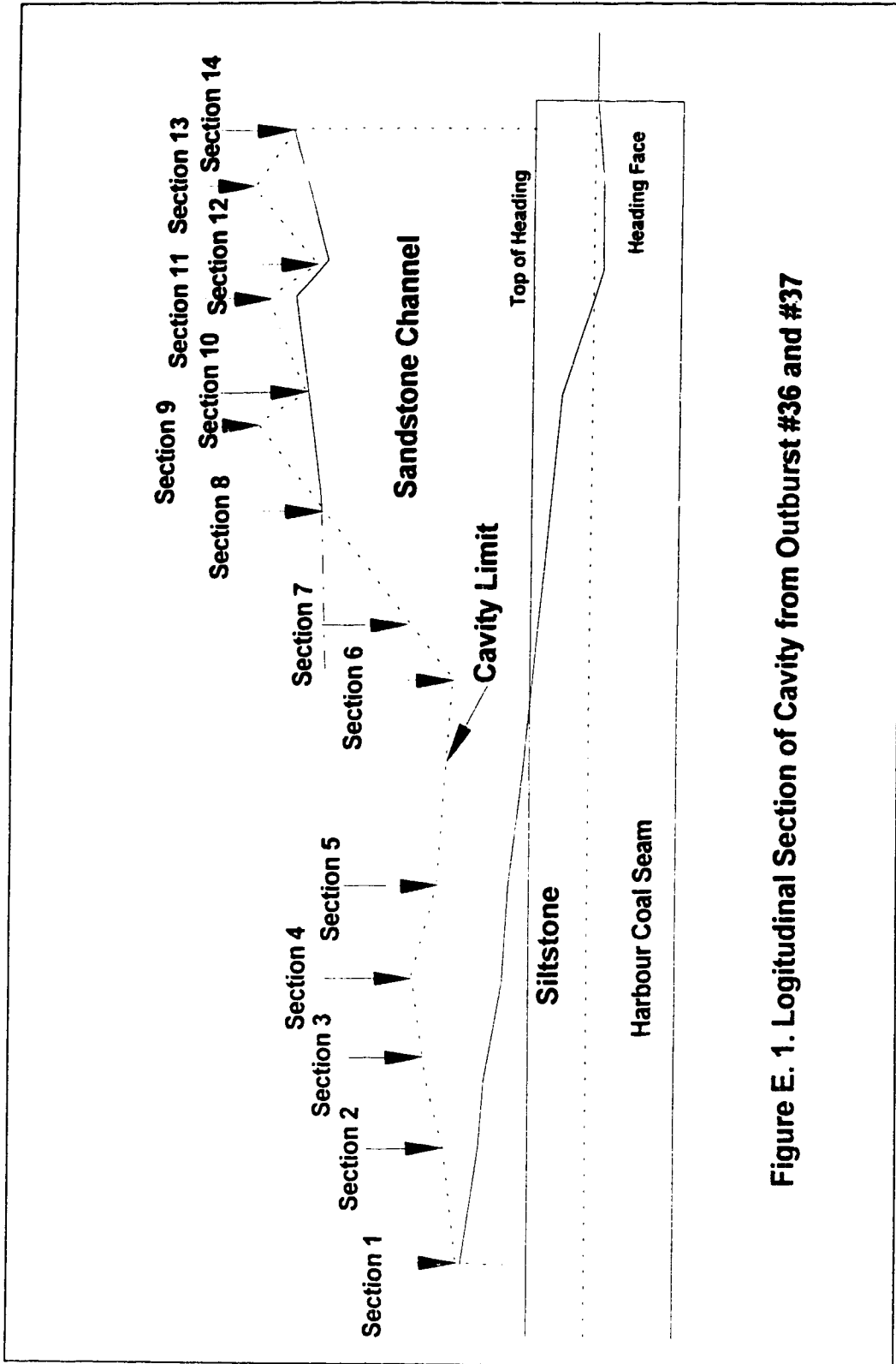
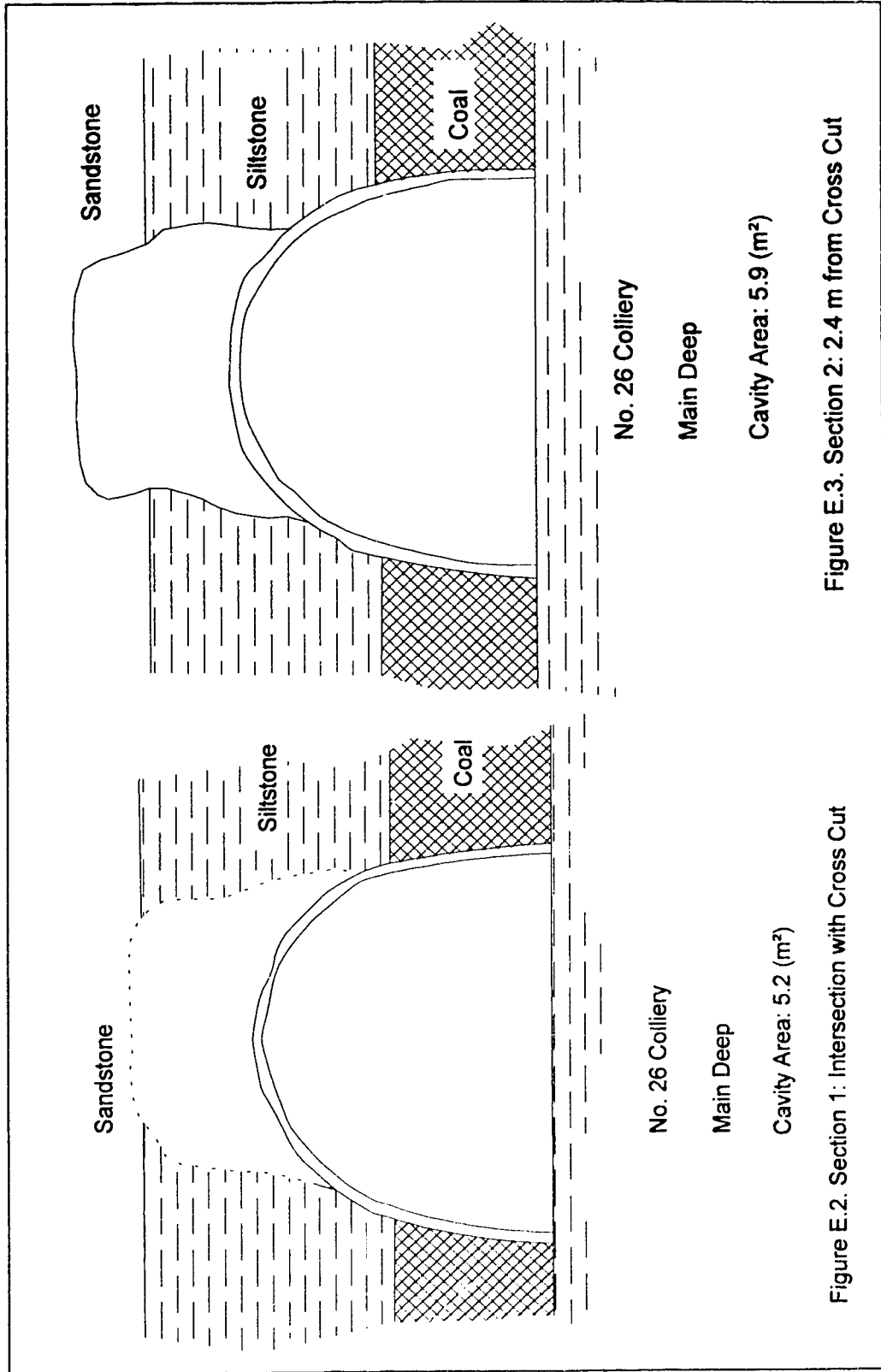
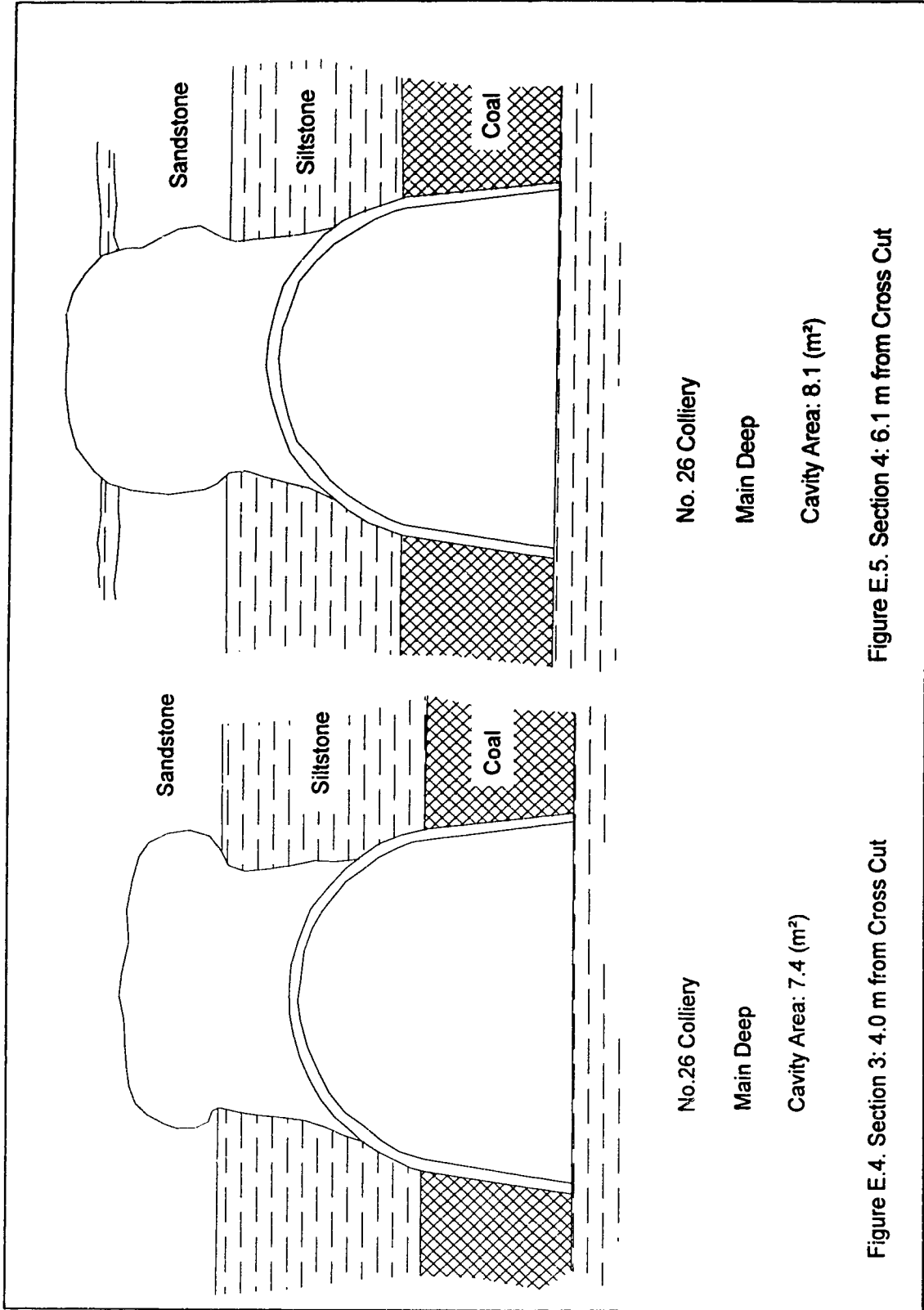


Figure E. 1. Logitudinal Section of Cavity from Outburst #36 and #37





No. 26 Colliery
Main Deep
Cavity Area: 7.4 (m²)

No. 26 Colliery
Main Deep
Cavity Area: 8.1 (m²)

Figure E.4. Section 3: 4.0 m from Cross Cut

Figure E.5. Section 4: 6.1 m from Cross Cut

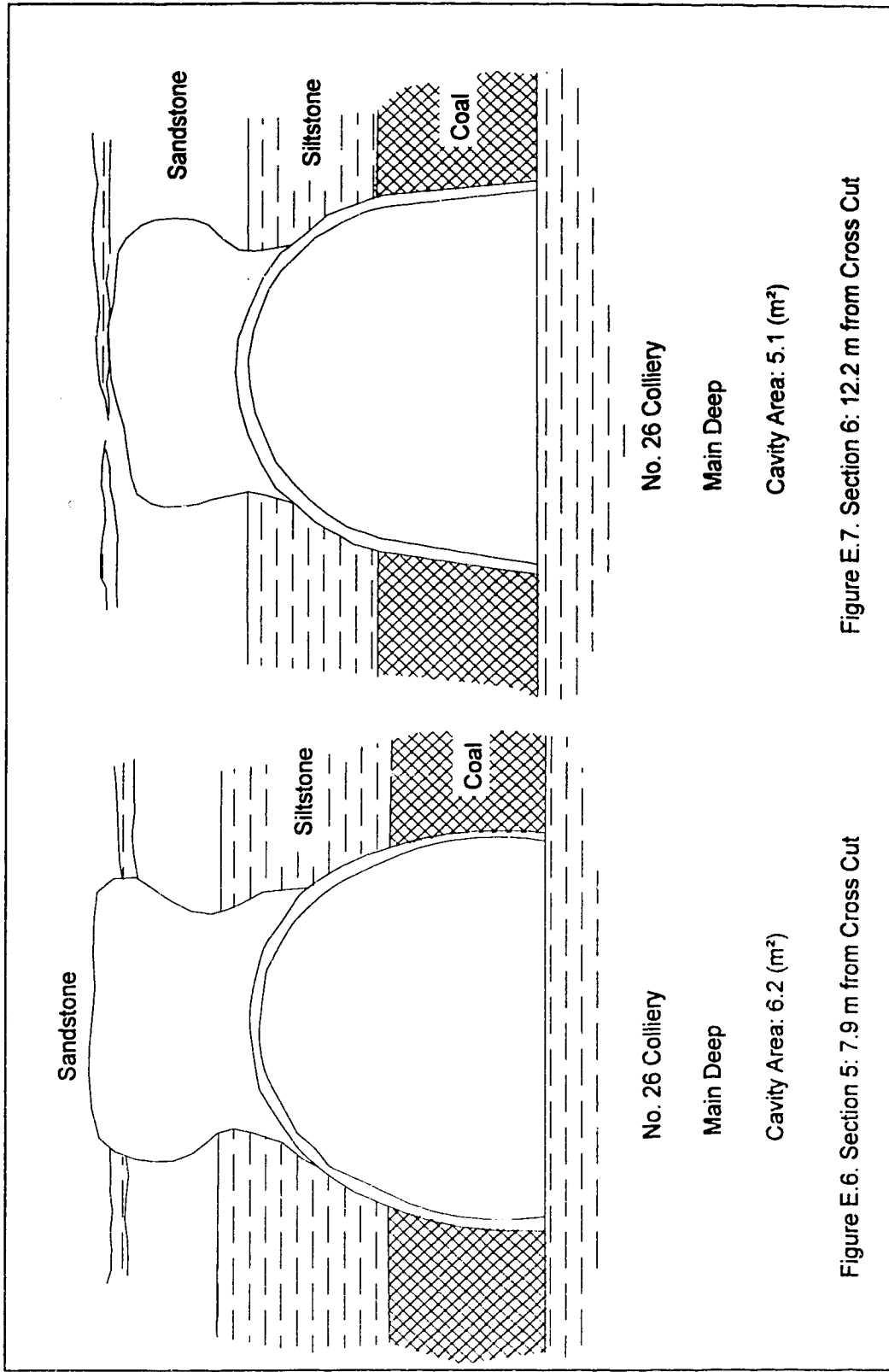
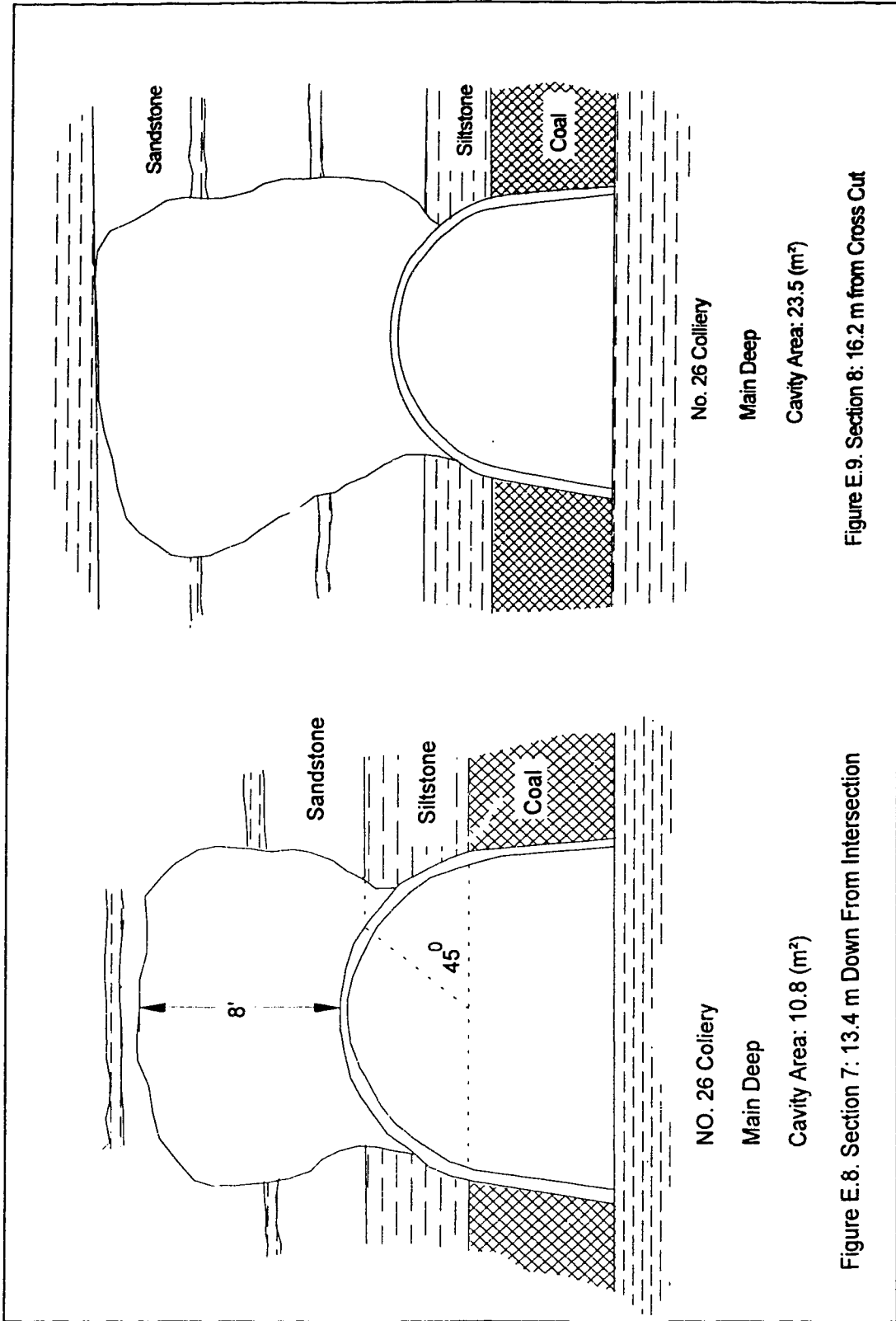


Figure E.6. Section 5: 7.9 m from Cross Cut

Figure E.7. Section 6: 12.2 m from Cross Cut



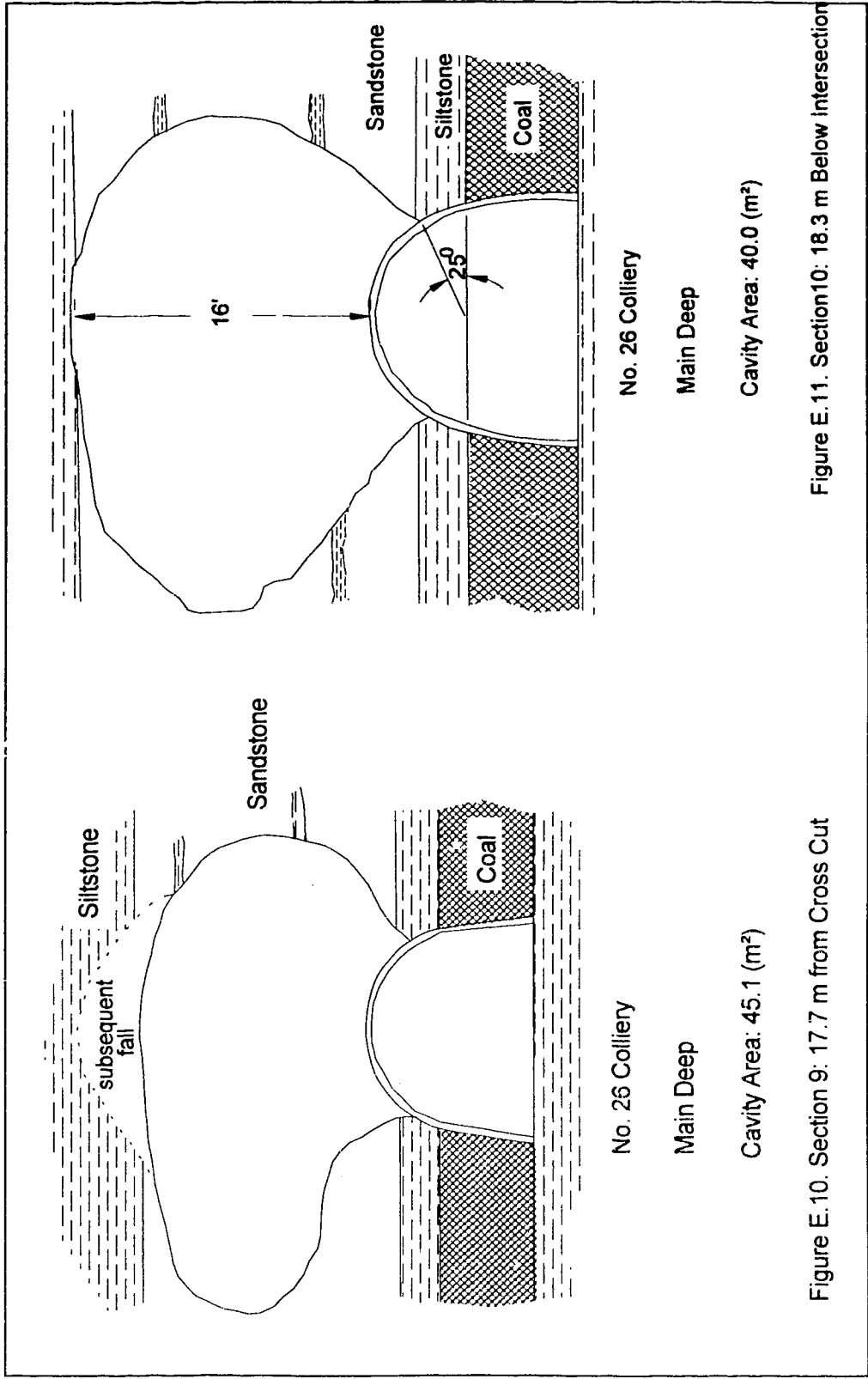
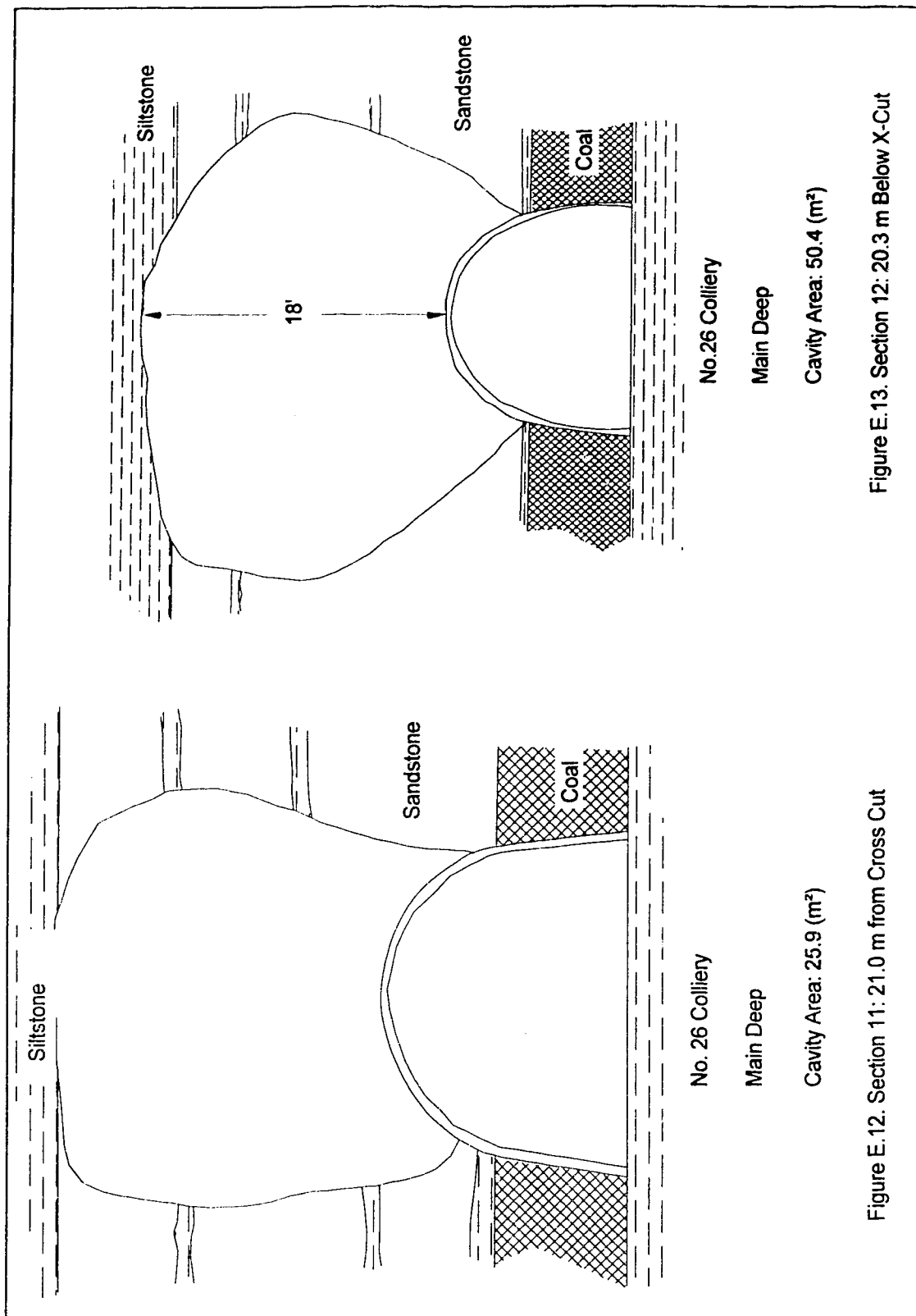


Figure E. 10. Section 9: 17.7 m from Cross Cut

Figure E. 11. Section 10: 18.3 m Below Intersection



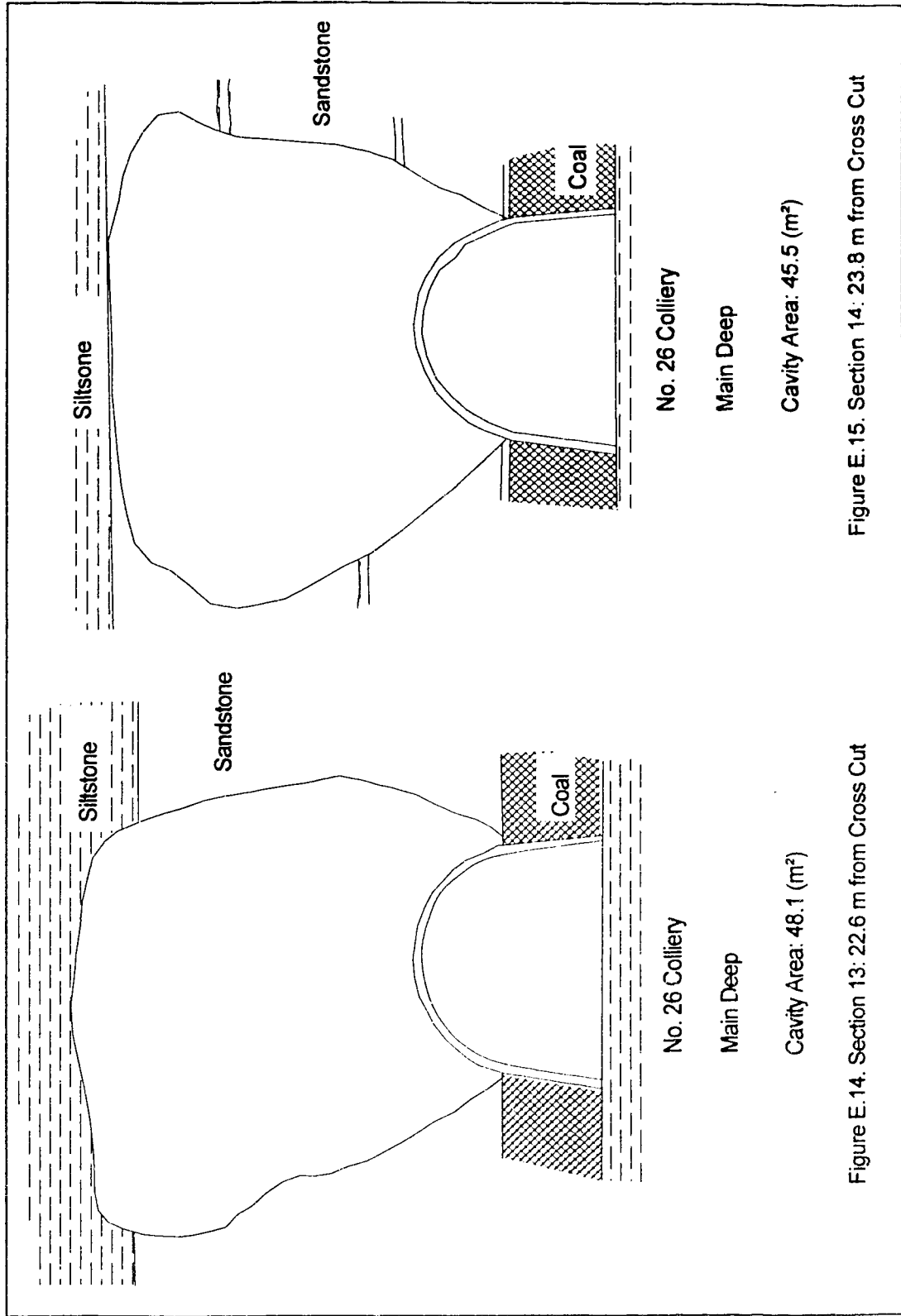
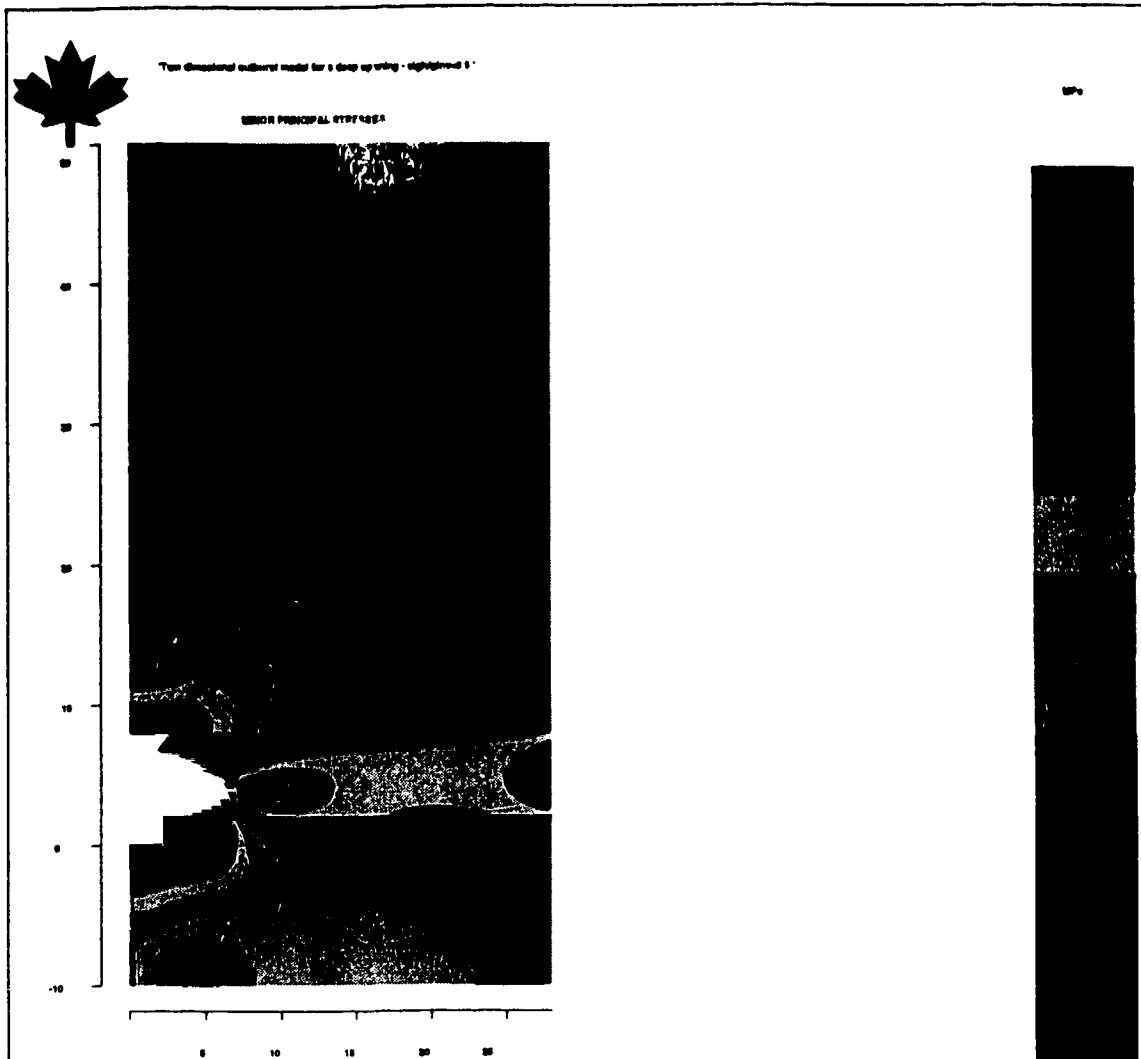


Figure E.14. Section 13: 22.6 m from Cross Cut

Figure E.15. Section 14: 23.8 m from Cross Cut

Appendix F.
Cavity Shape and Size Resulting from the Empty Cavity Model

Twelve cavities obtained from application of the empty cavity model to the entry case have been presented in this appendix. They result from the different conditions.

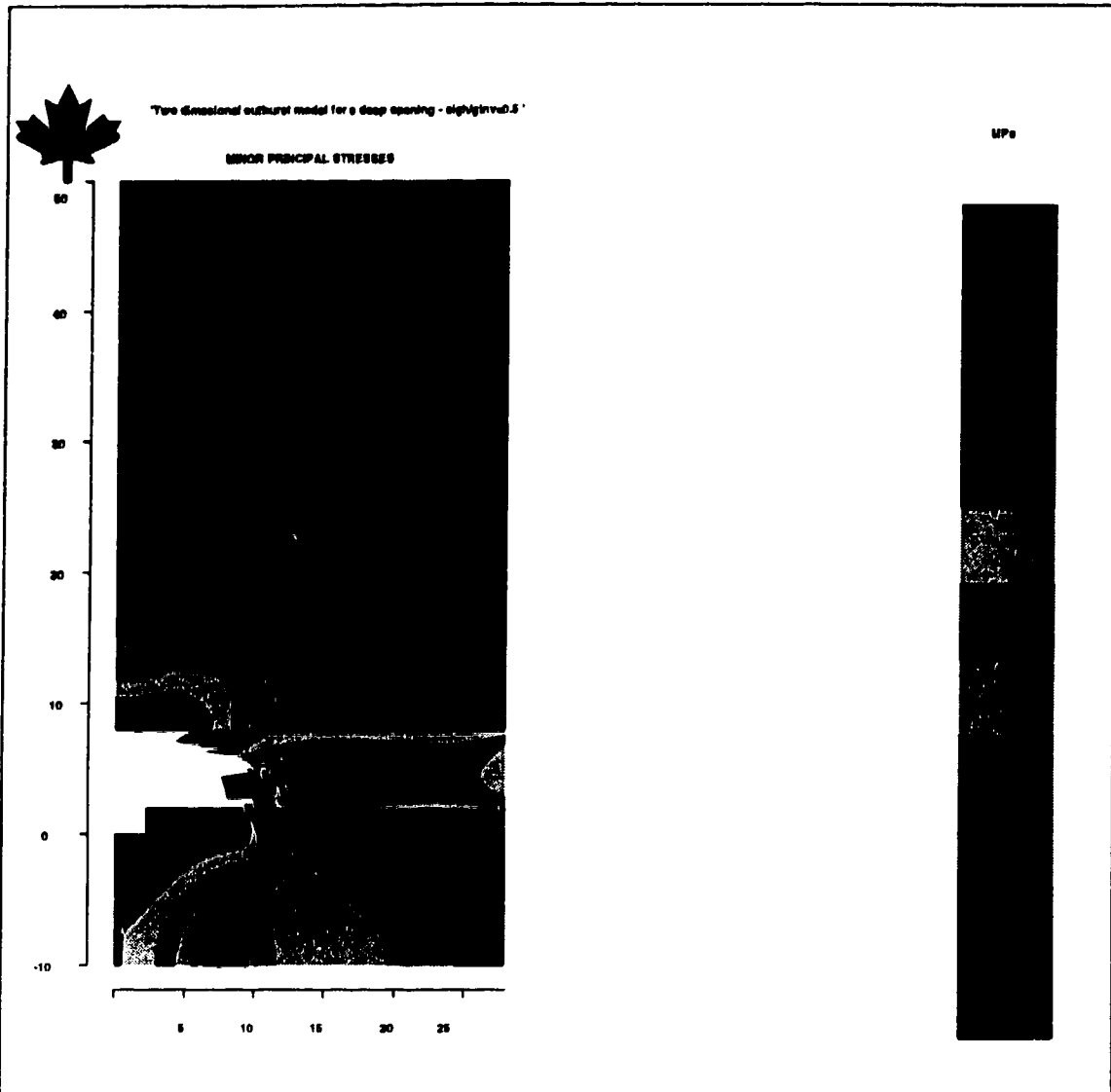


Compared input data and result:

Stress ratio: 0.5
 Gas pressure: 2.7 MPa
 Sandstone height: 3.8 m
 Exposure angle: 0°

Stablized cavity size: 50.4 m²

Figure F.1. Stabilized Cavity from Empty Model

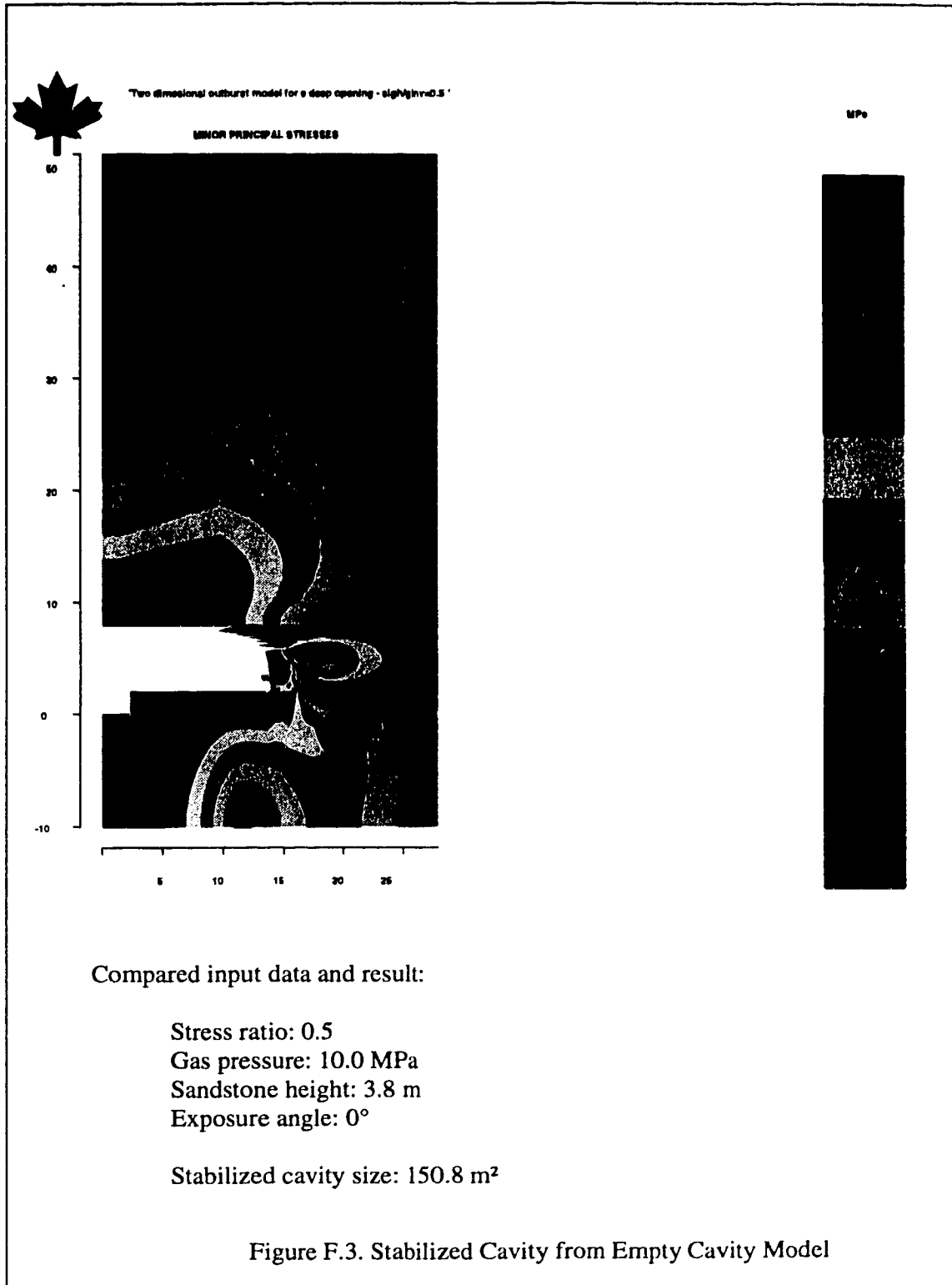


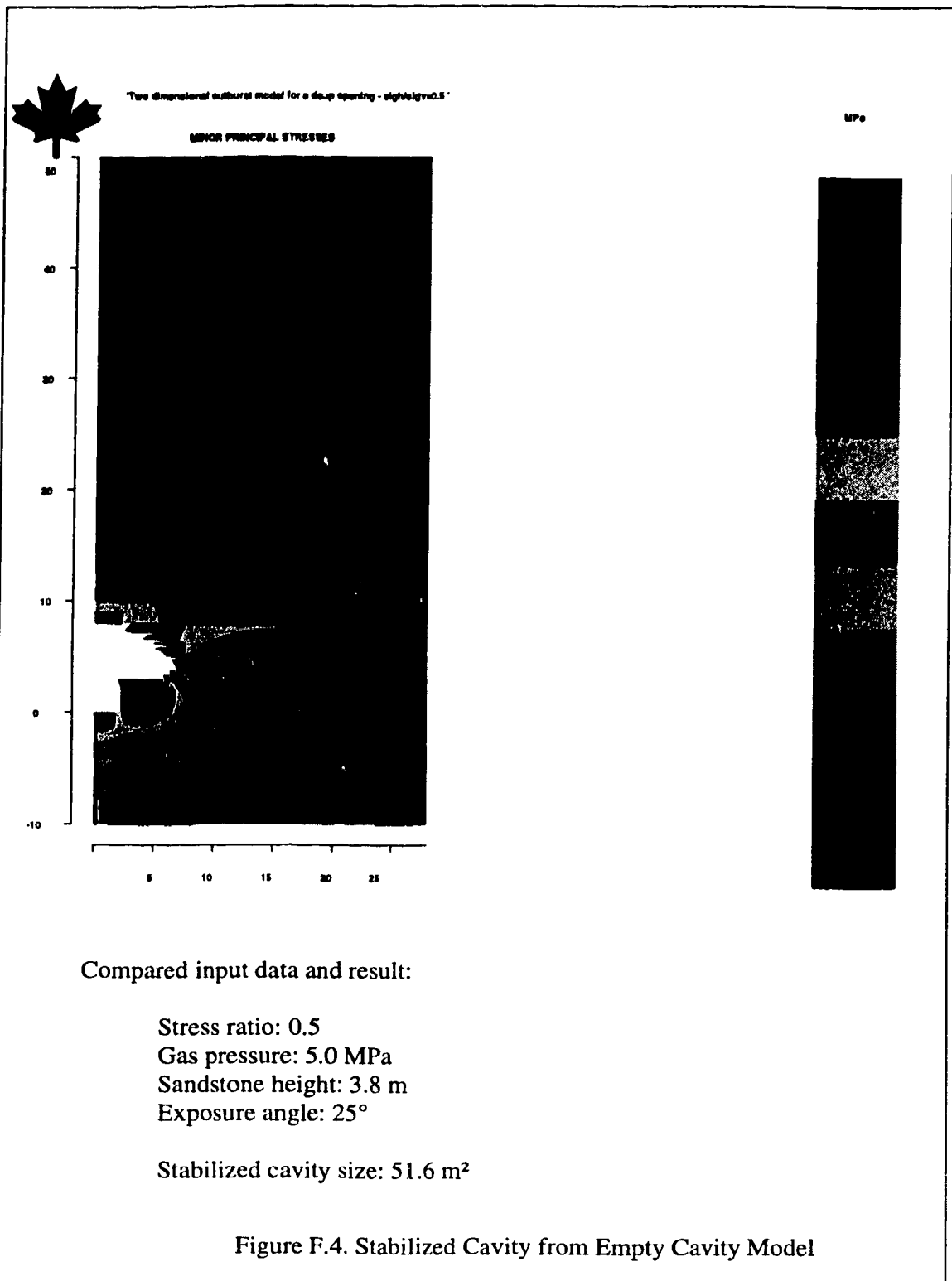
Compared input data and result:

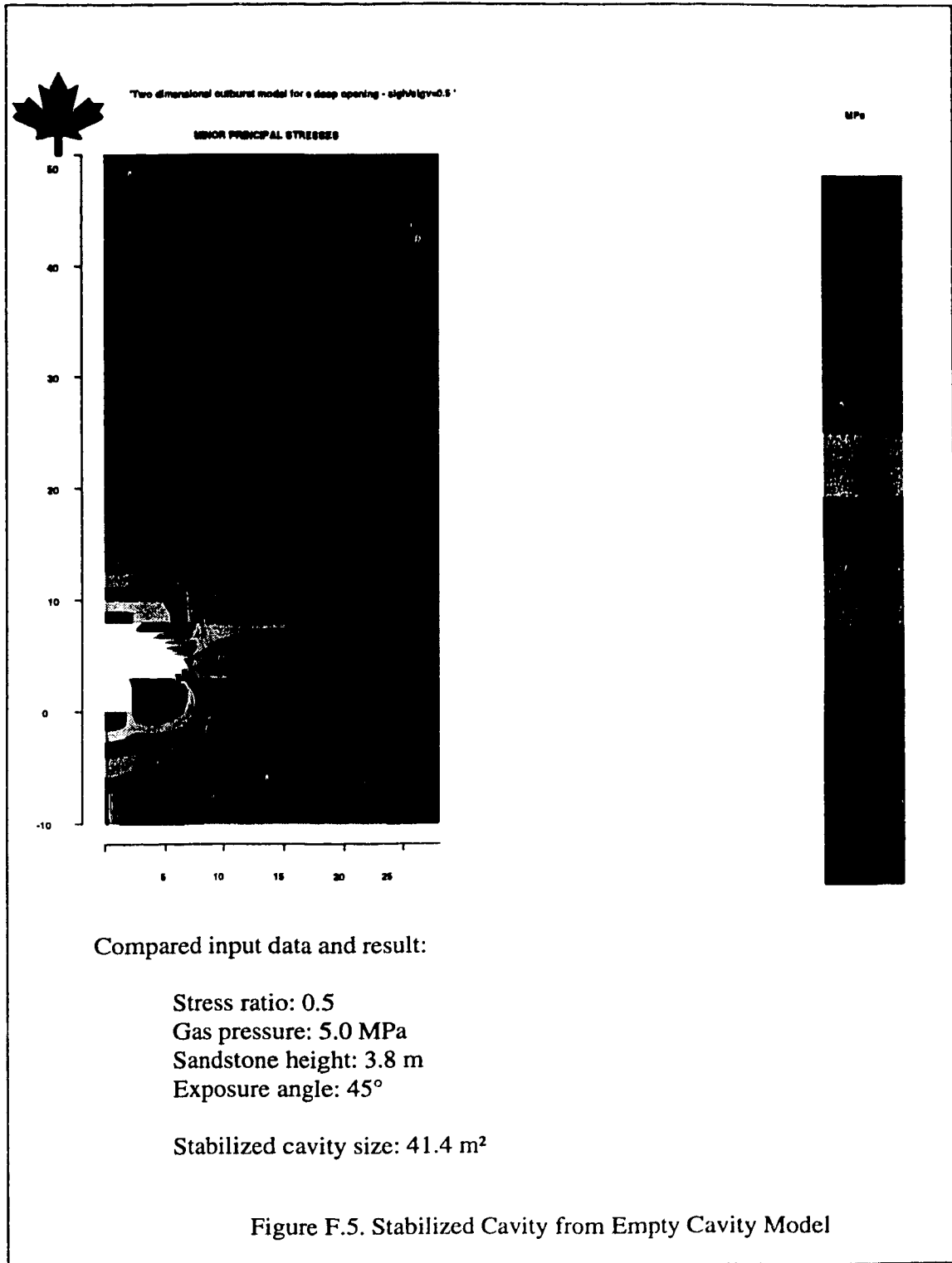
Stress ratio: 0.5
 Gas pressure: 4.0 MPa
 Sandstone height: 3.8 m
 Exposure angle: 0°

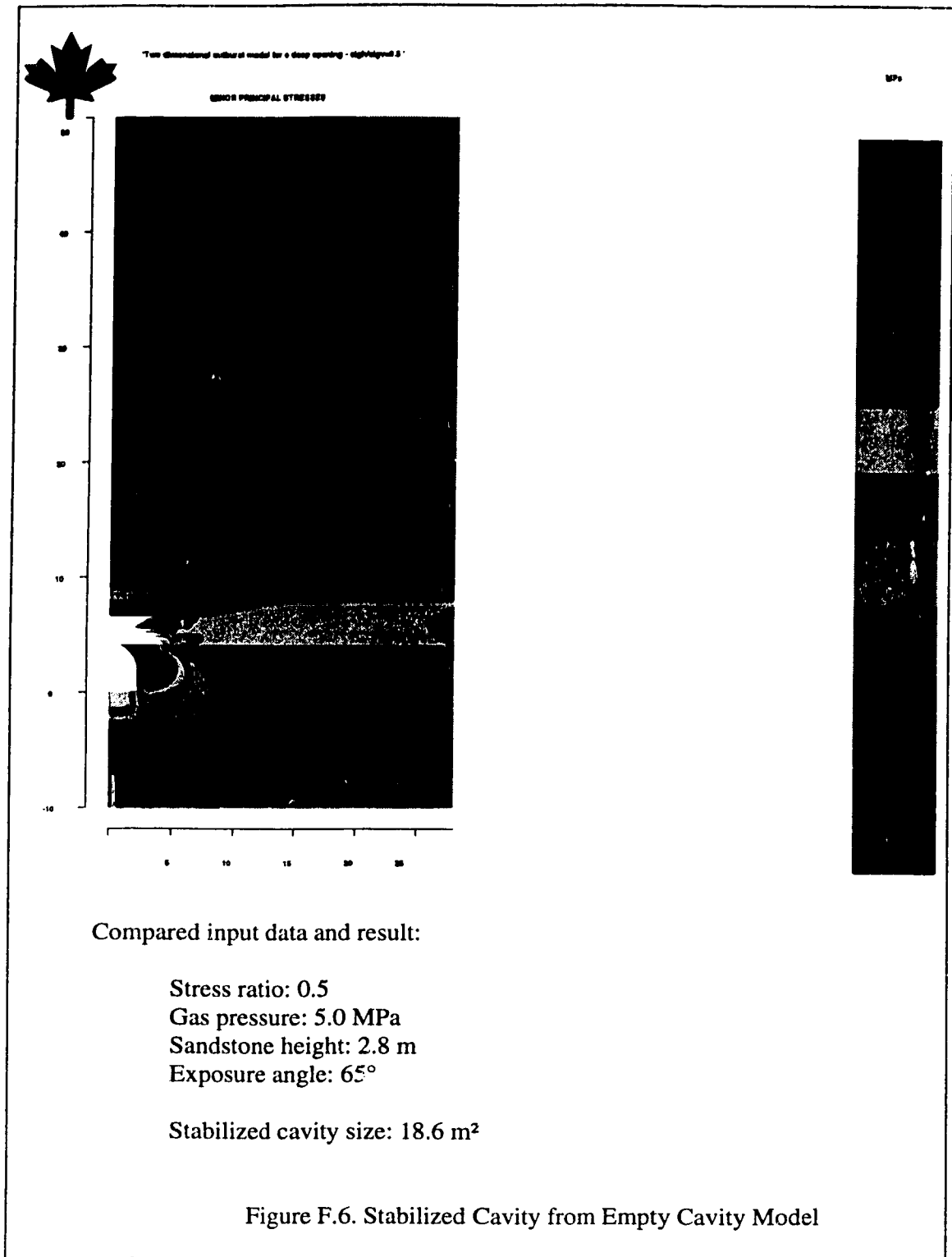
Stabilized cavity size: 88.0 m²

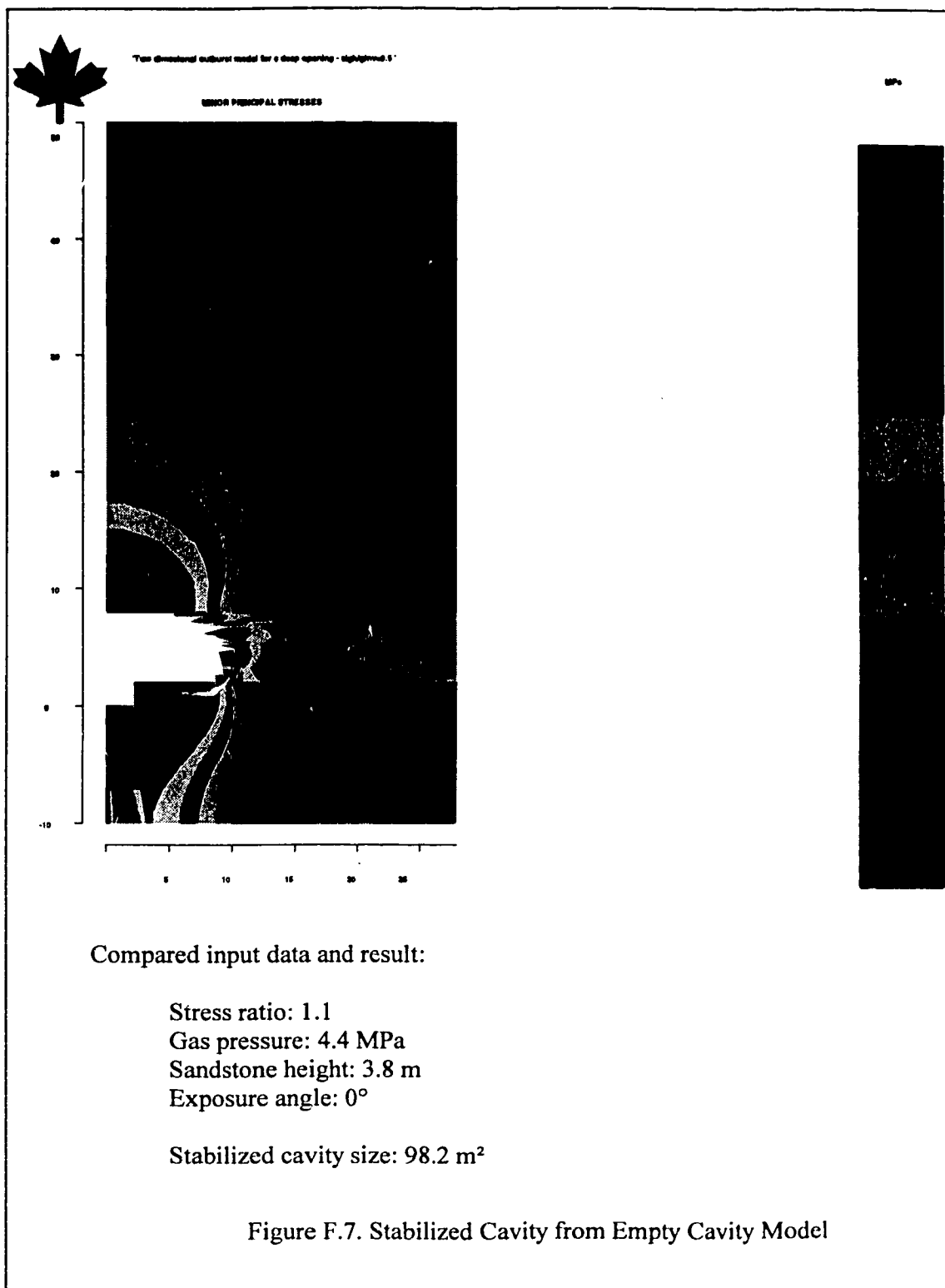
Figure F.2. Stabilized Cavity from Empty Cavity Model

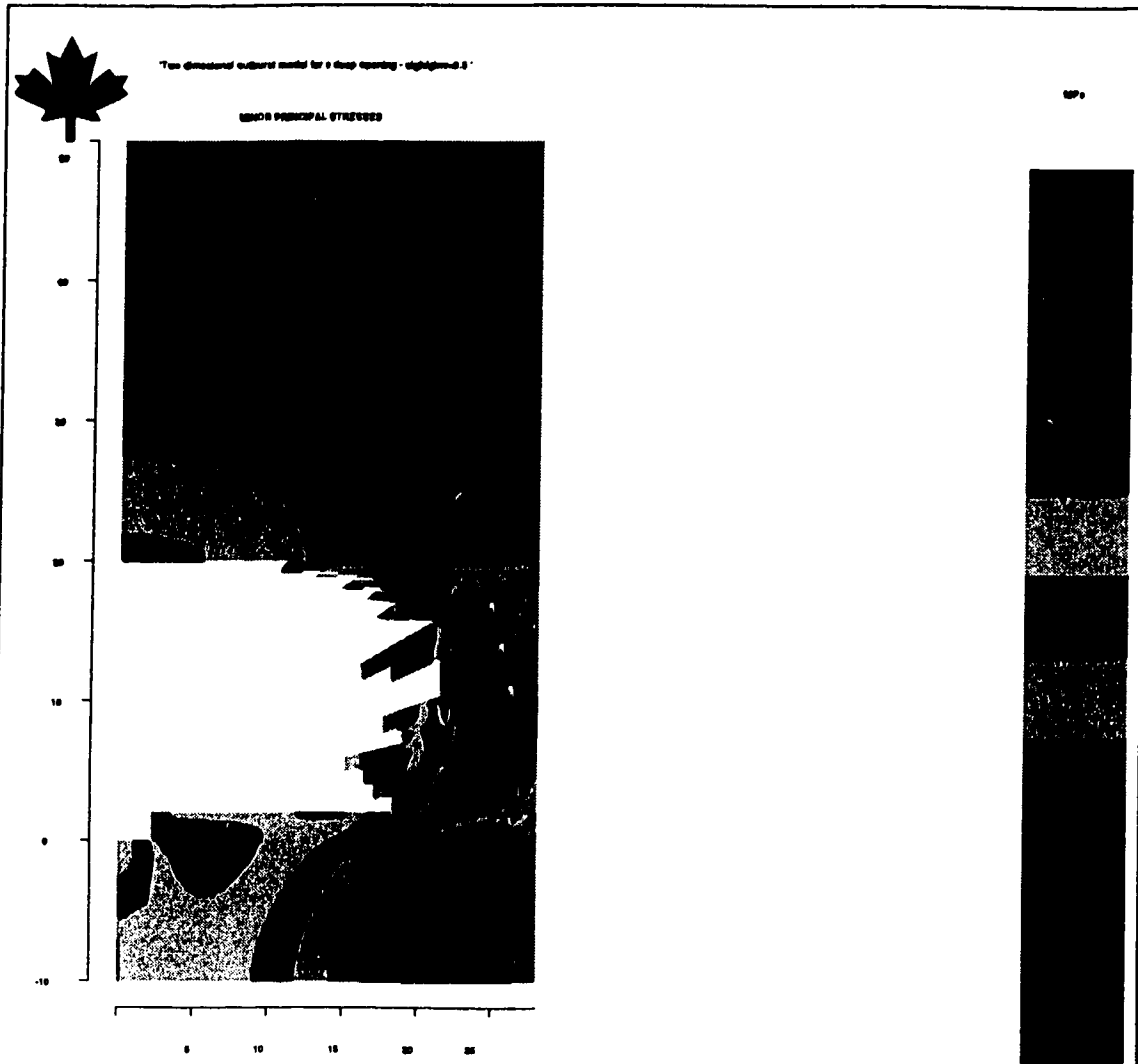










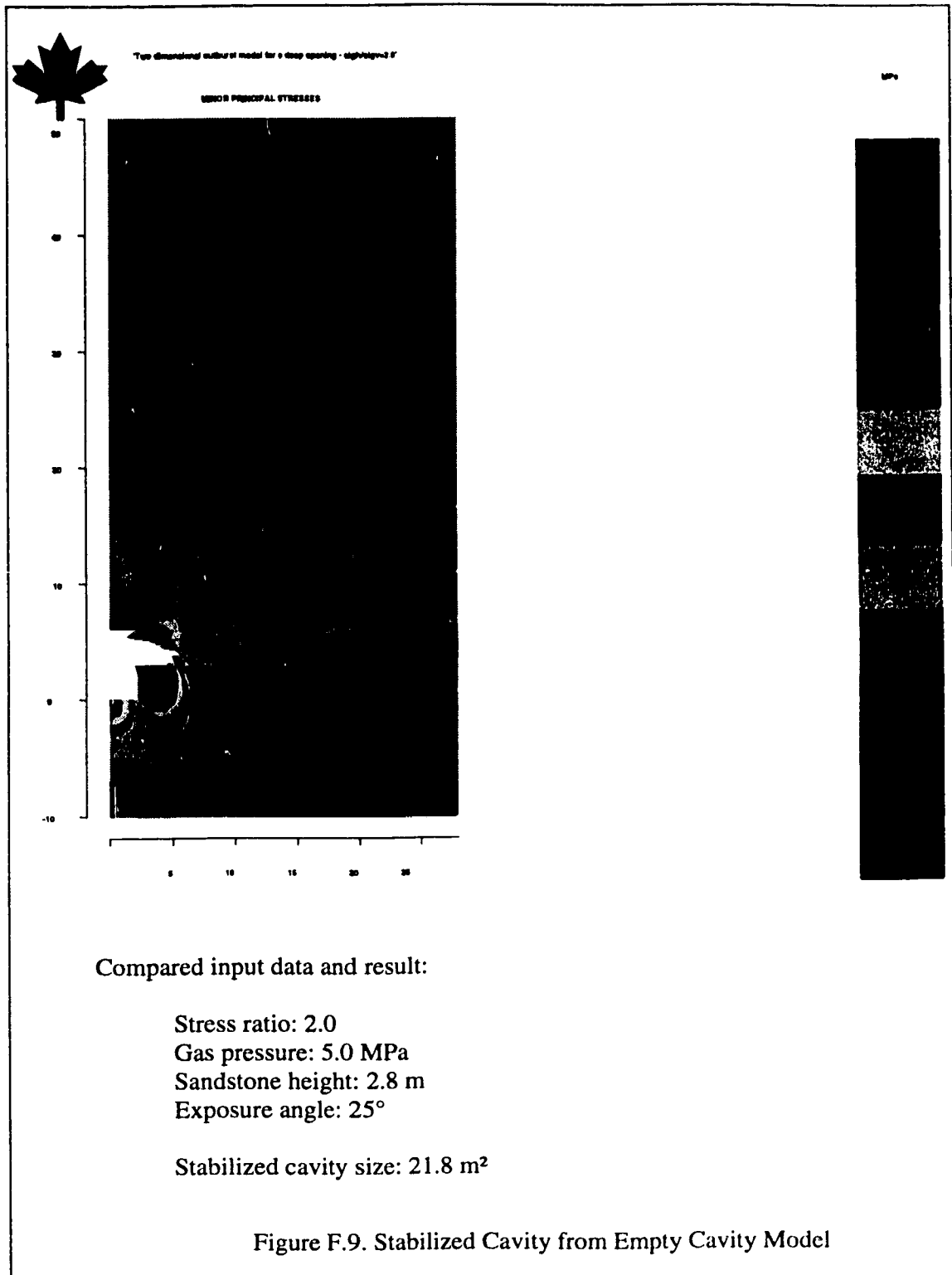


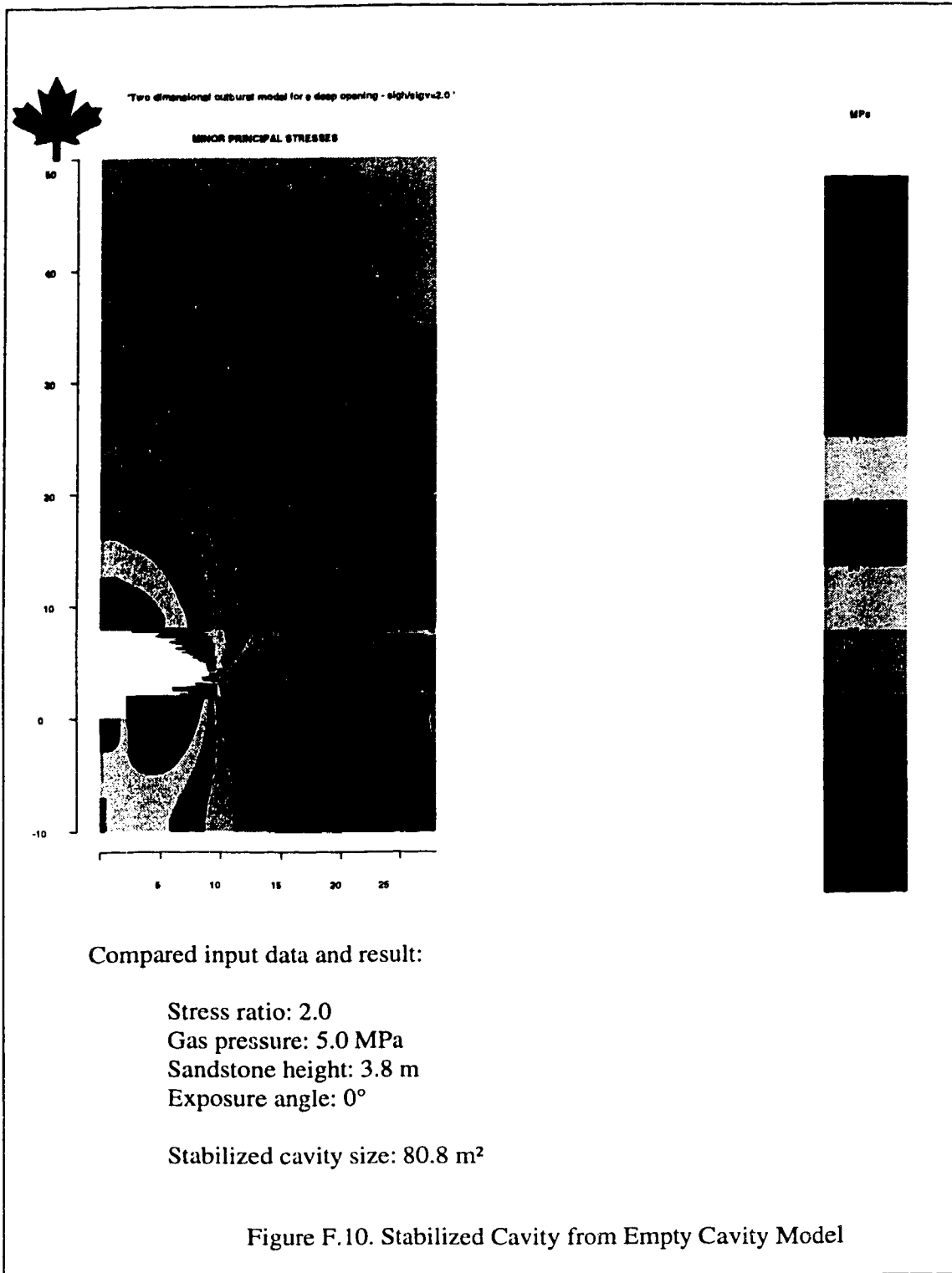
Compared input data and result:

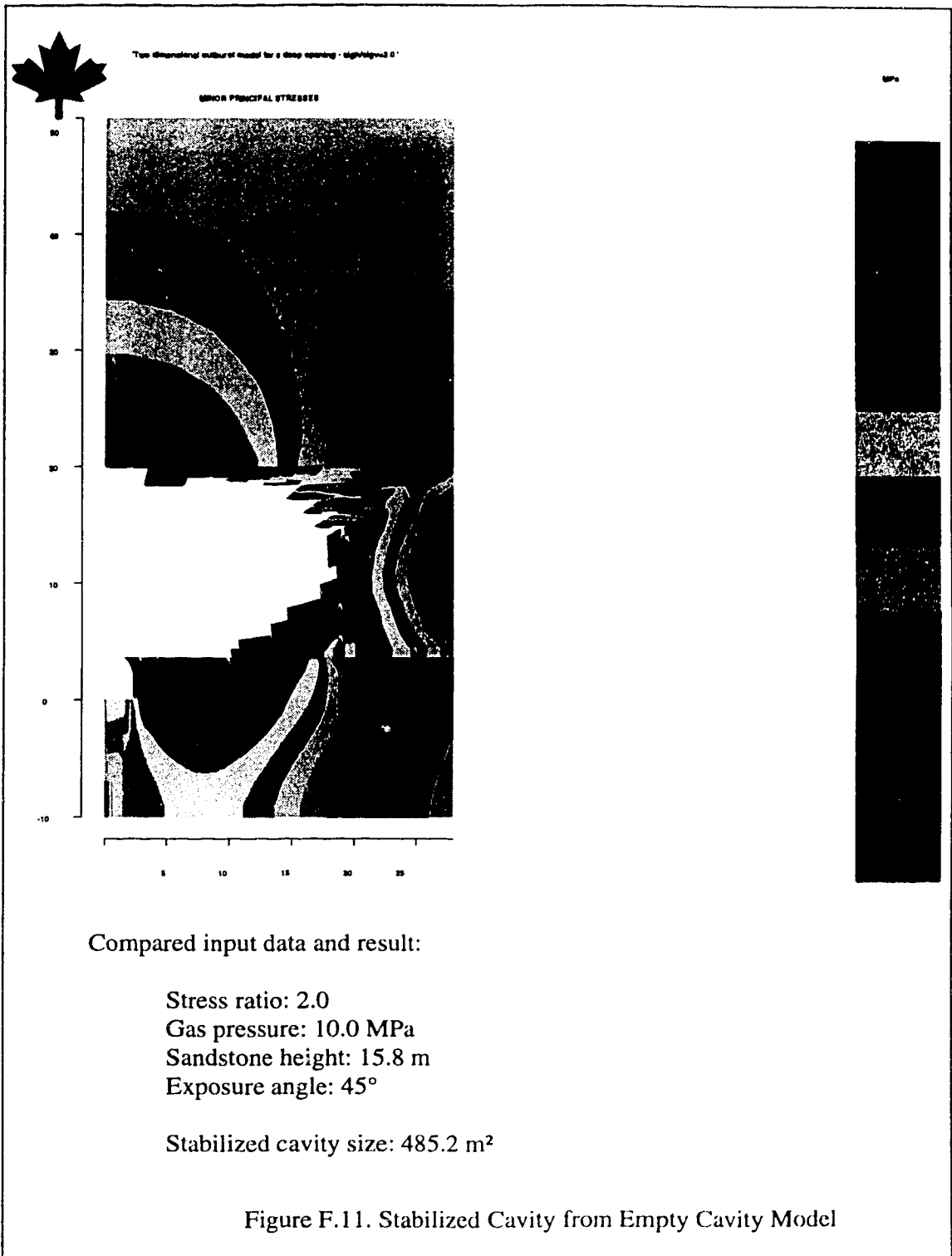
Stress ratio: 1.1
 Gas pressure: 4.6 MPa
 Sandstone height: 15.8 m
 Exposure angle: 0°

Cavity size: deemed to go to infinity

Figure F.8. Infinity Cavity from Empty Cavity Model

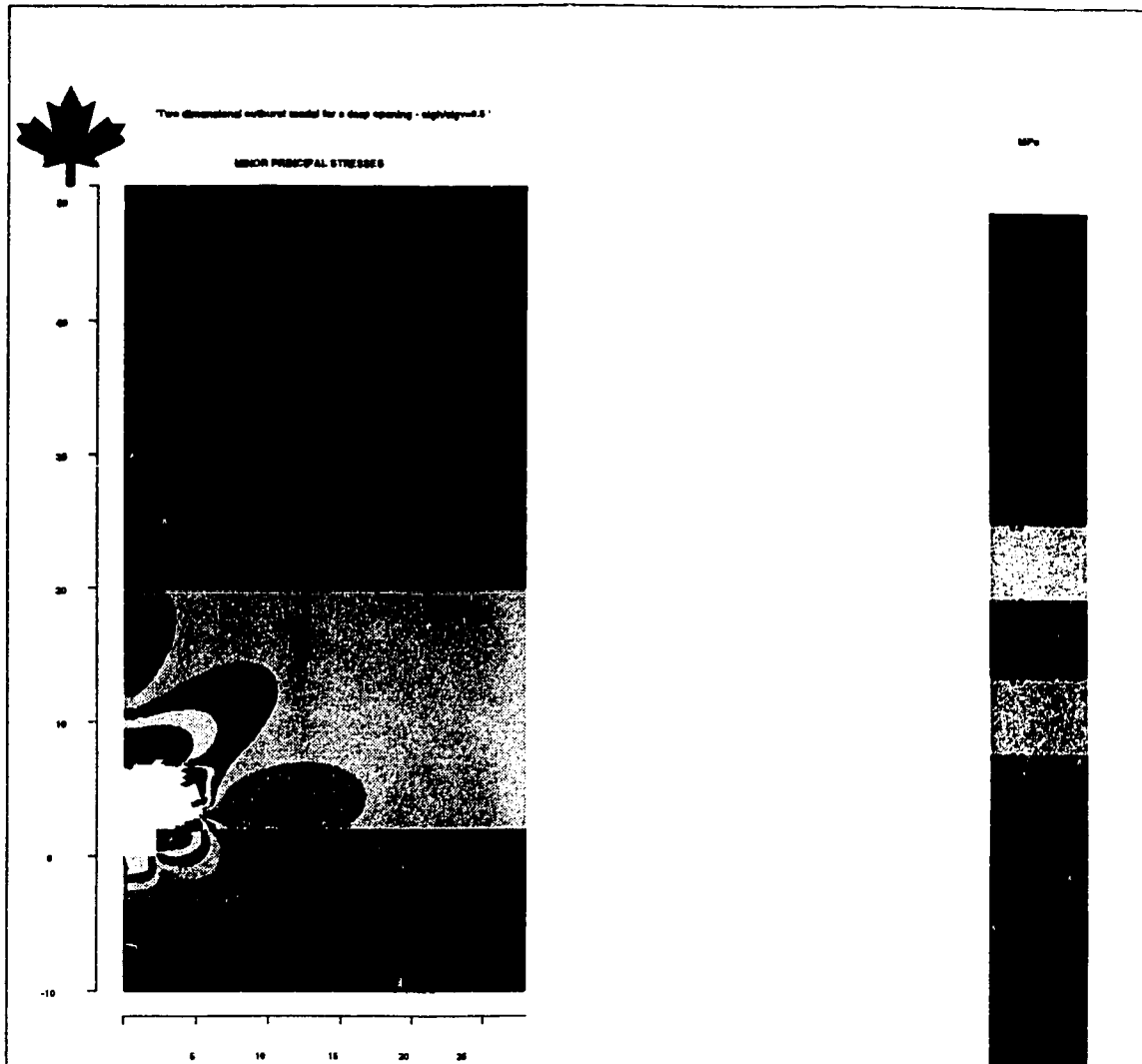






Appendix G.
Cavity Shape and Size Obtained from Filled Cavity Model

The stabilized cavities and infinity cavity by applying the filled cavity model are illustrated in this appendix. They are obtained under the same other conditions but different gas pressures.

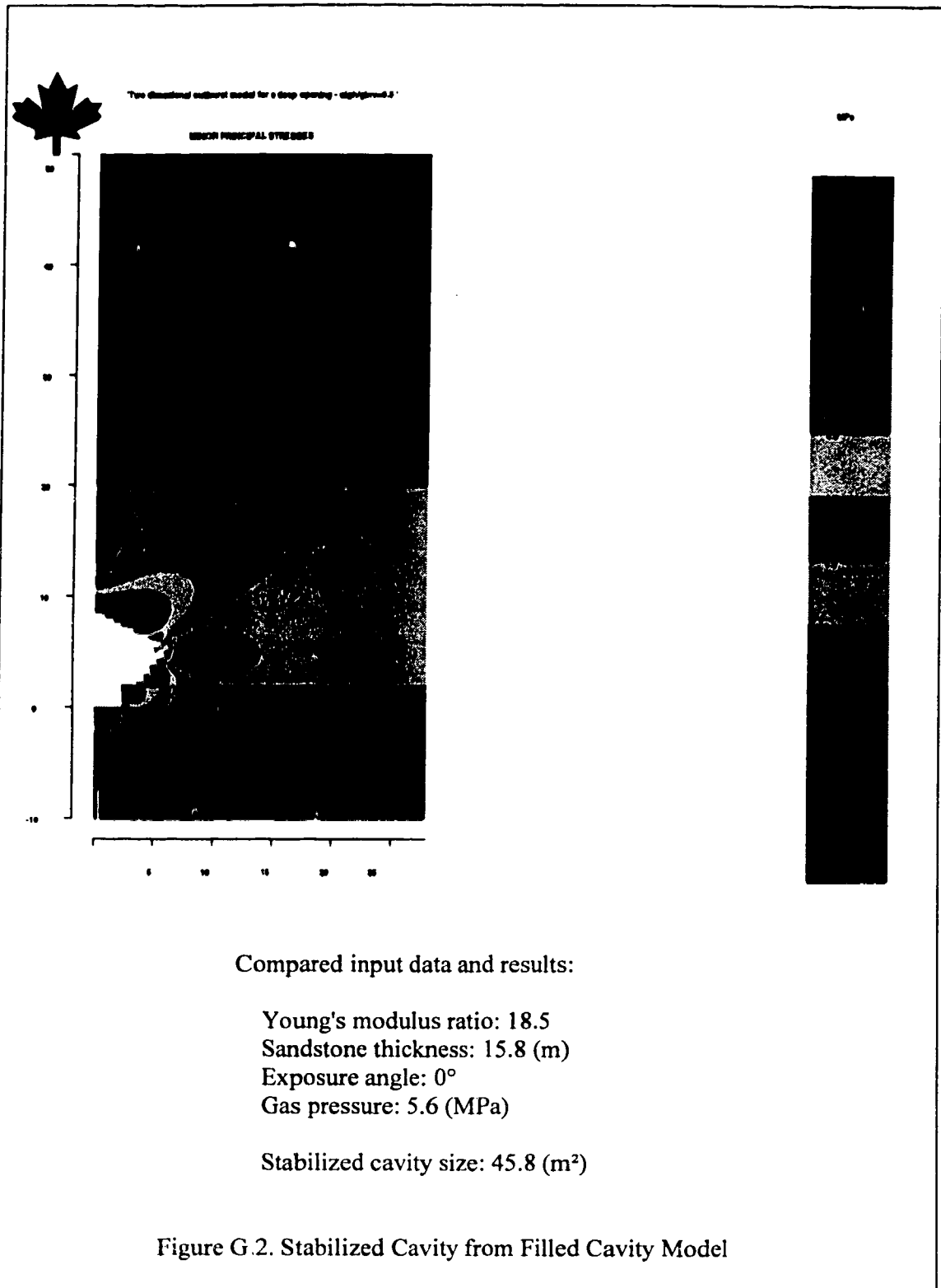


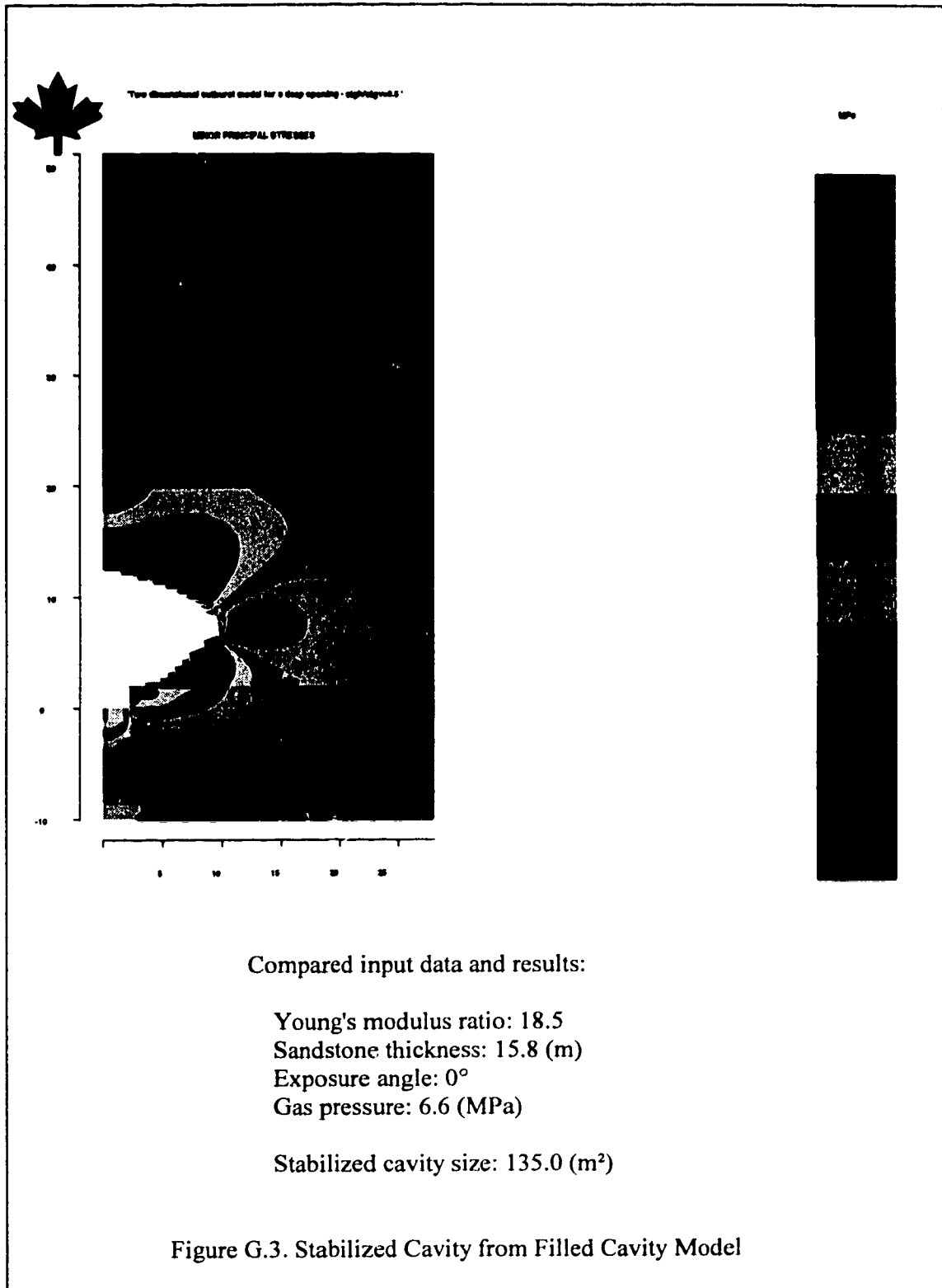
Compared input data and results:

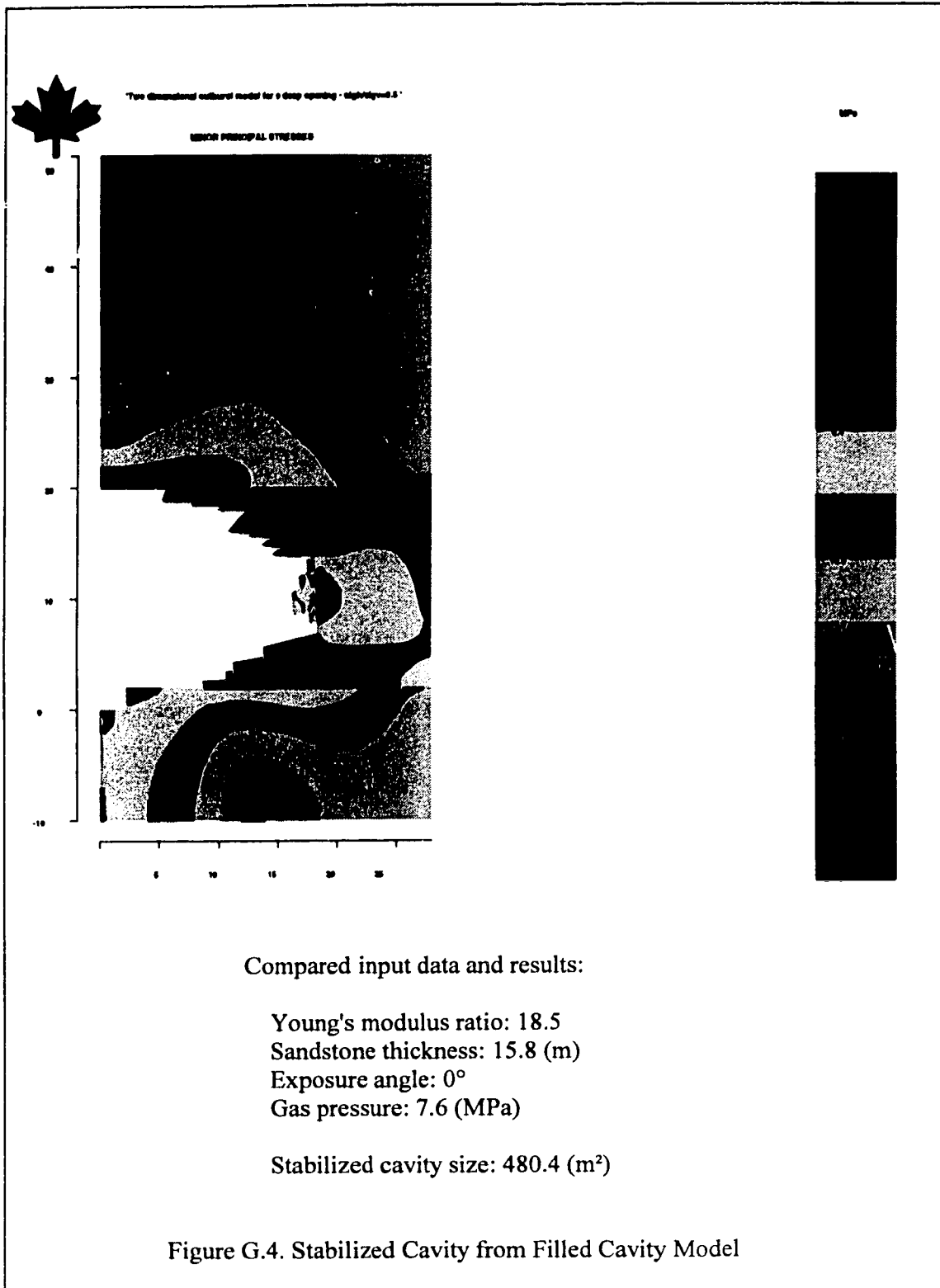
Young's modulus ratio: 18.5
 Sandstone thickness: 15.8 (m)
 Exposure angle: 0°
 Gas pressure: 4.6 (MPa)

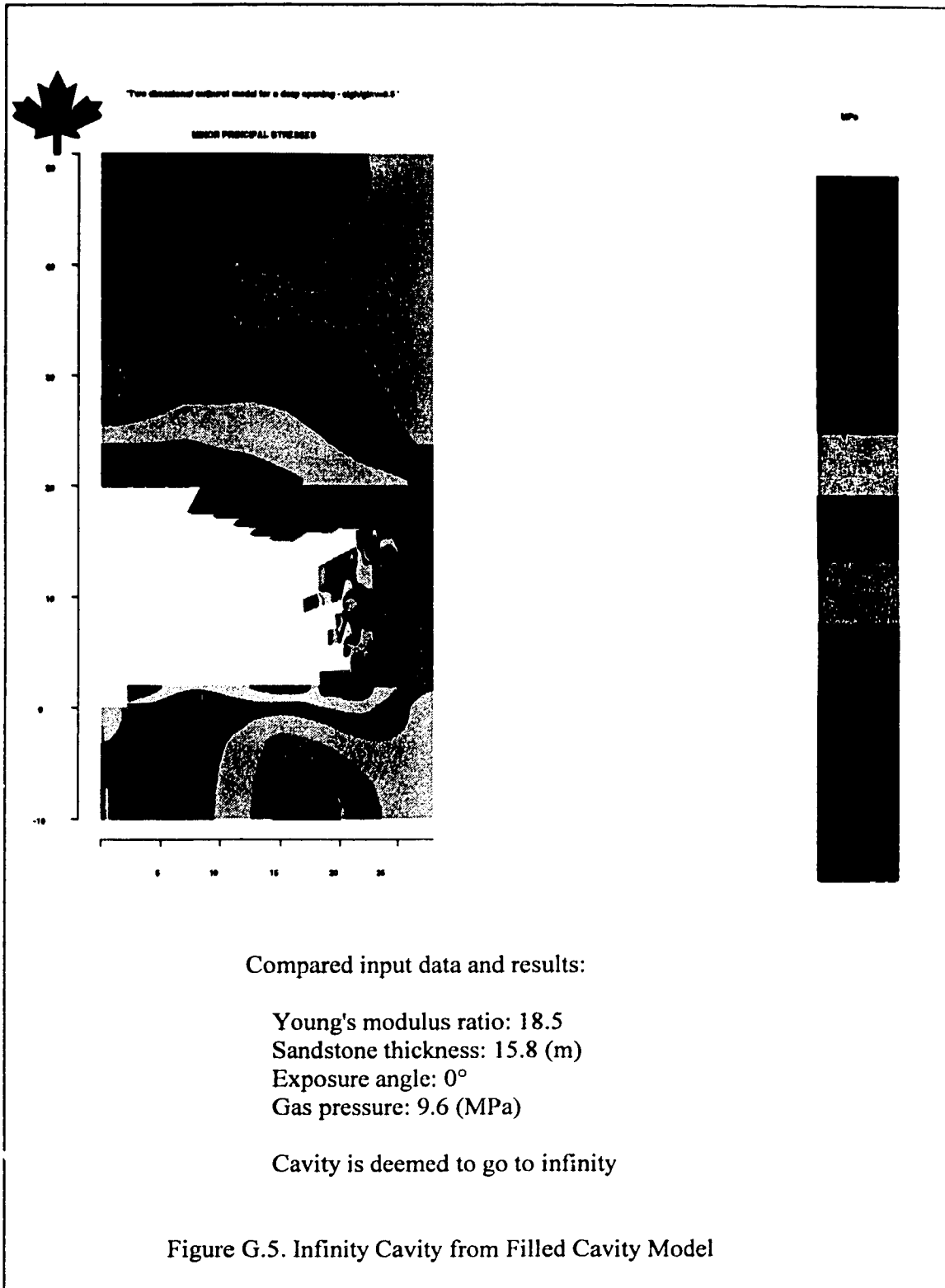
Stabilized cavity size: 37.0 (m²)

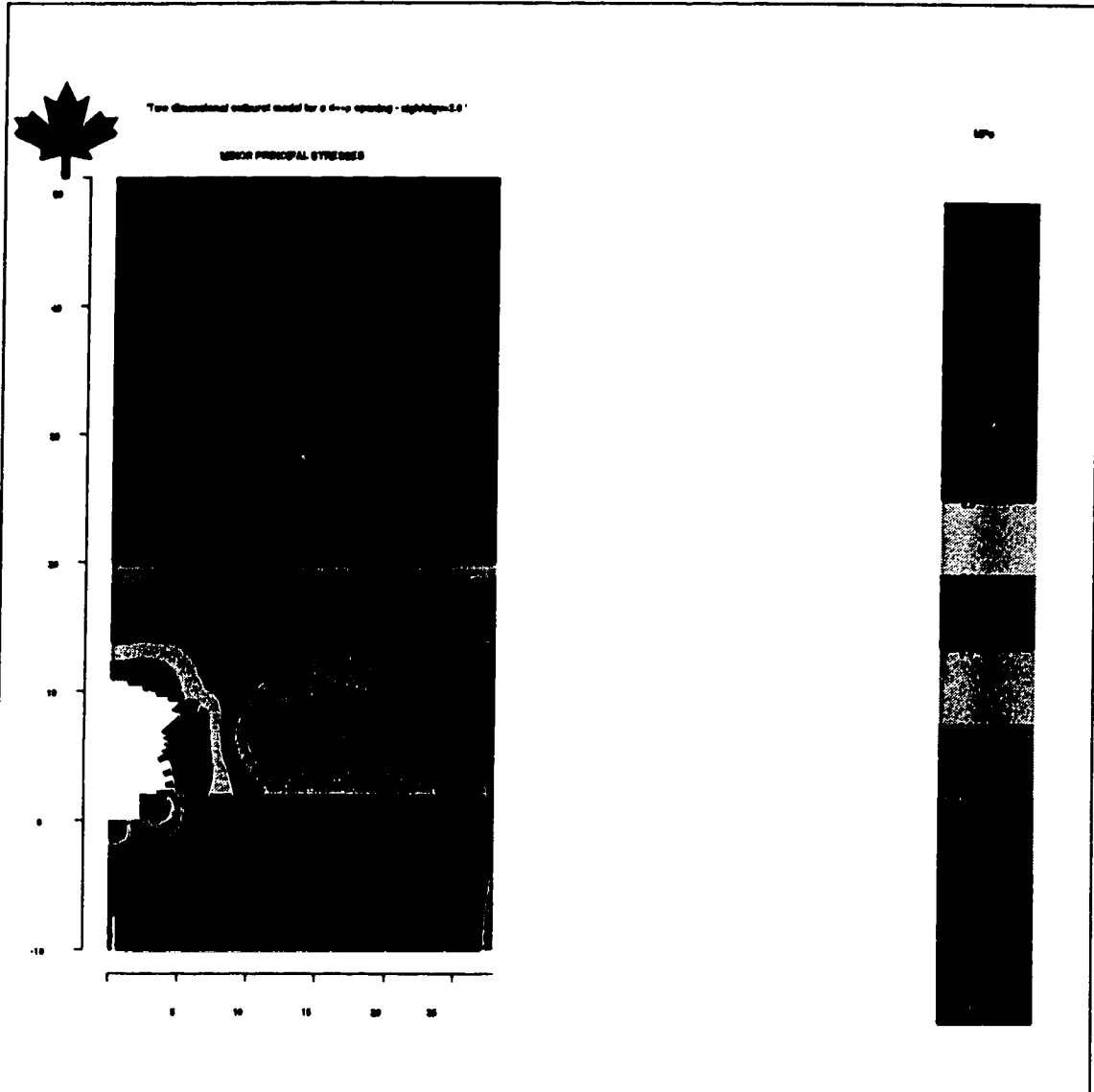
Figure G.1. Stabilized Cavity from Filled Cavity Model











Compared input data and results:

Young's modulus ratio: 18.5
 Sandstone thickness: 15.8 (m)
 Exposure angle: 0°
 Gas pressure: 5.6 (MPa)

Stabilized cavity size: 50.8 (m²)

Figure G.6. Stabilized Cavity from Filled Cavity Model